Hydrogeological modelling of the saltwater intrusions in the Southern Central Region of Vietnam under changing scenarios: the case of Luy River catchment

MSc. Linh Dieu PHAM

A dissertation submitted to Ghent University in fulfilment of the requirements for the degree of Doctor of Science: Geology

UNIVERSITEIT GENT

FACULTY OF SCIENCES

Promotion Commission:

Promotor: Prof. Dr. Ir. Thomas Hermans (Ghent University)

Copromotes: Prof. Dr. Ir. Frédéric Nguyen (Université de Liège)

Dr. Ho Huu Hieu (Vietnam Institute for Geosciences and Mineral)

Examination Committee:

Chairman: Prof. David Van Rooij (Ghent University)

Prof. Kristine Walraevens (Ghent University)

Dr. Thoang Ta Thi (Hanoi University of Natural Resources and Environment, Vietnam)

Dr. Nawal Alfarrah (Ghent University)

Prof. Dr. Ir. Alain Dassargues (Université de Liège)

This research was funded by:

VLIR-UOS TEAM2019 - 77923

BOF Grant DPO/WS/TB

Global Mind Funding

This research project was conducted at the Hydrogeology and Hydrogeophysics Research Unit, Department of Geology, Ghent University (Belgium).

© Linh Dieu Pham, 2024.

All rights reserved. No part of this publication may be reproduced in any form by print, photo, electronically or any other means without written permission from the author. To refer to this thesis: *Pham D.L. (2024) Hydrogeological modelling of the saltwater intrusions in the Southern Central Region of Vietnam under changing scenarios: the case of Luy River catchment.*

Acknowledgements

Someone wrote that a PhD is an extensive journey: you are aware of your starting point and your desired destination, but you don’t really know how to achieve your final objective. This state is so true in my case! I was a bit confident with a little knowledge about groundwater chemistry at the beginning, but hydrogeology is not only about that! There were so many definitions that I did not understand neither English meaning nor process themselves in the beginning! I was wondering how to calculate or measure accurately the parameters of natural processes. I did not know that everything has assumptions behind it or at least a simplification. The modeling part took so much time during my PhD! I did not know what I did wrong, either the way I constructed the model or the model itself… I had a feeling of failure! I joined some social activities to remove the stress. I went hiking and biking to have some fun… It worked a bit, but the deep inside stress was still there; happiness was not complete! I was always feeling the heavy thing in my mind and on my shoulder. To be honest, I wanted to give up a few times!

As I write this acknowledgement, I believe I have nearly overcome that challenging period. And the achievement would not have been possible without the support of my supervisors, colleagues, friends, and family.

First of all, I would like to thank my direct supervisor, Thomas, who has been accompanying and supporting me from the beginning until now! I will never forget the image that he was looking for me before the exam to make sure that I could pass it! Thomas, thank you so much for your encouragement, your patience, and the lessons that you gave to me! I will carry my blue notebook, filled with all your drawings and explanations, with me for as long as possible - most of the time, I have to rewrite your words to ensure I can read them later 😉 I have never seen anyone who is as devoted and equitable with the student as Thomas! Thank you, Thomas! We become better because of your kindness!

I would like to thank my co-supervisor Frédéric! We are a little bit far from each other, but I always feel closely when I see his family name 😊 Thanks Fred, for the suggestions you made during the meetings, the decisions, the support, and the strategy you gave me during my PhD research! I hope I will have an opportunity to work closer with you in the near future.

I would also like to thank Hieu, my promoter on the Vietnam side. Thanks for giving me the opportunity to work on this interesting research and with the wonderful people! At the end, I can say that all the decisions you made in terms of the project are absolutely right! And the rightest one is choosing us to work on it! 😊

I would like to take this chance to say thanks to the experts of groundwater modeling - Vu Thanh Tam in Vietnam and Alexander Vandenbohede in Belgium! I appreciate your explanations and practical advice on how to construct hydrogeological models and deal with convergence issues when the model was (not) running. I am grateful for all your help!

This work would not have been feasible without the cooperation of my colleagues and PhD students from the Applied Geophysics and Hydrogeology sections. Thanks, Diep, for her accompanying me throughout this project period. We went through both good and hard times together; I hope you also appreciate the value of this time as much as I do. I was also with Robin from the field to the lab, and I have never encountered someone with such a keen curiosity about everything as he does. Good luck with your adventure, Robin!

I am grateful to be with Marieke, who has a gift of understanding and explanation for colleagues and students. She is the one who sometimes forgets about her own work to help others. Thanks Marieke, for sharing your knowledge, introducing me to the model troubleshooting, and engaging in conversations about work and life issues. I understand why you are chosen to be a PhD assistant! It is really a pleasure to share the office with you!

With Luka, thanks for checking the model error, looking at solver packages and teaching me how to read the output file of the model. My last steps of modeling progressed faster with your help!

I am delighted to have joined the team alongside Wouter, Elien, Lore, Le, Arsalan, Liming, Hamdi, and Guillaume. I appreciate all of your support, participation in team activities, occasional chatting, coffee, and pingpong games. I wish you all the best of luck in your future career!

I would also like to express my gratitude to Mizanur, Mazeda, George, Alemu, and Adugnaw for their discussions, talks, and knowledge sharing with me during my time working in the office and occasionally chatting online. I am grateful to Jill for analysing our water samples as fast as possible during the Covid crisis. I would like to extend my gratitude to Marion, Kurt, and Wim for their consistent assistance and talk during my stay!

I would like to say thanks to my close friends Long, Chien, Yen, Huong, Hue, and Phuong Anh! Thanks for spending time with me; join me in hiking, biking, drinking, and arguing! Being with you guys made the study life more enjoyable!

Last but not least, I would like to say many thanks to my family: my Mum, who always cares about me and my little family, asking if I am healthy enough; mention me taking care of myself; to my Dad in heaven - I hope you are happy with your kids! To my husband and kids: I am a lucky woman to have you guys! Thanks for your unconditional love, your support, your patience, and being proud of me. I look forward to returning home and enjoying my parent job with you soon! To my brother, sister, and nephews: thanks for your encouragement and being proud of me! I am almost done now!

I would also like to take this opportunity to say thanks to Vinh - he is my relative uncle but also my GIS expert - who has been following me from the very beginning of my career until now. Thanks for all your help and encouragement!

I am grateful to Fanny from OBSG, the families of Rik, Phuong Anh and Lam, as well as Tim and Araceli, for their assistance with my accommodation during my stay in Ghent.

And many thanks to the jury members who helped me improve this doctoral thesis! I would like to send my special appreciation to Kristine for her lectures in the groundwater chemistry course and her encouragement during the last steps of my PhD.

Abstract

The salinity distribution of coastal aquifers often reflects the complex evolution of region related to marine transgressions and regressions, and are only rarely in equilibrium with current boundary conditions. Characterizing such aquifers requires describing the recharge and discharge zones, the chemical composition of the groundwater and the aquifer's geometry and properties. Under climate change, a comprehensive understanding of aquifers is essential for sustainable water resource management and economic development. A multidisciplinary approach is necessary due to the ongoing interaction of meteorological and geographic conditions, groundwater chemistry processes, and hydrogeological properties.

In this thesis, we study the groundwater resources of the Luy River catchment aquifers, in the Binh Thuan province, Vietnam. First, we estimate the recharge for the study area in order to quantify the amount of water infiltrating into the aquifers. Two approaches, namely the soil moisture balance (SMB) and water-table fluctuation (WTF) methods, are utilized. The water balance uses a tank-type model that takes into account many factors such as precipitation, runoff, flow through the unsaturated zone, and evapotranspiration by plants which are determined by soil properties, vegetation type and boundary conditions. It necessitates data regarding the geomorphology, land use, vegetation cover, and meteorology. The other method relies on the fluctuations in groundwater levels over time to estimate recharge using observation wells. Groundwater level fluctuations are observed throughout time in both deep and shallow wells. Due to the short monitoring period, the WTF approach is just employed to verify the approximate amount of recharge estimated using the SMB method. The average recharge obtained using the SMB methodology over a 42-year observation period amounts to 312 mm/year in the alluvial plain and 531 mm/year in the dunes, and is of the same order of magnitude as the values found using the WTF method.

Second, we analyze the chemical composition of groundwater samples obtained during both the dry and wet seasons in the study area. Our goal is to determine the specific hydrochemical mechanisms that are causing the salinization and changes observed in the shallow aquifer of the study regions. The study focuses on analyzing the distribution of chemical components in groundwater and identifying signs that indicate processes of freshening and salinization. These indicators include cation exchange processes, chloride concentration, ionic delta, water facies variation, and geochemical modelling. Unexpectedly, the findings show that freshening is the dominant process in the aquifers, and it is more advanced in the rainy season than the dry season. The deeper aquifer experiences more severe salinization during the dry season as a result of insufficient recharge and excessive aquifer exploitation. Salinity can vary quickly over short distances, and saltwater intrusion extends further inland and at deeps than previously thought. Using these new findings, we create a new conceptual framework to explain the progression of salinization in the research area. This framework considers the natural dilution of originally saline groundwater during the last high water stand that occurred about 6000 years ago, when seawater completely filled the aquifers. The low-permeability material traps this saltwater, slowing down freshening processes and thus extending its residence time. This trapped paleo-groundwater can act as a secondary source of salinity for saltwater intrusion when freshwater at shallow depth is extracted for irrigation; salinization then occurs by upconing or lateral migration. This conceptual model serves as the foundation for creating a groundwater model of the research area, which will ultimately result in the formulation of sustainable management strategies for this coastal region. These strategies aim to prevent any further degradation of the groundwater resources.

This conceptual model is then tested numerically. An initial three-dimensional stratigraphic model is created using the available well logs, geophysical data, and geochemical data. The first numerical model objective is to investigate the impact of aquifer properties on the distribution of freshwater and saltwater over extended periods of time. It seeks to verify the hydro-chemical conceptual model by examining if the time frame of the freshening process aligns with the hydraulic properties and water balance in the catchment area, assuming no groundwater exploitation. Additionally, the study aims to analyze the current distribution of saline groundwater from different hypotheses regarding saltwater sources. Lastly, it aims to evaluate the potential for groundwater resource development in the face of freshening and saltwater intrusion threats. As such, we consider this model primarily as a conceptual tool. However, we verified the accuracy of the model by qualitatively comparing the simulated findings with the actual measurements of groundwater levels and salt concentrations, which serve as an indicator of the chemical composition of the groundwater. The findings confirm that the presence of paleo-groundwater in the study area is a realistic hypothesis. They suggest that during long-term freshening processes, saltwater becomes trapped inside the clay aquitard and the lower aquifers. The difference in density between saltwater and freshwater exacerbates this trend. The top and bottom elevations of the aquifers are also affecting the saltwater distribution. The most realistic scenario's saltwater distribution pattern aligns with the results of geophysical investigation carried out in the study area and the hydrochemical conceptual model.

Finally, we focus on sustainable groundwater resource management for the study area. The same groundwater model is used, but a calibration step is carried out to ensure the model can reproduce current observations. We combine all the findings from previous sections, along with sea level rise and climate change scenarios, to provide a picture of the distribution of saltwater in the aquifers over the next 50 years. We also identify potential reservoirs in the study area that could serve as valuable resources for abstraction while minimizing the impact of saltwater intrusion. The results indicate that over the next 50 years, saltwater will continue to be present in the aquifers in its natural state, even without any pumping, which is coherent with the findings of the long-term simulation. If groundwater remains abstracted as it currently is, saltwater may infiltrate inland, approximately 1 km from the coastline. In combination with the pumping in the alluvial and sea level rise, saltwater is forecast to intrude to the inland about 5 km from the river mouth. The salinity will increase in the shallow aquifer due to upconing. The dune system has a significant capacity for freshwater and could serve as freshwater reservoirs in the future. This is particularly valuable since it assists in reducing the problem of saltwater intrusion on the alluvial plain. This approach might be integrated with regulated aquifer recharge, wherein the surplus precipitation during the rainy season could be kept within the dune system to augment the groundwater reservoir in the dunes.

Samenvatting

Kustgrondwaterreserves weerspiegelen vaak een complexe evolutie van mariene transgressies en regressies en zijn slechts zelden in evenwicht met de hedendaagse randvoorwaarden. Om dergelijke aquifers te karakteriseren moeten de aan- en afvoerzones, de chemische samenstelling van het grondwater en de geometrie en eigenschappen van de aquifer worden beschreven. Bij klimaatverandering is een uitgebreid begrip van aquifers essentieel voor duurzaam waterbeheer en economische ontwikkeling. Een multidisciplinaire aanpak is noodzakelijk vanwege de voortdurende interactie tussen meteorologische en geografische condities, chemische processen in het grondwater en hydrogeologische eigenschappen.

In dit proefschrift bestuderen we de grondwatervoorraden van de watervoerende lagen van het stroomgebied van de Luy rivier, in de provincie Binh Thuan, Vietnam. Eerst schatten we de aanvulling voor het studiegebied om de hoeveelheid water die infiltreert in de watervoerende lagen te kwantificeren. Twee benaderingen worden gebruikt, de bodemvochtbalans (SMB) en de grondwaterstandfluctuatie (WTF). De eerste maakt gebruik van een tankmodel dat rekening houdt met vele factoren zoals infiltratie, afvloeiing, stroming door de onverzadigde zone en wateropname door planten die worden bepaald door bodemkwaliteit, de randvoorwaarden en evapotranspiratie. Hiervoor zijn gegevens nodig over de morfologie, het landgebruik, de vegetatiebedekking en de meteorologie. De andere methode is gebaseerd op de fluctuaties in grondwaterniveaus in de loop van de tijd om de aanvulling te schatten met behulp van waterniveaus in observatieputten. Grondwaterpeilschommelingen worden in de loop van de tijd waargenomen in zowel diepe als ondiepe putten. Vanwege de korte meetperiode wordt de WTF-methode alleen gebruikt om de aanvulling die geschat is met de SMB-methode te verifiëren. De gemiddelde aanvulling bereikt met de SMB methode, 312 mm/jaar in de alluviale vlakte en 531 mm/jaar in de duinen, is vergelijkbaar met de waarden gevonden met de WTF methode.

We analyseren de chemische samenstelling van grondwatermonsters die zijn verkregen tijdens zowel het droge als het natte seizoen in het studiegebied. Ons doel is om de specifieke hydrochemische mechanismen te bepalen die de verzilting en veranderingen in de ondiepe watervoerende lagen veroorzaken. Het onderzoek richt zich op de analyse van de verdeling van chemische componenten in het grondwater en het identificeren van tekens die duiden op processen van verzoeting en verzilting. Deze indicatoren zijn onder andere kation uitwisselings processen, chlorideconcentratie, ionische delta, variatie in hydrochemische facies en geochemische modellering. De bevindingen tonen aan dat verzoeting het dominante proces is in de watervoerende lagen en dat dit proces in het regenseizoen meer gevorderd is. De diepere aquifer ondervindt ernstigere verzilting tijdens het droge seizoen als gevolg van onvoldoende aanvulling en overmatige aquifer exploitatie. Het zoutgehalte kan snel variëren over korte afstanden en zoutwaterintrusie breidt zich verder landinwaarts en op diepte uit. Met behulp van deze nieuwe inzichten creëren we een nieuw conceptueel kader om de progressie van verzilting in het onderzoeksgebied te verklaren. Deze houdt rekening met de natuurlijke verdunning van het oorspronkelijk zoute grondwater dat tijdens de hoge zeewaterstand zo'n 6000 jaar geleden werd aangevuld. Slecht doorlatend materiaal houdt dit zoute water vast, waardoor het langer aanwezig blijft. Het kan fungeren als een secundaire zoutbron voor zoutwaterintrusie wanneer zoet water op geringe diepte wordt onttrokken voor irrigatie; verzilting vindt plaats door verticale of laterale migratie. Het conceptuele model dient als basis voor het maken van een grondwatermodel van het onderzoeksgebied, dat uiteindelijk zal resulteren in de formulering van duurzame beheerstrategieën voor dit kustgebied. Deze strategieën zijn erop gericht om verdere achteruitgang van de grondwaterbronnen te voorkomen.

Dit conceptuele model wordt vervolgens numeriek getest. Er wordt eerst een driedimensionaal stratigrafisch model gemaakt met behulp van de beschikbare boorgatmetingen, geofysische en geochemische data. Het doel van het numerieke model is om de invloed van de eigenschappen van de aquifer op de verdeling van zoet en zout water over langere perioden te onderzoeken. Het probeert het hydrochemische conceptuele model te verifiëren door te onderzoeken of het tijdsbestek van het verzoetingsproces overeenkomt met de hydraulische eigenschappen en de waterbalans in het stroomgebied, ervan uitgaande dat er geen grondwater wordt geëxploiteerd. Daarnaast heeft de studie als doel om de huidige verspreiding van het zoute grondwater te analyseren vanuit verschillende hypotheses met betrekking tot zoutwaterbronnen. Tot slot is het de bedoeling om het potentieel voor de ontwikkeling van grondwaterbronnen te evalueren in het licht van verzoeting en de dreiging van zoutwaterintrusie. Als zodanig beschouwen we dit model voornamelijk als een conceptueel hulpmiddel. We hebben de nauwkeurigheid van het model echter geverifieerd door de gesimuleerde resultaten te vergelijken met de werkelijke metingen van grondwaterniveaus en zoutconcentraties, die dienen als indicator voor de chemische samenstelling van het grondwater. De bevindingen suggereren dat zout water tijdens langdurige verzoeting vast komt te zitten in de kleiaquitard en de diepere watervoerende lagen. Het verschil in dichtheid tussen zout en zoet water versterkt deze trend. De top en onderkant van de aquifers hebben ook invloed op de zoutwaterverdeling. Het zoutwaterdistributiepatroon van het meest realistische scenario komt overeen met de resultaten van het geofysisch onderzoek van Cong-Thi et al. uit 2021 en het hydrochemische conceptuele model van Pham et al. (2022).

Tot slot richten we ons op duurzaam grondwaterbeheer voor het studiegebied. Hiervoor wordt hetzelfde model gebruikt, maar er wordt een kalibratiestap uitgevoerd om ervoor te zorgen dat het model de huidige waarnemingen kan reproduceren. We combineren alle bevindingen uit de voorgaande hoofdstukken, samen met scenario's voor zeespiegelstijging en klimaatverandering, om een beeld te krijgen van de verdeling van het zoute water in de watervoerende lagen in de komende 50 jaar. We identificeren ook potentiële reservoirs in het studiegebied die kunnen dienen als waardevolle bronnen voor grondwaterextractie terwijl de impact van zoutwaterintrusie tot een minimum wordt beperkt. De resultaten geven aan dat er de komende 50 jaar zout water in de aquifers aanwezig zal blijven in zijn natuurlijke staat, zelfs zonder pompen. Als er grondwater wordt onttrokken zoals nu het geval is dan kan zout water landinwaarts infiltreren tot op ongeveer 1 km van de kustlijn. In combinatie met het pompen in de alluviale vlakte en zeespiegelstijging zal zout water naar verwachting ongeveer 5 km vanaf de riviermonding het binnenland binnendringen. Door een verticale stroming vanuit de diepere lagen zal het zoutgehalte in de ondiepe watervoerende laag toenemen. Het duinsysteem heeft een aanzienlijke zoetwatercapaciteit en kan in de toekomst dienen als zoetwaterreservoir. Dit is vooral waardevol omdat het helpt om het probleem van zoutwaterintrusie in de alluviale vlakte te verminderen. Deze aanpak kan worden geïntegreerd met kunstmatige aquifer aanvulling, waarbij het neerslagoverschot tijdens het regenseizoen binnen het duinsysteem kan worden gehouden om het grondwaterreservoir in de duinen te vergroten.

List of Abbreviations

ASL	Above sea level.
BC	Boundary condition.
DEM	Digital elevation model.
EC	Electrical conductivity.
ERT	Electrical resistivity tomography
IPCC	Intergovernmental Panel on Climate Change
Kh	Horizontal hydraulic conductivity.
Kv	Vertical hydraulic conductivity.
LGM	Last Glacial Maximum.
NAWAPI	National Center for Water Resources.
MODFLOW	MODular three-dimensional finite-difference groundwater FLOW model
MT3DMS	Modular 3-dimensional multi-species transport model
RSME	Root mean square error.
SL	Sea level
SWI	Saltwater Intrusion
SMB	Soil Moisture Balance
WTF	Water-table Fluctuation.
TDS	Total dissolved solids.
TVD	Total variation diminishing, is a numerical solver for advective solute transport.
USGS	United States Geological Survey

Contents

Acknowledgements i

Abstract v

Samenvatting ix

List of Abbreviations xiii

Chapter 1. Introduction 1

Chapter 2. Site description 14

- 2.1 General description 14
- 2.2 Topography, Land Use and Surface Water 14
- 2.3 Climate 16
- 2.4 Geology and Hydrogeology 17

Chapter 3. Estimating groundwater recharge for Luy River plain in Binh Thuan, Vietnam 25

- 3.1 Introduction 26
- 3.2 Study area description 27
- 3.3 Materials and methods 29
  - 3.3.1 Soil moisture water balance method 30
  - 3.3.2 Water table fluctuation method 35
- 3.4 Results and discussion 36
  - 3.4.1 Groundwater recharge calculated using SMB 36
  - 3.4.2 Groundwater table fluctuation 44
- 3.5 Discussion 50
- 3.6 Conclusion 52

Chapter 4. Groundwater salinization and freshening processes in the Luy river coastal aquifer, Vietnam 54

4.1 Introduction 55
4.2 Methods 58
4.2.1 Water Sampling 58
4.2.2 Chemical Analysis 60
4.2.3 Geochemical Analysis 60
4.3 Results 63
4.3.1 Chemical Composition and Ion Distribution of Water Samples 63
4.3.2 Classification of Water 67
4.3.3 Hydrochemical Facies Using Piper and HFE-D Diagrams 69
4.3.4 Ionic Relation and Origin of Solutes 71
4.3.5 Water/Rock Interaction and the Origin of Solutes 73
4.3.6 Speciation-solubility calculations 74
4.3.7 Variation of hydrogeological parameters of groundwater with time76
4.4 Conceptual model of the salinity evolution in the Luy river catchment . 82
4.5 Conclusions 86
Chapter 5. Groundwater modelling to validate saltwater intrusion and freshening processes identified from hydrochemistry in a coastal groundwater system in Vietnam..88
5.1 Introduction 89
5.2 Study area 93
5.3 Methods 97
5.3.1 Hydro-stratigraphic model 97
5.3.2 Conceptual model 102
5.3.3 Model construction 103
5.3.4 Mathematical model 106
5.3.5 Numerical model 110
5.3.6 Formulation of scenarios 112
5.4 Results 114
5.4.1 Freshening and saltwater intrusion in homogeneous conditions . 115
5.4.2 Scenario 4: realistic model 123

5.4.3 Scenarios 5, 6, and 7 128
5.5 Discussion 132
5.6 Conclusion 134
Chapter 6. Simulating groundwater management scenarios in the salinized Luy River aquifer systems under climate change 136
6.1 Introduction 136
6.2 Study area and available data 138
6.3 Methodology 144
6.3.1 Climate change and sea level rise 144
6.3.2 Groundwater modelling 146
6.3.3 Formulation of scenarios 148
6.4 Results and discussion 149
6.4.1 Model calibration 149
6.4.2 Simulation of scenarios 154
6.4.3 Discussion 163
6.5 Conclusion 165
Chapter 7. Conclusion and Recommendation 167
References 175
Appendix 192
Appendix 1 Geological map of Bac Binh and Tuy Phong districts (Segers, 2024) 192
Appendix 2 Compilation of relevant geological formations and deposits (sedimentary facies), derived from multiple sources (Segers, 2024) 193
Appendix 3 Chemical component of groundwater samples in the Luy River catchment collected in the rainy season 2020 195
Appendix 4 Chemical component of groundwater samples in the Luy River catchment collected in the dry season 2021 200
Appendix 5 Fresh-Salt waters in the mixing line 201
Appendix 6. Lithological well logs 202

Chapter 1. Introduction

Freshwater is a replenishable and fluctuating natural resource but is also limited. As part of its natural cycle, water evaporates from various water bodies (seas, lakes, and rivers) and is transpired by vegetation, forming clouds, and finally finds its way back inland as precipitation, replenishing surface reservoirs but also aquifers (USGS, 2021). Approximately 2.5% of the total water on Earth is freshwater, with most of it being stored in solid form in glaciers and ice caps. Groundwater accounts for around 30.1% of the total, while fresh surface water represent only about 1% (Figure 1.1). As the globe's largest freshwater storage, groundwater is a life-sustaining resource that supplies water to billions of people both for drinking water production and agriculture. In addition to its significance in irrigated agriculture and food security, groundwater is also vital for energy production, human health, and the provision of ecosystem services, for example through maintaining a baseflow in rivers during dry periods.

Nature always follows its own principles and functions in a balanced manner (Zekâi 2015). Human activities that consume more freshwater than nature replenishes can cause water shortages and negatively impact the surrounding environment and ecosystems. Groundwater contamination reduces freshwater availability. Some of the major sources causing contamination are landfills, septic systems, storage tanks, hazardous waste sites, and the widespread use of chemicals. Another urgent concern is saltwater intrusion (SWI), which usually occurs in coastal areas (Bear 1999; Appelo and Postma 2005).

Coastal zones are commonly defined based on the distance-to-coast (100 km from the coast) and elevation data (below 50 m elevation) (Neumann et al., 2015; Ramkumar et al., 2019). Human settlements tend to be more concentrated in coastal areas due to the economic advantages of ocean navigation, coastal fisheries, tourism, and recreation.

Approximately 40% of the world's population resides in coastal regions (Figure 1.2, United Nations 2020). These areas are experiencing growing challenges to their ecosystems, such as habitat conversion, land cover change, and pollution, particularly in terms of groundwater contamination. High population concentration in low-elevation coastal zones increases vulnerability to sea-level rise and coastal hazards.

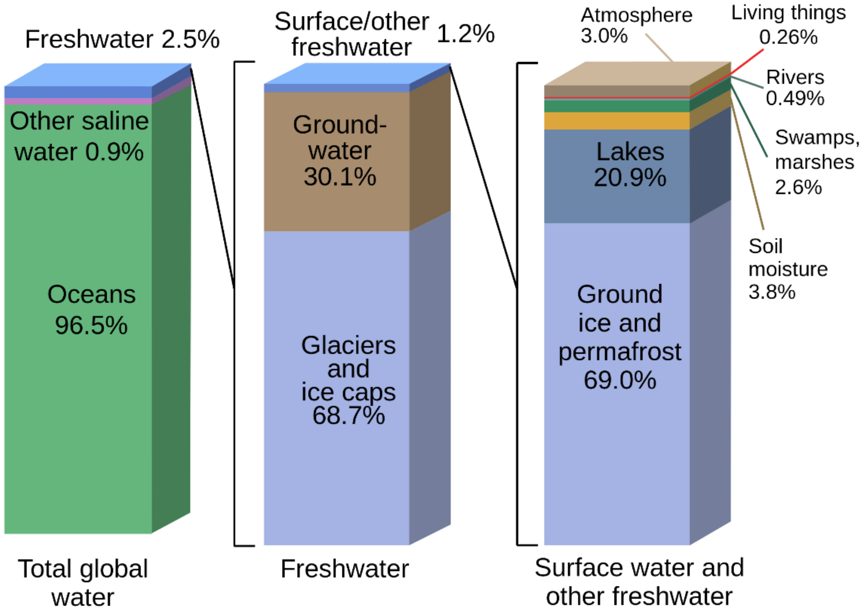

Figure 1.1 Earth's water distribution (USGS 2021)

The impacts of saltwater intrusion and global climate change have profound effects on the residents of coastal areas, as well as on accessibility to groundwater and water demand. According to Fox weather’s report (2024), world’s population forecast to peak in 2080 at 10.13 billion. Over the next 50 years, population growth as well as water demands are projected to push all the coastal communities into water scarcity conditions (Neumann et al., 2015).

Aquifers in low-lying coastal areas around the world are at risk of saltwater intrusion due to factors such as density-driven flow, tidal influence in estuaries, high groundwater extraction rates, low recharge rate, or excessive water drainage (Ramkumar et al., 2019, Bosserelle et al., 2022; Zamrsky et al., 2024). These threats are expected to increase in severity as a result of climate change. Therefore, sustainable management of groundwater resources is essential.

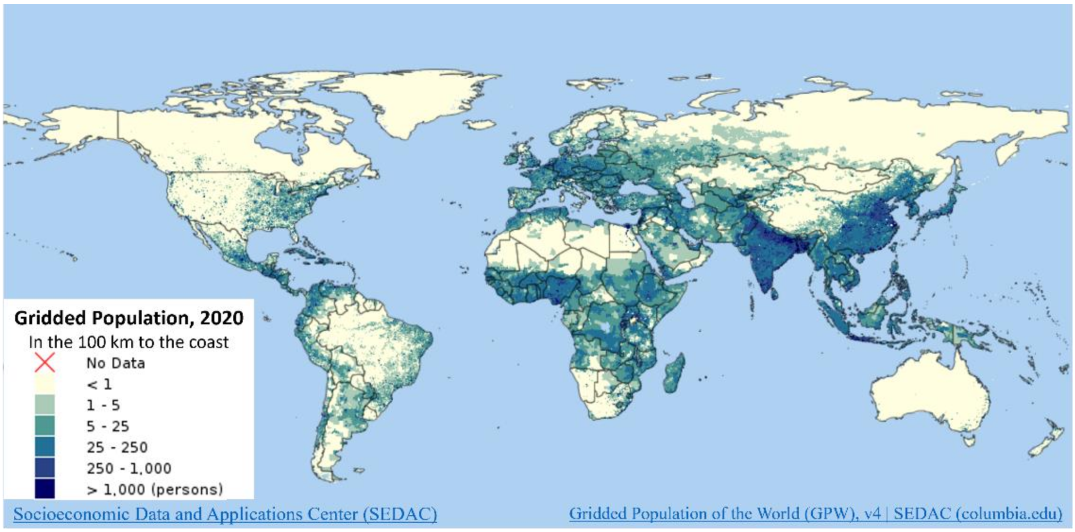

Socioeconomic Data and Applications Center (SEDAC)

Gridded Population of the World (GPW), v4 | SEDAC (columbia.edu)

Figure 1.2 The world population in 2020 (United Nations, 2020)

Groundwater is highly susceptible to contamination due to agricultural, industrial, and urban activities (Hem 1985; Appelo and Postma 2005). Local communities must face the ongoing and inescapable pollution of the environment, both from past events as well as current sources of pollution. Consequently, the characterization and evolution of aquifers in relation to the pollution of groundwater and the movement of dissolved substances is a highly relevant topic.

A comprehensive understanding of aquifers requires a multidisciplinary approach due to the ongoing interaction of hydrogeological properties, groundwater chemistry processes, and meteorological and geographic conditions. In other words, we must acquire some knowledge about the geometry and the properties of the aquifer, including the presence and extent of confined and unconfined units and their hydraulic properties (porosity, specific yield, hydraulic conductivity), the recharge and discharge zones of the aquifer, the chemical composition of the water, to understand which processes govern the aquifer system.

Groundwater recharge is a vital aspect in maintaining the water balance and is a crucial element in any groundwater flow model. Accurately assessing this element is challenging, however it is essential in the management of aquifers. The water balance technique is widely utilized to estimate groundwater recharge (Thornthwaite and Mather, 1957; Bakundukize et al., 2011). The method uses a tank model that takes into account factors such as runoff, infiltration, flow through the unsaturated zone depending on soil properties and boundary conditions, as well as evapotranspiration. The necessary data includes information regarding the topography, land use, plant coverage, and weather conditions. One alternative approach to assessing groundwater recharge involves analysing the variations in groundwater levels over a certain amount of time (Healy and Cook 2002). The variation of groundwater level through the time are usually recorded in monitoring wells.

Examining the factors that control groundwater geochemistry and figuring out the stage and cause of salinization will help in effectively assessing the appropriate groundwater quality for both drinking and irrigation purposes, as well as suggesting appropriate management strategies (Appelo and Postma 2005). To evaluate contamination caused by SWI and freshening processes, the most straightforward approach is to utilize indicators derived from the chemical components of groundwater (Appelo and Postma, 2005; Barlow 2013). The indicators of cation exchange processes, such as cation exchange codes (Walraevens and Van Camp, 2004; Stuyfzand, 1986) and chloride (Cl) conservative element (Appelo and Postma, 2005), are of particular interest as they can provide information about whether freshening or salinization processes are dominant and even the current stage of the process (Andersen et al., 2005). In addition, the hydrochemical facies can be used to assess the progression of saltwater intrusion over time and space (Giménez, 2019). However, there may be a time lag between changes in the factors causing saline intrusion and their impact on the hydrochemical signature. The response to salinization is typically faster than the response to freshening (Walraevens and Van Camp, 2004).

Once we have a good conceptual model of the aquifer system, we can use numerical models as tools to investigate the origins of saltwater, thereby enhancing our understanding of the driving forces and significant factors that govern the magnitude of saltwater intrusion. By applying this method, it is possible to identify and effectively control regions that are susceptible to climate change and sea level rise.

Modelling can be considered as an essential step in quantifying many flow and solute transport problems and in general many hydrogeological challenges (e.g., Hill and Tiedeman, 2007). Models not only assist in quantifying water related processes, but also provide valuable understanding of the system under investigation. Additionally, once it has been shown that the models can replicate past behavior (calibration), they can be used to predict how groundwater will behave in the future, help with decision-making, and allow the exploration of different management strategies.

The primary utility of simulation is not its ability to make accurate predictions, but rather its capacity to facilitate the investigation process. One can identify the system's features by implementing tests on the model's properties, which are extremely helpful when attempting quantitative predictions. In fact, most model parameters are uncertain, and some are correlated. Barnett et al. (2012) offer a comprehensive set of modeling guidelines that encompass the entire modeling process, including the establishment of modeling objectives, the creation of conceptual models, the architecture of the groundwater system, the design and construction of the model, the calibration, and the sensitivity analysis process. Barnett et al. (2012) also propose a range of modeling methods, providing a comprehensive outline of the principes involved in analyzing predictive uncertainty. The key in groundwater modeling studies is therefore to recognize the limitations of the model, and avoid the over-interpretation of prediction.

In theory, a groundwater flow model simulates hydraulic heads and groundwater flow rates within and across the boundaries of the system under consideration. A solute transport model is used to simulate the concentrations of substances dissolved in groundwater. In general, groundwater transport in the aquifer follows three main processes: advection, molecular diffusion, and dispersion. This way, groundwater's dissolved components also move in the aquifer. Since fresh groundwater and saltwater have different densities, we must incorporate these differences into our groundwater transport model to account for saltwater pollution.

A model is the ultimate integration of all knowledge, including hydrological data, lithological data, sedimentological data, water quality, and geophysical data available in a certain area, but requires a lot of input. In a steady-state model, the hydraulic conductivity of all hydrogeological layers must be provided. Specific storage and specific yield are additional mandatory inputs for transient flow. Dealing with solute transport, effective porosity and dispersivity are additional input parameters. Furthermore, we need to consider the recharge rate, boundary conditions, and which processes are governing the system. Finally, a calibration strategy must be developed to derive these hydraulic and solute transport parameters, based on field observations of the hydraulic head and saline concentrations.

Vietnam has an elongated roughly S-shape extending from north to south distance over 1,650 km from the latitudes 8° to 24°N, with a coastline 3444 km long, excluding islands (Figure 1.3). According to a recent worldwide remote sensing investigation, Vietnam has 3,069 km^2 of tidal flats, ranking it as the tenth most tidal flat-prone country (Murray et. al. 2019).

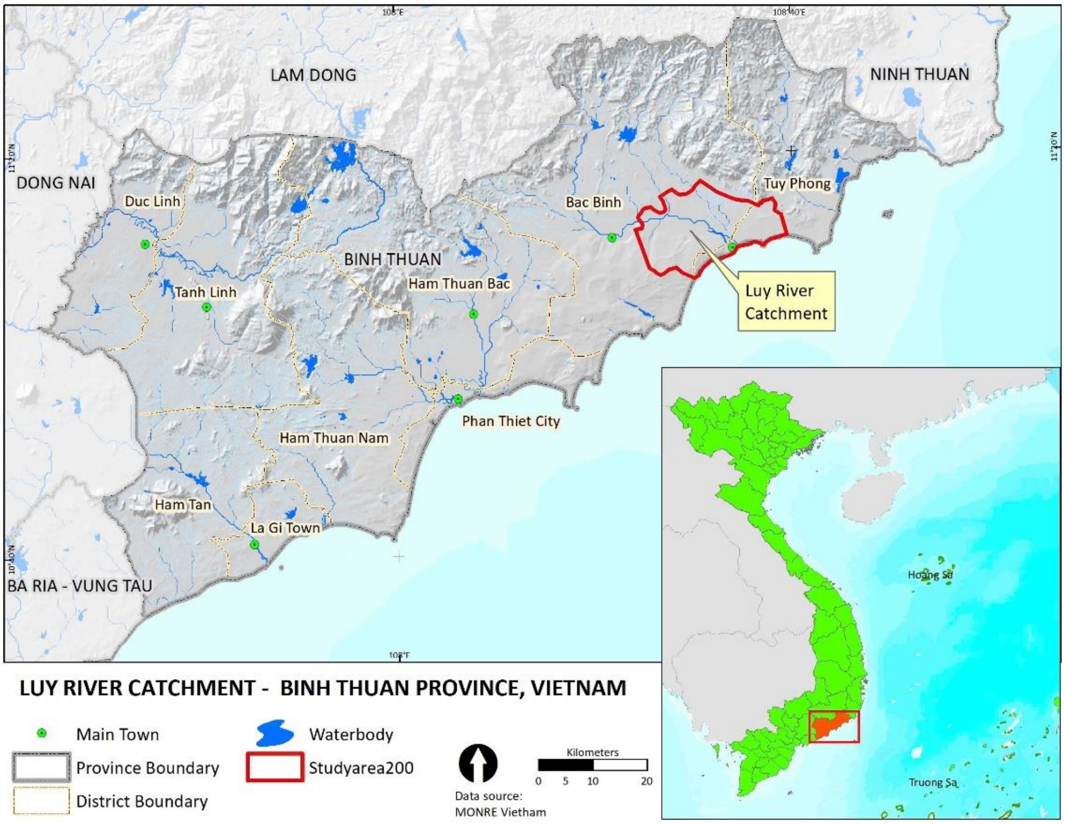

Figure 1.3 Location of the study area

Vietnam's land is mostly hilly and densely forested, with mountains and hills accounting for 75% of the surface area, mostly located on the north and west sides of the country, while tropical forests cover around 42% of the country. Parts of the Red River Delta in the north and the Mekong River Delta in the south occupy the flat land, which makes up about 25% of Vietnam's land. The remainder of the flat land is located in the central part of Vietnam, including the alluvial plains that follow the multitude of river systems crossing the country. These coastal lowlands are the narrow flat parts located on the East with rivers discharging in the Vietnamese Eastern Sea, boarded on the landward side, by the prominent Truong Son Mountain chains.

Due to differences in latitude and the marked variety in topography, Vietnam's climate varies greatly between regions. In general, Vietnam experiences a temperate, dry winter and a hot summer in the north, a tropical monsoon in the central part, and tropical savannah in the south. Some typical parts of Central Vietnam have semi-arid to arid weather. Seasonal variations in the mountains, plateaus, and northernmost areas are much more dramatic, with temperatures varying from 3 °C in December and January to 37 °C in July and August. During the monsoon seasons, Vietnam receives high rates of rainfall, with an average amount of 1,500 to 2,000 mm/year.

In the central part of Vietnam, the topography gradually decreases from the west at the mountainside to the east toward the coastline; this often causes flooding, especially in parts with poor drainage systems. Tropical depressions, tropical storms, and typhoons also pose a threat to the country. Vietnam has 55% of its population living in low-elevation coastal areas; this makes Vietnam one of the most vulnerable countries to Climate Change.

In the last decade, most urban water supply systems were built without effective management. The Vietnam Water Supply and Sewerage Association (VWSA) found that water production capacity exceeded demand in 2008, although service coverage was still low. Most of the clean water supply system is underdeveloped, which prevents proper distribution of clean water.

One third of 727 district and town have piped water, which take only a small proportion of population. Water safety in urban and rural water delivery systems is also a problem. Most industrial enterprises discharge untreated effluent onto waterways in the areas where the government does not take measures to address the issue. The home wastewater is dumped untreated into the environment and pollutes surface water (British Business Group Vietnam, 2017).

Local and foreign Universities and Institutes have worked together to introduce water filtration devices to improve water access in recent years. Local residents are concerned about the substantial public health risks of pollution-contaminated water and high groundwater arsenic levels (University of Technology Sydney, 2018). About 78% of Vietnam's population has improved sanitation - 94% in urban areas and 70% in rural areas. According to a 2015 survey, 21 million Vietnamese still lack access to improved sanitation (University of Technology Sydney (2018). The construction ministry reported in 2018 that the water supply and drainage industry was using advanced technology and IT to address sanitation difficulties but faced funding, climate change, and pollution issues (Vietnam News 2018a). The health ministry also plans to develop statewide water inspection units since June 2019. Since poor or contaminated water supplies and unclean conditions create many health difficulties each year, inspections should be done systematically (Vietnam News 2018b).

Binh Thuan is located in south-central Vietnam, one of the driest parts of the country. In this area, groundwater is the most vital source of water for domestic supply. Groundwater is the source of potable water for about 260000 people (Nawapi 2015), and its use for irrigation has recently increased. Shallow aquifers are the major water supply sources, and many household-owned wells serve as irrigation wells.

Up to now, the southern central coast of Vietnam has received little attention. Investigations by the National Center for Water Resources (NAWAPI) revealed saltwater contamination in both river estuaries and further inland, threatening the availability of freshwater for irrigation and drinking purposes (Nawapi, 2015, 2018). These early investigations delineated the SWI zone based on the total dissolved solids (TDS), and concluded, based on the spatial patterns, that SWI was caused by direct infiltration from surface water in the river estuaries. However, these conclusions were derived from mostly shallow boreholes, without a detailed analysis of the geochemical composition, and could not explain the occurrence of saltwater further inland.

Climate change poses a severe threat to the region, compounding the already complex situation. Sea level rise and droughts might drive salt water further inland, and management strategies such as increased groundwater extraction are additional stress factors for the groundwater resources. The latest IPCC predictions about sea level rise and precipitation can be combined with groundwater models to investigate the future evolution of SWI and predict its impacts on water salinity and local communities. This can serve as a first to formulate water management strategies (such as pumping rate limitation, artificial freshwater recharge, construction of additional freshwater storage ponds, or alternative use of surface and groundwater, among others) to mitigate the adverse effects of climate change, that can be tested using groundwater models to estimate their effectiveness.

The aim of this work is to use numerical models as tools to investigate the origins of saltwater, thereby enhancing our understanding of the driving forces and significant factors that govern the magnitude of saltwater intrusion. By applying the integrated methods, it is possible to identify and effectively control regions that are susceptible to climate change and sea level rise, thereby predicting how groundwater will behave in the future, helping with decision-making, and allowing the exploration of different management strategies.

A hydrogeological system is characterized by complex and interacting aspects such as precipitation, evapotranspiration, land use, soil type, sediment properties, groundwater abstraction, and aquifer geometry (Figure 1.4). Hydrogeological models become uncertain when the presence, properties, and extent of these aspects remain inadequately quantified, which is always the case to a certain level (Hermans et al., 2023).

.

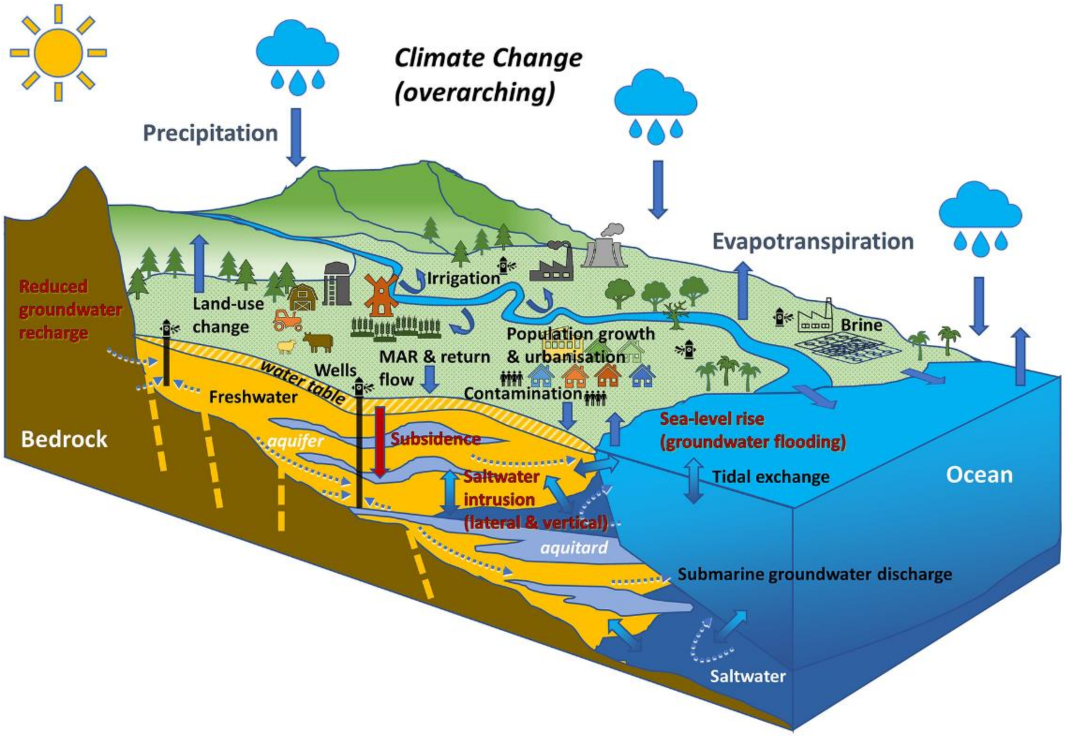

Figure 1.4 Schematic portraying the issues, opportunities and dynamics related to ground water and its management at the coast in light of future climate change, sustainable development and drought threats (from Dodd and Rishworth, 2023). This demonstrates key issues relevant to coastal urban reliance on groundwater.

Therefore, we have based our approach for constructing the groundwater management system of our study area located in the Luy River catchment, Binh Thuan region on our research on the water balance and saltwater distribution. The site is situated on a coastal alluvial plain with complex shallow aquifers in arid and semi-arid weather conditions, and is therefore particularly difficult to characterize.

The thesis is organized as followed. Chapter 2 of the thesis is a site description that reviews the characterization of topography, climate conditions, land use, geology, and hydrogeology in the study area. It presents a comprehensive overview of the study site in the Luy River catchment.

Chapter 3 presents the application of the Soil Moisture Water Balance and Water-Table Fluctuation methods to estimate the recharge for the Luy river plain. This chapter aims to investigate how shallow aquifers react to climatic variables, estimate groundwater recharge, and understand their spatiotemporal distribution, all of which are critical components of long-term water management strategies. The findings will also be used for groundwater modeling in the following phases of the study (Chapter 5 and 6).

Chapter 4 is dedicated to identifying the origin of saltwater intrusion in the Luy River catchment, as this constitutes a necessary step to propose a sustainable management of the groundwater resources in the study area. A thorough hydrochemical analysis of newly acquired water samples is proposed to identify which processes are taking place and what the origin of the high salinity is. A new hydrogeochemical survey in the Luy River catchment is performed, including both shallow and deep wells and samples collected during both the dry and wet seasons. The study corresponds to the first in-depth hydrochemical analysis of the seawater freshening and intrusion processes based on water composition, as well as the first attempt to identify their seasonal variations in the region. In addition, an integrated interpretation of the new datasets with the available geophysical results is proposed to distinguish the effect of recent saltwater intrusion from freshening processes, which are still the dominant processes controlling water quality at the catchment scale. The study culminates in a conceptual model of seawater intrusion that considers both natural and anthropogenic effects, as well as seasonal cycles. This conceptual model serves as a foundation for future groundwater modeling and management.

In Chapter 5, a three-dimensional (3D) stratigraphic model is first constructed based on the existing well logs and geophysical and geochemical data. Then, density-dependent flow and solute transport is simulated over long periods of time to find out: (1) how aquifer properties affect the freshwater and saltwater distributions and to verify numerically the hypothesis behind the hydro-chemical conceptual model built in Chapter 4, i.e., to see if the time scale of the freshening process fits with the hydraulic properties and water balance in the catchment under the current natural conditions (i.e. absence of groundwater exploitation); (2) analyze the current saline groundwater distribution originating from various hypotheses of saltwater sources, and (3) assess the potential of groundwater resource development under freshening process and saltwater intrusion threats. The model's validity is tested by comparing the simulation results to actual heads and salt concentration, which constitutes a proxy for the hydrochemical composition of groundwater.

The groundwater model is further refined and calibrated in Chapter 6 to reproduce current observations and serve as a management tool for groundwater management. This chapter examines the impact of global climate change and rising sea levels on the groundwater system of the coastal plain in the Luy River basin. We model the effects of saltwater intrusion on the groundwater system, considering forecasted sea level rise, annual fluctuations in groundwater recharge, groundwater extraction, the initial salinity distribution, and the hydrogeological characteristics of the aquifers. By examining the fluctuations in the simulated groundwater levels and the structure of the salt-freshwater boundary, we can evaluate the probable effects of climate change on the groundwater reserves in the research area. Subsequently, we will offer suggestions for the sustainable management of groundwater resources in the designated region, while considering the discoveries made in the study.

The thesis ends with a discussion and general conclusions.

Chapter 2. Site description

This chapter has been published in:

Pham D.L., Cong-Thi, D., Segers, T., Huu, H.H., Nguyen, F., Hermans, T., 2022. Groundwater Salinization and Freshening Processes in the Luy River Coastal Aquifer, Vietnam. Water 14 (15), 2358 pp.

2.1 General description

Binh Thuan is the sole region in Vietnam that possesses indigenous deserts characterized by a diverse array of barren landscapes, encompassing salt deserts and degraded land. If this situation has several advantages for the growth of tourism as it has recently attracted many visitors to this area, the province is nevertheless currently experiencing desertification, a phenomenon that significantly affects agricultural production, the ecology, and socio-economic activity. According to local residents, there are times when there is no rain for the entire year. Certain farmers are compelled to allow their crops to desiccate due to the scarcity of irrigation water. The lack of freshwater resources has emerged as the most urgent issue in this area.

2.2 Topography, Land Use and Surface Water

The study area is the alluvial plain of the Luy River located in the two coastal districts of Tuy Phong and Bac Binh, Binh Thuan province (Figure 2.1). The population in 2018 of these districts is 269,249 inhabitants with a density of 102 inhabitants/km² (DONREBT, 2020). The study area belongs to the Luy river basin, which originates from high mountains in the eastern border of the Di Linh Plateau in the Lam Dong province and flows to the Phan Ri River mouth. In 2008 and 2009, the Dai Ninh (Lam Dong province) and Bac Binh (Binh Thuan) hydropower plants were constructed in the upstream part which increases the freshwater supply in the catchment globally. The hydropower reservoirs are recharged by water from the Dong Nai River system and these reservoirs play a significant role in the management of the freshwater supply to the Luy river basin during the dry season, providing irrigation water for the production of rice in the study area. However, the dam overflow resulting from heavy rains during the rainy season combined with water releases from these hydropower stations also sometimes cause floods in the study area (VINWATER, 2020). In addition, riverine SWI occurs in the downstream part through the Luy river estuary during high tides. TDS measurements in the Phan Ri River mouth during the summer 2019 show values of 15 to 20 g/L up to 5 km inland (Figure 2.1). These measurements were recorded during high tide when the TDS value is supposed to be the most affected by SWI from the Luy river estuary.

The study area is bounded in the northwest by a mountainous area with altitude ranging from 1200 to 2000 m above sea level which is covered by 70 to 100% of forest. The elevation declines sharply from 1200 to 300 m and then regularly from 300 to 100 m into the coastal plain. The south of the study area is delineated by the red sand dune, adjacent to the Vietnamese Eastern Sea, with elevation ranging from 100 to 300 m. The southeast of the study area is limited by the white sand dune complex, also adjacent to the Vietnamese Eastern Sea. The alluvial plain is relatively flat, with the elevation sloping gently from west to east.

The main crops cultivated in this plain are dragon fruit plants and rice depending on the water supply and irrigation network in each location. Rice is typically cultivated where irrigation water from dams is available, whereas dragon fruit, which is more drought and salinity resistant, is cultivated in other areas, generally relying on groundwater for irrigation.

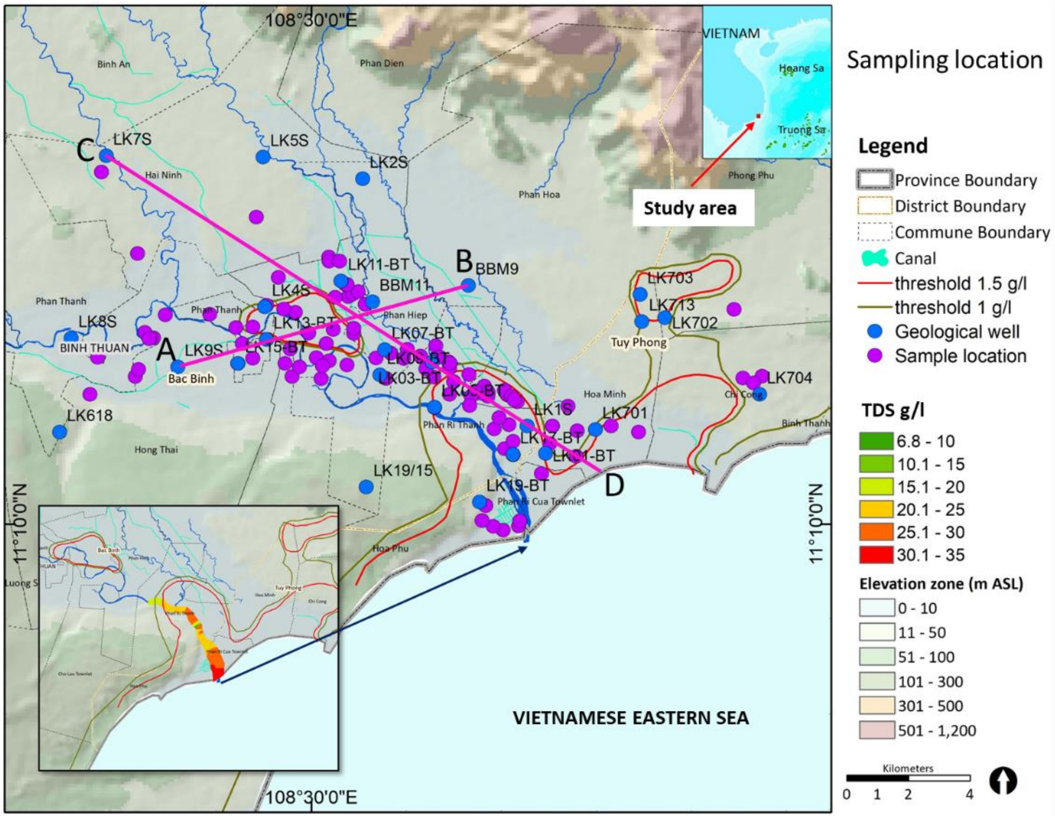

Figure 2.1 The location of the study area with the topography, sample location and TDS measurement in the Phan Ri River mouth in the summer 2019, AB and CD cross section lines following the chapters.

2.3 Climate

The Binh Thuan province has a typical semi-arid climate with the rain season from May to October and the dry season from November to April. The climate is characterized by low rainfall, high evaporation and strong land winds. The 1982–2019 meteorological data collected in the Phan Thiet station located 50 km south of the study area shows that the mean monthly temperature varies from 25.2 ◦C in January to 28.7 ◦C in May (Figure 2.2). The average monthly humidity changes from 75.1% in January to 84% in September. The average monthly evaporation varies from 91.2 mm in October to 140.8 mm in March whereas the average monthly rainfall reaches its highest value of 194 mm in September and minimum value of 0.4 mm in February.

The Tuy Phong and Bac Binh districts have 6 dry months per year with less than 100 mm of monthly rainfall. With a variety of typical deserted lands including sand, stone or salt deserts and degraded land, the province is facing desertification, which has a strong impact on overall agricultural production, the environment and socio-economic activities (Gobin et al., 2012; Gobin et al., 2016; Le et al., 2019).

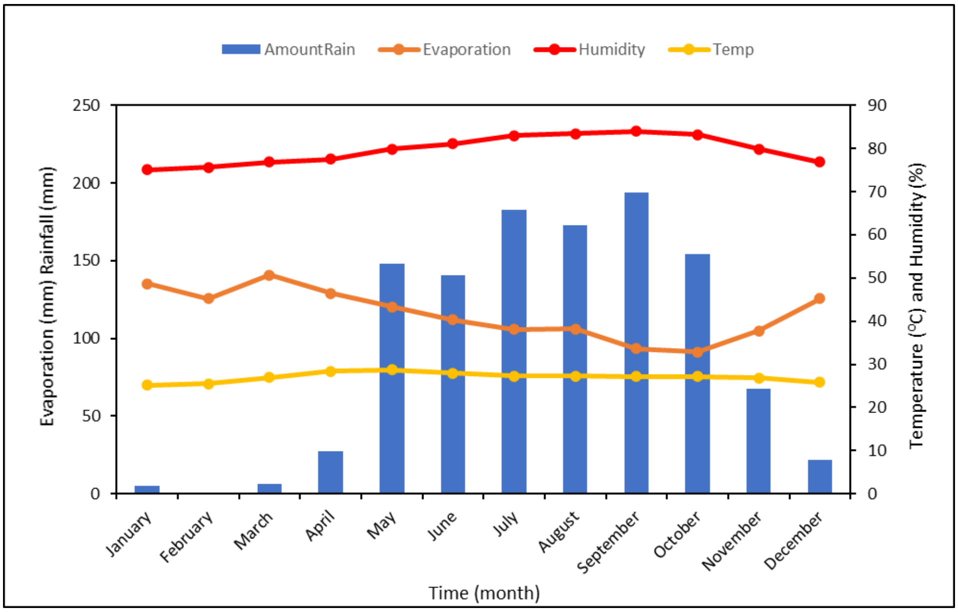

Figure 2.2 The average monthly evaporation (mm), rainfall (mm) and humidity (%) and temperature (°C) in the study area in period of 1979 – 2021

2.4 Geology and Hydrogeology

The area has a complicated geological and evolutionary history. Segers (2024) provides a detailed description of the geological formations present in the subsurface of the research region and surrounding area, including their structural characteristics and the sequence of the processes that formed them. An updated geological map (Appendix 1) was also reconstructed in that work based on available maps (in Vietnamese). Previous investigations in the area mostly focused on regional geology on a larger scale, and discrepancies and inaccuracies were identified in the existing literature and database.

At its base, the region primarily consists of fractured rocks composed of fine-grained sediments from the Mid-Jurassic and igneous plutons and their volcanic counterparts from the Late Mesozoic. These ancient strata have experienced numerous tectonic phases, leading to the development of a complex system of faults that became the basement. Marine and reworked aeolian sand deposits from the Late Cenozoic overlie them near the coast. For the purposes of this work, we concentrate more on the sediments formed in the Quaternary.

Currently, most of the coastal region is covered with recently formed sand layers, primarily from the Mid-Late Pleistocene to Holocene periods. The shoreline is mainly composed of extensive sandy barriers that rise up to 160 meters above the current sea level. These barriers are located in front of a wide alluvial coastal plain. During the Quaternary period, climatic change had a significant impact on the formation of coastal depositional environments. Glacial-interglacial alternations result in eustatic sea level (SL) fluctuations, causing cycles of marine incursions and regressions that repeatedly modify the erosion-deposition dynamics in the region. The sand is carried from the Truong Son mountains, which are close by, to the continental shelf by rivers when sea level is low. Waves reshape the sand once it reaches the continental shelf, depositing it again during interstadial and interglacial transgressions. Aeolian reworkings occur during periods of decreased vegetation and landscape instability. Murray-Wallace et al., 2002; Schimanski & Stattegger, 2005; Nghi et al., 2007; Quang-Minh et al., 2009).

The division of transgression periods in Vietnam is subject to numerous debates and updates. In this study, we follow the literature of Nghi et al. (2007). According to that, throughout the Quaternary, there were five cycles of SL (Appendix 2) change that brought about five sediment cycles: (1) Early Pleistocene (Q_1^1); (2) Middle-Late Pleistocene ($Q_1^{2\text{-}3a}$); (3) Late Pleistocene (Q_1^{3b}); (4) latest Pleistocene – Middle Holocene ($Q_1^{3c} – Q_2^2$); and (5) Late Holocene (Q_2^3).

1- The first sedimentary cycle (Q_1^1) corresponds to the alluvial sediments from the Tuy Phong Formation, specifically from the Early-Mid Pleistocene period, referred to as $aQ_1^{1\text{-}}$

^{2}*tp*. The presence of gravel and sand in the formation is indicative of the regression and subsequent transgression during deglaciation. The existence of certain laterally displaced pebbles and gravel indicates that the sediment has experienced the termination of the cycle, characterized by a period of weathering.

2- The second sedimentary cycle (Mid-to-Late Pleistocene, $Q_1^{2\text{-}3a}$) is characterized by the presence of old sandy bars and tombolo lagoonal facies in the previous coastal plain (Nghi et al., 2007). A sedimentary deposit consisting of alluvial-proluvial facies, dating back to the Late Early Pleistocene ($apQ_1^{2.2}$) is a strong indication of the initiation of a new cycle. Gravel and pebble deposits deposited by river floods can be observed in the vicinity of the Luy River, downstream from adjacent mountainous areas.

The Phan Thiet Formation ($mQ_1^{2\text{-}3}pt$), in the Mid-Late Pleistocene characterized by red sands, is widely distributed in the coastal area, especially on the right bank of the Luy River. The sandy coastal barriers can be classified into two parts: an outer barrier consisting of white Holocene sands and an interior barrier composed mainly of reddish sands with cores of older white-grey sand.

3- The third sedimentary cycle in Late Pleistocene, Q_1^{3b}, is considered by the presence of the upper Phan Thiet Formation ($m^bQ_1^{2\text{-}3}pt$) which consists of yellow-reddish sands that make up the massive inner barrier succession. During the Late Pleistocene, there was a period of rising sea levels that caused the deposition of a significant amount of white quartz sands. Over time, these sands underwent weathering, resulting in their color changing to yellow and reddish tones due to infiltration (Nghi et al., 2007).

The white marine sands ($mQ_1^{3.2}$) partially contributed to the formation of a smaller white dune system located on the banks of the Luy River. The sand dunes rise to an elevation of 40 meters above sea level, overlaying the previous Phan Thiet deposits. The smaller dune system is also partially covered by aeolian reworkings of older reddish sands (vQ_1^{3}). The alluvial-marine sands ($amQ_1^{3.2}$) are extensively visible in the area located behind the dune sands at higher elevations.

4- The fourth sedimentary cycle, which occurred from the last Pleistocene to the Early-Mid Holocene (Q_1^{3c}-Q_2^{1-2}), began with the continuation of the previously described accelerated aeolian reworking during the Last Glacial Maximum (LGM). The decrease in sea level during this time period resulted in increased erosion between the coastal barrier sands and the marine sand sheet further inland. This erosion created the necessary space for the deposition of Holocene fluvial valley-fill and lagoonal sediments.

The fourth cycle is defined by a Flandrian transgression sedimentary facies consisting of sandy silts and clays that are attributed to deltaic facies (amQ_2^{1-2}). This facies covers a large portion of the alluvial-coastal plain. Additionally, there are silty clays that contain a significant amount of organic material and peat, which are characteristic of marshy facies (Nghi et al., 2007). Although there are no wetland sediments found in the research region, the study has noted the existence of plant humus in Mid-Holocene alluvial-marine deposits. The alluvial-marine sediments gradually change into alluvial sediments (aQ_2^{1-2}) toward further upstream. Marine sediments (mQ_2^2) are found in short, narrow, and elongated deposits along the shoreline. In contrast, aeolian deposits, specifically (vQ_2^2), are more extensive and cover parts of a huge dune system with yellow-brownish, small-grained quartz sands. Aeolian activity has occurred in multiple phases throughout the Quaternary period. These phases have led to periods of recurrent sand accumulation, resulting in the vertical expansion and elongated shape of the dune system (Quang-Minh et al., 2009).

The increased rates of sedimentation resulted in the development of thick sand deposits during the Holocene period on the continental shelf (Schimanski & Stattegger, 2005). These deposits were later reshaped and relocated by the combined forces of tides and waves, ultimately giving rise to new sand barriers (Quang-Minh et al., 2009). The outer white barrier sands of the huge coastal dune system were generated following the post-glacial marine transgression between approximately 8,000 and 6,000 years ago. Additional sand deposits have been added more recently through aeolian reworking throughout the Late Holocene period (Murray-Wallace et al., 2002; Quang-Minh et al., 2009).

5- In the Late Holocene, these white sand barriers underwent reworking to give rise to the formation of recent dune sands (vQ_2^{2-3}). The fifth sedimentary cycle included recent reworkings (vQ_2^3) that occurred approximately 3,000 years ago to the present. These reworkings may be associated with a Late Holocene regression phase, during which sea level decreased to its current level. This information is supported by studies conducted by Nghi et al. (2007) and Quang-Minh et al. (2009). Marine sediments (mQ_2^{2-3} and mQ_2^3), alluvial-marine sediments (amQ_2^{2-3}), alluvial sediments (aQ_2^{2-3} and aQ_2^3), and black marine-bog sediments (mbQ_2^3) are present in various locations within the alluvial plain. These sediments are typically found along the coast and along rivers, occurring as tiny deposits. The area is experiencing ongoing dune development, and there has been a recent phase of sand buildup around 0.2 thousand years ago, which is likely due to mining activity (Quang-Minh et al., 2009).

In the study area, we only observe a portion of the full five sediment cycles, which correspond to the five cycles of sea level change. The Luy river plain is mostly covered by fluvial–marine sediments originating from the Pleistocene and Holocene (Figure 2.3). The fluvial–marine sediments from the middle to late Pleistocene are distributed in the higher parts of the plain characterized by sequences of round gravel, sand and grits or sand intercalating with silt and clay forming terraces of the Luy river tributaries. The middle–late Holocene sediments are found in the lower part of the plain which is mainly made up of clay, clayey silt mixed sand, brown yellowish or greyish silty sand containing various amounts of foraminifera, shell fragments, lithoclasts and plant fragments (Hoang, 1997).

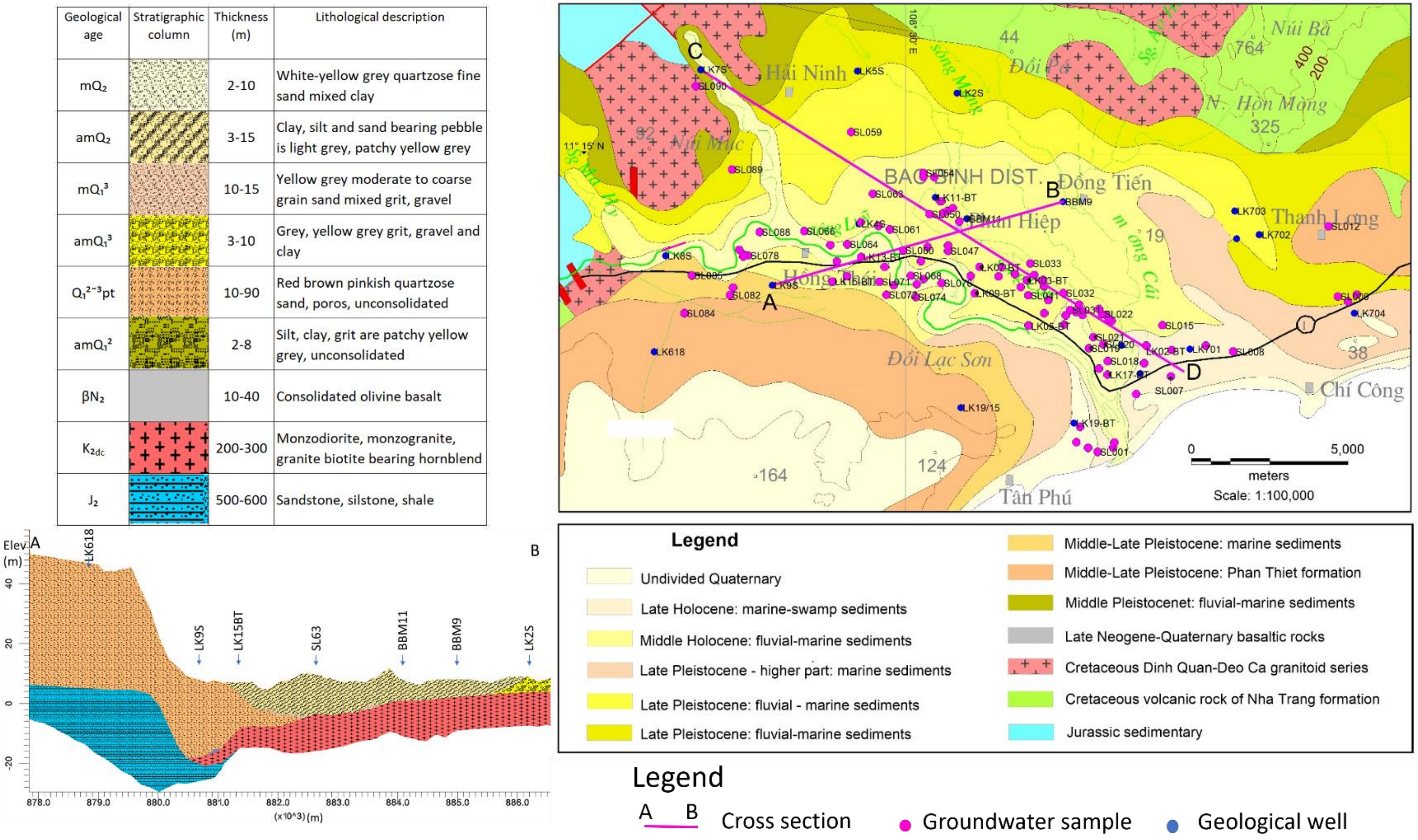

Geological age	Stratigraphic column	Thickness (m)	Lithological description
mQ_2		2-10	White-yellow grey quartzose fine sand mixed clay
amQ_2		3-15	Clay, silt and sand bearing pebble is light grey, patchy yellow grey
mQ_1^3		10-15	Yellow grey moderate to coarse grain sand mixed grit, gravel
amQ_1^3		3-10	Grey, yellow grey grit, gravel and clay
$Q_1^{2-3}pt$		10-90	Red brown pinkish quartzose sand, poros, unconsolidated
amQ_1^2		2-8	Silt, clay, grit are patchy yellow grey, unconsolidated
βN_2		10-40	Consolidated olivine basalt
K_{2dc}		200-300	Monzodiorite, monzogranite, granite biotite bearing hornblend
J_2		500-600	Sandstone, silstone, shale

Elev (m)
A
B
LK618
LK9S
LK15BT
SL63
BBM11
BBM9
LK2S
40
20
0
-20
878.0
879.0
880.0
881.0
882.0
883.0
884.0
885.0
886.0
(x10^3) (m)
C
D
Hải Ninh
BAC BINH DIST.
Đông Tiến
Thanh Lương
Chí Công
Tân Phú
Đồi Lạc Sơn
Núi Mực
Núi Bà
N. Hòn Mòng
Đồi Pá
11° 15' N
108° 30' E
0
5,000
meters
Scale: 1:100,000
Legend
Undivided Quaternary
Late Holocene: marine-swamp sediments
Middle Holocene: fluvial-marine sediments
Late Pleistocene - higher part: marine sediments
Late Pleistocene: fluvial - marine sediments
Late Pleistocene: fluvial-marine sediments
Middle-Late Pleistocene: marine sediments
Middle-Late Pleistocene: Phan Thiet formation
Middle Pleistocenet: fluvial-marine sediments
Late Neogene-Quaternary basaltic rocks
Cretaceous Dinh Quan-Deo Ca granitoid series
Cretaceous volcanic rock of Nha Trang formation
Jurassic sedimentary
Legend
A B Cross section
Groundwater sample
Geological well

Figure 2.3 The geological map, stratigraphic column of the study area and cross section along the line AB, modified from Hoang P. (1997).

The thickness of the Holocene aquifer is thin in the right bank (2 – 4 m) but it increases in the left bank from 2 to 20 m. In contrast, the Pleistocene aquifer is thick on the right bank, due to the high altitude of the sand dune, and is thinner on the left bank.

The Holocene and Pleistocene aquifers can sometimes be distinguished as an un-confined aquifer and a confined aquifer, respectively, when semi-continuous clay layers and lenses are present, but otherwise they just lie on each other sequentially (Figure 2.3). They are underlined by granite and granitoid from the Cretaceous and sandstone, claystone and siltstone from the Jurassic. These layers have a limited water storage capacity and are considered as secondary fractured aquifers in the study area.

Water recharge to the aquifers mainly comes from precipitation during the wet season and surface water including through irrigation practices. Outflows occur at the Luy river estuary, and its tributaries, and underground discharge to the sea, whereas abstractions occur through pumping for irrigation, aquaculture farming and mining activities. The construction of the hydropower reservoirs in the upstream part since 2008 has been increasing the freshwater supply to the aquifer as it also supplies the study area with fresh surface water through irrigation channels. On the contrary, it might have increased riverine SWI by reducing the average flowrate in the Luy river.

Figure 2.4 illustrates the piezometric map in the study area expressed in freshwater head above the reference level (mean sea level at elevation 0). The main hydraulic gradient is along the Luy river with a secondary component perpendicular to it. Note that locally the natural gradient is perturbed due to water abstractions or irrigation practices.

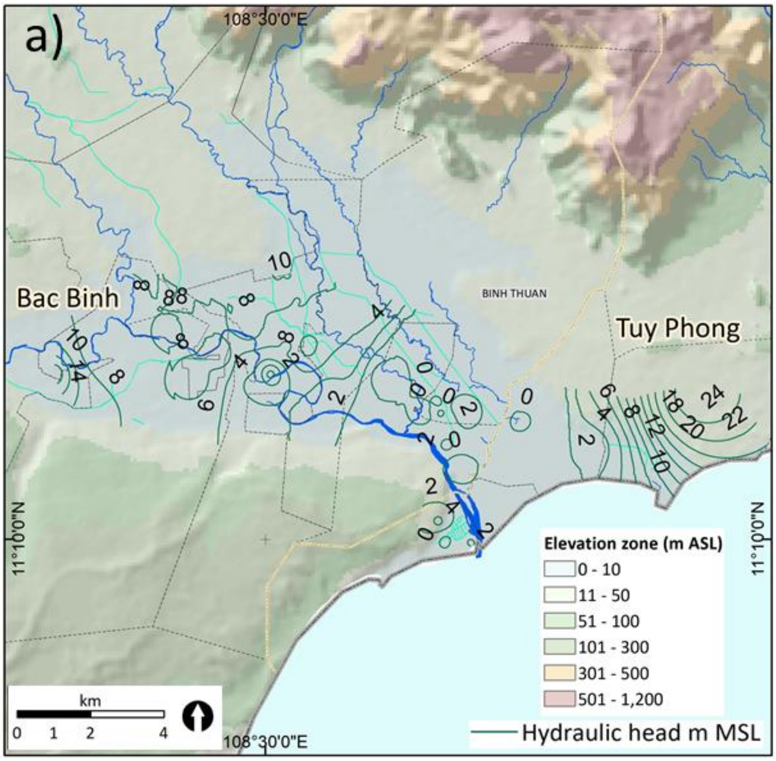

Figure 2.4 (a) The elevation of the water table from the freshwater wells in the study area measured in the summer 2020.

The white and red sand dunes complexes are characterized by higher water levels. In the upstream part, the piezometric table remains above sea level while in the central of the plain and near the coast, the water table is close to sea level or sometimes even below. Note that the piezometric map was produced by interpolation ignoring the interaction with surface water bodies (river and seas). It is just meant to illustrate the main direction of flow in the study area.

Chapter 3. Estimating groundwater recharge for Luy River plain in Binh Thuan, Vietnam

Pham Dieu Linh[1,3,*], Cong-Thi Diep[1,3], Hieu Huu Ho[3], Frédéric Nguyen[2], Thomas Hermans[1]

[1] Laboratory of Applied Geology and Hydrogeology, Department of Geology, Ghent University, Krijgslaan 281-S8, 9000 Ghent, Belgium

[2] Liege University and KU Leuven, B- 4000 Liège and 3000 Leuven, Belgium

[3] Vietnam Institute of Geosciences and Mineral Resources (VIGMR), 100000 Hanoi, Vietnam

* Correspondence: Linh.PhamDieu@UGent.be

Abstract: Groundwater recharge is an essential component of the water balance and in any groundwater flow model. It is a critical element in aquifer management, but also one of the most challenging aspects to evaluate effectively. This is particularly applicable in semi-arid environments, where the recharging processes are highly variable. This study estimates the recharge for the Lur River catchment, Vietnam. Two methodologies, specifically the soil moisture balance (SMB) and water-table fluctuation (WTF) techniques, are employed. The water balance employs a tank-type model that considers many parameters, including precipitation, runoff, flow through the unsaturated zone, and evapotranspiration by plants, which are influenced by soil qualities, vegetation type, and boundary conditions. It requires data on geomorphology, land use, vegetation cover, and meteorology. The WTF method depends on temporal variations in groundwater levels to estimate recharge through observation wells. Fluctuations in groundwater levels are noticed throughout time in both deep and shallow wells. Owing to the limited monitoring duration, the WTF methodology is utilized solely to validate the projected recharge quantity derived from the SMB method. The mean recharge derived from the SMB methodology over a 42-year observation period is 312 mm/year in the alluvial plain and 531 mm/year in the dunes, comparable to the values obtained using the WTF method. At the same time, the actual evapotranspiration

(AET) and runoff in the alluvial plain and the dunes are estimated. The AET values for the alluvial plain and the dunes are 708 mm/year and 599 mm/year, respectively, while the runoff values are 118 mm/year and 0.8 mm/year, respectively.

Keywords: Recharge, Soil Moisture Balance, Water Table Fluctuation, Coastal area

3.1 Introduction

Groundwater recharge is a key component for water balance and in any groundwater flow model. It is one of the crucial factors in aquifer management, which is also one of the hardest factors to accurately assess. This is especially true in semi-arid regions, where the recharging processes are very unpredictable. Direct measurement of groundwater recharge is challenging (Lerner et al. 1990), it is thus typically estimated through indirect methods. Recharge estimation methods can be categorized as direct, water balance, flux, and tracer methods (Kinzelbach et al., 2002). These techniques generate estimates at multiple temporal and spatial scales, covering a wide range of complexity and cost. Information on different methods is contained in references such as Simmers (1997), Lerner et al. (1990), and Scanlon et al. (2002). Each method has advantages and disadvantages, and one should exclude the ones that are not suitable in a certain area or for which the data available are poor. In general, it is advised to use several different approaches and compare the outcomes (Healy and Cook 2002). For example, in the context of salinized aquifer, the chloride mass balance method is not appropriate because of the multiple origins of the conservative chloride anion (Eriksson and Khunakasem 1969, Gee et al., 2004).

This study aims to estimate the recharge for the Luy river plain using the Soil Moisture Balance (SMB) (Thornthwaite and Mather (1957), Bakundukize et al. (2011) and Water-Table Fluctuation (WTF) methods (Healy and Cook, 2002; Healy, 2010). The water balance method is based on a tank model, which considers runoff, infiltration and flow through the unsaturated zone according to soil properties and boundary conditions, and evapotranspiration. It requires information on the morphology, land use, vegetation cover and meteorological data. The meteorological data from 1979 to 2021 was collected for the study area. The calculations will be based on daily records for rainfall and evaporation, land use maps for different years (1990, 2000, 2010, and 2019), and a soil map.

Another method for estimating groundwater recharge is based on the fluctuations in groundwater levels over time to estimate recharge. This approach is termed the WTF method and is applicable only to unconfined aquifers (Healy and Cook 2002). An estimate of specific yield is required to deduce the recharge from monitored water levels in one or more wells or piezometers. The data from observation wells in the study area were collected from 2020 to 2021. The variation of groundwater level through the time were monitored in seven monitoring wells using CTD-divers, in both deep and shallow wells. Given the limited monitoring period, the WTF method is only used to validate the order of magnitude of the recharge obtained by the SMB method.

This study's goals are to investigate how shallow aquifer reacts to climatic variables, estimate groundwater recharge, and understand its spatiotemporal distribution, all of which are critical components of long-term water management strategies. The findings will also be used for groundwater modelling in the following phase of the study (Chapter 5).

3.2 Study area description

According to Binh Thuan Department of Natural Resources and Environment (BDNRE, 2020), in 2018, the total area of Binh Thuan was 794,393 ha, with 46%, or 361,426 ha, being agricultural and 43%, or 344,393 ha, being forest.

The soil map from Gobin et al., (2012) showing the study area is mainly covered by sandy soils (Arenosols) along the coast as part of huge coastal dune complexes located on the two side banks of the Luy river (Figure 3.1). The cultivation of drought tolerant crops such as cassava, cashew and mango are found on Ferralic and Arenosols. Along the Luy river alluvial plain are found Fluvisols and locally Gleysols. These alluvial soils have a variable texture depending on local conditions of sedimentation: they can be very clayey or very sandy depending on their position in the landscape and vicinity to the main river. The alluvial soils where the climate is dry, are often used for the cultivation of the dragon fruit. Where there is more water supply in the alluvial soils, wetland rice cultivation is dominating. In the mountain areas, these are highly weathered, red, clayey soils mostly coved under tropical humid rainforest. Leptosols, mostly formed on granite outcrops, cover a small area of the study area. Between the coastal dunes and the mountains an undulating floodplain is found with clay enriched subsoils (Figure 3.1), comprising Haplic Acrisols, Luvisols and Lixisols. A minor percentage of soils is saline and occur mainly at the transition between sand dune areas and plains where evapotranspiration rates outweigh rainfall thereby encouraging salt accumulation. Irrigated agriculture takes place mainly on Acrisols, followed by Ferralsols, Luvisols and Fluvisols. Rice is the main crop grown as a staple meal, and irrigation is prioritized for this crop. The cultivation of dragon fruit as a commercial crop for both domestic and international markets is gaining popularity.

Following the classification of Gobin et al., (2012), in terms of texture, the study area can be divided into two main types of soil:

- Silty clay loam soil with three different horizons: sandy loam (0-20 cm), organic sandy loam (20-100 cm) and sandy clay (100 -200 cm). This soil profile may be typical for Ferralsols, Fluvisols, and Acrisols. They are distributed mostly in the plains and the weathering zone in mountains.
- Sandy soil with two different horizons: sandy (0-20 cm) and loamy sand (20-200 cm). This soil profile typical for Arenosols, and is usually found along the coast of the study area.

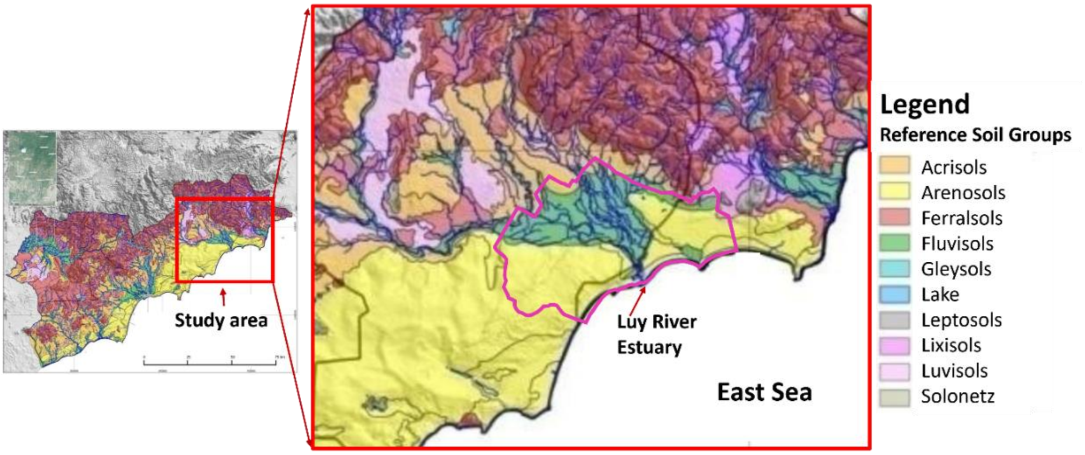

Figure 3.1 The soil map of the study area (extracted from Gobin 2012). The purple polygon is the model area of chapter 5.

3.3 Materials and methods

Groundwater recharge is a complex function of several factors and mechanisms, including climate patterns, soil types, land use, physiographic characteristics, depth to the water table, antecedent soil moisture, properties of the geological materials, interaction between surface and groundwater, available groundwater storage among others, which may not be known or estimated accurately (Sophocleous, 2004). As a result, estimations of groundwater recharge always contain significant errors and uncertainties (Dages et al., 2009; Sophocleous, 2004; Fitzsimons & Misstear, 2006).

In this study, two different groundwater recharge estimation techniques are applied. The recharge calculations using Thornthwaite and Mather soil moisture balance approach using the meteorological data for the period from 1979 to 2021 based on hydrological years (starting from September and ending in August the next year), soil types and land use maps (Figure 3.2) in the study area. Additionally, the groundwater table response of the study area aquifer has been characterized using time series to apply the water table fluctuation method. Given the limited time series available, the latter is mostly used to validate the SMB estimates.

3.3.1 Soil moisture water balance method

The soil moisture water balance method was developed by Thornthwaite and Mather (1957) and is calculated based on the following components: Potential maximum retention after runoff begins (S), Water capacity of the root-zone (CAP), curve number coefficient to estimate runoff (CN), Precipitation (P), Runoff (RO), Potential Evapotranspiration (PET), and Accumulated Water Loss (APWL). The different terms of the soil moisture budget are computed in an excel sheets for all hydrological components instead of a separate excel sheet per component as applied by Bakundukize et al. (2011). The basic principles and the mathematical formulation of the model which was proposed earlier by Thornthwaite and Mater (1957), are thoroughly discussed by Bakundukize et al. (2011). We use daily time steps rather than monthly time steps summing rainfall and evapotranspiration, in order to more accurately represents actual precipitation event, PET, and surface runoff.

The monthly and daily climate data were first sorted into hydrologic years in Binh Thuan which start from September, and ends at the end of August. This choice was based on the average monthly precipitation data (Figure 2.2) showing the maximum rain value. This allows to fix soil moisture storage at the beginning of the hydrologic year assuming it is at its maximum value (Ritter, 2006). Furthermore, the concept of hydrologic year reflects the natural climatic reality in the sense that it commences with the end of the season of maximum groundwater recharge (ensuring maximum initial moisture). It then takes into account the utilization of soil moisture during the dry season, and terminates just before soil moisture reaches its peak again (Ritter, 2006).

PET: Potential Evapotranspiration

Potential evapotranspiration is the amount of water that would be evaporated under an optimal set of conditions, among which is an unlimited supply of water. If the demand for water largely exceeds that which is actually available, soil moisture is depleted and plants eventually die (Ritter, 2006). In this study, potential evapotranspiration is estimated using the Penman-Monteith formula which was modified by Allen et al. (1998), the potential evapotranspiration can be mathematically expressed as follows:

$$\mathrm{PET} = \frac{0.408\Delta(R_n - G) + \gamma\frac{900}{T+273}u_2(e_s - e_a)}{\Delta + \gamma(1+0.3u_2)} \text{ (Equation 3.1)}$$

where PET = reference potential evapotranspiration (mm day^{-1}), R_n = net radiation at the crop surface ($MJm^{-2}day^{-1}$), G = solar heat density ($MJm^{-2}day^{-1}$), γ = psychrometric constant (kPa $°C^{-1}$), T= mean air temperature (°C), u_2 = wind speed at 2 m height (m s^{-1}), e_s = saturation vapor pressure (kPa), e_a = actual vapor pressure (kPa), $e_s - e_a$ = saturation vapor pressure deficit (kPa), Δ = slope of the saturation vapor pressure curve (kPa $°C^{-1}$).

The data consists of daily records of air temperature (maximum and minimum), daily air humidity (average relative and minimum), daily sunshine duration, total of daily rainfall and daily wind speed maximum. The FAO modified Penman-Monteith evapotranspiration (ET0) was calculated using the PET calculator software.

The standard Penman-Monteith method for estimating PET was applied in this research. Computation of the standard Penman-Monteith equation on a daily basis was performed using the PET calculator software from FAO based on the meteorological data collected from 1979 to 2021 in the Phan Thiet stations approximately 50km south to the study area.

Curve number (CN)

The curve number is one of the factors affecting surface runoff calculation. According to the United States Department of Agriculture (USDA) (1985) the key elements that determine CN are the hydrologic soil group (HSG), cover type, treatment, hydrologic condition, and antecedent runoff condition (ARC). In this study, the CN value is taken from USDA 1985 which estimates the CN based on the average antecedent runoff condition for urban, cultivated agricultural, other agricultural, arid and semiarid range land uses. CN is calculated based on the rate of distribution of crop types grown on the different soil types.

Surface runoff

The daily runoff in the study area can be estimated based on the curve number method. In this study the calculation for the runoff will take place for the entire period (1979–2021).

The produced curve number will be for normal antecedent soil moisture conditions (AMC), where an adjustment for dry and wet AMC conditions will be made based on specific equations described in the following parts.

The SCS Runoff Curve Number (CN) method is described in detail in NEH-4 (SCS 1985). The SCS runoff equation is:

$$\mathrm{RO} = \frac{(\mathrm{P} - 0.2\mathrm{S})^2}{(\mathrm{P} + 0.8\mathrm{S})} \ (\text{if } \mathrm{P} > 0.2\mathrm{S}, \text{otherwise } \mathrm{RO} = 0) \text{(Equation 3.2)}$$

where RO = runoff (mm) P = rainfall (mm) S = potential maximum retention after runoff begins (mm)

Potential maximum retention after runoff begins (S) includes water retained in surface depressions, water intercepted by vegetation, evaporation, and infiltration. It is related to the soil and cover conditions of the watershed through the CN:

$$\mathrm{S} = \frac{254000}{\mathrm{CN}} - 254 \text{ (Equation 3.3)}$$

Water capacity of the root-zone (CAP)

The water capacity of the root-zone, or soil capacity, is the maximum water content of the soil available for plants without gravitational water. It is calculated by multiplying the root depth (mm) by the water holding capacity (in volume %). The latter is calculated by the difference between the field capacity and the wilting point. Soil capacity is characteristics for the soil texture and land use practice of an area, and estimated using the water capacity estimating table of Thornthwaite and Mather (1957).

Accumulated potential water loss (APWL)

During the dry season (Peff < PET), there is a deficit of water for plants represented by the APWL. The latter simply cumulatively increases by the difference between PET and P_{eff}. The soil moisture (SM) is calculated using Equation 3.4 while the actual evapotranspiration is AET = P_{eff} + ΔSM, and no groundwater recharge occurs.

$$\mathrm{SM} = \mathrm{CAP} \times \exp^{\frac{\mathrm{APWL}}{\mathrm{CAP}}} \text{(Equation 3.4)}$$

where Potential Evapotranspiration (PET) in mm; Effective rainfall (P_{eff}) in mm, Accumulated Potential Water Loss (APWL) in mm, Actual Evapotranspiration (AET) in mm.

During the wet season, when the potential evapotranspiration (PET) is less than the precipitation (Peff), the soil moisture (SM) increases by the difference between Peff and PET, until it reaches the field capacity of the soil. This allows the soil moisture to be determined. The APWL decreases and can be calculated according to equation 3.5.

$$\mathrm{APWL} = -\mathrm{CAP} \, \mathrm{x} \ln\left(\frac{\mathrm{SM}}{\mathrm{CAP}}\right) \text{ (Equation 3.5)}$$

When the value of (P-RO-PET) is positive (surplus), then the recharge

$$R_N = (P - RO - PET) - (CAP - SM) \text{ (Equation 3.6)}$$

where R_N is natural groundwater recharge

In the dry season, the value of (P-RO-PET) is negative (deficit), and there is no recharge into groundwater. The SMB method equations are summarized in Table 3.1.

Identifying the initial point for the computation of soil moisture utilization is the most challenging aspect. The cycle is repeated successively until the soil moisture storage at the end of a wet or dry season is identical to the value for the same season in a previous cycle.

Table 3.1 Annual soil – water budget calculations (Thornthwaite and Mather, 1957)

	Wet Season			**Dry Season**
	SUR = (P – RO) – PET > 0			**SUR = (P – RO) – PET < 0**
		SM < CAP		
	SM = CAP	(P – RO) – PET ≤ CAP – SM	(P – RO) – PET > CAP – SM	
SM	CAP	SM + (P-RO) – PET	CAP	CAP x $e^{-\mathrm{APWL/CAP}}$
R_N	(P – RO) – PET	0	(P – RO) – PET – (CAP – SM)	0
AET	PET	PET	PET	(P – RO) + ΔSM
DEF	0	0	0	PET – AET

P = precipitation (mm); RO = runoff (mm); PET = potential evapotranspiration (mm); APWL= accumulated potential water loss (mm) (PET – (P – RO)) accumulated for subsequent dry days; AET = actual evapotranspiration (mm); SM = water stored in soil; CAP = soil capacity (mm): maximum water content of soil, without gravitational water (= average rooting depth (mm) × water content at field capacity (in volume %); ΔSM = change in SM; DEF = deficit (PET – AET) (mm); SUR = surplus ((P – RO) – AET) (mm); R_N = natural groundwater recharge (SUR − ΔSM) (mm).

3.3.2 Water table fluctuation method

The method referred to as the WTF technique is specifically suitable for unconfined aquifers. Aside from the monitoring of water levels in one or several wells or piezometers, an estimate of specific yield is required.

The WTF technique operates under the assumption that increases in groundwater levels in unconfined aquifers are a result of recharge water reaching the water table (Healy and Cook, 2002). It therefore ignores other processes such as the influence of nearby discharge zones (springs, streams), the presence of drains, or the surplus of infiltration from upstream run-off and lateral flow. The calculation for recharge is as follows:

$$\mathrm{R} = \mathrm{S_y} \times \frac{\Delta \mathrm{H}}{\Delta \mathrm{t}} \text{ (Equation 3.7)}$$

where, R – recharge during the period of time Δt, S_y – specific yield, ΔH – water level rise.

A thorough study is performed on the mechanisms responsible for variations in water levels in unconfined aquifers. The concept of specific yield is examined closely, and methods for measuring it in both theoretical and field settings are evaluated. In order to estimate the overall recharge value using the WTF technique, it is necessary to apply Equation 3.7 to each individual water level rise. For the purpose of calculating the total recharge, we assign the value Δh to represent the difference between the highest point of the rise and the lowest point of the predicted antecedent recession curve at the time of the peak. The annual recharge is estimated by cumulating the individual rainfall events following equation 3.8:

$$Recharge_{annual} = S_y \times \sum \Delta H \text{ (Equation 3.8)}$$

where S_y – specific yield, ΔH – water level rise in a hydrological year.

The antecedent recession curve represents the path that the well hydrograph would have taken if there had been no precipitation causing a rise in water levels.

3.4 Results and discussion

3.4.1 Groundwater recharge calculated using SMB

One of the factors influencing runoff potential estimates is the hydrologic soil group. Soil in the area can be assigned to two groups: A (sandy soil) and D (silty clay soil) according to the definition from the United States (USDA, 1986). This impacts the rate of water infiltration when the soils are not protected by vegetation, are thoroughly wet, and receive precipitation from long-duration storms. Based on the land use maps presented for the different time periods (Figure 3.2) the study area is mainly covered by agriculture crops as observed in the field and described in Gobin et al. (2012). The vegetation in the area varies from moderately deep-rooted crops (dragon fruit, rice, and shrubs) to orchards (cassava, cashew, and mango) or closed nature forests (as shown in the land use maps). In general, those crops can be considered as the cover type of the brush-brush weed-grass mixture, with brush being the major element in the fair hydrologic condition based on the cover description in the USDA (1986). The runoff curve numbers for the hydrologic soil groups of silty clay and sand in the study area, estimated in USDA (1986) corresponding with the cover types, are 35 and 77, respectively. This determination of curve number depends on the watershed's soil and cover conditions, which the model represents as hydrologic soil group, cover type, treatment, and hydrologic condition.

The root zone varies from 0.25 to 1.5 m, according to Thornthwaite and Mather (1957) as well as observation in the field. In the study area, the root zone can be specified into two types based on the rate of crop distribution on the soil types. Rooting depth equals 0.75 m in sandy soil and 0.8 m in silty clay soil.

Thornthwaite and Mather (1957) suggested the values of water capacity for combinations of soil textures and vegetation types for moderately rooted crops, which are presented in Table 3.2. This data was supported by the Vietnam - Belgium bilateral project: "Monitoring climate Impact and disaster Resilience of Vietnamese Agro-ecosystems" (MNERVA). Vietnamese code (MOST): NDT.96.BE/20; and Belgium code (BELSPO): BL/67/VT44.

The soil capacity estimated for the sandy soil and silty clay soil corresponding to the vegetation is 75 mm and 200 mm respectively.

The initial soil moisture for actual recharge calculation is estimated based on the starting time of the hydrological year is in September. Whereas the rainy season reaches its peak, the soil is assumed to be at field capacity, and soil moisture is at its maximum, which equals the soil capacity.

Table 3.2 Suggested values of water capacity for combinations of soil textures and vegetation types in the study area based on Thornthwaite & Mather (1957)

HSG	Soil texture	Area (%)	Water holding capacity (% volume) = water content at field capacity	Cover type	Rooting depth (m)	Water capacity of the root-zone (CAP) (mm)	Curve number
A	sandy	50	10	Moderately rooted crops (corn, cereals, cotton, tobacco)	0.75	75	35
D	silty clay	50	25	Moderately rooted crops (corn, cereals, cotton, tobacco)	0.8	200	77

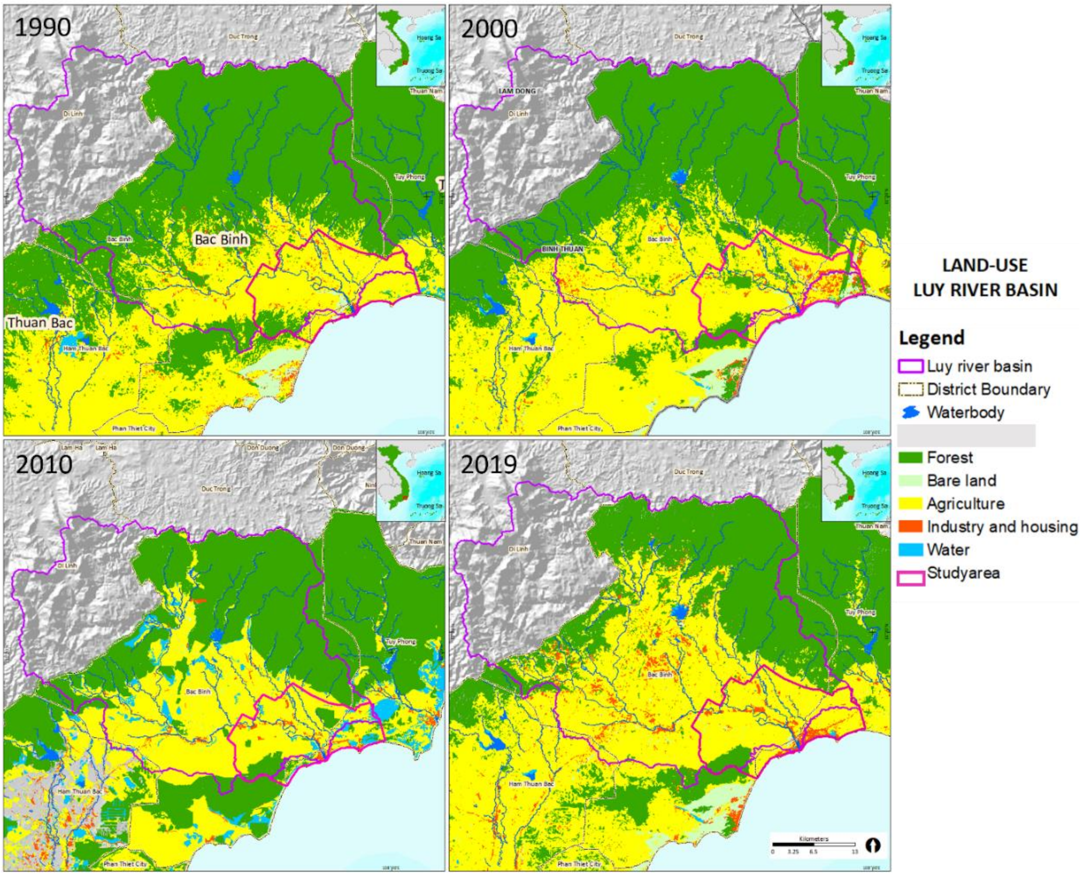

Figure 3.2 Land use maps of the Luy River catchment changed during the time period from 1990 to 2019

The input data was calculated based on the distribution of soil types and crops grown on them. The potential evapotranspiration, surface runoff, plant available water, accumulated potential water loss, soil moisture, actual evapotranspiration and recharge were calculated following equations 3.1-3.6 model (section 3.3.1) using daily time steps. The daily recharge to the aquifer is then aggregated per year and processed in Table 3.1 for 42 years. Table 3.3 and 3.4 show the outcomes of yearly precipitation, runoff, potential evapotranspiration, actual evapotranspiration and recharge results for sandy and silty clay soil types, respectively. The annual values are summed from calculated daily values.

Table 3.3 The results of annual precipitation, runoff, potential evapotranspiration, actual evapotranspiration and recharge for loamy sand soil type

Year 1979	**PREC mm/yr**	**RO mm/yr**	**PET mm/yr**	**RECH mm/yr**	**AET mm/yr**	**RECH mm/day**
1980	1176	0.0	1306	604	572	1.65
1981	1211	5.3	1213	750	476	2.06
1982	1269	3.4	1095	620	667	1.70
1983	815	0.0	1274	394	443	1.08
1984	1099	0.0	1234	598	507	1.64
1985	956	0.0	1338	415	562	1.14
1986	1043	0.0	1276	478	567	1.31
1987	1110	0.0	1407	500	617	1.37
1988	827	0.0	1443	274	559	0.75
1989	1476	0.6	1268	895	586	2.45
1990	842	0.0	1538	265	581	0.72
1991	1278	0.0	1642	622	664	1.70
1992	1000	0.0	1610	425	583	1.17
1993	818	0.0	1601	181	675	0.49
1994	1278	0.0	1389	665	616	1.82
1995	1107	0.0	1560	522	585	1.43
1996	1078	0.0	1327	546	571	1.50
1997	1294	1.0	1319	674	622	1.85
1998	673	0.0	1331	195	481	0.53
1999	2025	0.3	1068	1359	667	3.72
2000	1314	0.0	1143	725	596	1.99
2001	1464	24.8	1249	781	662	2.14
2002	1058	0.8	1320	478	581	1.31
2003	1139	0.0	1287	594	550	1.63
2004	1220	0.0	1171	637	587	1.74
2005	795	0.1	1368	310	492	0.85
2006	1334	0.4	1316	697	653	1.91
2007	1319	0.0	1338	723	597	1.98
2008	1373	0.0	1368	712	704	1.95
2009	1062	0.0	1592	308	753	0.85
2010	768	0.0	1672	187	607	0.51
2011	1437	0.2	1469	771	690	2.11
2012	1239	1.0	1545	457	792	1.25
2013	1040	0.0	1571	484	567	1.32
2014	1097	0.0	1525	466	655	1.28

2015	878	0.0	1545	410	511	1.12
2016	1097	0.0	1621	429	695	1.18
2017	1098	0.0	1288	464	643	1.27
2018	960	0.0	1283	439	529	1.20
2019	1091	0.0	1326	467	624	1.28
2020	862	0.0	1293	437	449	1.20
2021	966	0.0	1137	336	630	0.92
Average	1119	0.9	1373	531	599	1.45

Table 3.4 The results of annual precipitation, runoff, potential evapotranspiration, actual evapotranspiration and recharge silty clay loam soil type

Year	**PREC**	**RO**	**PET**	**RECH**	**AET**	**RECH**
1979	**mm/yr**	**mm/yr**	**mm/yr**	**mm/yr**	**mm/yr**	**mm/day**
1980	1176	151	1306	329	696	0.90
1981	1211	162	1213	480	592	1.31
1982	1269	200	1095	350	751	0.96
1983	815	68	1274	237	535	0.65
1984	1099	117	1234	366	622	1.00
1985	956	66	1338	278	634	0.76
1986	1043	41	1276	303	701	0.83
1987	1110	116	1407	287	714	0.79
1988	827	71	1443	132	665	0.36
1989	1476	228	1268	567	687	1.55
1990	842	37	1538	168	661	0.46
1991	1278	102	1642	422	761	1.16
1992	1000	57	1610	292	661	0.80
1993	818	56	1601	38	776	0.10
1994	1278	164	1389	403	729	1.11
1995	1107	105	1560	306	696	0.84
1996	1078	90	1327	309	726	0.85
1997	1294	130	1319	458	709	1.26
1998	673	45	1331	104	597	0.29
1999	2025	297	1068	951	778	2.61
2000	1314	134	1143	471	717	1.29
2001	1464	283	1249	397	787	1.09
2002	1058	148	1320	269	643	0.74
2003	1139	96	1287	371	681	1.02
2004	1220	102	1171	395	728	1.08

2005	795	103	1368	123	580	0.34
2006	1334	140	1316	475	736	1.30
2007	1319	168	1338	418	734	1.15
2008	1373	186	1368	400	841	1.10
2009	1062	45	1592	111	906	0.30
2010	768	61	1672	129	675	0.35
2011	1437	180	1469	451	834	1.24
2012	1239	150	1545	229	871	0.63
2013	1040	79	1571	346	626	0.95
2014	1097	67	1525	317	753	0.87
2015	878	84	1545	220	632	0.60
2016	1097	144	1621	145	839	0.40
2017	1098	114	1288	227	766	0.62
2018	960	76	1283	282	611	0.77
2019	1091	96	1326	245	750	0.67
2020	862	115	1293	184	591	0.50
2021	966	92	1137	134	741	0.37
Average	1119	118	1373	312	708	0.86

The annual runoff estimates from 1979 to 2021 indicates that in the sandy soil type, the runoff is 0.9 mm/year, significantly lower than the runoff of 118 mm/year seen in the silty clay soil. This is coherent with field observations, as this soil type is present in the dunes where there are no streams and all the precipitation either evaporates or infiltrates into the aquifers. For the silty clay loam soil, the runoff is still limited because of soil texture distribution, and it is also located in the alluvial plain of the Luy River where the slope is small. Due to the larger runoff value in the alluvial plain area, its recharge is lower (312 mm/year) in comparison to the dune side (530.7 mm/year). Figure 3.3 shows the evolution of the yearly recharge rate and runoff for two soil types distributed in the study area in response to precipitation and evapotranspiration over the past 42 years. In general, yearly precipitation mostly varies from 800 to 1400 mm. It reaches its minimum value in 1998 with 673 mm/year and its maximum in 1999 with 2024 mm/year. The recharge rate has a proportional relationship with precipitation since it reaches its peak in 1999 in both calculations of soil type, whereas the evapotranspiration value is lowest in this year. The average recharge represents 28% of the volume of precipitation in the silty clay soil type and 47% in the case of sandy soil. The run-off in the dune (sandy soil) is almost 0, explaining the higher recharge rate. In dry months, the PET is generally higher than the precipitation so that the AET is lower than the PET. In both silty clay soil and sandy soil, AET is also lower than the effective precipitation because, when calculated on a daily basis, infiltration after strong rain events is possible. AET in the sandy soil is lower than in silty clay soil.

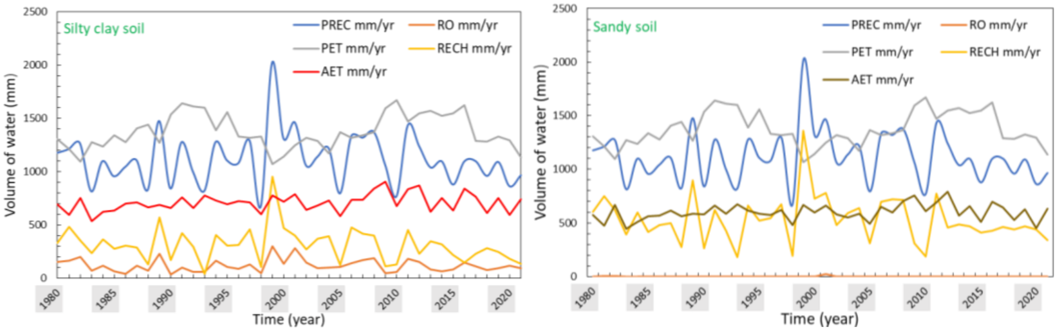

Figure 3.3 The evolution of the precipitation, evapotranspiration, runoff and recharge over the 42 years for two types of the soil distributed in the area.

The forty-two year monthly calculated recharges for the two types of soil in response to precipitation and evapotranspiration are presented in Figure 3.4. The precipitation reaches its peak in September, then decreases regularly to zero in February, increasing again until August of next year. The actual evapotranspiration varies relatively with the precipitation and recharge values in both soil types. The recharge rate is driven by the difference and becomes very low or equal to zero in the dry months from December to April next year. This recharge trend will be used to model the transient behavior of the groundwater system in Chapter 5.

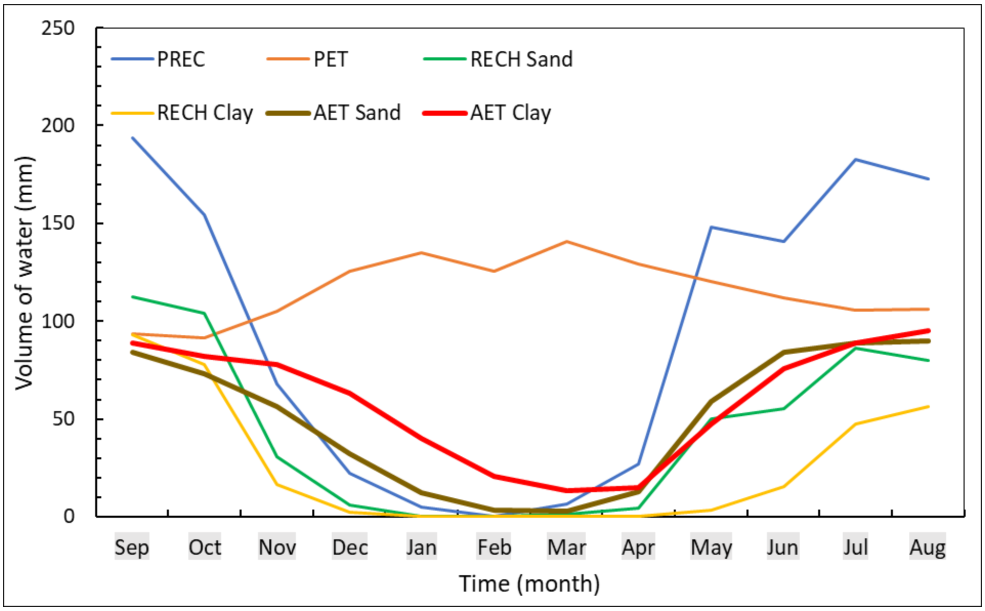

Figure 3.4 Forty-two year average monthly calculated recharge for the sandy soil and silty clay soil corresponding with the monthly precipitation and evapotranspiration in the area.

3.4.2 Groundwater table fluctuation

The water table fluctuation method (WTF) calculates recharge by multiplying the change in water level over time by the specific yield. Since the study area contains shallow aquifers and the significant variation in precipitation between dry and rainy seasons, it is appropriate to apply this method for recharge estimation. However, it ignores the interaction with the river, the effect of small streams, canals and drains, as well as possible impact of irrigation on the water levels and lateral flow.

The water table fluctuation during the seasons was monitored in the research area using CTD-Diver devices installed in seven monitoring wells. The water-level basically rise in the wells in response to rainfall. Recharge is expected to occur in the rainy season during the months from May to October which have a high amount of rain. The wells at these location are predominantly a combination of deep and shallow wells corresponding to lower and upper aquifers, with the exception of one deep well (LK19BT). The well locations are shown in Figure 3.5.

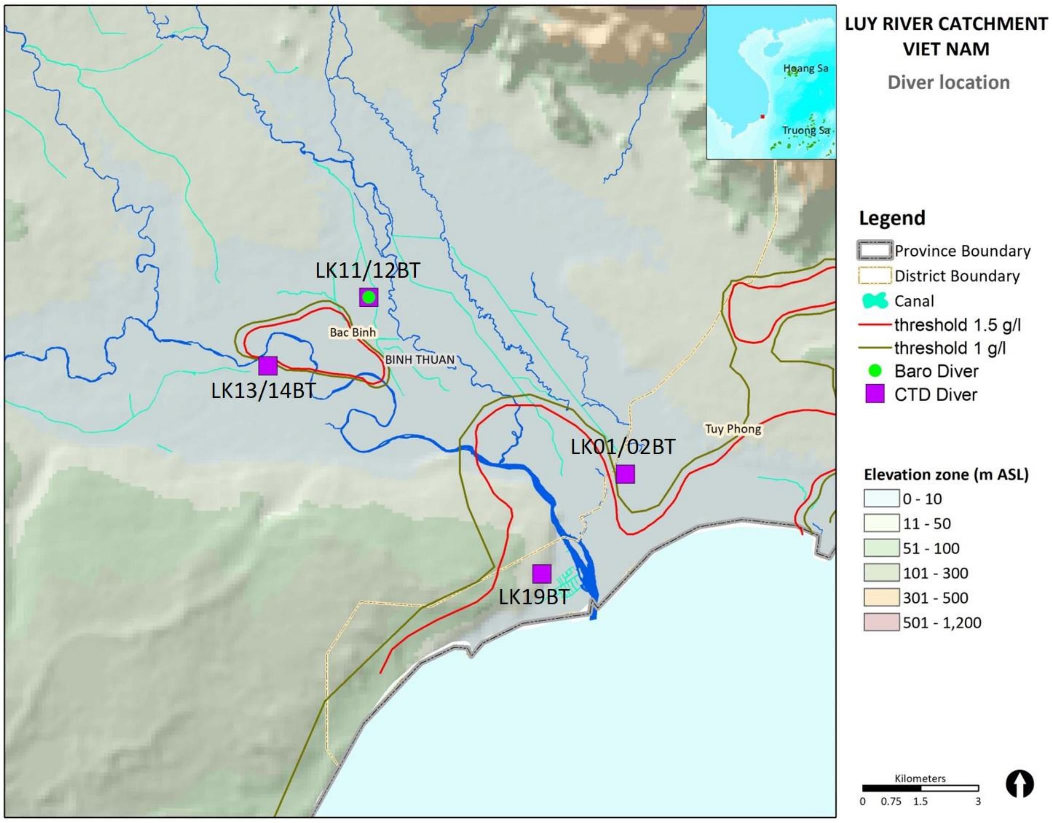

Figure 3.5 Location of the monitoring wells in the study area.

Most of the observation wells are located in the alluvial plain. The sediment or soil layer is a mix of clay, silt, and sand; one of them is located in the foot of the sand dune (LK19BT). Based on the statistics on the specific yield complied by Johnson (1967) and the soil types distributed in the area, a specific yield of 0.155 for sediment in the alluvial plain and another of 0.21 for sediment on the dune side will be used for WTF calculations.

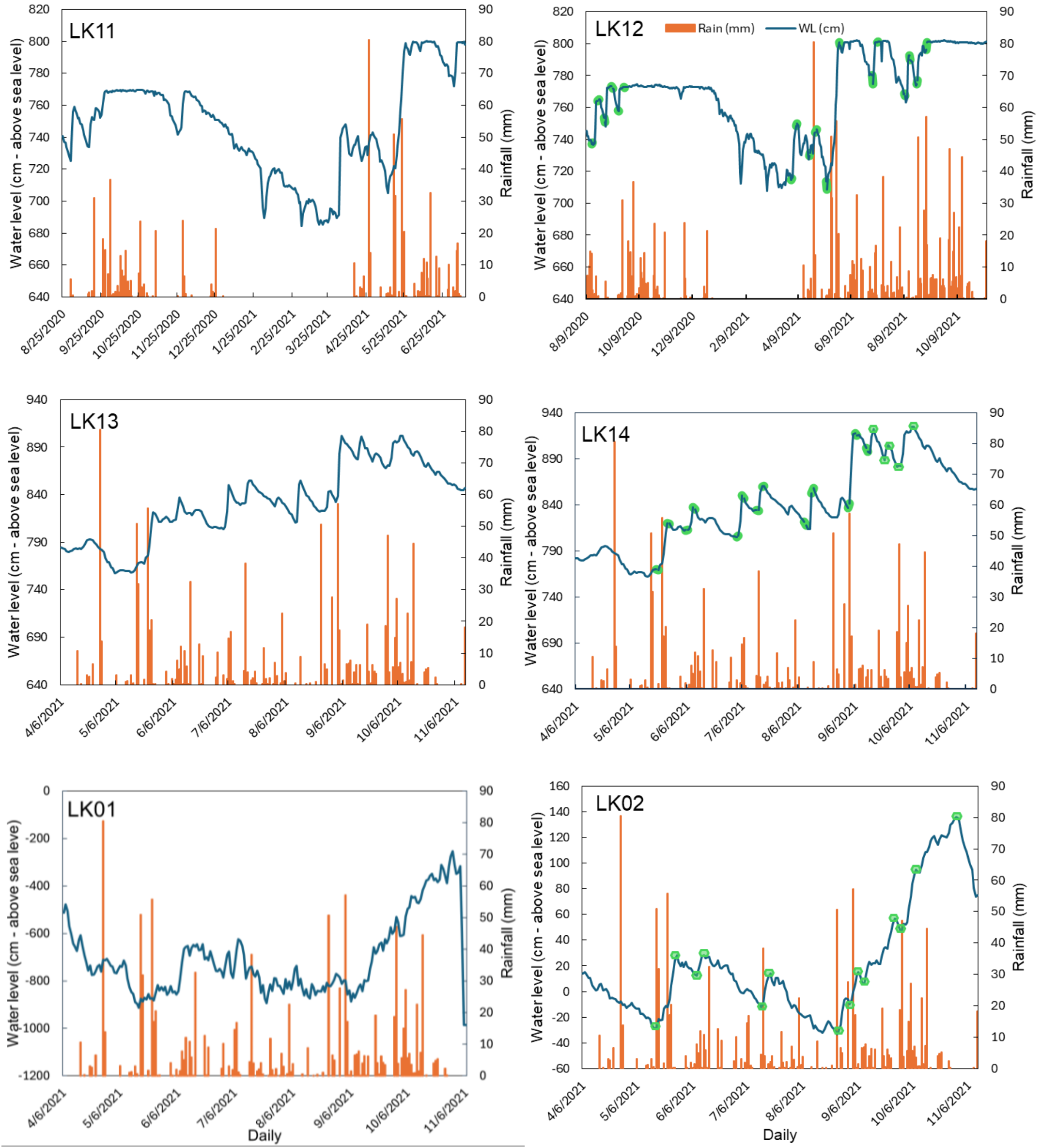

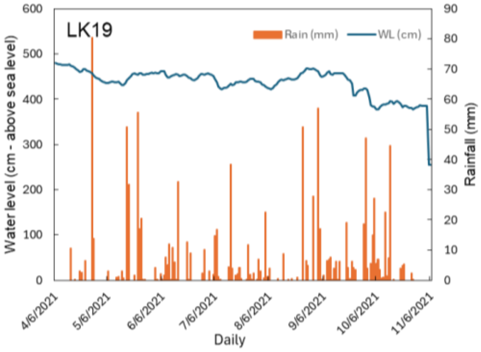

Figure 3.6 The variation of water level (expressed as level above the sea level) in the observed wells and daily rainfall in the study area at the same period. The green dots show lows and peaks of the water level used for calculating the recharge.

Figure 3.6 shows the variation of water level in the observed wells and the daily rainfall in the study area. The observation clearly demonstrates a substantial correlation between the water level in all the wells and the changing seasons. The first two graphs of the wells LK11 and LK12 depict the peaks in the water level during the rainy season (August-October) and then a continuous decrease until the end of the dry season (April). The second part of the graph from May to November 2021 corresponds to the recharge season. Remarkably, the water level in LK11BT and LK12BT is fluctuating even during the dry months when the rainfall is zero. This is likely caused by irrigation occurring in the area. For the rainy months, the water level reaches a plateau corresponding to a water level of about 8 m which is stable during almost the entire rainy season. This likely indicates the influence of the nearby canal which has a fixed water level and is therefore draining the aquifer.

Among the observed wells, LK01BT and LK19BT are screened in the sandy layer (lower aquifer), which is semi-confined under clay lenses. The WTF method is not appropriate for the condition of the wells as they are not shallow. LK19 BT clearly shows less variations in the water table throughout the year with no direct link with the precipitation. LK01BT has fluctuations similar to its shallow counterpart (LK02BT), but with a much larger amplitude. They both display a steady increase in water level at the end of the rainy season, which might indicate these locations receives lateral recharge from the dunes. LK01BT is also much more saline.

The other wells can be assumed to be screened in the unconfined aquifers, at each site, the deeper screen has similar water levels and fluctuations suggesting that they are located in the same aquifer what is confirmed by the absence of confining clay layers in the borehole log description. The water table at these wells varies smoothly throughout the rainfall events, which produce measurable changes in water level in the observed wells. This is attributed to the recharge of these short-term signals by the storage capacity and then partly discharge again in the surface water, causing the recession.

The green dots in Figure 3.6 indicate the short-term rise in the water table during each rain event. Tables 3.5, 3.6, and 3.7 show the water level rise in response to the amount of rainfall, as well as the calculated recharge per day for each shout-term rise, for observed wells LK12, LK14, and LK02. The recharge rate for each short-term rise is different and obviously affected by the amount of rainfall received throughout the water level rise phase. This recharge rate is limited to the rainfall season; consequently, following equation 3.8.

Table 3.5 Water fluctuation during the short-term signals and calculated recharge at the term for well LK12. Date Hmin: the day water level at the low point; Hmin WL at the low point; Hmax: WL at the high point; ΔH: water level rise = Hmax-Hmin; Rainfall: amount of rain in those days; Days: number of days WT increasing; Recharge: calculated by WTF method.

Date (Hmin)	Hmin cm	Hmax cm	ΔH mm	Rain mm	Days	Recharge mm/day	Recharge mm/year
8/17/2020	736.79	764.95	281.6	10.9	7	6.23	
8/31/2020	748.18	773.36	251.8	6.2	6	6.50	
9/15/2020	757.95	773.08	151.3	34.6	7	3.35	
3/25/2021	711.21	750.02	388.1	0	15	4.01	
4/21/2021	727.31	746.21	189.1	103.4	10	2.93	
5/12/2021	708.51	800.66	921.5	182.5	15	9.52	
7/4/2021	774.85	800.92	260.6	33.3	4	10.10	
7/14/2021	788.85	801.91	130.60	46.70	4.00	5.06	
8/11/2021	763.31	798.73	354.15	100.60	21.00	2.61	
SUM			2928.59				453.93

Table 3.6 Water fluctuation during the short-term signals and calculated recharge at the term for well LK14. Date Hmin: the day water level at the low point; Hmin WL at the low point; Hmax: WL at the high point; ΔH: Hmax-Hmin; Rainfall: amount of rain in those days; Days: number of days WT increasing; Recharge: calculated by WTF method.

Date (Hmin)	Hmin cm	Hmax cm	ΔH mm	Rain mm	Days	Recharge mm/day	Recharge mm/rainy season
5/14/2021	762.60	819.73	571.27	181.5	14	6.32	
6/4/2021	812.22	837.40	251.75	16.4	6	6.50	
7/3/2021	805.30	847.22	419.23	36.3	5	13.00	
7/14/2021	834.06	860.78	267.19	48.2	5	8.28	
8/11/2021	813.28	858.17	448.92	9.3	4	17.40	
9/2/2021	836.41	917.12	807.06	74.4	4	31.27	
9/14/2021	895.95	922.35	264.04	6.3	3	13.64	
9/22/2021	888.61	904.56	159.47	13.8	3	8.24	
9/29/2021	881.41	920.50	390.84	134.4	11	5.51	
SUM			3579.77				554.86

Table 3.7 Water fluctuation during the short-term signals and calculated recharge at the term for well LK02. Date Hmin: the day water level at the low point; Hmin WL at the low point; Hmax: WL at the high point; ΔH: Hmax-Hmin; Rainfall: amount of rain in those days; Days: number of days WT increasing; Recharge: calculated by WTF method.

Date (Hmin)	Hmin cm	Hmax cm	ΔH mm	Rain mm	Days	Recharge mm/day	Recharge mm/rainy season
5/16/2021	-29.39	28.01	573.99	177.90	13.00	6.84	
6/8/2021	12.06	26.90	148.46	74.20	8.00	2.88	
7/14/2021	-12.48	14.17	266.44	50.30	6.00	6.88	
8/26/2021	-31.08	12.70	437.78	113.50	11.00	6.17	
9/9/2021	5.62	56.88	512.59	68.70	18.00	4.41	
9/29/2021	48.36	135.90	875.43	227.80	32.00	4.24	
SUM			2814.69				436.28

With more than a year of observation, the water level in the wells LK11BT and LK12BT reaches the maximum level in September and the minimum level in February. The estimated annual recharge for LK12 is 454 mm/year, with a specific yield of 0.155. The observations in wells LK14 and LK02 were recorded during the rainy season of 2021, and it was not a full hydrological year. However, applying the cumulation of water level fluctuation, the estimated recharge for that period is 436 mm in LK02 and 555 mm in LK14. The time record and the rainfall in the period are different from the estimation in the well LK12 therefore we cannot compare them together. The result can also be affected by the specific yield value we set for each soil type.

3.5 Discussion

Soil moisture balance and water table fluctuation methods were used to estimate groundwater recharge storage inside the site. In the soil moisture balance method, the soil texture and of course the topography play an important role since they control how much water infiltrate into the aquifer. Evapotranspiration is also taken into account, it is affected by the crops growing in the soil and the weather state in the study area.

The average recharge (312 and 531 mm/year in the alluvial plain and the dune respectively) estimates obtained using the SMB approach are in the same order of magnitude as the values obtained using the WTF method (Table 3.8), which however correspond to a single year. From Table 3.3 and Table 3.4, the recharge in 2020 and 2021 was supposed to be below average (184 and 134 mm for the alluvial plain and 437 and 336.4 mm/year for the dune area), which is significantly lower compared to the estimated recharge of 454 mm in that period for the WTF method. The WTF is obviously dependent on local conditions as well as on the estimated value for the specific yield, which makes rather uncertain. The estimated recharge is indeed directly proportional to the specific yield. We use a value of 15% which is rather high for silty clay loam. The local conditions are averaged out in the SMB approaches, since we simplified the study area within two main zones. This shows that, determining the most effective approach is challenging, especially at the catchment scale. The reliability of the outcome increases with the abundance of data. This gives us confidence that the SMB method can be applied to estimate average recharge rate since data is available over a larger period of time. However, the SMB only considers the precipitation as input and not irrigation. It is expected that some return flow from irrigation is participating to the recharge, as is indicated by the WTF, with some wells showing increase in water level during the dry season.

Table 3.8 Estimates of groundwater recharge rates, in mm/year, for the coastal area in Binh Thuan, Vietnam in both SMB and WTF methods

Material/location	Recharge (mm/year)	
	SMB method	WTF method
		2020 - 2021
Silty, clay, mixed sandy loam soil/alluvial plain	312	454
Loamy sand soil/dune side	531	

Scanlon (2004) and Scanlon et al. (2006) found a relationship between recharge and precipitation based on the observation in the semiarid and arid regions in the Southwestern U.S:

$$R = 0.15(P - 42)\ for\ P > 42, R = 0\ for\ P \leq 42\ (Eq. 8)$$

where P is precipitation (cm/year) and R is the recharge.

Their relationship suggests that recharge decreases linearly as precipitation decreases from 80 cm/year to about 42 cm/yr. Recharge approaches zero when the precipitation is below that value. They suggested that recharge was minimal or negligible in semi-arid conditions at precipitation rates below 50 cm/yr. The average precipitation for 42 years in the study area is 111.8 cm/year. Applying this correlation to the study area obtains a recharge rate of 105 mm/year, which is particularly lower than the rates derived from the aforementioned two techniques. This is likely explained by the difference in climate between the two regions and we conclude that this empirical relationship is not applicable to the Luy River catchment. This further stresses the importance of local recharge estimates.

Unfortunately, there was no dedicated studies before ours in the study area to compare our estimates. Nguyen (2015) used a range value from 0.6 to 791 mm/year in his model, but there is no justification about the chosen values. Ta T.T. et al (2019) used a value of recharge ranging between 18-730 mm/year in their study in the Ninh Thuan province which is adjacent to Binh Thuan.

3.6 Conclusion

This study uses the daily rainfall and evapotranspiration variations for the past 42 years and two years of observation of water level fluctuations to estimate the recharge rate in the Luy River catchment. The long-term average (42 years) rainfall is 1118 mm/year, and the potential evapotranspiration is 1373 mm/year. The area was divided into two parts for recharge estimation. The first part is found on the alluvial plain and consists of silty clay loam type of soil. The second part corresponds to the dune complex in the area, is characterized by a loamy sand soil type. From the soil moisture balance method, the runoff in the alluvial plain is 118 mm/year (10.6% of rainfall), and the recharge rate is 312 mm/year (28% of rainfall). On the dune side, the runoff is 0.9 mm/year (0.08% of rainfall), and recharge is 531 mm/year (47% of rainfall).

The result obtained from the water level fluctuation method in 2020 - 2021 in the alluvial plain is 454 mm/year. They were obtained from a limited number of wells for a short period of time, and are therefore not suited to calculate yearly recharge average. Moreover, water level changes are not only caused by rainfall infiltrating to become recharge but also ocean tides, earth tides, barometric pressure changes, pumping, drainage, lateral flow and estimated specific yield. Therefore, the estimated value for the period 2020-2021 seems to overestimate the recharge of the SMB for the corresponding year. We therefore trust the estimation from the SMB method, obtained for longer period of time, as a good estimation of the average recharge rate in the study area.

Recharge is a complex function of multiple environmental factors, including precipitation duration and intensity, temperature, radiation, wind, soil type, geology, antecedent moisture conditions, and vegetation. Due to the significance of understanding recharge rates, considerable resources have been dedicated to the measurement or estimation of recharge. Based on Scanlon's definition, the research region does not fall under the classification of arid or semi-arid settings due to its average annual precipitation of 1118 mm. Nevertheless, the extended period of drought, flooding, and seawater intrusion pose significant challenges in the research area. These phenomena may be attributed to the significant variation in precipitation levels between the dry and wet seasons, as well as a higher amount of evapotranspiration in the region.

Chapter 4. Groundwater salinization and freshening processes in the Luy river coastal aquifer, Vietnam

This chapter has been published in:

Pham D.L., Cong-Thi, D., Segers, T., Huu, H.H., Nguyen, F., Hermans, T., 2022. Groundwater Salinization and Freshening Processes in the Luy River Coastal Aquifer, Vietnam. Water 14 (15), 2358 pp.

Pham Dieu Linh[1,3,*], Cong-Thi Diep[1,3], Tom Segers[1], Hieu Huu Ho[3], Frédéric Nguyen[2], Thomas Hermans[1]

[1] Laboratory of Applied Geology and Hydrogeology, Department of Geology, Ghent University, Krijgslaan 281-S8, 9000 Ghent, Belgium
[2] Liege University and KU Leuven, B- 4000 Liège and 3000 Leuven, Belgium
[3] Vietnam Institute of Geosciences and Mineral Resources (VIGMR), 100000 Hanoi, Vietnam
***** Correspondence: Linh.PhamDieu@UGent.be

Abstract: The Vietnamese Binh Thuan province located along the Southern Central part of the coast is one of the driest in the country. The population is relying largely on groundwater for irrigation, and the groundwater resources are threatened by climate change and saltwater intrusion in river estuaries. Recent studies, however, reveal that the extension of saltwater intrusions was larger than expected, raising some doubts on the actual origin of the intrusions. In this study, we use the geochemical characterization of groundwater samples collected in both the dry and rainy seasons in the Luy river coastal area to identify hydrochemical processes responsible for the salinization and variations taking place in the shallow aquifers. The distribution of chemical components of groundwater and the indicators presenting the freshening and salinization processes, such as cation exchange code and chloride conservative element, the ionic delta, the HFE-diagram, and geochemical modelling, were studied. The results show that 65% of the samples exceed the WHO limit for drinking water and 100% of them have a degree of restriction on use from slight–moderate to severe in potential irrigation problems according to FAO. The findings indicate that freshening is the dominant process in the aquifers, and it is more advanced in the rainy season. Due to a lack of recharge and aquifer exploitation, salinization is more severe in the deeper aquifer and during the dry season. Saltwater intrusion is not limited to the zone close to the river but extends further inland and at depth, and salinity can vary quickly over short distances. Based on these new insights, we develop a new conceptual model for the evolution of salinization in the Luy river catchment involving a natural freshening process of connate water combined with anthropic influence. The conceptual model will form the basis for the development of a groundwater model of the study area and eventually lead to sustainable management scenarios for this coastal region, preventing further deterioration of the groundwater resources.

Keywords: hydrochemistry; freshening; saltwater intrusion; coastal aquifer

4.1 Introduction

Saltwater intrusion is one of the most widespread threats occurring in coastal areas worldwide (Werner et al., 2013). It does not only decrease water quality by raising salinity to levels exceeding acceptable drinking and irrigation water standards but also threatens the prospective exploitation of coastal aquifers and soil salinization. Many studies have been carried out in coastal areas across the globe to understand the problem of saltwater intrusion, for example, in Africa (Van Camp et al., 2014; Idowu and Lasisi, 2020), America (Lyles 2000; Barlow and Reichard, 2010), Asia (Parck et al., 2012; Prusty and Farooq, 2020), Australia (Werner and Gallagher, 2006; Morgan and Werner, 2015) and Europe (Walraevens et al., 1993; Custodio 2010).

Seawater encroachment inland is the most common cause for the increase in salinity. This often occurs in arid and semi-arid regions where groundwater constitutes the main freshwater resource and additional pressures related to climate change, such as sea level rise, changes in recharge patterns and groundwater withdrawal have impacted the hydrologic balance in the coastal aquifers (Park et al., 2005; Bennetts et al., 2006; Petalas and Lambrakis 2006; Alfarrah and Walraevens, 2018). Salinization can also be the result of upconing, where saltwater is present at depth and rises due to groundwater extraction (Werner et al., 2009). The presence of fossil seawater might also be a source of salinity (UNESCO, 1987; Custodio, 1997; Werner et al., 2013). This old seawater can primarily be found in low permeability formations, such as clay and silty clay where it stays entrapped in the sediments. As opposed to saltwater intrusion, freshening processes are also common in coastal aquifers, for example through infiltration of rainwater, reduction in exploitation flowrate or artificial recharge (Appelo, 1994; Walraevens and Van Camp, 2004; Andersen et al., 2005; Lambrakis, 2006; Walraevens et al., 2007; Russak and Sivan, 2010; Antonellini et al., 2015; Sarker et al, 2021a). The freshwater recharge gradually infiltrates through the shallow soil toward the aquifers, leading to changes in salinity and groundwater chemistry. Through its 3444 km long coast, Vietnam is particularly vulnerable to SWI. Several local hydrogeochemical studies on saltwater intrusion have been performed in Vietnam (Nguyen et al., 2014; Larsen, et al., 2017; Kim et al., 2017; Hoang et al., 2018; Bauer, et al., 2022; Ha, et al., 2022). Those studies mostly focused on the Red River delta and Mekong delta - the areas located in the north and south of Vietnam, respectively.

In terms of the project, we have applied some new methods to investigate the saltwater intrusion happening in the area. A recent geophysical study in the Luy River catchment based on electrical resistivity tomography (ERT) (Cong-Thi et al., 2021) revealed the deeper part of the coastal aquifer along the downstream part of the Luy River is mostly occupied by saltwater, whereas the distribution of salinity in the shallow part is extremely variable. Large variations of salinity are observed at short distances, without any apparent correlation with the distance to the Luy river and its tributaries, highlighting a complex distribution of salinity. This geophysical survey showed that the estimation from NAWAPI for the extension of the SWI zone was underestimated and that the current situation was likely not the result of recent river water infiltration only, but a consequence of the evolution of the context in the catchment involving both natural and anthropic processes. The main objective of this part is to identify the origin of saltwater intrusion in the Luy River catchment, as this constitutes a necessary step to propose a sustainable management of the groundwater resources in the study area. Our recent geophysical data raised some serious doubts about the origin of the salinity (river infiltration), but it is not sufficient on its own to draw definitive conclusions. Therefore, we propose a thorough hydrochemical analysis of newly acquired water samples in order to identify which processes are taking place and what is the origin of the high salinity. This will eventually allow us to propose a new conceptual model of the aquifer in agreement with both geophysical and geophysical data.

In coastal aquifers, the situation is often very complex with several saltwater intrusion and freshening processes playing a role at the same time (Werner et. al., 2013). Although the mapping of the total dissolved solid content, as can be obtained from geophysical data (Cong-Thi et al., 2021; Hasan et al., 2020; Hermans et al., 2012; Sarker et al., 2021b), is a first necessary step, this is often not sufficient to reveal the complexity and the dynamics of the processes taking place (Bear et al., 1999). Identifying factors governing groundwater geochemistry and the identification of the stage and cause of salinization will assist in efficiently evaluating the suitable groundwater quality for irrigation and drinking water purposes and to propose adapted management strategies (Appelo and Postma, 2005). The most direct way to investigate contamination by seawater intrusion and freshening processes is to use indicators derived from groundwater chemical components (Bear et al., 1999; Appelo and Postma, 2005; Barlow 2013). The indicators of cation exchange processes, such as cation exchange codes (Walraevens and Van Camp, 2004; Stuyfzand, 1986) and chloride (Cl) conservative element (Appelo and Postma, 2005), are of particular interests as they can reveal if freshening or salinization processes are dominant and even the current stage of the process (Andersen et al., 2005). Similarly, the evolution of the hydrochemical facies can evaluate how saltwater intrusion is evolving with time and space (Giménez, 2019), although there might be a delay between a change in the drivers of saline intrusion and its effect on the hydrochemical signature, the response to salinization being faster than the one to freshening (Walraevens and Van Camp, 2004).

For the objective of this study, we perform a new hydrogeochemical survey in the Luy river catchment, including both shallow and deep wells and samples collected during both the dry and wet season. Our study corresponds to the first in-depth hydrochemical analysis of the seawater freshening/intrusion processes based on water composition as well as the first attempt to identify their seasonal variations. In addition, we propose an integrated interpretation of the new datasets with the available geophysical results to distinguish the effect of recent saltwater intrusion from freshening processes that are still the dominant processes controlling water quality at the scale of the catchment. The final result of our study is a conceptual model of seawater intrusion, taking into account natural and anthropic effects with the effect of seasonal cycles, which serves as a basis for future groundwater modelling and management.

4.2 Methods

Our methodology is based on newly acquired water samples all over the alluvial plain of the Luy River catchment. The extension of the study area was based on previous data that were available (previous samples and geophysical data) to cover the zones where saltwater intrusion is encountered. The upstream part of the Luy river basin is known to be fresh (Nawapi, 2015), and SWI is known to be the main issue for groundwater quality in the downstream part. The analysis of the hydrochemistry of the water sample is used to identify the origin of saltwater intrusions. In Section 4.4, the results of the hydrochemical analysis will be combined with existing data to derive a conceptual model of the SWI processes in the study area.

4.2.1 Water Sampling

The objective of the sampling campaign was to provide a better coverage of the unconsolidated aquifer than previous studies (Nawapi, 2015; 2018). Ninety groundwater samples were collected in the summer of 2020 from both dug wells and drilled wells owned by farmers using the USGS protocol (Claassen, 1982). These wells are typically used for irrigation purposes and are often abandoned by the farmers when they become too saline. They are all potentially factors of SWI by inducing lateral flows or upconing if saline water is present in the vicinity. Because those samples were mostly shallow (<5 m: 6 samples - 7%, from 5 to <15 m: 69 samples - 76%, >15 m: 9 samples - 10% and 6 samples - 7%: no information of depth) and that ERT data (Cong-Thi et al., 2021) identified a clear distinction between the shallow and deeper aquifer, 10 nested wells with screen intervals in both the shallow and deep parts of the aquifer were drilled. These are forming the new monitoring network in the Luy river catchment and provide 20 additional samples. In addition, most wells were revisited in April 2021 during the dry season. Wells in which the TDS (converted from measured electrical conductivity - EC in the field with TDS (mg/L) = 0.65 × EC (µS/cm) – groundwater was around 25°C and air temperature was from 30 - 35°C) was significantly different with an absolute difference greater than 500 mg/L (corresponding to 15 wells) and the wells of the monitoring network were resampled for comparison with the wet season. The location of the samples is shown in Figure 2.1. For major cation and anion analysis, the samples were collected through a 0.45 µm cellulose acetate filter. Samples for cation analysis (Al, Ca, Fe, K, Mg and Na) were filtered and collected into 50 mL polyethylene (PE) bottles and acidified to 1% with HNO_3. Samples for anion analysis (F, Cl, Br, SO_4) were filtered and collected into 50 mL PE bottles with no further treatment. Samples for NO_3, NO_2 and PO_4 determinations were filtered and collected into 50 mL PE bottles adding 1% chloroform. Samples for determining the total dissolved inorganic carbon (DIC) were not filtered but were collected into 100 mL bottles and were analyzed on the same day.

All bottles were rinsed 3 times before sampling and completely filled with the sample to avoid air contact and afterward stored at a temperature of +5 ◦C and sent to Belgium for analysis in the Laboratory for Applied Geology and Hydrogeology, Department of Geology, Ghent University.

4.2.2 Chemical Analysis

Major cations (Na^+, K^+, Ca^{2+}, Mg^{2+}, FeTotal and MnTotal) were analyzed by inductively coupled optimal emission spectrometry (ICP-OES) and major anions (Cl^-, SO_4^{2-}, NO_3^-, PO_4^{3-}, NH_4^- and NO_2^-) were analyzed using a spectrophotometer (Shimadzu UV1800). Br^- and F^- anions were analyzed by an ion-specific electrode. pH was measured onsite using a pH electrode calibrated against commercial buffer solutions. The dissolved inorganic carbon (DIC) concentrations were measured using an alkalinity titration.

Among 110 water samples, 54 samples have an ionic balance error within ±5% whereas the charge balance of 43 samples range within ±5–10%. Twelve samples have an ionic balance error between ±10–20% and one sample has an ionic balance error of 41%. The latter was completely left out of the analysis process. In this study, samples with an ionic balance error up to 20% were kept for analysis to maximize the number of samples. The high error for some samples is attributed to the difficult sampling conditions, the conservation of the samples during transport and the dilution of the samples for analysis because of the high salinity. The ionic balance for the 33 samples collected during the dry season is below 10%.

4.2.3 Geochemical Analysis

The analysis of the data involved four steps: (1) the classification of water using the Stuyfzand's classification (Stuyfzand, 1986); (2) the evolution of hydrochemical facies using (Piper, 1944) and HFE-D diagrams (Giménez and Sánchez, 2015); (3) the estimation of the origin of solutes using conservative element behavior and calculation of aqueous speciation and mineral saturation indices; (4) the calculation of the expected composition based on conservative mixing.

4.2.3.1 Stuyfzand's Classification

In Stuyfzand's classification, the primary type of water uses the Cl^- content (in mg/L) corresponding with the codes <150 = F-Fresh, 150–300 = Fb-Fresh-brackish, 300–1000 = B-Brackish, 1000–10,000 = Bs-Brackish-salt, 10,000–20,000 = S-Salt and >20,000 = H-Hyperhaline. We also use Stuyfzand's cation exchange code which determines if cation exchange has taken place and the original component of the exchange. According to Stuyfzand (1986), the surplus of (Na + K + Mg) often points at a (former) freshwater encroachment and the deficit of (Na + K + Mg) often points at a (former) saltwater intrusion. The cation exchange code also plays a significant role in the examination of salinization and freshening processes because it characterizes the composition of end-members. In the coastal aquifers, seawater (SW) and freshwater (FW) are considered as two end-members that are characterized by the water types of S-NaCl0 and F-$CaHCO_3$0, respectively. Following this, the sum of Na^+, K^+ and Mg^{2+} in meq/L is corrected for the seawater contribution specified from the Cl^- content. The cation exchange code is given following the sign of the cation exchange parameter (Na + K + Mg) corrected, with a margin of error of $\sqrt{0.5Cl}$ (negative code = deficit, positive code = surplus, θ code – within margin error = equilibrium). The Cl^- content is assumed to be a conservative component originating from seawater only.

4.2.3.2 Hydrochemical Facies Using Piper and HFE-D Diagrams

The Piper diagram plots the main cations and anions using relative concentration expressed in meq/L in a multivariate diagram including a cation triangle and an anion triangle and a transferred rhomb. The latter are also indicators of salinization/freshening processes caused by cation exchange. The water type of the first fresh-water end-member is $CaHCO_3$0 and the salt water end-member is NaCl0. The facies of the samples shifting from $CaHCO_3$0 → $CaCl^-$ → $NaCl^-$ → NaCl0 on and above the mixing line present the salinization process with "-" expressing a deficit of marine cations. On the other hand, the samples located below the mixing line are experiencing freshening processes and the facies of the waters vary from NaCl0 → $NaCl^+$ → $NaHCO_3^+$ → $MgHCO_3^+$ → $CaHCO_3^+$ → $CaHCO_3$0 with the "+" describing a surplus of marine cations.

The alternating sequence between freshening and salinization processes can be recognized by the evolution of the chemistry of the major ions over time (Giménez, 2014) used a Hydrochemical Facies Evolution Diagram (HFE-Diagram) to describe the seawater intrusion based on the evolution of hydrochemical facies. The HFE-Diagram is plotted in terms of the relative percentages of anions and cations, in which Cl^- represents the seawater end-member, whereas HCO_3^- or SO_4^{2-} corresponds to the dominant anion in fresh groundwater (Giménez and Sánchez, 2015). The base-exchange reactions were described following the percentages of (Na^+ + K^+) and Ca^{2+}. The blue mixing line is situated between the FW/SW end-members. Besides the mixing line, there are two transitions indicating the evolution of water samples according to freshening and saltwater intrusion processes. Different sub-stages can be identified, using the salinity evolution estimated through the proportion of Cl^-: in the freshwater intrusion (FwI) phase, represented by the top left curved arrow, the freshening sub-stages (f1, f2, f3, f4 and FW) can be identified. In the opposite sector of the diagram, the saltwater intrusion (SwI) sub-stages belonging to intrusion phases are represented (i1, i2, i3, i4 and SW).

4.2.3.3 Origin of Solutes Using Conservative Element Behavior, Aqueous Speciation and Mineral Saturation Indices

The origin of solutes and their mixing were assessed using the relationship of Cl^- and other ions. Cl^- and Br^- were considered as the characteristic saline elements because of their conservative behavior with their hydrophilic character and small ionic size. They neither take part in significant ion-exchange reactions at low temperatures nor are adsorbed onto mineral surfaces. As they are highly soluble, they only form minerals during extreme evaporation conditions when halite starts to precipitate (Alcalá and Custodio, 2008). The major ions were plotted against Cl^- content and compared with the mixing line to inspect whether ions were enriched or depleted. The calculations of aqueous speciation and mineral saturation indices were carried out using the aqueous geochemical modelling code PHREEQC (Parkhurst and Appelo, 2013). For these calculations, the saturation index of calcite, dolomite, gypsum and halite for each water sample were examined to see if specific rock/water interaction had occurred.

4.2.3.4 Expected Composition Based on Conservative Mixing

The chemical interactions between fresh and saltwater were detected by calculating the expected composition based on conservative mixing of saltwater and freshwater, and then comparing the result with the measured concentrations in the water sample, Cl^- being considered as a conservative component. Assuming no Cl^- component came from the dissolution of halite, the fraction of seawater f_{sea} was calculated using the Cl^- concentration of the sample (Andersen et al., 2005; Appelo and Postma, 2005) following Equation (1):

$$f_{sea} = \frac{m_{Cl^-,sample} - m_{Cl^-,fresh}}{m_{Cl^-,sea} - m_{Cl^-,fresh}} \ (1)$$

Where $m_{Cl^-,sea}\ and\ m_{Cl^-,fresh}$ were taken from the seawater composition from (Turekian, 1968) and freshwater from Luy river catchment with the lowest Na^+ and Cl^- contents, respectively.

The concentration of ion i, by conservative mixing of seawater and freshwater, was then calculated by Equation (2):

$$m_{i,\ mix} = f_{sea} \text{ x } m_{i,\ sea} + (1 - f_{sea}) \text{ x } m_{i,\ fresh}, \ (2)$$

where mi is the concentration of i (mmol/L), f_{sea} the fraction of seawater in the mixed water and subscripts “mix”, “sea” and “fresh” indicate a conservative mixture, seawater and freshwater, respectively. During the reactions, any change of the concentration mi, react was simply determined by Equation (3):

$$m_{i,\ react} = m_{i,\ sample} - m_{i,\ mix}, \ (3)$$

where $m_{i,sample}$ is the measured concentration in the sample.

If $m_{i,\ react}$ is greater than zero, it indicates the groundwater was enriched with respect to species i, whereas a $m_{i,\ react}$ lower than zero suggests depletion compared to plain mixing.

4.3 Results

4.3.1 Chemical Composition and Ion Distribution of Water Samples

Except for four samples taken from wells drilled through the bedrock, which is located between 20 and 50 m below the surface except in the upstream part of the study area, samples were collected from the shallow unconsolidated aquifers.

A statistical summary of the hydrochemical parameters is presented in

Table 4.1. Minimum and maximum values of the TDS are 985 and 16,155 mg/L respectively, with an average value of 1617 mg/L, illustrating the large variability in salinity. The pH ranges in the expected interval for groundwater from 4.2 to 8.7.

Na^+ is the most abundant cation in the water samples with concentration ranging from 10 to 4902 mg/L. Ca^{2+} ranges from 3.2 to 979 mg/L and Mg^{2+} from 1.9 to 912 mg/L. The highest value of K^+ is 150 mg/L and the lowest one is 0.25 mg/L.

For the anions, the concentration of Cl^- varies from 16.2 to 4935 mg/L and SO_4^{2-} ranges from 0 to 4219 mg/L. This largest value, which is higher than the SO_4^{2-} concentration from seawater (2750 mg/L), was collected from LK07-BT, likely indicating another source of contamination. NO_3^- concentration varies from 0.2 to 340 mg/L and PO_4^{3-} concentration from 0 to 19 mg/L.

Figure 4.1 shows the well screen position and the contour plots of the TDS value, Cl^-, Na^+, Ca^{2+}, Mg^{2+}, SO_4^{2-}, HCO_3^-, NO_3^- and Br^- distribution along the transect DC (see Figure 2.1), using samples located on or in the direct vicinity (less than 1 km) of the section line.

Despite the lack of samples located below −10 m, the TDS, Cl^-, Na^+, Mg^{2+} and Br^- and to a lesser extent SO_4^{2-} show similar patterns and constitute evidence of saltwater presence in the lower aquifer as all the samples collected just above the bedrock show the highest values.

The distribution of HCO_3^- in Figure 4.1h is quite different and likely brings information regarding freshwater recharge. The Ca^{2+} concentration has a mix pattern, showing influence of both freshwater recharge and salinization.

The NO_3^- concentration is large (greater than 50 mg/L) in the upper aquifer, showing that groundwater is polluted, likely due to the extensive use of fertilizers for agriculture. The concentration decreases in deeper samples, as expected from natural nitrate reduction.

Table 4.1 Basic statistical descriptors of the physicochemical parameters from groundwater and surface water: n—number of samples, max—maximum, min—minimum, med—median, ave—average and std.—standard deviation. Units: Temperature (Temp) in ◦C, EC in µS/cm (25 ◦C), total dissolved solids (TDS) and ions in mg/L.

	pH	**EC**	**TDS**	**Na^+**	**K^+**	**Ca^{2+}**	**Mg^{2+}**	**FeTotal**	**Mn^{2+}**	**NH_4^+**	**Cl^-**	**SO_4^{2-}**	**NO_3^-**	**HCO_3^-**	**PO_4^{3-}**	**Br^-**
Depth from 3.5 to 110m																
N	110	110	110	110	110	110	110	110	110	110	110	110	110	110	110	110
Max	8.7	35,509	16,155	4903	150	979	912	31	23	15	4,935	4,219	341	1022	20	108
Min	4.2	162.0	85.6	8.9	0.3	3.3	2.0	0.0	0.0	0.0	16.2	0.0	0.2	0.0	0.0	0.3
Med	7.3	1,471.5	984.6	173.7	5.6	53.0	25.9	0.0	0.2	0.1	138.4	104.6	22.3	366.0	0.3	2.5
Ave	7.2	2,968.9	1,617.1	358.9	20.6	85.3	51.6	1.5	0.8	0.8	425.1	210.3	48.7	404.0	0.9	7.7
Std	0.68	4,856.1	2,055.7	622.8	30.7	130	110.3	4.5	2.4	2.1	877.8	444.6	61.8	239.4	2.3	16.9
WHO standards of maximum value for drinking water (mg/l)																
			600	200			50				250	250	50			
Degree of Restriction on Use for irrigation																
			ml	meq/l							meq/l		mg/l	mg/l		
Slight to			450-													
Moderate			2000	> 3							4-10		5-30	1.5-8.5		
Severe			> 2000	> 9							> 10		> 30	>8.5		

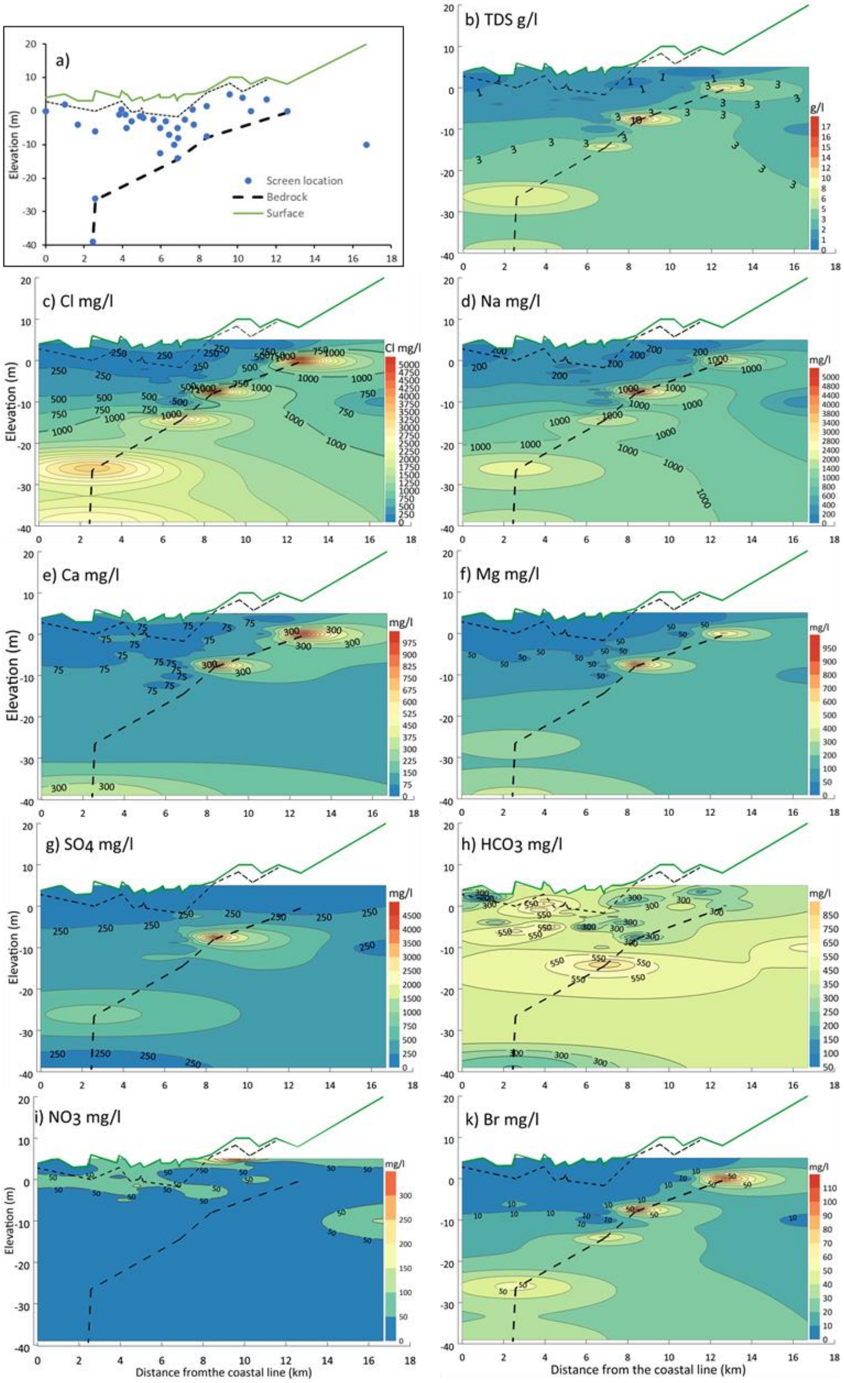

Figure 4.1 (a) Vertical well screen positions along the DC profile in Figure 2.1. The thick black dashed line indicates the bedrock surface, the green line is the surface elevation line, and the thin black line is the elevation of the water table in the wells. (b–j) interpolation of TDS and ion concentration from water samples along profile DC.

Among the 110 water samples, 72 water samples are exceeding the WHO limit (WHO, 2017) for drinking water (

Table 4.1) for at least one ion, including Mg^{2+}—18 samples, Na^+—48 samples, Cl – 33 samples, SO_4^{2-}—24 samples, NO_3^-—41 samples and TDS—53 samples. Following the guidelines for evaluation of water quality for irrigation given by Ayers and Westcot (Ayers and Westcot, 1985) (

Table 4.1), all water samples have a degree of restriction on use for irrigation including TDS—82 samples, Na^+—46 samples, Cl^-—30 samples, NO_3^-—32 samples and HCO_3^-—70 samples for the slight–moderate degree; and TDS—19 samples, Na^+—48 samples, Cl^-—24 samples, NO_3^-—46 samples and HCO_3^-—32 samples for the severe degree.

4.3.2 Classification of Water

According to Stuyfzand’s classification, 56% of the water samples are fresh whereas 19% and 15% are fresh-brackish and brackish, respectively. Only 10% of the samples in the Luy river catchment are brackish-salt. The spatial distribution of water types in terms of Cl^- content is shown in Figure 4.2a. Most brackish-salt water samples are located along the Luy river close to the sea and at larger depth. However, some brackish and brackish-salt samples taken at depth less than 15 m are located far from the coast up to 15 km inland. Globally, there is no clear trend in the distribution of salinity in shallow samples. This observation confirms geophysical observations that identified a strong variability at the small scale (Cong-Thi et al., 2021). Samples collected in the pairs of shallow/deep wells also systematically indicate a higher salinity at depth.

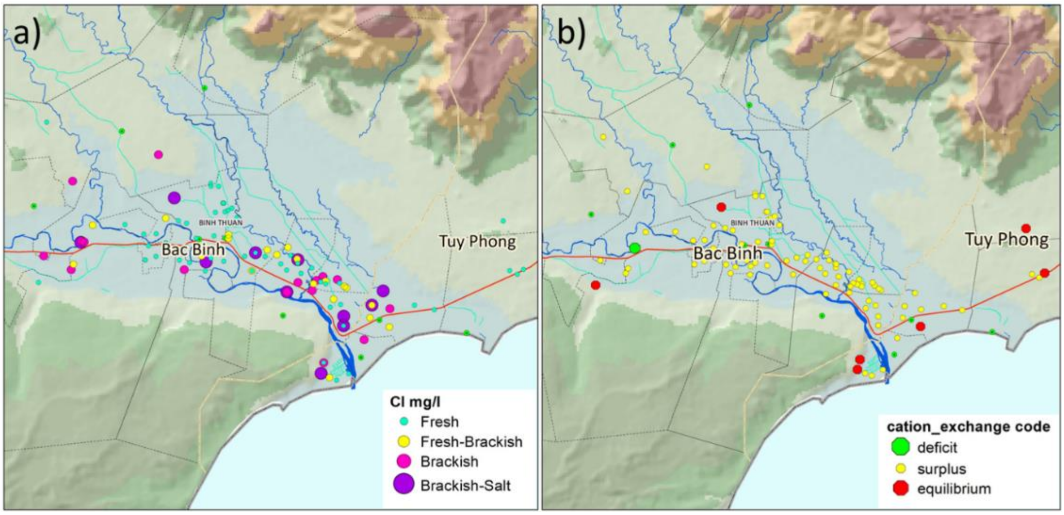

Figure 4.2 (a) Water type distribution based on the Cl^- content and (b) the distribution of cation exchange code of water samples in the Luy river catchment.

Figure 4.2b illustrates the spatial distribution of the cation exchange code. Most samples in the Luy river catchment show a surplus of (Na + K + Mg), indicating that freshening processes are dominant. This can be counterintuitive as the local population is experiencing salinization of its water resources (Tran, 2020). However, freshening processes are generally acting at a longer time scale than salinization (Walraevens and Van Camp, 2004). The hydrochemical composition of water needs more time to respond to a new equilibrium compared to hydrodynamics. Therefore, from the observations, it seems that most of the samples in the Luy River have been experiencing freshening processes from the past, even if salinization processes might take place in the present.

Most of the samples in equilibrium are located in the dunes on the sides of the Luy river; only one sample is located in the plain. This suggests that the chemical composition of groundwater has reached an equilibrium in these locations, which can be related to a preferential recharge in dune areas (Paepen et al., 2022). Only one sample in deficit is observed, located far away from the coast.

4.3.3 Hydrochemical Facies Using Piper and HFE-D Diagrams

The Piper diagram in Figure 4.3a shows the groundwater composition and water types. The NaCl water type is the most abundant (44.5% of the samples) whereas the Na-Mg-SO_4 water type represents the minority (1.8% of the samples). The mixing Na-HCO_3-Cl water type corresponds to 20.9% and the Ca-Mg-HCO_3, Ca-Mg-Cl-SO_4 and Na-HCO_3 water types represent 15, 13 and 5% of the samples, respectively.

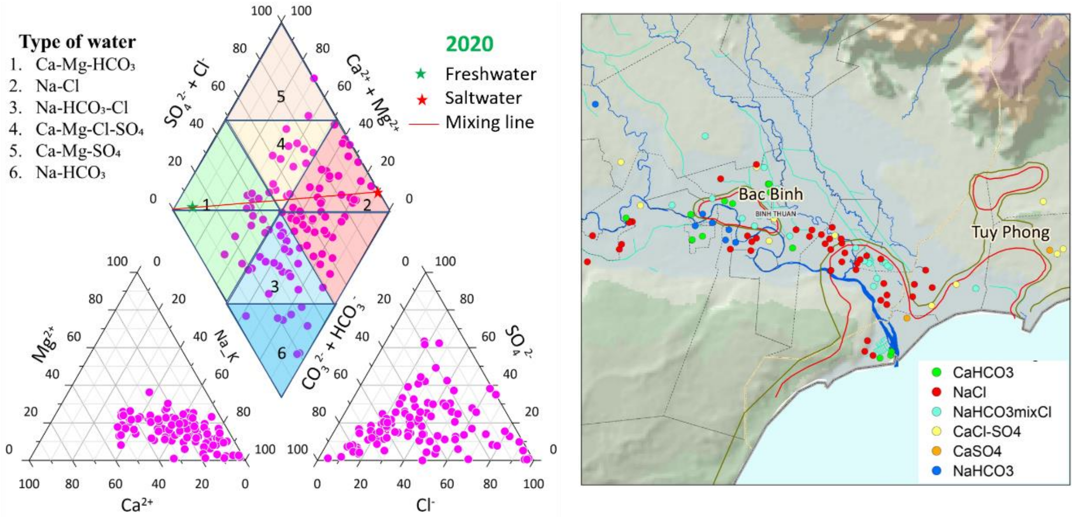

Figure 4.3 (a) Piper diagrams of groundwater samples in the Luy river catchment (the purple dots) and (b) water type from the Piper diagram distribution.

The distribution of the water types from the Piper diagram is mapped in Figure 4.3b. The NaCl water type extends along the Luy river from the coastal line to around 18 km inland. The distribution of groundwater samples in the Piper diagrams shows that the freshening process is dominant.

Figure 4.4a illustrates the distribution of groundwater samples in the HFE diagram. The 8 sub-stages of freshening and saltwater intrusion combined with their water type are mapped in Figure 4.4b and listed in Table 4.2. The map reveals that the freshening phase extends largely in the study area, which is characterized by the sub-stages of proximal facies f4 + FW and f3. This can be explained by the abundance of the shallow water samples and the lack of deep-water samples. The distal facies corresponding to sub-stages f2 and f1 are less abundant and some occurrences are observed far from the coast. The main recharge areas are recognized by the freshening facies that are most proximal to the FW end-member observed on the right bank of the Luy river and at the higher elevation parts in the left bank.

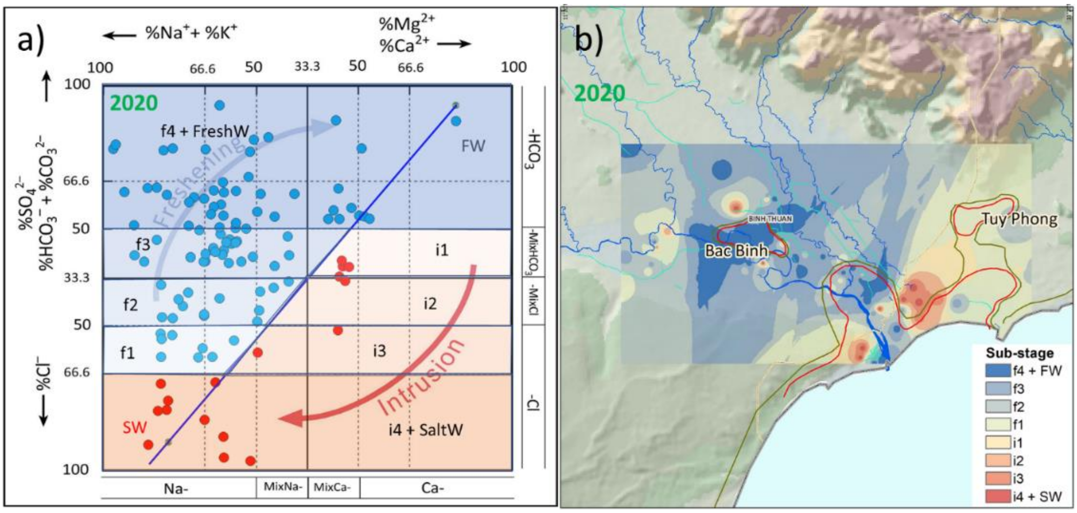

Figure 4.4 (a) HFE diagram and (b) distribution of sub-stages of water samples in the Luy river catchment, the red balls are the samples in the intrusion zone and the blue balls are in the freshening zone.

Table 4.2 Distribution of sub-stages in freshening and intrusion phases for 110 water samples collected in the rain season 2020.

	FW+f4	f3	f2	f1	i1	i2	i3	SW+i4	Total
Number	45	26	14	8	4	1	2	1	110
Percentage	41	24	13	7	3.5	1	1.5	1	100
freshening					intrusion				
	proximal	←	distal			distal	→	proximal	

Saltwater intrusion is observed in the coastal zone with the proximal facies i3 and SW + i4 at different depths in both deep and shallow wells. These samples might result directly from the sea or the estuary. Both the proximal and distal saltwater intrusion facies are also observed locally far inland, mostly from shallow wells of less than 15 m depth. The saltwater and salinization processes in the shallow boreholes (less than 15 m depth) might be explained either by infiltration from the river, when close to it, by upconing processes from the deeper aquifer when the shallow aquifer is exploited or by the existence of clay lenses where saltwater has been trapped.

4.3.4 Ionic Relation and Origin of Solutes

The composition of groundwater samples was plotted using pairs of ions (Figure 4.5). Figure 4.5a,b show the relation of Na^+ versus Cl^-; the halite dissolution was added as the 1:1 line. Samples lying on the mixing line or 1:1 line indicate simple mixing processes and halite dissolution, respectively. Most of the samples observed above the mixing line and 1:1 line shows an Na^+ surplus that might originate from cation exchange in freshening processes. The Na^+/Cl^- vs. Cl^- ratio diagram shows that almost all samples are located above the seawater ratio line, confirming an excess of Na^+, with a few samples located on the mixing line.

Figure 4.5c shows the correlation of Ca^{2+} versus Cl^-. Many samples located above the theoretical mixing line indicate an excess of Ca^{2+}. The presence of an excess in the majority of samples indicates that the saltwater intrusion process is occurring concurrently with freshening in various locations. The graph illustrates how cation exchange during salinization causes the excess Ca^{2+}. This enrichment of Ca^{2+} may also come from calcite/dolomite dissolution or freshwater recharge. This will be further investigated using the saturation index.

Figure 4.5d shows the relation of Ca^{2+} versus HCO_3^- adding the calcite dissolution line. The high HCO_3^- value indicates the freshwater environment and the bicarbonate enrichment. The much higher HCO_3^- content (a thousand mg/l) combined with the excess of Ca^{2+} might be related to the second stage of calcite dissolution.

The SO_4^{2-} anion is considered to originate primarily from seawater. The surplus of sulfate in the SO_4^{2-} vs Cl^- diagram (Figure 4.5e) where most of the water samples are located above the mixing line, suggests not only a seawater origin but also another contamination source such as fertilizers or due to pyrite oxidation.

The plot of NO_3^- vs Cl^- in Figure 4.5f shows the enrichment of nitrate up to 5.5meq/l. The excess of nitrate is believed to stem from infiltration of fertilizers from the surface as agriculture activities are intense in the Luy river catchment.

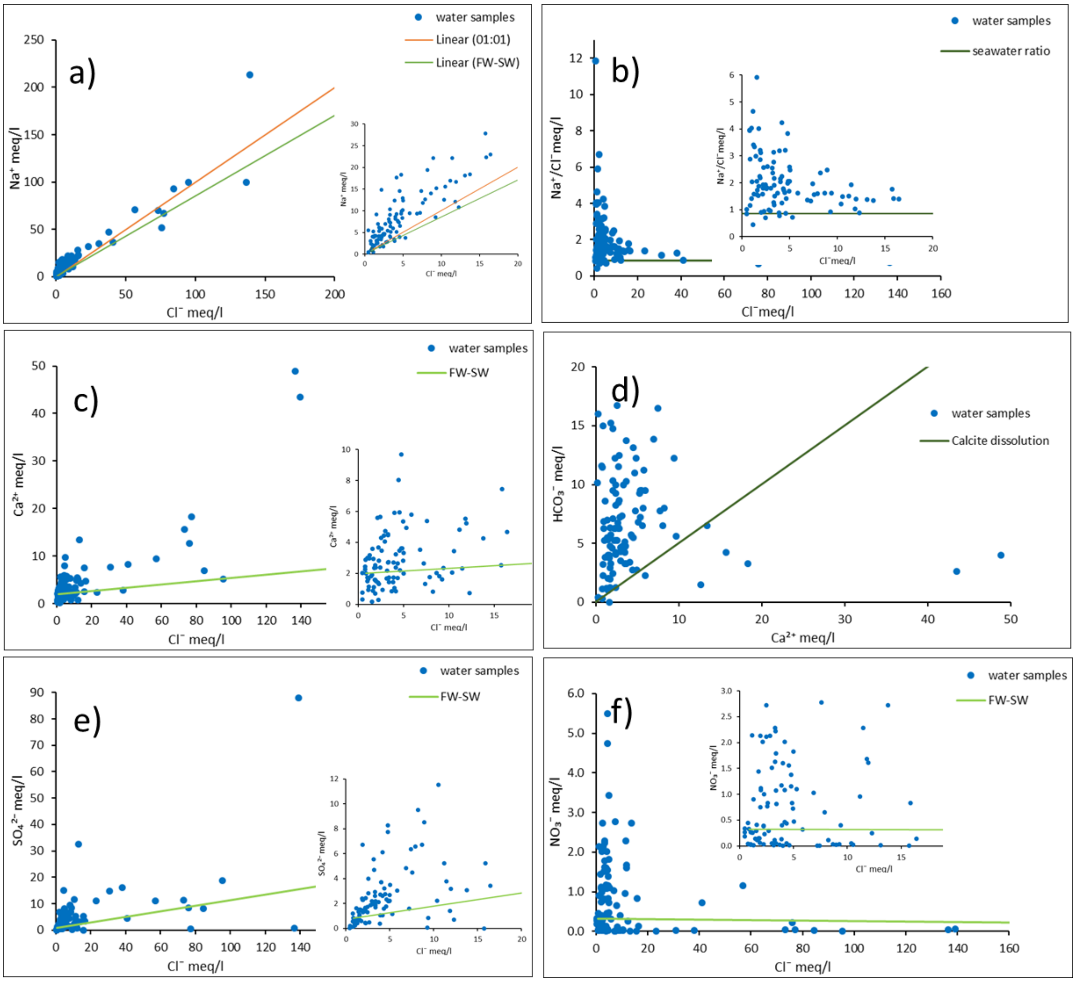

Figure 4.5 Plots of Na^+ (a), Ca^{2+} (c), HCO_3^- (d), SO_4^{2-} (e) and NO_3^- (f) with respect to Cl^- and their ionic ratios (b) for groundwater samples.

4.3.5 Water/Rock Interaction and the Origin of Solutes

The Luy river plain is characterized by shallow Holocene sediments including clay, silt, sand mixed with gravels, grits and pebbles or shelf fragments originating from fluvial-marine sediments. The deeper sediments consist of fine to medium grain quartz sand from the Pleistocene. The bedrock mainly consists of granite, sandstone and siltstone, which also surrounds the basin in its upstream part. If Ca^{2+}, Mg^{2+}, SO_4^{2-} and HCO_3^- are resulting from calcite, dolomite and gypsum dissolution, then an equilibrium should exist between cations and anions (Fisher and Mullican, 1997). It also means water samples should be in or close to the 1:1 linear trend. The cation exchange factor plays a significant role in the freshening and salinization process (Walraevens and Van Camp, 2004). In a saturated solution, Ca^{2+} and Mg^{2+} supplied by calcite, dolomite and gypsum dissolution are replaced by Na^+ originating from NaCl. On the other hand, HCO_3^- presents the calcite and dolomite dissolution and Cl^- and SO_4^{2-} record how much halite and gypsum are dissolved, respectively. It can also be derived from seawater. A diagram of ($Ca + Mg - SO_4 - HCO_3$) versus ($Na + K - Cl$) (Figure 4.6a) is plotted to examine the amount of Na^+ gained or lost relative to the supply by halite dissolution and the gain and loss of Ca^{2+} and Mg^{2+} related to the supplement by gypsum, calcite and dolomite dissolution. The linear correlation of these parameters with a slope of −1 suggests (Figure 4.6b) the cation exchange governs the composition of groundwater, and the lower right corner in the diagram represents the participation of cation exchange in the freshening process (Fisher and Mullican, 1997).

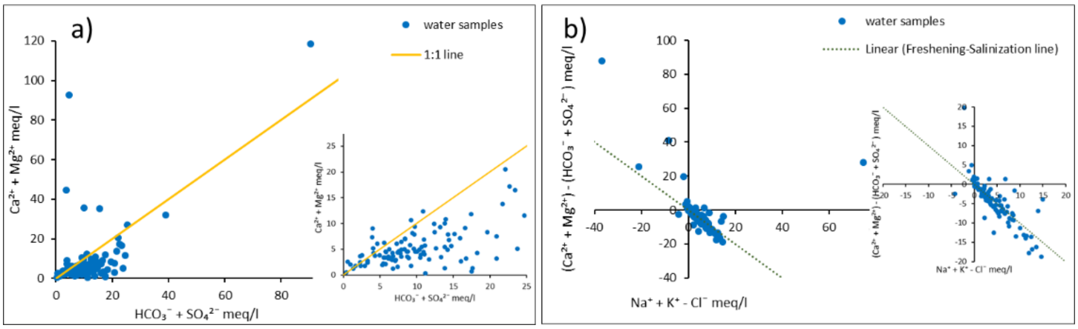

Figure 4.6 Relationship between (HCO_3 + SO_4) versus (Ca + Mg) and (Ca + Mg - SO_4 - HCO_3) versus (Na + K – Cl).

The water samples are located mostly under the 1:1 line presenting an enrichment of HCO_3^- + SO_4^{2-} and a deficiency of Ca^{2+} + Mg^{2+}, then the residual negative charge of HCO_3^- + SO_4^{2-} must be balanced by Na^+. This suggests cation exchange processes are occurring during freshening and confirms the analysis of the processes of freshening and saltwater intrusion from other analysis.

4.3.6 Speciation-solubility calculations

The most common forms of calcium in sedimentary rock are carbonates. There are two crystalline forms, calcite and aragonite with the same formula $CaCO_3$, and the mineral dolomite can be described as $CaMg(CO_3)_2$. Other calcium minerals common in sediments consist of the sulfates gypsum ($CaSO_4.2H_2O$) and anhydrite ($CaSO_4$) and more rarely, fluorite (CaF_2). Calcium can also exist as a component of some types of zeolites and montmorillonite. The dissolution of the retained shells can be simply represented as the ion Ca^{2+} in the solution.

According to Hem (1985), in some conditions, a bicarbonate concentration near 1000 mg/l correspond to about 10% of the calcium found in $CaHCO_3^+$ form. Similarly, more than half the calcium might be represented in the form of the $CaSO_4$ ion pair if sulfate concentrations is above 1000 mg/l.

The saturation index of calcite, dolomite, halite and gypsum is plotted in Figure 4.7 against the concentration in Cl^-, used as a proxy for salinity. 56% of the water samples represented in Figure 4.7a are supersaturated with respect to calcite. Such index value reflects groundwater containing an abundant amount of calcite with sufficient resident time to reach equilibrium, calcite will be precipitated in suitable conditions. The rest of the samples are undersaturated with respect to calcite suggesting the samples might come from an environment poor in calcite or where Ca^{2+} has another form or has not reached equilibrium due to short residence time. Figure 4.7b shows that dolomite has a similar trend with 57% oversaturated samples with dolomite respectively reflecting a dolomite enriched environment.

The principal source of carbon dioxide species that produce alkalinity in surface or groundwater is the CO_2 gas fraction of the atmosphere, or the atmospheric gases present in the soil or the unsaturated zone lying between the surface of the land and the water table (Hem, 1985). When CO_2 dissolves in water, gaseous CO_2(g) becomes aqueous CO_2 (aq), and form carbonic acid, H_2CO_3 that can favor calcite dissolution.

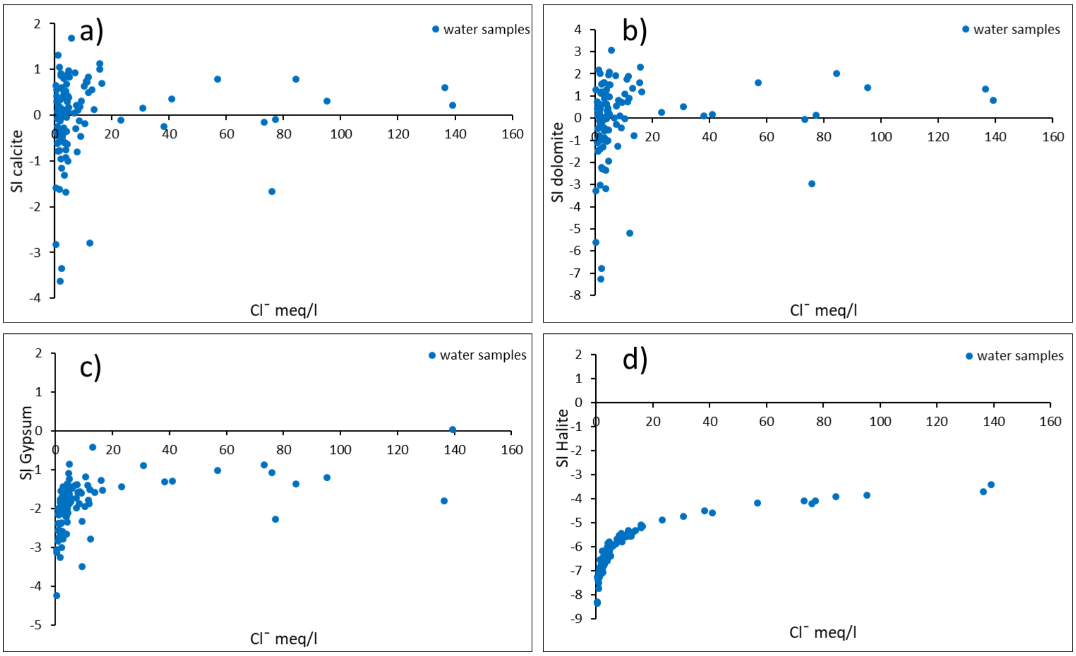

Figure 4.7 Saturation index for calcite, dolomite, gypsum and halite versus Cl^- concentration.

Fifty-six percent of water samples have a positive saturation index with respect to calcite and dolomite. Then the HCO_3^- concentration could increase in the water samples following the dolomite and calcite dissolution reactions. It also causes higher Ca^{2+} and Mg^{2+} concentrations which will be adsorbed by clay and desorbed Na^+ in the water samples. This process can explain the high HCO_3^- concentration and the apparent enrichment of Ca^{2+} (Figure 4.5c). Therefore, a high HCO_3^- concentration is produced from calcite and dolomite dissolution at a pH less than 6.3.

The water samples are all undersaturated with respect to halite suggesting there are no mineral formed of halite in the study area. The same observation is valid for gypsum except for one oversaturated sample which may relate to the dissolution of gypsum from previous saltwater intrusion (Gomis et al., 2000).

An ionic delta was calculated for all major cations Na^+, Ca^{2+}, Mg^{2+} and K^+ and anions HCO_3^-, SO_4^{2-} and NO_3^-. The result confirms the cation exchange during the freshening/saltwater intrusion processes, as well as the enrichment of the anions SO_4^{2-} and NO_3^- in some samples, indicating pollution.

4.3.7 Variation of hydrogeological parameters of groundwater with time

The sampling campaign was repeated during the dry season of 2021. We could only record information from 90 out of the 110 wells visited in 2020, the other ones were either dry or had been abandoned. Only 20 wells had lower TDS values from 15 to 4821 mg/L, while 70 wells had higher TDS from 7 to 32054 mg/l. Figure 4.8 shows the locations of the wells with increasing and decreasing salinity as well as the water level going up or down between the two measuring periods. In general, the salinity increased, mostly in the wells located in the left bank and decreased in the right bank of the Luy river. Water level seems to go down in the inland part and rise up in the estuary area which might be a result of the tides. Based on these results, 33 groundwater samples were collected, including the 18 water samples from our new monitoring wells (except the 2 that were dry) and the 15 samples that had an absolute difference in TDS value greater than 500 mg/l.

The 33 water samples collected in both the rain season 2020 and dry season 2021 were used to analyze their temporal evolution (

Table 4.3). On average, the concentration of all the ions increased except for stable PO_4^{3-} and decreasing of NO_3^- concentrations. The ions Na^+, Cl^- and SO_4^{2-} present extremely high concentrations at some locations in 2021 compared to 2020 (such as Na^+ – 8204mg/l, Cl^- – 19752 mg/l and SO_4^{2-} – 5865 mg/l) that identify the presence of saltwater in the groundwater samples ($Cl_{seawater}$ = 19000 mg/l) and a possible stronger SWI in the dry season.

Similar patterns of increasing salinity in the dry season are evident in the primary type of classification since the fresh and fresh brackish water types decrease from 57.6% to 30% in total while the brackish water and saltwater types increase from 12% to 27% and from 0% to 6% respectively. The brackish-salt water type decreases slightly from 30% to 27%. This suggests the salinity increases in both freshwater and saline water zones in the dry season.

The Stuyfzand classification in term of cation exchange code shows that the water samples which have a surplus code corresponding to water samples involved in freshening process (release of Na^+) decrease from 28 samples (85%) to 22 samples (67%). In contrast, the samples in deficit which indicate saline intrusion with cation exchange processes increase from 1 sample (3%) to 7 samples (21%). 4 samples (12%) are in equilibrium in both sampling periods, but not necessarily at the same locations. This is a confirmation of the increased salinity in the dry season. Figure 4.8 shows the location of the samples with their cation exchange codes changing between 2020 and 2021. The deficit code (indicating saltwater intrusion) is visible up to 14 km from the coast. This identifies the presence of saltwater intrusion at larger distance from the river in the dry season 2021. The salinization process can hardly be explained with direct intrusion from the river, but is likely related to pumping activities inducing some upconing from saltwater already present at depth or trapped in clay-rich zones.

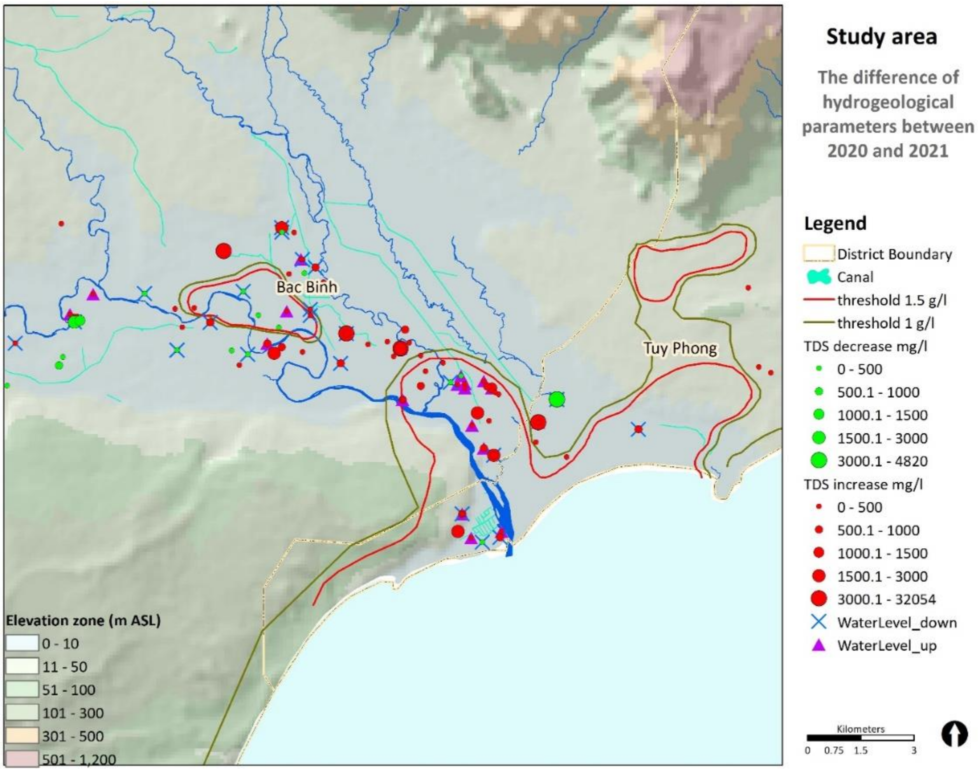

Figure 4.8 The difference of the hydrogeological parameters between 2020 and 2021.

Table 4.3 Summary of chemical composition variation of 33 water samples.

mg/L	**TDS**	**Na^+**	**K^+**	**Ca^{2+}**	**Mg^{2+}**	**Cl^-**	**SO_4^{2-}**	**NO_3^-**	**HCO_3^-**	**PO_4^{3-}**	**Br^-**
Increasing from 2020 to 2021 in 33 samples											
%	88	94	82	76	79	91	61	36	58	45	76
Max	23729	5921	303	306	1157	16372	1646	173	246	1	152
Min	3.7	0.4	0.1	1.3	0.1	0.8	2.2	0.4	3.7	0.1	0.2
Ave		453	22	69	93	1346	204	640	718	0.3	11
Decreasing from 2020 to 2021 in 33 samples											
%	12	6	18	24	21	9	39	64	42	21	21
Max	2056	512	23	129	12	990	621	36	267	4	12
Min	63	33	0.2	0.5	0.3	0.4	2.3	0.7	8.5	0.1	0.5
Ave	623	273	6	38	5	332	111	7	112	1	5

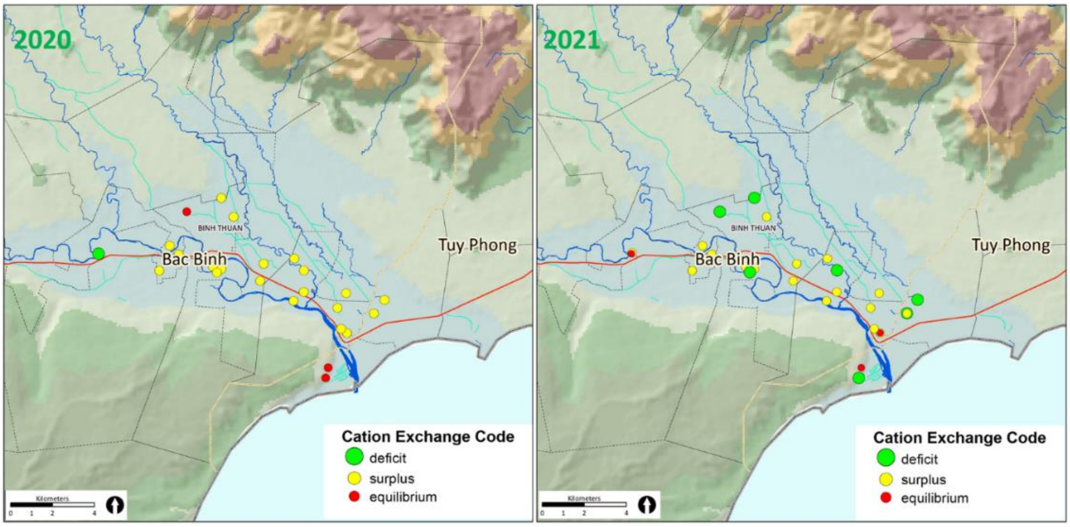

Figure 4.9 Distribution of the cation exchange codes of 33 water samples collected in 2020 (in rainy season) and 2021 (in dry season).

The water samples collected in 2020 and 2021 at the same locations are plotted in the HFE diagram to observe the water faces variation during the time periods (Figure 4.10).

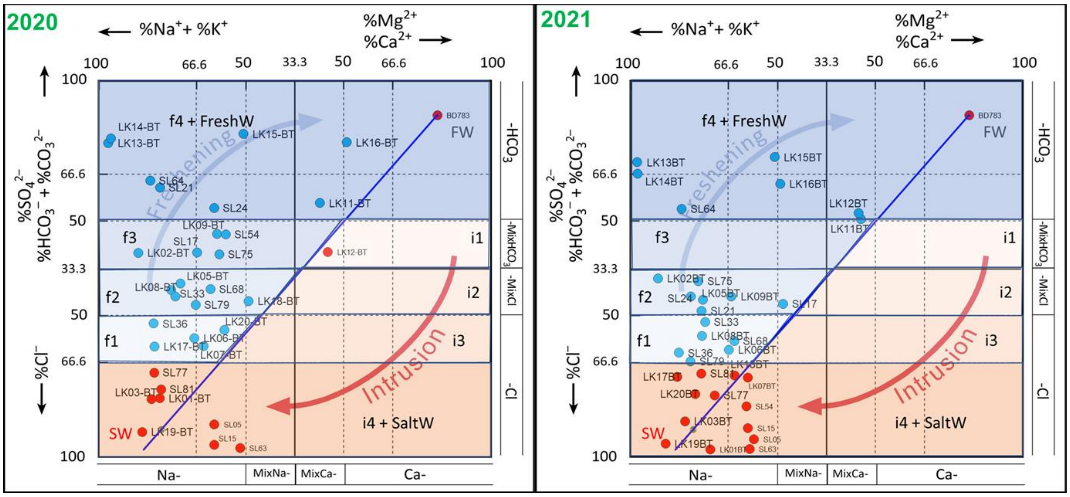

Figure 4.10 Representation of 33 samples collected in the rain season 2020 and dry season 2021 on the HFE-Diagram.

The distribution of sub-stages in freshening and intrusion phases for the two sampling periods is shown in Table 4.4. Water samples situated in the freshening field decrease from 73% in 2020 to 60% in 2021. The sub-stages range regularly from distal to proximal to the freshwater in the freshening field while there are few samples located in the distal and proximal facies in the intrusion field. The water samples located in the intrusion field at the two periods are mostly located in the seawater field which is located in the first quarter corner of the HFE-Diagrams. This representation identifies that freshening is the main process occurring in this study area resulting in an increase of the marine cations Na^+, K^+ and Mg^{2+} and decrease of Ca^{2+} in the groundwater, but that seasonal variations are impacting the freshening sub-stages.

Table 4.4 Distribution of sub-stages (in %) in freshening and intrusion phases for each sampling period.

	FW+f4 (%)	**f3** (%)	**f2** (%)	**f1** (%)	**i1** (%)	**i2** (%)	**i3** (%)	**SW+i4** (%)	**Total** (%)	**N**
July 2020	25	15	18	15	3	0	0	24	100	33
April 2021	21	0	21	18	0	0	0	40	100	33
freshening					intrusion					
proximal ← *distal*					*distal* → *proximal*					

The distribution of the water samples from Figure 4.10 shows that samples from the sub-stages f1, f2, f3 tend to move back to the seawater corner in the dry season 2021, what corresponds to a higher proportion of Cl^-.

4.4 Conceptual model of the salinity evolution in the Luy river catchment

In this study, 110 groundwater samples were collected and analyzed in the Luy River catchment. They confirm the presence of brackish to saline water in the unconsolidated coastal aquifer. The analysis of the chemical composition of the water samples brings new evidence to reveal the origin of the salinity:

1. In total, 65 % of the samples are exceeding the WHO limit for drinking water and a 100% of them has a degree of restriction on use from slight - moderate to severe in potential irrigation problems according to FAO;
2. Next to the salinity, the aquifer is locally strongly contaminated by nitrates, and to a lesser extent sulfates. The origin of the nitrate is attributed to the excessive use of fertilizers in the study area. Although leaking sceptic tanks and sewage systems cannot be excluded, most data were collected in rural zones dominated by agricultural fields where the use of fertilizers is documented;
3. The systematic collection of water samples in the deeper part of the aquifer has revealed the recurrent presence of saline water at depth, with a systematic increase of salinity at depth at locations where nested wells were installed. This observation is confirmed both by geophysical data acquired in the summer 2019 (Figure 4.11, Cong-Thi et al., 2021) and interviews performed with the farmers. It confirms that estimation of the fresh-saline interface from previous studies based only on shallow wells underestimated the actual extent;
4. If the downstream and deeper part of the aquifer is systematically saline, the distribution of salinity in the upstream part is complex, with sharp variations at short distances making it difficult to predict the salinity. Saline water samples have been detected as far as 14 km inland. These observations are also confirmed by the geophysical survey (Cong-Thi et al., 2021).

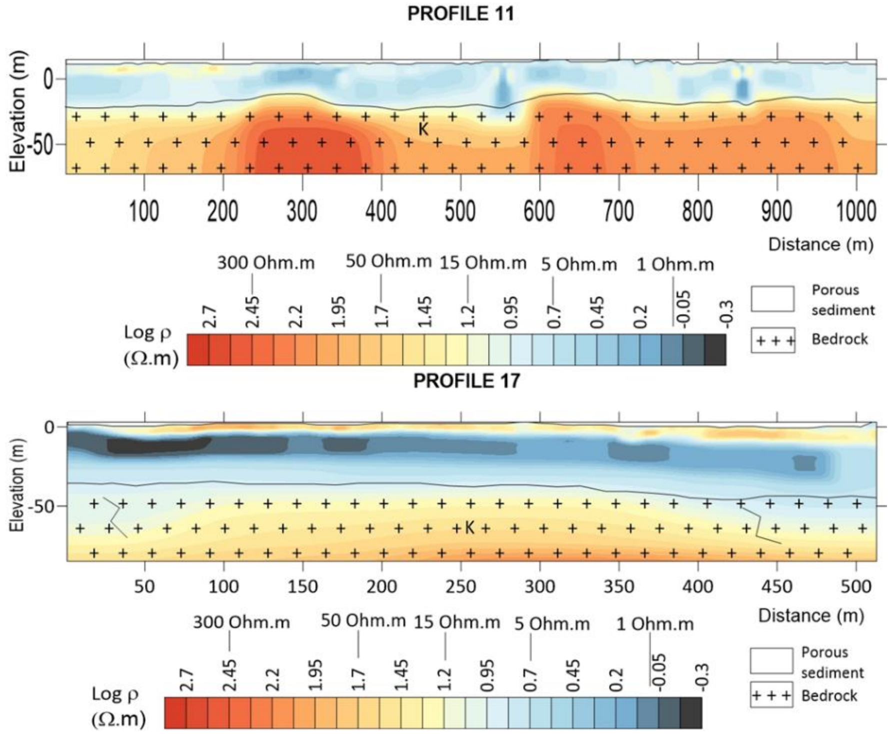

Figure 4.11 The presence of saline water at depth (modified from Cong-Thi et al., 2021).

5. The chemical composition of most of the water samples clearly shows a domination of freshening processes in the coastal aquifer. The Stuyfzand classification, the Piper diagram, the HFE diagram and the analysis of the correlation with conservative anions demonstrate that the aquifer is dominated by NaCl and $NaHCO_3$ water types with a systematic excess in Na^+. This points towards an enrichment of Na^+ related to cation exchange processes during freshening processes. This is likely the results of the natural freshening of the aquifer since the last water high stand. The freshening of the aquifer is likely a slow process, considering that (i) the shallow aquifer is drained by the Luy River and its tributaries, (ii) the bottom of the aquifer is up to several tens of meters below sea level and (ii) the climate is semi-arid with limited recharge. Although this observation seems counterintuitive at first sight given that the local population is experiencing salinization of the water resources, we think that the presence of

fossil saltwater both at depth and trapped in low permeability area can act as a secondary salinization source when the shallow and thin fresh aquifer is exploited. This is further supported by the samples located in the dune areas, which show a water composition in equilibrium. Dunes are preferential recharge zones where freshening processes can occur at a faster rate.

6. Seasonal variations in the salinity exist in the aquifer, although they are limited. 78% of the sampled locations experienced an increase in salinity between the summer 2020 (wet season) and the spring 2021 (dry season), but it was significant (TDS increases greater than 500mg/l) only in 21% of the locations (19 samples in 90 samples recorded in 2021). This increase in salinity is characterized by a shift in the chemical composition of the sample. Although freshening processes remain dominant, the freshening signature is less pronounced. This is likely a result of the absence of recharge during the dry season, combined with the local exploitation of the shallow aquifer for agriculture and aquaculture and the presence of saltwater at depth and trapped in low permeability zones, resulting in upconing and salt migration. This is also confirmed by the experience of farmers who often see their wells becoming saltier and sometimes dry during the dry season.

Based on the above observations, we propose a new conceptual model for the evolution of the salinity in the Luy river catchment. The simplified hydrogeological processes of relevance to saltwater intrusion and freshening are represented in Figure 4.12 following the CD profile direction (Figure 2.1).

During the last transgression, corresponding to the high water stand about 6000 years ago, the study area was largely invaded by the sea and the pores of the aquifer were filled by seawater, except in the high elevation dune area and highland (Figure 4.12a). When the water level started to decrease, freshwater recharge from the surface through rainfall and underground from the adjacent mountainous areas initiated the freshening of the aquifer resulting in the current chemical signature. However, the plain is mainly made up of clays, clayey and silty sand which have a relatively low permeability. Combined with a typical semiarid climate where recharge is limited, an important draining system through the Luy River and its tributaries, this saltwater has a long residence time and the aquifer has not reached a new equilibrium yet, especially at depth and in low permeability zone (Figure 4.12b). This presence of paleo-groundwater can explain why groundwater salinity can change from fresh to brackish over short distances in clayey areas, and why the deep aquifer is still saline because of density-driven flow. At the opposite, the dune areas have been freshened more quickly, and constitute important freshwater reserves in the area.

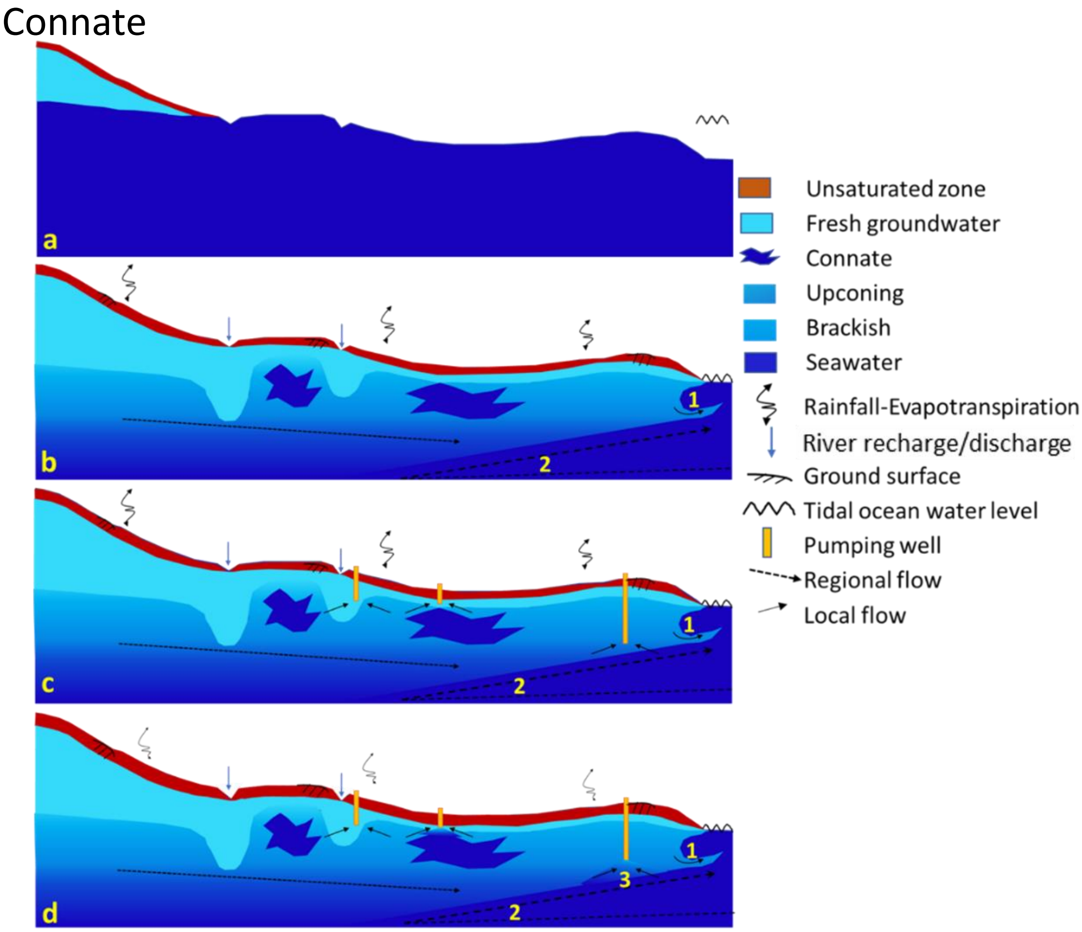

Figure 4.12 Simplified diagrams of the coastal aquifer in the Luy river catchment: 1- coastal fringe processes such as tidal seepage face and upper seawater recirculation zone, 2- density driven circulation in the seawater zone, 3- seawater upconing due to well pumping.

The saltwater intrusion and freshening processes in the different time: a- Seawater covered the catchment during the past transgression, b- natural freshening, c and d- freshening and saltwater intrusion affected by human activities during rainy and dry seasons respectively.

Locally, this paleo-groundwater can act as a secondary source of salinity for salt-water intrusion when freshwater at shallow depth is extracted for irrigation – salinization occurs by upconing or lateral migration as illustrated in Figure 4.12c,d. In the wet season, there is the development of a freshwater lens on top, which is likely exploited and drained by the river in the dry season, resulting in decreasing water level and upconing. Close to the Luy river, direct infiltration of saltwater is possible during high tides, especially in the dry season when the flow rate is limited. However, the large-scale spreading of river infiltration should be limited by the overall draining character of the river. Irrigation with freshwater from dams can also affect the recharge pattern and further perturb the natural situation. This new conceptual model of the aquifer should be tested in future work. The acquisition of isotopic data should allow to identify more clearly the freshening and salinization source and as well as the age of groundwater (Craig, 1961; Fritz and Fontes, 1989). Groundwater modelling could also be used to test the hypothesis to verify if the timescale of the freshening processes is consistent with the hydraulic properties and the water balance in the catchment (Zwertvaegher et al., 2013; Lebbe 2018).

4.5 Conclusions

The hydrogeochemical analysis of 110 groundwater samples collected from the Luy river coastal aquifers in the summer 2020 was studied and complemented by 33 new analyses made after the dry season in the spring 2021. The general chemical composition of groundwater was analyzed however the isotope components of hydrogen, oxygen and carbon which uses to estimate the origin and age of groundwater are missing. We also need more water samples in the deeper aquifer, then we will have a completed understanding the processes occurring at the depth.

The findings support the current freshening trend in the aquifer. In comparison to the dry season, the freshening characteristic is more advanced in the rainy season. Salinization is stronger in the deeper aquifer and during the dry season which results of a lack of recharge and exploitation of the aquifer. They also confirm the observations from geophysical data revealing that (i) saline intrusion is not limited to the zone close to the river but extends further inland and at depth; (ii) salinity can vary quickly at short distance.

These analyses allowed us to propose a new conceptual model for the evolution of salinization in the Luy river catchment explaining the salinity distribution, the freshening trend and the salinization during the dry season. We consider that saltwater originally in place after the last water high stand has been progressively freshened by recharge from precipitation and from the mountainous area explaining why samples in elevated areas show freshwater facies and an equilibrium. This freshening process is not complete in the low-lying areas, at depth and in clay-rich zones where paleo-groundwater is still entrapped. This saltwater acts as a secondary salinization source during the dry season when the farmers exploit the thin shallow freshwater lens present in the Holocene aquifer.

This conceptual model is extremely important for the management of water resources in this semi-arid region of Vietnam particularly vulnerable to climate change. Combined with an analysis of the water balance (recharge: precipitation, fluxes, river and canal recharges and discharge: pumping, evaporation, and river drain) and of the hydraulic conductivity of the aquifer layers, it will form the basis for the development of a groundwater model of the study area and eventually to sustainable management scenarios for this coastal region, preventing further deterioration of the groundwater resources. In view of rising sea levels in the future due to climate change, saltwater intrusion in the river estuary will increase instead of decrease. It is recommended to reduce the future exploitation of the aquifers and increase the surface water recharge through irrigation or artificial recharge to ensure a sustainable use of the groundwater resource in this coastal region and to prevent further deterioration of quality in the shallow groundwater.

Chapter 5. Groundwater modelling to validate saltwater intrusion and freshening processes identified from hydrochemistry in a coastal groundwater system in Vietnam

Pham Dieu Linh[1,3,*], Marieke Paepen[1], Cong-Thi Diep[1,3], Alexander Vandenbohede[5], Tam Vu Thanh[4], Hieu Huu Ho[3], Frédéric Nguyen[2], Thomas Hermans[1]

[1] Laboratory of Applied Geology and Hydrogeology, Department of Geology, Ghent University, Krijgslaan 281-S8, 9000 Ghent, Belgium
[2] Liege University and KU Leuven, B- 4000 Liège and 3000 Leuven, Belgium
[3] Vietnam Institute of Geosciences and Mineral Resources (VIGMR), 100000 Hanoi, Vietnam
[4] National Center for Water Resources Planning & Investigation (NAWAPI) 100000 Hanoi, Vietnam
[5] De Watergroep, Brussels, Belgium
* Correspondence: Linh.PhamDieu@UGent.be

Abstract

Groundwater management requires an in-depth knowledge of hydrogeological processes taking place in aquifers. In case of saltwater intrusion processes, many factors may influence the salt concentrations, including natural factors (sea level, river estuaries, freshwater recharge), hydraulic properties, anthropic factors (water extraction, drainage) and the past history of the region (presence of paleogroundwater). In such a context, groundwater numerical models can provide valuable information about the functioning of the hydrogeological systems and evaluate the influence of the above-mentioned factors. In this study, we validate a conceptual model of saltwater intrusions based on hydrochemical analysis using a numerical model, in particular if the timing of freshening processes is in line with the presence of paleogroundwater. A three-dimensional stratigraphic model of the Luy River catchment, Binh Thuan province, Vietnam, is constructed using the existing well logs, geophysical data, and geochemical data. Several scenarios are then simulated for long

period of times (up to 5000 years) to analyze how freshening processes are influence by the hydraulic properties and geometry of the aquifer system. The results indicate that during extended periods of freshening, seawater becomes confined in the clay aquitard and the lower aquifers. This trend is worsened by the difference in density between saltwater and freshwater. The saltwater distribution is also influenced by the upper and lower boundaries of the aquifers. The saltwater distribution pattern in the most plausible scenario validates the conceptual model.

5.1 Introduction

Saltwater intrusion is one of the most common threats to coastal communities across the world (Werner et al. 2013). It not only degrades water quality by increasing salinity over acceptable drinking and irrigation water standards, but it also jeopardizes potential exploitation of coastal aquifers and may yield soil salinization.

Seawater encroachment inland is the most typical source of salinity rise, which often occurs in arid and semi-arid regions where groundwater constitutes the main freshwater resource. In addition, climate change poses a number of threats to aquifer systems that can lead to salinization, such as rising sea levels, changes in the recharge, and groundwater withdrawal, all of which can change the hydrologic balance in coastal aquifers (Park et al. 2005, Bennetts et al. 2006, Petalas and Lambrakis 2006). Salinization may also occur as a consequence of upconing, where saltwater is present at depth and rises up due to groundwater extraction (Werner et al. 2009). The presence of fossil seawater might also be a source of salinity (UNESCO 1987, Custodio 1997, Werner et al. 2013). This ancient saltwater is mainly found in low-permeability formations like clay and silty clay, where it remains trapped in the sediments (Pham et al., 2022; Cong-Thi et al., 2024).

Freshening processes, in contrast to saltwater intrusion, can also occur in coastal aquifers, for example, via freshwater recharge, decrease in exploitation flowrate, or artificial replenishment (Appelo 1994, Andersen et al. 2005, Lambrakis, 2006, Walraevens et al.

2004, Russak and Sivan 2010, Antonellini et al. 2015, Sarker et al. 2021). Freshwater recharge progressively infiltrates through the shallow soil toward the aquifers, causing decrease in salinity and chemical changes in the groundwater.

The Luy River catchment area is located on Vietnam's Southern Central coast, which is one of the driest regions of the country. According to a recent geophysical study using electrical resistivity tomography (Cong-Thi et al. 2021) in the Luy River catchment, saltwater predominates in the deeper portion of the coastal aquifer along the downstream portion of the Luy River. In contrast, the distribution of salinity in the shallow part is highly erratic. Salinity is distributed in a complicated manner, with large changes seen over very short distances and seemingly unrelated to proximity to the Luy river and its tributaries, but rather linked to the presence of clay layers and lenses (Cong-Thi et al., 2024).

Pham et al. (2022) has shown in a hydrochemistry study (Chapter 4) that freshening is the dominant process in the Luy River aquifers, and it is more pronounced in the rainy season. Due to a lack of recharge, the higher density of saltwater, and aquifer exploitation, salinization is more severe in the deeper aquifer and during the dry season at locations where groundwater is extracted for irrigation. They hypothesize that fossil saltwater entrapped within clay-dominated geological formations, originally infiltrated during the last water high stand about 6000 years ago, is the most probable source of saline groundwater, whereas the seawater entrance into the river estuary during rising tides causes the salinization along the downstream part of the river and its tributaries.

Modelling the density-dependent groundwater flow coupled with solute transport of the groundwater system in the past can be used to assess the current state of freshwater and saltwater distributions and to predict the effects of possible management actions (Oude Essink et al. 2010; Lebbe et al., 2012). A few studies have applied numerical saltwater transport models to simulate paleo-saltwater intrusion, and freshening processes as well as assessment of climatic and human impacts on groundwater resources (Vandenbohede, A., 2003; Giambastiani et al, 2007, Delsman et al. 2014; Antonellini et al 2015; Meyer et al. 2019), but such large-scale models remain rare in the literature. The complexity of simulating density-dependent flow at transport at the catchment scale for long period of times often leads to simplification of the system. Montcoudiol et al. (2017) for example simplified a complex catchment into a 2D cross-section and ignored density effects to speed up simulation processes. Aside rare exceptions (e.g., Zwertvaegher et al., 2013), the geological changes that occurred during the long simulation periods are ignored or simplified.

The most practical integration of monitoring and modelling of pollution/salinization in groundwater may be found in administrative and management decision-making processes. However, even the concept of model validation is debatable (Konikow and Bredehoeft, 1992), especially when long time-scales are considered. Before findings may be integrated into other economic, technical, political, or institutional models, every operational model must be calibrated with field data, which is typically impossible for models spanning hundreds of years. Such models must therefore mostly be seen as numerical tools to better understand the hydrogeological system.

For the Luy River coastal aquifer, Nguyen M.K. (2015) has developed a groundwater flow model in his PhD thesis about the characterization of groundwater reservoirs in the whole province of Binh Thuan. However, working at the large scale, the study did not investigate saltwater intrusion or freshening processes in the area. Ta T.T. (2019) studied saltwater intrusion in the coastal aquifers of the neighboring Ninh Thuan province, which has similar climate conditions and sedimentary processes as our study area. This research chose the saltwater initial concentration for the running density model based on the evidence of saltwater intrusion located further inland, which prevents using such model to test hypotheses related to freshening and salinization processes that can take place over long period of time. Such understanding is nevertheless essential to develop long-term groundwater management strategies. For the study area, Cong-Thi et al. (2021) and Pham et al. (2022) have found that the salinity distribution was more complex that initially estimated based on shallow boreholes (NAWAPI, 2018)

Pham et al. (2022) proposed a conceptual model explaining the current distribution of salinity. During the last transgression, corresponding to the high water stand about 6000 years ago, the study area was largely invaded by the sea and the pores of the sediments were filled by seawater, except in the high elevation dune area and highlands. This is illustrated by the presence of recent marine deposits up to 20 km inland. When the water level started to decrease, freshwater recharge from the surface through rainfall and inflow from the adjacent mountainous areas initiated the freshening of the aquifer, resulting in the current chemical signature. However, the alluvial plain is mainly made up of clays, clayey and silty sands which have a relatively low permeability. The bottom of the unconsolidated aquifer is also largely below the current sea level. Combined with a typical semi-arid climate where recharge is limited, an important draining system through the Luy River and its tributaries, this saltwater is expected to have a long residence time and the aquifer has not reached a new equilibrium yet, especially at depth and in the low permeability zones. This presence of paleo-groundwater can explain why groundwater salinity can change from fresh to brackish over short distances in clayey areas (Cong-Thi et al., 2024a), why the deep aquifer is still saline because of density-driven flow and why salinity can increase locally when the shallow freshwater lens is exploited for irrigation. At the opposite, the dune areas have been freshened more quickly, due to preferential recharge (see Chapter 3) and constitute important freshwater reserves in the area. Locally, this paleo-groundwater can act as a secondary source of salinity for saltwater intrusion when freshwater at shallow depth is extracted for irrigation, salinization occurs by upconing or lateral migration. Close to the estuary, direct salinization from the river can occur.

In this study, a three-dimensional (3D) stratigraphic model is first constructed based on the existing well logs, geophysical and geochemical data. Then, density-dependent flow and solute transport is simulated over long periods of time to find out: (1) how aquifer properties affect the freshwater and saltwater distributions and to verify numerically the hypothesis behind the hydro-chemical conceptual model, i.e., to see if the time scale of the freshening process fits with the hydraulic properties and water balance in the catchment under the current natural conditions (i.e. absence of groundwater exploitation); (2) analyze the current saline groundwater distribution originating from various hypotheses of saltwater sources, and (3) assess the potential of groundwater resource development under freshening process and saltwater intrusion threats.

Given that calibration would only be feasible for the most recent times for which observations are impacted by groundwater extraction, and a full sensitivity analysis would be unattainable due to the long simulation, no attempt is made to calibrate the model in this chapter (see Chapter 6). As a result, we consider our model to be largely a conceptual tool. Nonetheless, we tested the model's robustness by comparing the simulation results of the most realistic simulation scenario to the piezometric map and salt concentration, which constitutes a proxy for the hydrochemical composition of groundwater. This ensures that the model can qualitatively simulate natural flow within the aquifer in a realistic way. The model is calibrated in the next chapter to reproduce current observations and serves as a management tool for groundwater management.

The groundwater flow and saltwater transport models are constructed for these objectives using the SEAWAT software packages coupling MODFLOW-2000 with MT3DMS (Gue and Langevin, 2002). The data required for the model, including natural recharge, boundary conditions, river and drainage packages, is described in the methodology section.

5.2 Study area

The study zone is constituted by the downstream part (coastal plain) of the Luy River and its tributaries. It is surrounded in the northwest by a hilly terrain with altitudes ranging from 1200 to 2000 m above sea level and covered from 70 to 100% with forest. The terrain drops dramatically from 1200 to 300 m, then gradually from 300 to 100 m onto the coastal plain (Figure 2.1). The southern boundary is defined by a red sand dune system near to the Vietnamese Eastern Sea, with elevations varying from 100 to 300 m. The white sand dune complex, which is also next to the Vietnamese Eastern Sea, limits the research region to the southeast. The limit of the model corresponds to crests in the dune complexes, assumed to correspond to groundwater divides. The alluvial plain is rather flat, with an elevation between 0 and 50 m gradually descending from west to east. The Vietnamese Eastern Sea constitutes the seaside limit of the model. Depending on the water availability and irrigation network in each site, the major crops planted on this plain are dragon fruit plants and rice. Rice is normally grown where dam irrigation water is available, but dragon fruit, which is more drought and salt tolerant, is grown in other locations, frequently using groundwater for irrigation.

Water recharge to the aquifers mainly comes from precipitation during the wet season and surface water, including through irrigation practices, and adjacent flow from the mountainous area. Appling the Soil Moisture Balance method in the period 42 years for calculating the recharge rate in the study area, an average recharge of 422 mm/year was estimated, with higher values in the dune complexes (531 mm/year) compared to the alluvial plain (312mm/year) (Chapter 3).

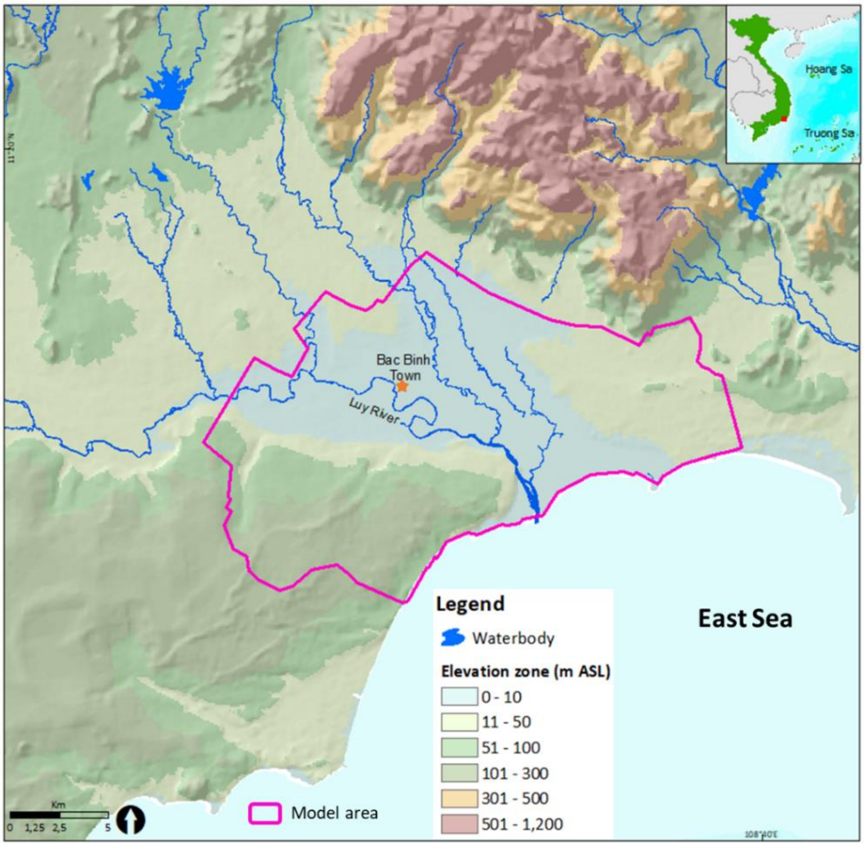

Figure 5.1 Map of the study area indicating the model boundary in the topography background.

Several research projects have studied the geology in the area (Hoang P., 1997; Nguyen D.T., 1999; Nguyen V.C., 2001; Nguyen DT (ed) (1999)). These studies indicate that the upper part of the area consists of unconsolidated sediments from the Holocene and the Pleistocene periods. The Holocene formation consist mostly of clay, clayish silt mixed sand, brown yellowish or greyish silty sand and the Pleistocene formation includes fine coarse sands, round gravel, or sand intercalating with silt and clay. The thickness of the Holocene sediments is thin in the right bank of the river (2–4 m) but it increases in the left bank from 2 to 20 m. In contrast, the Pleistocene formation is thick on the right bank, due to the high altitude of the sand dune, and is thinner on the left bank. The hard rock consisting of granite and granitoid from the Cretaceous and sandstone, claystone and siltstone from the Jurassic is located at depth around -40 m at the sea, decreasing in the upstream part and finally outcropping in the mountains and hills (Figure 2.3).

Research on the potential of groundwater resources for drinking and irrigation purposes has been conducted since 1992 (Nguyen T.G. et al., 1992; Cao D. G. et al., 2008; Nawapi, 2015, 2018). The studies from the National center for Water Resources (Nawapi, 2015, 2018) combined all information from previous studies of well logs and well testing, the groundwater samples, as well as the geophysics data, to make a hydrogeological map of the Binh Thuan province.

Pumping tests were carried out in local residential wells and newly drilled wells (Nawapi 2018) in Bac Binh district to assess the hydraulic conductivity, specified yield, and specific storage of the aquifers (54 wells). According to the results, the hydraulic conductivity covers a broad range from 0.7 to 46.9 m/d in both Holocene and Pleistocene aquifers. The flow rate recorded in the wells varies from 0.06 to 4.5 l/s. The most prospective groundwater resource in the area was observed in coarse-grained and fine-grain sediments of the Quaternary formations (amQ_1^2, $Q_1^{2-3}pt$, amQ_1^3, and mQ_1^3, Figure 2.3). There was also a lower potential for groundwater in the fracture zones of hard rock formations. The clay in the top part of the amQ_1^2, amQ_1^3, and the bottom part of the amQ_2 is considered to be an impermeable layer between the Quaternary formations.

Since 2008, the Dai Ninh hydropower reservoir in the upstream part has recharged the freshwater supply to the Luy River with an average rate of about 27m³/s, as it also supplies the study area with fresh surface water through irrigation channels. The Luy River and streams in the study area are mostly draining the shallow unconfined aquifer system and therefore contribute to seasonal groundwater discharges. However, decreasing the average flowrate in the Luy River during the dry season combined with high tide sequence can induce riverine SWI. Locally, the natural gradient is perturbed due to water abstractions or irrigation practices. Outflows occur at the Luy river estuary to the sea, whereas abstractions occur through pumping for irrigation (about 23,258 m³/day in Bac Binh and Tuy Phong districts, Tran T.D. 2020), aquaculture farming, and mining activities.

5.3 Methods

5.3.1 Hydro-stratigraphic model

For a given region, different conceptual hydrogeological models can be built depending on how the available data are used and interpreted (Troldborg et al. 2007; Seifert et al. 2012). This could have a major effect on the calibration and the prediction of the models. Consequently, 3D stratigraphic modelling can prove helpful as a framework for creating a realistic hydrogeological model, especially for areas with significant hydrogeological variations.

For this study area, three-dimensional hydro-stratigraphic modelling is performed based on collected well-log records and geological-hydrogeological maps and cross-sections exiting in the area. There were 24 geological boreholes logs available from previous studies and 10 new wells were drilled for this study (Cong-Thi, 2024b). The log description was used for analyzing and interpolating the 3D hydro-stratigraphic model. The stratigraphic column of the formations in the study area is constructed based on the geological map and the exiting literatures (Figure 2.3).

To identify the possibility of contact between hydrogeological units, lithological classes - which are subsequently categorized based on their layering sequence and an understanding of the local hydrogeology - are derived from the lithological intervals found in the well logs. Cross-sections were built to interpret the continuity of units between the boreholes. The GMS 10.7 software is used as a tool for extrapolating these contacts from boreholes using the inverse distance weighted method to create a 3D hydro-stratigraphical solid model of the study area.

At the bottom of the stratigraphic column, there is a group of drilling intervals that have different thicknesses. These intervals mostly consist of low permeable rocks such as sandstone, siltstone, shale, granite, and solidified basalt. These rocks were formed between the Neogene and Jurassic periods. When there are fractures present, this cluster can be considered as a secondary aquifer.

Directly above the bedrock is a cluster of lithology intervals with significant permeability. These intervals are composed of unconsolidated sediments that formed during the Pleistocene period. The thickness of the intervals varies from around 100 meters in the well situated in the dune complex on the right bank of the Luy River to a few meters only in certain wells on the left bank. Additionally, it is also absent from certain wells. The cluster consist of grit, gravel, clean sand, coarse sand, and clay-mixed sand found in amQ_1^2, $Q_1^{2-3}pt$, amQ_1^3, and mQ_1^3 formations.

At the highest point of the stratigraphic column, there is a cluster of drilling intervals that consist of unconsolidated sediments deposited mostly during the Holocene period. The intervals comprise clayey sand, sand mixed with clay, and clay mixed with grey sand bearing gravel, grit, and sand found in mQ_2, amQ_2, and amQ_1^3 formations. The permeability of this cluster is moderate, and its thickness ranges from 2 to 20 meters (NAWAPI, 2018).

The amQ_2 and amQ_1^3 formations consist of a series of deposits composed of grey-blackish clay, clay blended with fine-grained sand and gravel, and yellow-grey, moist, malleable bentonite clay. These formations can be classified as a Quaternary aquitard composed of sediments originating from both the Holocene and Pleistocene periods. Drilling intervals at certain locations, such borehole LK7BT or BBM9, indicate that the entire unconsolidated sediment consists of clay, or a combination of clay, sand, and silt. The pumping test conducted on these wells indicates that the extraction of water is either non-existent or extremely limited (NAWAPI, 2018).

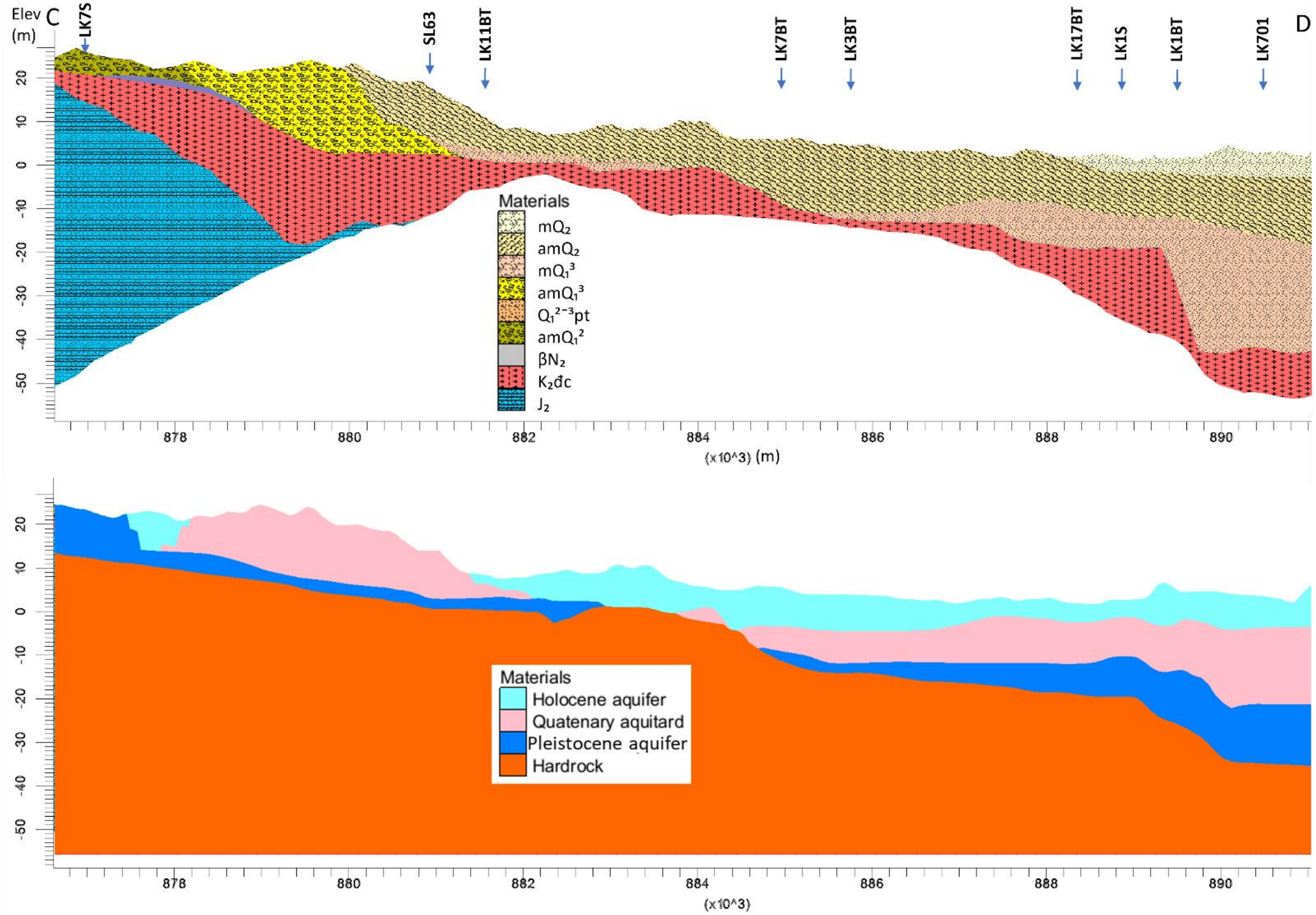

Figure 5.2 Distribution in depth of geological and hydrological units along cross-section C-D in Figure 2.3

Figure 5.2 illustrates the vertical distribution of geological and hydrogeological units along cross-section C-D. The classification of the Quaternary aquifers and aquitard is determined by the described methodology. Ten cross-sections are selected using the constructed 3D hydrogeological model (Figure 5.3). These cross-sections are then integrated in a fence diagram to assess the paths through which groundwater recharge, freshening and saltwater intrusion occur in the studied groundwater system.

The Holocene phreatic aquifer mostly occurs on the right bank of the Luy river in the alluvial plain part of the study area and along the river as shown in the geological map and hydrogeological fence diagram (Figure 5.3). The aquifer is up to 20 m thick and becomes thinner on the right bank and the northwest.

This aquifer is located on the plain of the main river and its tributaries, and therefore direct hydraulic interaction with these rivers is assumed. This aquifer is hydraulically isolated from the underlying Pleistocene aquifer by a 2–13m-thick aquitard. However, this aquitard is not continuous as the poorly permeable clay dominated deposits might be absent. The Holocene aquifer might sometimes lie directly above the Pleistocene. This is indicated by the groundwater levels from borehole LK01BT and LK02BT, drilled at the same location but screened at different depth, showing strongly different hydraulic and chemical conditions whereas similar value in those parameters are observed in LK11BT and LK12BT in both the Holocene and Pleistocene aquifers (Pham et al, 2022). Note that the discontinuity in the aquitard makes it difficult to model it accurately using an interpolated hydro-stratigraphic model, while its importance on the hydrogeological system makes it an essential component.

Therefore, the principal pathway for recharge of the Holocene aquifer is infiltration of rainwater through from the surface. Because the groundwater level observed in all shallow and dug wells within the study area is 3–5 m higher than the river and seawater levels, the groundwater flow in the Holocene aquifer is assumed to discharge to both the rivers and to the sea.

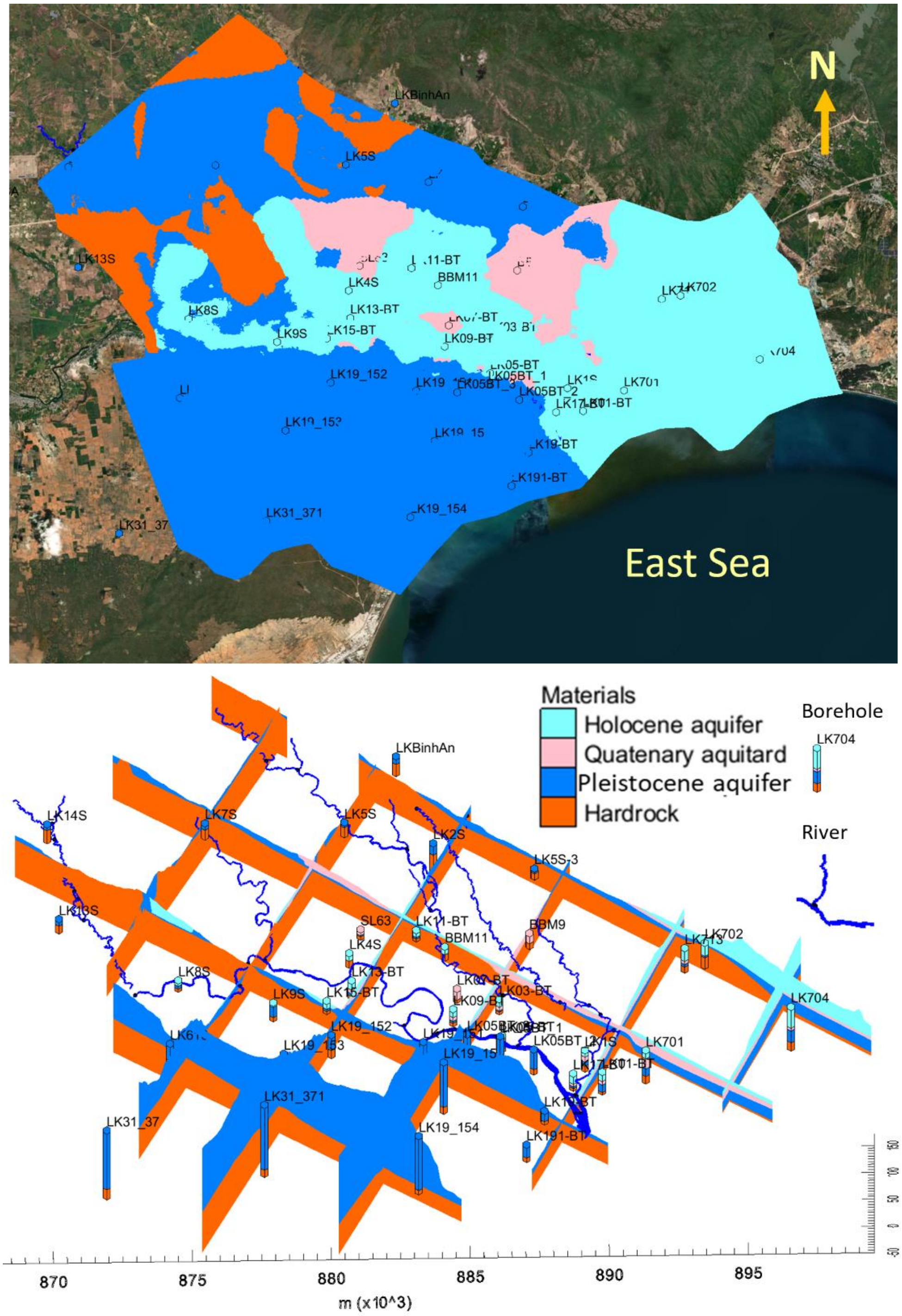

Figure 5.3 Stratigraphical fence diagram of the study area

The Pleistocene aquifer outcrops mainly on the right bank of the Luy river in huge sand dunes and thin layer in the northwest part, while in the remaining part it is covered by the Quaternary aquitard and/or Holocene aquifer. This aquifer occurs at elevation ranging from 20 m to -36 m, is 2–60 m thick and tends to be thicker towards the coast and the right riverbank (Figure 5.3). Where covered by the Quaternary aquitard, this aquifer is confined, with static water levels ranging from about 5 m below up to 1 m above the ground surface. Based on observed static groundwater levels in the boreholes SL84, SL82, SL36, LK1BT, and SL15, the groundwater in the Pleistocene aquifer flows from west to east, and from the dunes to the river plain. This aquifer is recharged by rainwater when outcropping or underlying directly the Holocene aquifer.

The Pleistocene aquifer directly overlies less permeable either granite formation from the Cretaceous or Jurassic which are considered as secondary aquifers. At these contact surfaces, the groundwater in the formations is assumed to have hydraulic connection with the Pleistocene aquifer as the groundwater level observed in the wells (SL56 and SL89) drilled in these formations lies within the distribution depth interval of the Pleistocene aquifer. However, inflow from these formations into the Pleistocene aquifer is not significant as the specific discharge and hydraulic conductivity are small compared with that of the Pleistocene aquifer.

The hard rock aquifer outcrops in the high mountains Northwest of the area and a lateral inflow resulting from the natural gradient is expected to enter the study area. This gradient can be roughly estimated from the recharge occurring in the mountains where this aquifer is in interaction with the surface water system. Given the connection with the Pleistocene aquifer, this lateral inflow can also contribute to recharging the latter in the study area.

5.3.2 Conceptual model

The model is built following the conceptual model for the evolution of the salinity in the Luy river catchment, which is described in Pham et al., (2022). During the last transgression, corresponding to the high water stand about 6000 years ago, the study area was largely invaded by the sea, and the pores of the aquifer were filled with seawater. The initial condition for the model therefore uses saltwater at a concentration of 35 kg/m³. When the water level started to decrease, freshwater recharge from the surface through rainfall and underground from the adjacent mountainous areas initiated the freshening of the aquifer. We simulate this process by imposing fresh conditions to the recharge (0.45 kg/m³), the river system and the Northwestern boundary conditions. Although conditions have changed in time, we use current recharge estimation to test how long it takes for the aquifer system to freshen.

First, the model is tested in homogeneous conditions assuming clean sand/sand mixed with grit or clay covers the whole area. Second, the model is run with a more realistic 3D hydro-stratigraphic distribution based on 4 layers, from top to bottom: the Holocene aquifer, the discontinuous Quaternary aquitard, the Pleistocene aquifer, and the hard-rock layer (Figure 5.3). Finally, scenarios where the Quaternary aquitard is continuous, no flow occurs at the Northwestern boundary and the surface recharge is larger are also addressed to provide a broader overview of saltwater intrusion and freshening processes in the area.

5.3.3 Model construction

Model domain and boundary conditions

The study area is about 25 km from west to east and about 15 km from north to south, so about 375 km². The modelled area was discretized into a regular model grid of 122 rows and 144 columns resulting in cells with dimensions of 200 m × 200 m. The model was first converted from these four hydrogeological units (the top Holocene aquifer, the Quaternary aquitard, the Pleistocene aquifer, and the hard-rock aquifer) to a four-layer model. Every layer was subdivided into 3 uniform sublayers, so that the model contains a total of 12 layers and 210086 model cells.

The model area can be found in Figure 5.1. The elevation of the top of the model was determined using a 30-meter resolution digital elevation model (DEM). The bottom of the model is restricted to a depth of – 60 m, where the bed rock is present. The coastal boundary is defined as a specified head sea boundary where the equivalent fresh groundwater level is at the sea level under normal conditions (average water level), and the sea water concentration for influx is 35 kg/m^3. The constructed model should be regarded as a regional groundwater flow and transport model which is adequate to simulate regional flow and transport patterns but may not be sufficient to describe freshwater/saltwater transition zones accurately. The northwest boundary follows the limit between the floodplain and the highlands in the northwest. The latter represent a catchment area of 169,160 ha, The recharge through rainfall for the whole catchment has been estimated to be about 40% of the precipitation (Kotchoni, 2019), which equals 240 mm/year. The total recharge rate in the highland area of 169160 ha is 1112285 m^3/day. Assuming the totality of the recharge flows into the study area, the incoming flux is equal to the recharge rate divided by the cross-sectional area along the northwest boundary, divided between the 12 layers at the northwest boundary of the model. The salinity of freshwater is assumed to be 0.45 kg/m^3.

Along the remaining model boundaries located in both dune complexes, no-flow boundaries were defined. These boundaries correspond to topographic crests located at the limit of the Luy river catchment; it is assumed that they also correspond to groundwater divides.

The Luy River and its main tributaries are defined as river boundary conditions with the river stage and river bottom extracted from the 30-meter resolution DEM. The numerous small streams of the floodplain (nowadays often replaced by canals used for drainage and irrigation) are modelled using the drain package. Irrigation is not included as it is assumed to have played a negligible role in the past history.

The model follows a constant simulation approach through time. It does not account for river salinity nor the tides. It assumes that the recharge is constant through time as well, and the geology and topography are fixed at the current situation. Considering the coarse resolution of the model, the geology of the model was simplified, not all heterogeneity is represented.

Hydrological stresses

The hydrological stresses comprise recharge through precipitation and lateral flow interactions with the Luy River and drainage to streams. The groundwater recharge rate was calculated from the soil moisture balance method (Thornwait and Mayer, 1957). Based on geography, soil types, and land use, two main zones were identified in the study area, namely the sand dunes and the alluvial plain. The calculated annual average recharge rate is about 422 mm/year, 531 mm/year in the dunes, and 312mm/year in the plain (Chapter 3).

The Luy River and its main tributaries flow from the northwest to the southeast and crosses the model area. The River package in MODFLOW was used to simulate groundwater discharge to and possible recharge from the rivers with a conductance of 0.025 m^2/day/m. There are a number of smaller streams (nowadays channelized) that receive groundwater discharge in the alluvial plain: they were defined with the Drain package as a polygon covering the alluvial plain at the depth of 1m below the surface with the conductance value given as the river of 0.025 m^2/day/m^2.

Model parameters

The hydraulic conductivity values were derived based on a small number of pumping tests (Nawapi, 2015), the geological properties from drilling data, and empirical lithology estimates (Domenico and Schwartz 1990) (Table 5.1). The large variability is the results of the heterogeneity of the deposits. Given the objective of testing how freshening and saltwater intrusion processes relate to time and hydrogeological parameters, and to avoid using many parameters to represent the varying hydraulic conductivity, homogeneous values were chosen for each hydro-stratigraphic unit. Vertical hydraulic conductivities were approximated to be 10% of horizontal values and applied for all further simulations.

Effective porosity is one of the less well documented parameters in the hydrogeological literature, with reported ranges for unconsolidated sediments from 1 to 40% (Woessner and Poeter, 2020). Effective porosities reported for relatively short scale tracer experiments are commonly below 10% (e.g., Worthington, 2022). At larger scale such as the catchment scale, Worthington et al. (2019) and Kidmose et al. (2023) noted that the effective porosity tend to the total porosity because of the influence of the matrix storage. If a higher effective porosity will lead to lower advection velocity, and therefore longer travel times for water particles, using an effective porosity equal to the total porosity avoids using a dual-porosity model for freshening studies. Indeed, if the actual effective porosity is lower than the total porosity, the diffusion from the immobile to the mobile water would still lead to slow freshening process at the representative elementary volume scale. Therefore, the effective porosity used in the transport model were chosen to be equal to the total porosity expected for unconsolidated sediments.

Table 5.1 The input parameters for the model simulation

Model layer	**Horizontal hydraulic conductivity (m/day)**	**Effective porosity**	**Dispersivity (m)** Longitudinal
Holocene aquifer	8	0.3	10
Quaternary aquitard	0.57	0.3	10
Pleistocene aquifer	18	0.3	10
Hardrock	0.05	0.03	10

5.3.4 Mathematical model

Mathematical models are representations of the reality using mathematical equations. Darcy’s law is a mathematical model that represents groundwater flowrate in porous media:

$$Q = KA\frac{\Delta H}{L} \text{ (Equation 5.1)}$$

where

Q is flow rate $[L^3/T]$

K is hydraulic conductivity [L/T]

ΔH/L is the hydraulic gradient [L/L]

A is the cross-section area of flow [L^2]

In all generality, both the hydraulic gradient and the specific discharge or Darcy's flux q [L/T] are expressed in vectorial form, while the hydraulic conductivity is expressed as a tensor:

$$\vec{q} = \boldsymbol{K}\vec{\nabla}H \text{ (Equation 5.2)}$$

The mass conservation principle coupled with Darcy's law allows to derive a differential equation for the main variable related to groundwater flow - the hydraulic head H. Based on the principle of mass conservation, the rate of accumulation of the mass stored in the representative elementary volume (REV) is equal to the algebraic sum of the mass fluxes across the faces of the element and the mass exchange due to sinks or sources. The mathematical expression for the conservation of mass as the governing equation for groundwater flow is:

$$-\nabla.(\rho\vec{q}) + \bar{\rho}q_s = \frac{\partial(\rho\theta)}{\partial t} \text{ (Equation 5.3)}$$

where

∇ is the divergence operator $\frac{\partial}{\partial x} + \frac{\partial}{\partial y} + \frac{\partial}{\partial z}$

ρ is the fluid density [ML^{-3}]

$\vec{q}$ is the specific discharge vector [LT^{-1}],

$\bar{\rho}$ is the density of water entering from a source or leaving through a sink [ML^{-3}],

q_s is the volumetric flow rate per unit volume of aquifer representing sources and sink [T^{-1}].

θ is the porosity [dimensionless], and

t is time [T]

For piezometers open to a given point, N, in an aquifer containing fresh water, the hydraulic head is defined as

$$h_f = \frac{P_N}{\rho_f g} + Z_N \text{ (Equation 5.4)}$$

where

h_f is the equivalent freshwater head [L]

P_N is the pressure at the point N [M/LT^2]

ρ_f is the density of freshwater [M/L^3]

g is the acceleration of gravity [L/T^2]

Z_N is the elevation at point N taken from a reference level [L]

In saline conditions, the density varies and measured hydraulic heads can be converted into equivalent freshwater heads using the following relation:

$$h_f = \frac{\rho}{\rho_f} h - \frac{\rho - \rho_f}{\rho_f} Z \text{ (Equation 5.5)}$$

Where ρ is the density of saline aquifer water and h is the measured hydraulic head.

Mass fluxes are found by multiplying the density of the fluid by its specific discharge, which is the volumetric flow per unit cross-sectional area of a bulk porous medium. Darcy's law for a fluid of variable density can then be expressed by the equations:

$$q_x = -\frac{k_x}{\mu} \frac{\partial P}{\partial x} \text{ (Equation 5.6)}$$

$$q_y = -\frac{k_y}{\mu} \frac{\partial P}{\partial y} \text{ (Equation 5.7)}$$

$$q_z = -\frac{k_z}{\mu} \left\lfloor \frac{\partial P}{\partial z} + \rho g \right\rfloor \text{ (Equation 5.8)}$$

where

q_x, q_y, q_z are the individual components of specific discharge,

μ is the dynamic viscosity [ML^{-1}T^{-1}]

k_x, k_y, k_z represent intrinsic permeabilities [L^2] along the three main axes with the z-axis being vertical.

g is the gravitational constant [LT^{-2}] and treated here as a positive scalar quantity.

In terms of equivalent freshwater head, Darcy's law can be expressed:

$$q_x = -K_{fx}\frac{\mu_f}{\mu}\left[\frac{\partial h_f}{\partial x}\right] \text{ (Equation 5.9)}$$

$$q_y = -K_{fy}\frac{\mu_f}{\mu}\left[\frac{\partial h_f}{\partial y}\right] \text{ (Equation 5.10)}$$

$$q_z = -K_{fz}\frac{\mu_f}{\mu}\left[\frac{\partial h_f}{\partial z} + \left(\frac{\rho-\rho_f}{\rho_f}\right)\right] \text{ (Equation 5.11)}$$

In terms of variable-density ground-water flow in porous media, the flow equation takes the general form of the partial differential equation

$$-\nabla.(\rho\vec{q}) + \bar{\rho}q_s = \rho S_p\frac{\partial P}{\partial t} + \theta\frac{\partial \rho}{\partial C}\frac{\partial C}{\partial t} \text{ (Equation 5.12)}$$

If the density is constant, the second term in the right hand side of the equation above is zero and the remaining density terms cancel.

The governing equation for variable-density flow in terms of freshwater head is therefore expressed in terms of freshwater head as

$$\frac{\partial}{\partial \alpha}\left(\rho K_{f\alpha}\left[\frac{\partial h_f}{\partial \alpha} + \frac{\rho-\rho_f}{\rho_f}\frac{\partial Z}{\partial \alpha}\right]\right) + \frac{\partial}{\partial \beta}\left(\rho K_{f\beta}\left[\frac{\partial h_f}{\partial \beta} + \frac{\rho-\rho_f}{\rho_f}\frac{\partial Z}{\partial \beta}\right]\right) + \frac{\partial}{\partial \gamma}\left(\rho K_{f\gamma}\left[\frac{\partial h_f}{\partial \gamma} + \frac{\rho-\rho_f}{\rho_f}\frac{\partial Z}{\partial \gamma}\right]\right) = \rho S_f\frac{\partial h_f}{\partial t} + \theta\frac{\partial \rho}{\partial C}\frac{\partial C}{\partial t} - \bar{\rho}q_s \text{ (Equation 5.13)}$$

where

α, β, γ represent a coordinate system aligned with the principal directions of permeability.

S_f is the specific storage in terms of freshwater head.

The term $\theta\frac{\partial \rho}{\partial C}\frac{\partial C}{\partial t}$ links the variable-density flow equation to the concentration of the dissolved species (salinity), which itself depends on transport processes, therefore coupling the flow equation to the transport equation. Solute mass is transported in porous media by the flow of groundwater (advection), molecular diffusion, and mechanical dispersion. The two latter are often grouped in a single term called hydrodynamic dispersion. The transport of solute mass in groundwater can be described by the following partial differential equation (Zheng and Bennett, 1995):

$$\frac{\partial C}{\partial t} = \nabla.(D.\nabla C) - \nabla.(\vec{v}C) - \frac{q_s}{\theta}C_s \text{ (Equation 5.14)}$$

where

D is the hydrodynamic dispersion tensor[L^2T^{-1}]

$\vec{v}$ is the advection velocity [LT^{-1}]

C_s is the solute concentration of water entering from sources or sinks [ML^{-3}]

θ is the effective porosity.

The fluid velocity can be estimated from the specific discharge $\vec{v} = \frac{\vec{q}}{\theta}$ and is therefore computed from the solution to the flow equation.

5.3.5 Numerical model

With a few exceptions of extremely simple systems, it is typically not feasible to solve the equations 13 and 14 analytically. Therefore, it is necessary to use numerical models to estimate the solution.

The SEAWAT code (Gue and Langevin, 2002) was developed to simulate three-dimensional, variable-density, transient groundwater flow in porous media. The source code for SEAWAT was developed by integrating MODFLOW (solving the flow equation) and MT3DMS (solving the transport equation) into a single program that solves equations 13 and 14 in a sequential way using the equivalent freshwater head. Both codes are using a finite-difference approach to solve the respective equations.

For each time-step, the cell-by-cell flow is calculated from the freshwater head gradients and relative density-difference term (Equation 13) using MODFLOW. The resulting flow field is transmitted to MT3DMS for the transport of solute (Equation 14). Subsequently, an updated density field is computed based on the new solute concentrations and reintegrated into MODFLOW as relative density-difference terms for the next time step. In that sense, SEAWAT is not really coupling the two equations but solves them sequentially.

The assumption is that the density of the fluid is determined exclusively by the concentration of dissolved components. The SEAWAT model incorporates the MT3DMS program's routines to simulate salt concentration that varies both in time and space. SEAWAT uses either an explicit or implicit approach to integrate the groundwater flow equation with the solute-transport equation. The explicit technique involves solving the flow equation one time for each timestep. The resulting advection velocity field is used afterwards in solving the solute-transport equation. This process of calculating the flow and transport equations is performed until all stress periods and the simulation are finished. This approach is sufficient when change in density between two-time steps are small. The implicit coupling approach involves solving the flow and transport equations numerous times for the same timestep until the maximum difference in fluid density between consecutive iterations is below a tolerance chosen by the user (Gue and Langevin, 2002). It is more accurate but also computationally more expensive.

In this study, the flow of groundwater with different densities is simulated to find out how aquifer properties affect the freshwater and saltwater distributions over long period of time and to verify numerically the hypothesis behind the hydrochemical conceptual model, i.e., to see if the time scale of the freshening process fits with the hydraulic properties and water balance in the catchment under present natural conditions. The characterization of the hydraulic properties and hydro-stratigraphic distribution in the study area follows the description of previous sections.

The groundwater flow part of the coupled model was run in steady state for each stress period, for all cases, i.e., since the stress factors remain constant, the variations in flow between stress periods are uniquely due to the change in concentration with the previous time-steps. This ignores the transience of the flow within stress-periods (e.g., Van Riet et al., 2022). This approach is justified since stress-periods are long, hydrological stress are constant, and input parameters in the model were estimated as average values. The time step was set to 30 days and multiplied by 1.05 to provide a smaller step at the start and a larger step subsequently. MT3DMS then set a transport time step, small at the beginning and increases it during the simulation. This approach also improves the convergence.

5.3.6 Formulation of scenarios

The purpose of this study is to find out how the properties of the aquifer affect the distributions of freshwater and saltwater and to test the hypothesis behind the hydrochemical conceptual model numerically. That is, to see if the time scale of the freshening process fits with the hydraulic properties and water balance in the catchment under natural conditions. To do this, scenarios for model simulations have been defined. The model was run with a starting salt concentration at 35 kg/m^3 in all active cells of the model. Since saltwater transfer takes a long time to achieve equilibrium and that density-dependent simulations are computationally expensive, these scenarios were first simulated for 100 years of freshening in natural conditions to assess the early freshening rates. Then the scenarios assumed to be the more realistic was run for a longer period (5000 years).

Scenario 1: homogeneous plain with hydraulic conductivity equals to 8 m/d

The model is initially evaluated under homogeneous conditions, where the hydraulic conductivity is set at 8 m/day. This value represents the highest range of values for the Holocene aquifer. This test aims to determine the rate at which freshening processes occur in a catchment that is solely filled with Holocene sediments of relatively high hydraulic conductivity, under natural conditions.

Scenario 2: homogeneous plain with hydraulic conductivity equals to 18 m/d

In this case, the model is tested in homogeneous conditions with a hydraulic conductivity of 18 m/day, which represents clean coarse sand mixed with fine sand characteristics of the sediments of the Pleistocene aquifer. This test provides insight into the rate at which the process of freshening occurs in the coarser sediments, as well as the spatial distribution of saltwater resulting from homogeneous hydraulic properties. In this scenario, the process of freshening is expected to occur rapidly.

Scenario 3: homogeneous plain with hydraulic conductivity equals to 0.8 m/d

The model is examined in uniform conditions, where the hydraulic conductivity of both the Holocene and Pleistocene aquifers, and the Quaternary aquitard equals 0.8 m/day. This test offers an in-depth view of the rate at which the process of freshening takes place in sediments with low permeability.

The model of the homogeneous cases follows a simulation spanning 100 years first, and then are also run for 1000 or 2000 years to assess the presence of any residual saltwater in the aquifers.

Scenario 4: "realistic" model

The model utilizes the hydro-stratigraphic distribution that more accurately represents the three-dimensional lithological situation (Figure 5.3). The composition consists of four distinct strata, arranged in a vertical sequence: the Holocene aquifer, the Quaternary aquitard, which is not continuous; the Pleistocene aquifer; and the bedrock. The hydraulic conductivity of the layers uses the values shown in Table 5.1. The model is first executed using identical boundary conditions and a 100-year time simulation, as in the preceding scenarios, to assess the evolution of freshening under similar circumstances. The model is additionally executed for 5000 years to observe the evolution in saltwater patterns resulting from extended freshening simulations.

Scenario 5: realistic model except for the presence of a continuous clay layer between the Holocene and Pleistocene aquifers

One of the crucial points in the study area is the existence of the semi-continuous clay layer and how it affects freshening. This scenario is run with a continuous clay layer identified in the alluvial plain side to test if there is a big discrepancy compared to a discontinuous clay layer.

Scenario 6: realistic model with a no-flow boundary at the Northwestern boundary

The model is evaluated in the northwest without considering an inflow boundary condition (i.e. implementing a no-flow boundary) since this boundary is located between the alluvial plain and the highlands in the northwest, which are much less permeable. This is the approach that was used in the model of Nguyen M.K. (2015).

Scenario 7: a larger recharge rate

Another scenario with a higher recharge rate is used in a simulation. This scenario investigates of an increased recharge from the surface by 20% does not result in an unexpectedly rapid refreshing.

5.4 Results

The location of the observation points is shown in Figure 5.4. They were chosen because they represent different situations in the hydrogeological system. Two points, DuneR and DuneL, are located in the dune complexes. They are meant to assess how fast saltwater freshens in a clean sand environment and the effect of elevation on the freshening process. LK1BT is close to the sea and river estuaries, while SL56 is close to the northwest boundary. The points SL63 and LK7BT are in the Quaternary aquitard. The point SL72 is located at the foot of the sand dunes on the right bank of the river. The observation points correspond to actual wells, but the latter are generally only screened at one specific depth, while for this model, we will also analyze the vertical distribution of salinity. The evolution of the freshening process with time is discussed in each scenario of the model simulation.

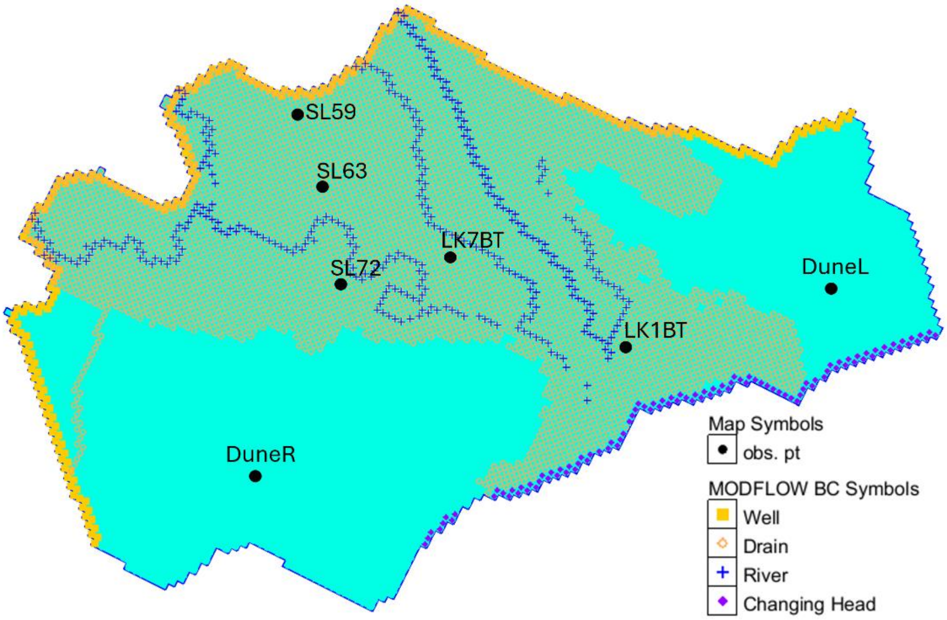

Figure 5.4 Model domain, boundary conditions and observation point locations.

For every scenario, we pay attention to layers 3, 6, 9, and 12, which correspond to the bottom of the Holocene aquifer, the Quaternary aquitard, the Pleistocene aquifer, and the hard rock respectively. Both saltwater spatial distribution in the layers and saltwater temporal evolution are presented in the following sections.

5.4.1 Freshening and saltwater intrusion in homogeneous conditions

These cases (scenarios 1 to 3) assume that the catchment is uniform in terms of the unconsolidated sediment. The last 3 layers are still simulated as hard rock with the corresponding hydraulic conductivity from Table 5.1. The models were initially simulated for a duration of 100 years in order to make a comparison with the other scenarios. We selected the points DuneR,and DuneL (dunes), LK7BT and SL63 (alluvial pain), and SL59 (close to NW boundary) to show the evolution of freshening.

Figure 5.5 shows the observation points after a 100-year simulation of scenarios 1, 2 and 3. In a homogeneous environment, most of the points located at higher elevations, such as

DuneL and DuneR, or the one that is close to the inflow boundary (SL59), are freshening very fast over time (15–40 years in the first 3 layers), whereas the points located in the plain are freshening much slower, such as LK7BT, and SL63. The freshening trend of most points follow a S-shape, with a slow freshening at the beginning, a period of almost linear decrease of salinity with time, followed by a reduction of the freshening rate.

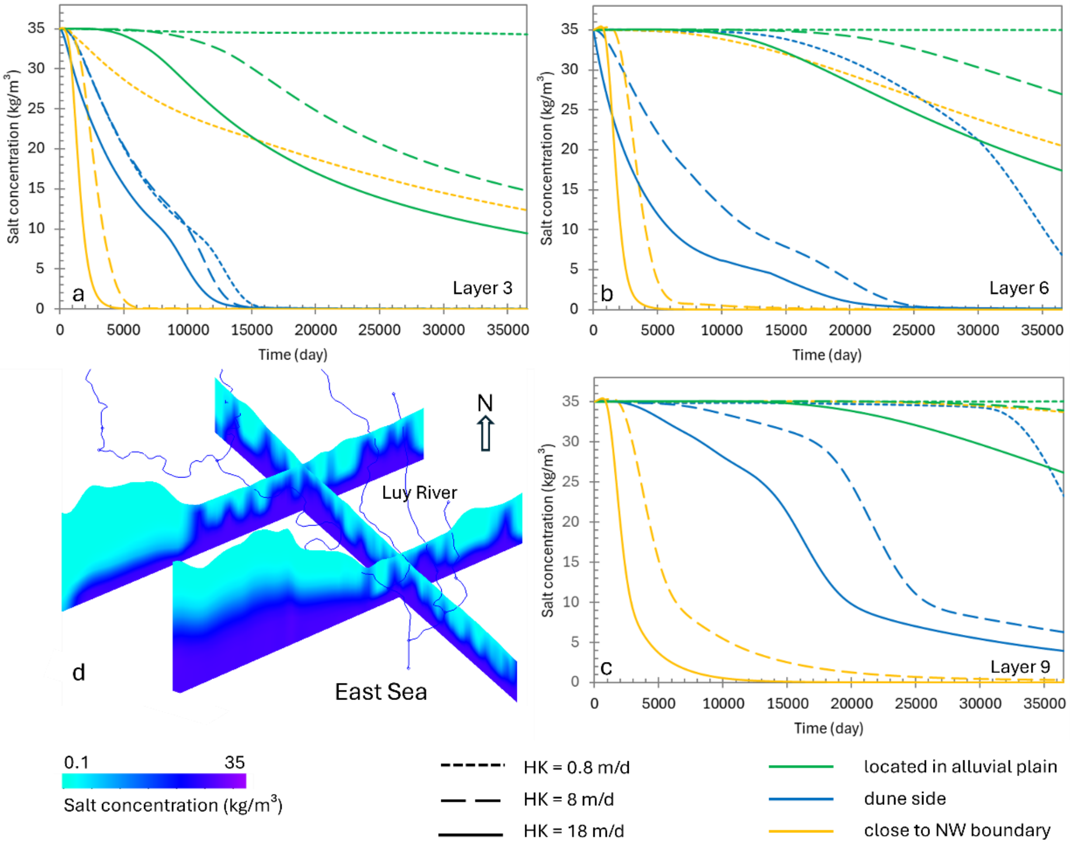

Figure 5.5 The observation points after a hundred-year simulation in layer 3 (a), layer 6 (b), and layer 9 (c). Cross sections (d) depict the effect of the river to the freshening process in the direction of the cross sections in Figure 2.3 for scenario 3.

In general, the freshening of the aquifer in case hydraulic conductivity (HK) equals 18 m/d follows a pattern similar to scenario 1 but happening at a faster rate as expected from the higher hydraulic conductivity. In contrast, for the low-permeability environment (HK = 0.8 m/d), the freshening process becomes slower for the deeper layers, and is globally significantly slower than in scenario 1 and 2. The curve having reached a steady freshening rate have a slope less steep than for previous scenarios, so that much longer freshening time should be expected. Figure 5.5 also shows cross-sections where the influence of local streams on the saltwater distribution is evident. As the surface water is mostly draining, the lower hydraulic head at the streams is responsible for a vertical component of the flow below them, which explains the higher salinities observe under the rivers.

Figure 5.6 shows saltwater distribution after a 100-year simulation for the scenario 1, 2, and 3 in the layers 3, 6, 9, and 12 in order from the top to bottom. In scenarios 1 and 2, the first six layers are freshening fast, and most of the locations are fresh after a 100-year simulation, except the locations around LK7BT, SL72, and SL63 in the alluvial plain. As expected, the freshening in the Pleistocene and hard rock part is slower. The bottom layer of the model is still fully saline everywhere at the end of the simulation period. This might be the result of either a low elevation or a low hydraulic conductivity defined for the secondary aquifer.

As freshwater replenishes the model from the top and flows into the model domain from the northwest border, the upper layers and the northwest boundary side experience a faster decrease in salinity. In contrast, the lower layers undergo a slower freshening process (Figure 5.6g,h,i,j,k,l). It demonstrates that, even under uniform conditions, the alluvial plain experiences a slower influx of fresh water compared to other areas. This might be caused by the fact that the aquifer in this part is below sea level. The alluvial plain is located on the left bank of the river, between the multiple branches of the river that are draining the aquifer, and not under the influence of fast freshening in the dune (higher recharge rate). The saltwater distribution is also affected by the draining river and stream which prevents infiltrating rainwater to percolate deep in the system. Figure 5.6 shows clearly the quite discontinuous pattern of saltwater being influenced by the river branches, especially in layers 6 and 9. The location SL72 situated at the base of the sand dunes, is likewise experiencing a reduced rate of freshening. Most points in the Pleistocene aquifer are experiencing fresher conditions in Scenario 2 compared to Scenario 1, while the bottom layer is still fully saline for all cases.

In the alluvial plain, the saltwater distribution is strongly affected by the surface water, with very sharp transition in salinity. Rivers play therefore a significant role in the distribution of saltwater. Saltwater appears trapped at the low elevations and below the base of the river, as illustrated in the cross sections in Figure 5.5d and in the layers in Figure 5.6a-l.

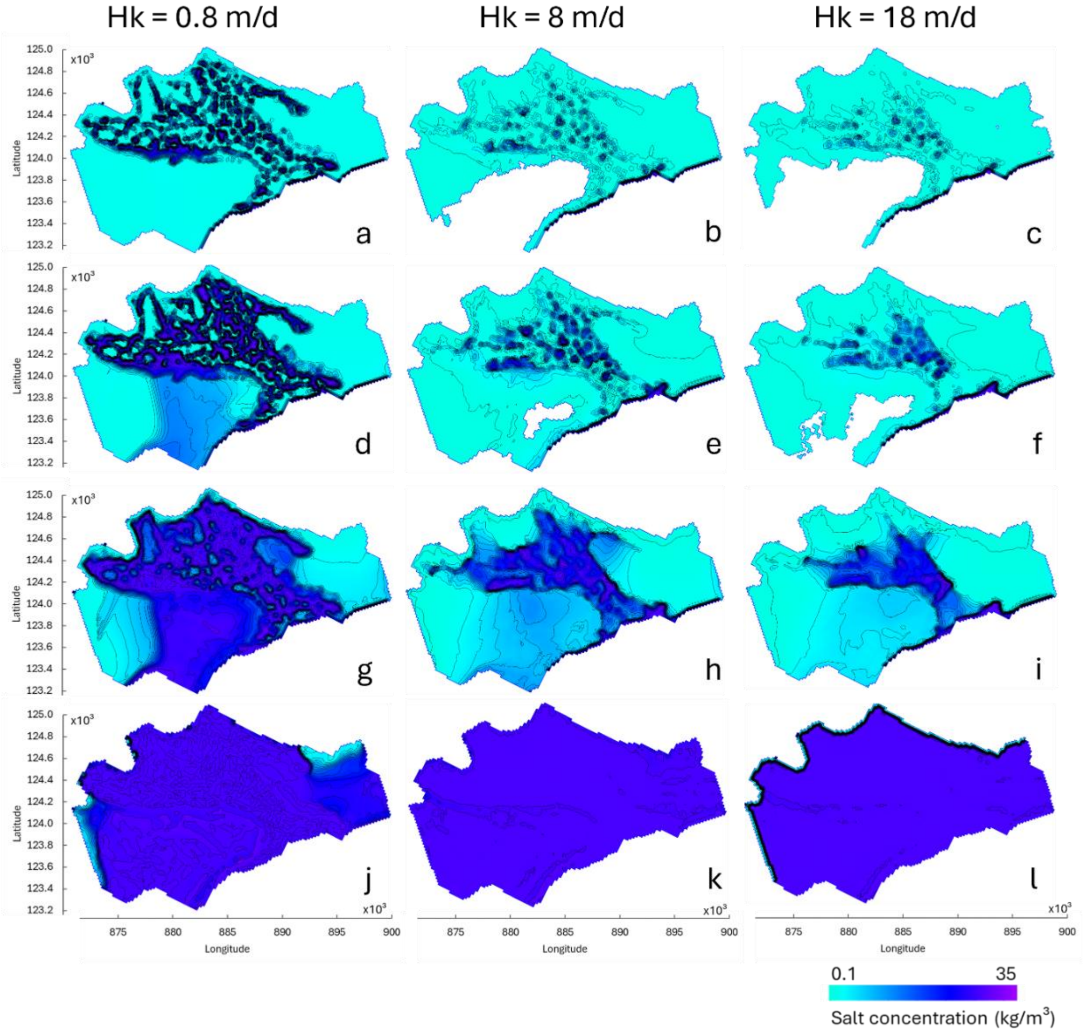

Figure 5.6 Saltwater distribution in the layers after a 100-year simulation for the scenario 1, 2, and 3 in the layer 3, 6, 9, and 12 in order from the top to bottom.

The incoming flux of the boundary from the west, together with the advantageous elevated position on the sides of the dune, are expected to speed up the process of freshening in those specific areas of the model, as depicted in Layer 9 of Figure 5.6. The thickness of the unconsolidated layers can influence it. Particularly the unconsolidated layers are thicker in the northeastern and southwestern areas of the model, compared to the alluvial plain, along the NW boundary. As a result of the low permeability of the sediments, the water levels are significantly higher in the dunes in the scenarios 3 compared to scenarios 1 and 2.

The model is simulated for 2000 years for scenarios 1, 2 and 3 to assess the time it would take for the homogeneous environment at a medium/high/and low permeability aquifers to freshen under current recharge scenarios.

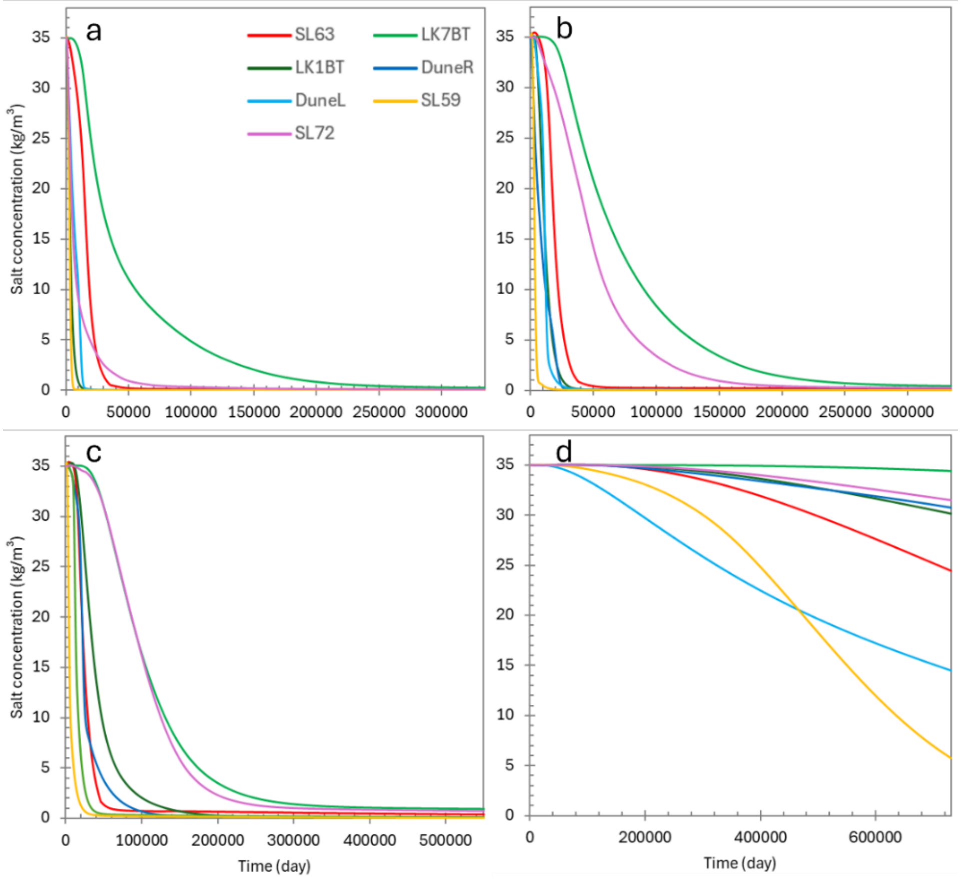

Figure 5.7 The observation points in case of 2000-year simulation for HK = 8 m/d, a – layer 3, b – layer 6, c – layer 9, and d – layer 12.

Figure 5.7 shows the observation points after a 2000-year simulation for scenario 1. In the medium permeability environment (HK = 8 m/d), the first three layers are completely fresh after 680 years, or 250000 days. In the sixth layer, it takes roughly 800 years to be completely freshen, while in the ninth layer, it takes about a thousand years. The observation points in layer 12 reveal that saltwater is still present at these areas after a 2000-year simulation.

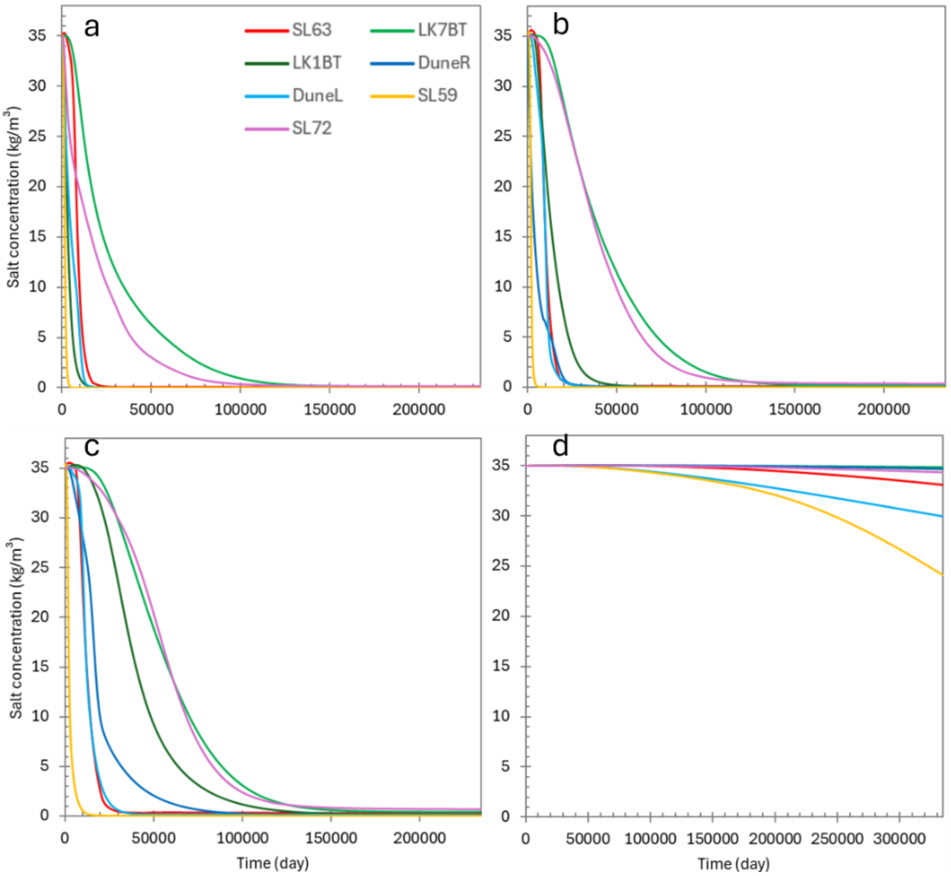

Figure 5.8 The observation points in case of 900-year simulation for HK = 18 m/d, a – layer 3, b – layer 6, c – layer 9, and d – layer 12.

Figure 5.8 depicts the observation points for the 900-year simulation for scenario 2. Obviously, in the high permeability environment of HK = 18 m/d, the freshening process occurs in the unconsolidated sediment much faster than in the medium permeability environment. After a simulation period of about 330 years, which is equivalent to 120,000 days, the aquifer in the third layer becomes completely fresh. In the sixth layer, the duration is around 150,000 days, equivalent to 410 years. In the ninth layer, the duration is approximately 170,000 days, equal to 465 years.

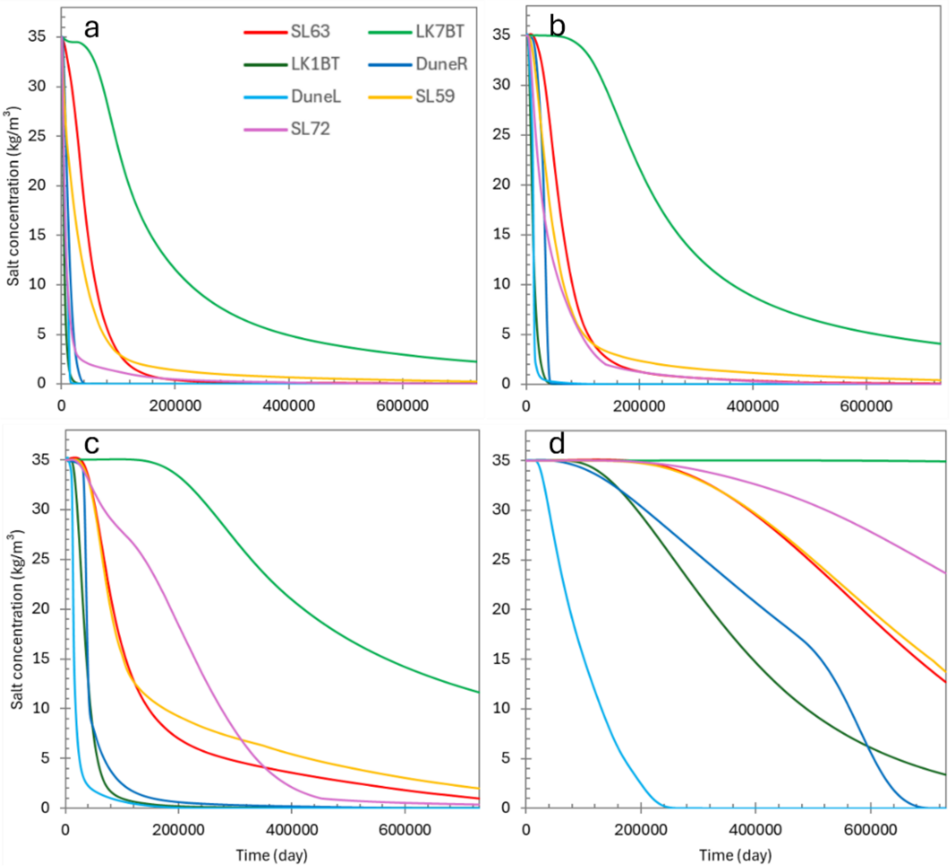

Figure 5.9 The observation points in case of 2000-year simulation for HK = 0.8 m/d, a – layer 3, b – layer 6, c – layer 9, and d – layer 12.

In contrast, in the low permeability environment of HK equivalent 0.8 m/d in scenario 3, the freshening occurs in the unconsolidated sediment more slowly than in the two previous cases (Figure 5.9). At the point LK7BT, located in the alluvial plain, there is still some saltwater in all layers after a 2000-year simulation. At other points, it takes around 1000 years and 1600 years to fully freshen the third and sixth layers, respectively. Layer 9 still contains some saltwater at the observation points of the alluvial plain.

Figure 5.10 illustrates the saltwater distribution after a 900-year simulation for the three scenarios1, 2, and 3. In general, the unconsolidated sediment layers are mostly fresh except for some saltwater remaining in the ninth layer of scenario 3 (HK = 0.8 m/d). The last layer of the model in the hard rock aquifer is also experiencing freshening, but at a rather low pace in scenario 2, likely because of the largest contrast in conductivity with the unconsolidated sediments. In contrast to expectations, the last layer of the model in scenario 3 underwent a significant freshening, similar to scenario 1 but at a slower rate. This can be attributed to the lower contrast in hydraulic conductivity between the hard rock aquifer and the unconsolidated aquifer for this scenario. Only at the sea, the salinity distribution follows the expected pattern of the interface with saltwater being found deeper as we move inland. This experiment demonstrates that even homogeneous conditions with relatively high hydraulic conductivity, the process of freshening occurs at a rather modest pace in the study area, and with significant lateral and vertical variations. This is the effect of a combination of factors including the recharge rate, the topography and the draining nature of the surface water bodies.

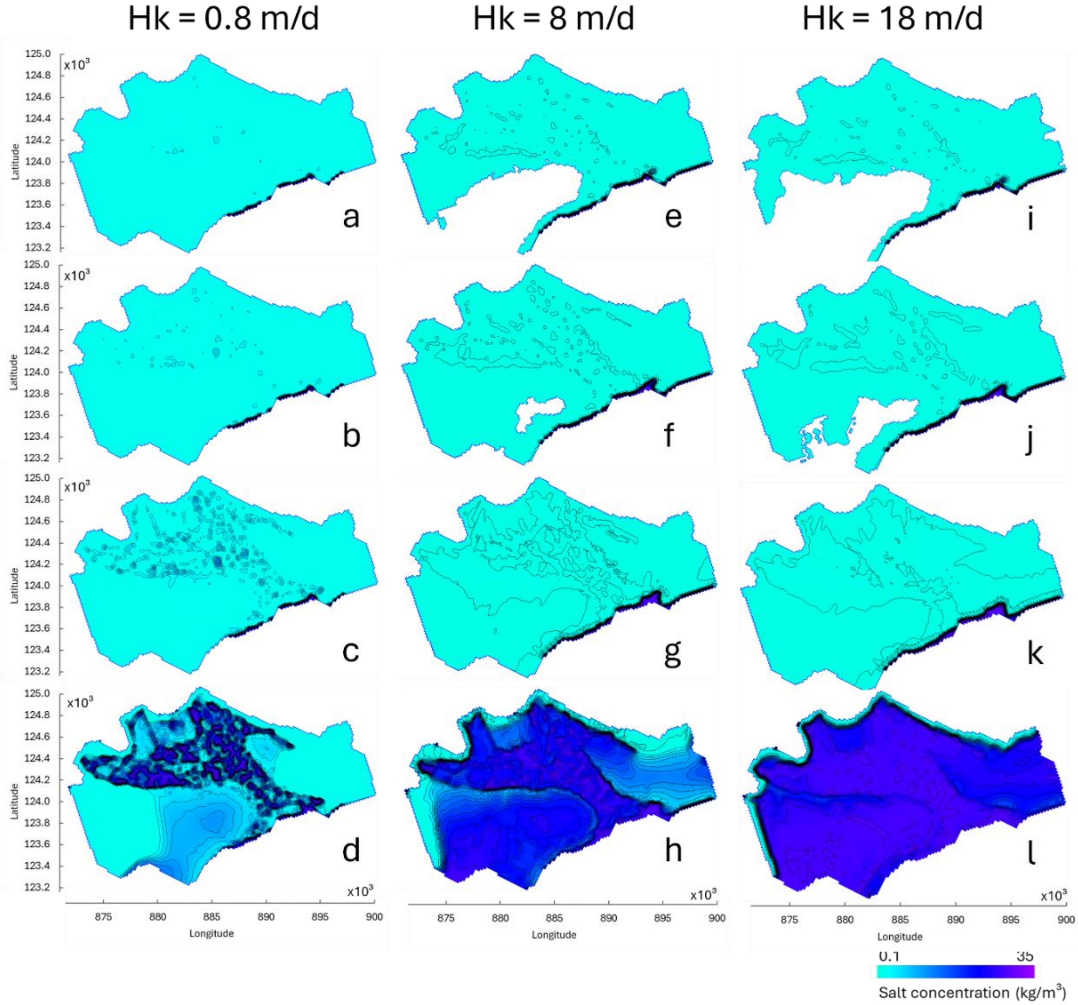

Figure 5.10 Saltwater distribution in the layers after a 900-year simulation for the scenario 1, 2, and 3 in the layer 3, 6, 9, and 12 in order from the top to bottom.

5.4.2 Scenario 4: realistic model

The actual model considering the observed hydrostratigraphy was run for 100 and 5000 years. Results are shown in Figure 5.11 and Figure 5.12, with a zoom on the first 100-year simulation plotted in Figure 5.13d and Figure 5.14a, b, and c, were they are compared to scenarios 5 to 7. In general, the points located at higher elevations, such as SL59, DuneL, and DuneR, are freshening faster over time, whereas the points located in the alluvial plain are freshening slower, such as LK7BT and SL63 and SL72. Most of the observed locations in Layer 3 follow a significant freshening trend, except for points SL63 and LK7BT, which are located at location where the clay lens is present. Therefore, the salt concentration does not change much at those observation point. SL72 is located at the foot of the sand dunes and receive the saltwater which is pushed from the high elevation dunes by freshwater recharge. After a hundred years, they are still displaying high salinities. The Pleistocene aquifer and hard rock are still mostly saline after 100 years.

The time series show clearly the evolution of salinity in the different layers. It takes about 50 years to be fresh in layer 3, but about 75 years in layer 6 for the observation points located on the sand dune side.

The saltwater distribution in the layers after a 100-year simulation is shown in Figure 5.14a, b, and c. Obviously, the top 3 layers are freshening fast, while in the lower layers, the salinity remain high except for the dunes. This is the result of the aquitard layer present in the alluvial plain, which prevents infiltrating water to percolate towards the deeper layers. In general, the top layers are freshening at a faster rate compared to other scenarios, whereas in the lower layers it occurs at a slower pace so that they still contain saltwater.

Since the freshening rate is quite slow for this configuration, we extended the simulation period to about 5000 years.

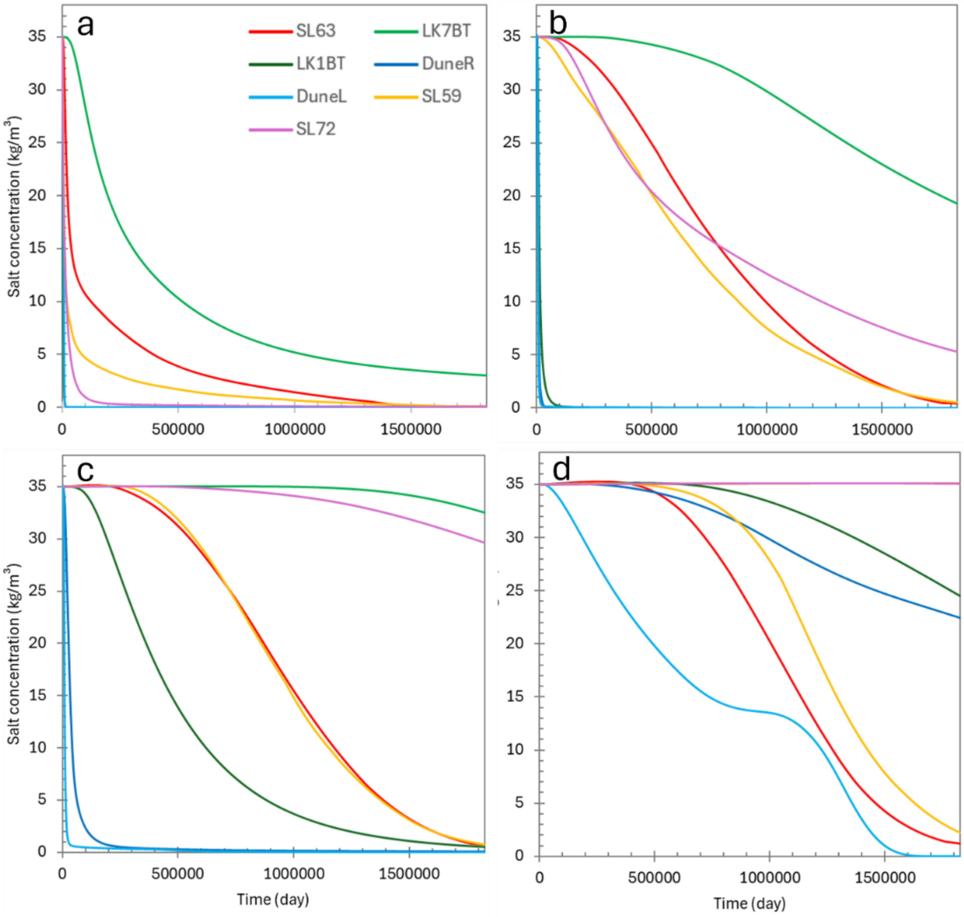

Figure 5.11. Observation points in case of reality in 5000-year simulation: (a) layer 3, (b) layer 6, (c) layer 9, (d) layer 12

Figure 5.11 and Figure 5.12 show the salinity evolution and final distribution for a 5000-year simulation. Compared to homogeneous cases for which all unconsolidated layers were fresh after less than 500 years in scenario 2, less than 1000 years in scenario 1, and less than 1600 years in scenario 3, this scenario illustrates that higher salinities are still observed locally in the Holocene aquifer, when present the aquitard is still saturated with salt water, and the Pleistocene aquifer is partly saline, except in the dune complexes and close to boundaries where it is recharged by the fluxes from the high mountains.

In the dunes, it takes less than 100 years of simulation to freshen layer 3, 250 years to freshen layer 6 and about 550 years to freshen layer 9. This observation shows that the dune systems constitute preferential recharge zone for the aquifers, due to their high elevation, the absence of the aquitard layer and of a draining river system.

As in previous scenarios, some points such as SL63, SL72 and LK07BT show a very slow freshening pattern with salty conditions after 5000 years of simulation. After 5000 years, the hard rock layer still contains a substantial amount of saltwater except close to the northwest boundary.

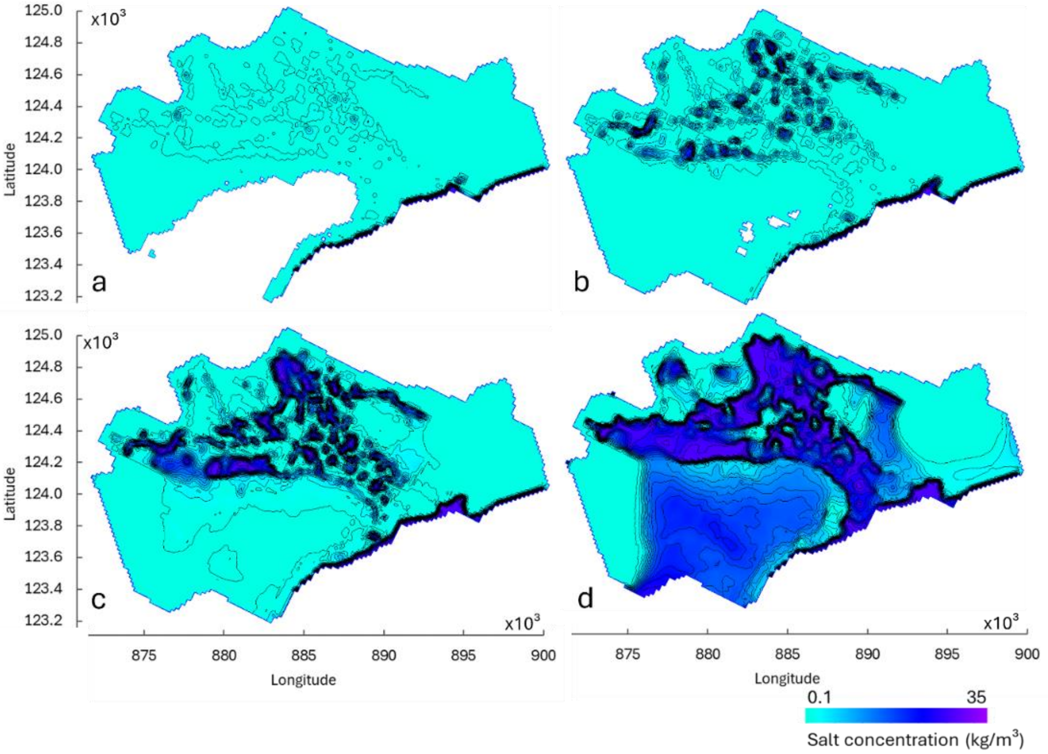

Figure 5.12 Saltwater distribution in the layers after 5000-year simulation: (a) layer 3, (b) layer (6), (c) layer 9, (d) layer 12

The last water high stand occurred 6000 years ago. However, the 5000-year simulation period already gives a good estimation of how the freshening processes have taken place since then. Given the monthly time steps used and the iterative nature of the coupling scheme with SEAWAT, simulations are slow to compute. The 5000-year simulations took about 17 days on an Intel Core E5-8500 CPU, 3.0GHz (64GB RAM). Simulating all the scenarios for such a long period of time would require excessive computational and memory requirement. In addition, some scenarios might run into convergence issues.

In addition, the simulations approach has neglected the variations observed during the last 6000 years in terms of recharge, river course, deposition and erosion processes, and land cover. It would therefore be unrealistic to attempt to reproduce the current situation with the model. The objective of the model was rather to evaluate the time scale at which the aquifer can be freshened.

Therefore, we can to some extent extrapolate the freshening rates observed for scenario 4. All simulations have shown that observation points behaved in a relative predictable way, with the first to experience a freshening being the first to be fully fresh with a S-shape trend. After an initial fast freshening, a steady freshening rate is occurring that then decreases at later stage. In all layers, LK7BT and SL72 are the last one to freshen, with a rate of 5 g/l for the last 250 years. It would therefore take at least another 750 years for the Holocene aquifer to be fresh (about 1500 years in total), which would still be an underestimation since the freshening rate decreases with time. For layer 6, SL 83 has a rate of freshening of about 2 g/l in the last 100 years so that it would take at least another 2000 years to be fully fresh. SL59 has an almost steady freshening rate of 1 g/l.100years, so that it would take more than 3000 years to be fully fresh. The Pleistocene aquifers is still mostly saline, and its freshening will take longer than the top layers.

We can therefore conclude that the timescale of freshening for the Luy River aquifer corresponds to a few hundred years in the dune complexes, to several thousands of years in the Pleistocene aquifer and clay rich zones of the alluvial plain. This is coherent with the observations made in Chapter 4 regarding the current salinity distribution.

5.4.3 Scenarios 5, 6, and 7

Three observation points located in the dunes, alluvial plain, and near the NW boundary are plotted in Figure 5.13a, b, and c for scenarios 5, 6, and 7 and compared with scenario 4 (Figure 5.13d).

The time series of salinity are exhibiting a different pattern in scenario 5 as opposed to previous cases (Figure 5.14d, e, f). Due to the presence of a continuous aquitard between the two aquifers, the process of freshening takes place at a slower rate in the Pleistocene aquifer. Sites at higher altitudes, like SL59, DuneL, and DuneR, are experiencing a more rapid process of freshening over time compared to scenario 4. On the other hand, points in the alluvial plain, such as LK7BT are undergoing a slower process of freshening. There is a significant disparity in the process of freshening between those places due to the presence of the clay layer separating the two aquifers, which impacts the flow paths in the unconsolidated layers.

The process of freshening is clearly occurring at a slow pace in the lower part of the alluvial plain, specifically in layers 3 and 6. The surface recharge cannot percolate towards the deepest layer and the draining role of the river contributes to removing this excess water from the aquifer. As a consequence, the Pleistocene aquifer is still almost completely saline. The right bank of the river exhibits a prominent saltwater pattern in layer 9, while layer 12 is still fully saline.

The influence of the upcoming flux from the northwestern border is obvious in scenario 5, since this particular section of the model exhibits a higher rate of freshening compared to other sections. The absence of inflow on the southern side of the sand dune (groundwater divide) causes a decrease in the rate of freshening. Additionally, the presence of the continuous clay in the alluvial plain restricts the flow from the dune side to the rest of the model domain, resulting in the observed patterns.

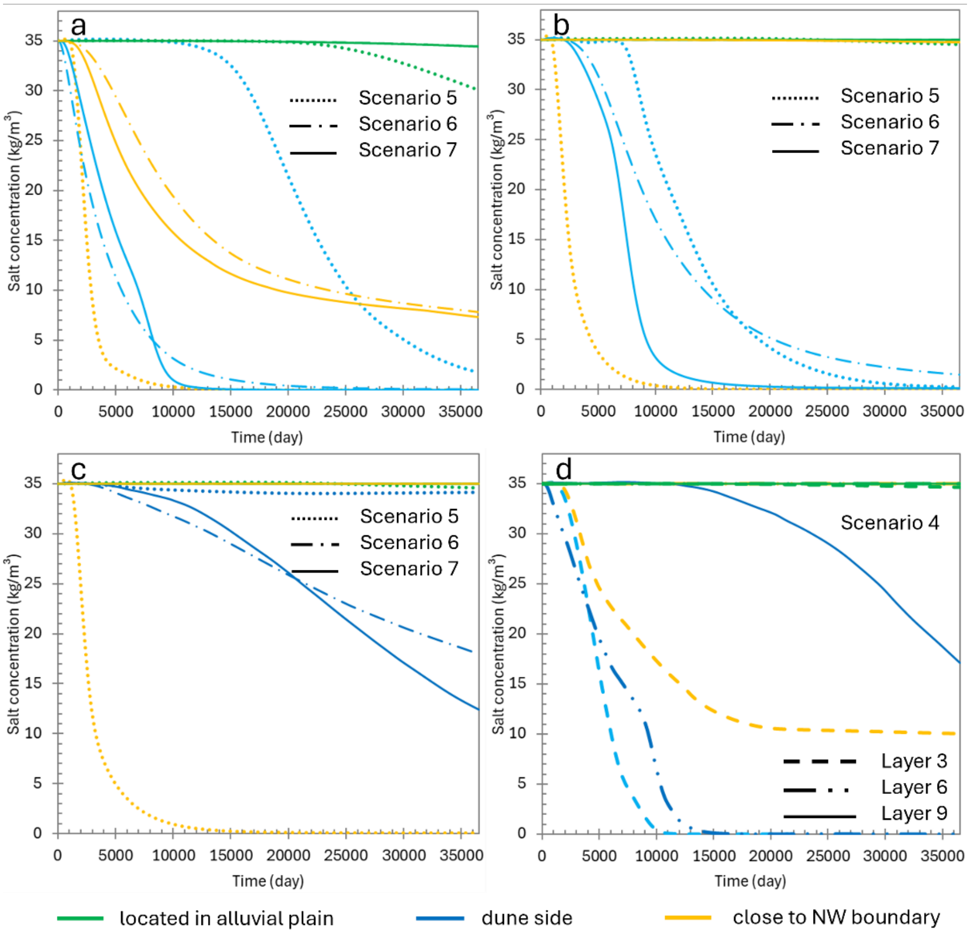

Figure 5.13 Observation points in scenarios 4, 5, 6, and 7 in 100-year simulation. The observation points of scenarios 5, 6, and 7 are ploted together in a – layer 3, b – layer6, c – layer 9.

The effect of no flow on the NW boundary in scenario 6 is clearly shown in the horizontal slices in Figure 5.14g, h, i. Since there is no freshwater coming from the upstream part of the catchment, only the surface recharge can freshen the saltwater further inland, while salty conditions prevail at depth, including at the boundary itself. The freshening rate are overall decreased compared to scenario 4 (Figure 5.14a, b, c). In contrast, increasing the recharge by 20% in scenario 7 is boosting the freshening process in all layers.

The combination of the simulations in the different scenarios allows us to have an overview of the freshening process and the saltwater distribution pattern at the different hydraulic properties and locations in the study area.

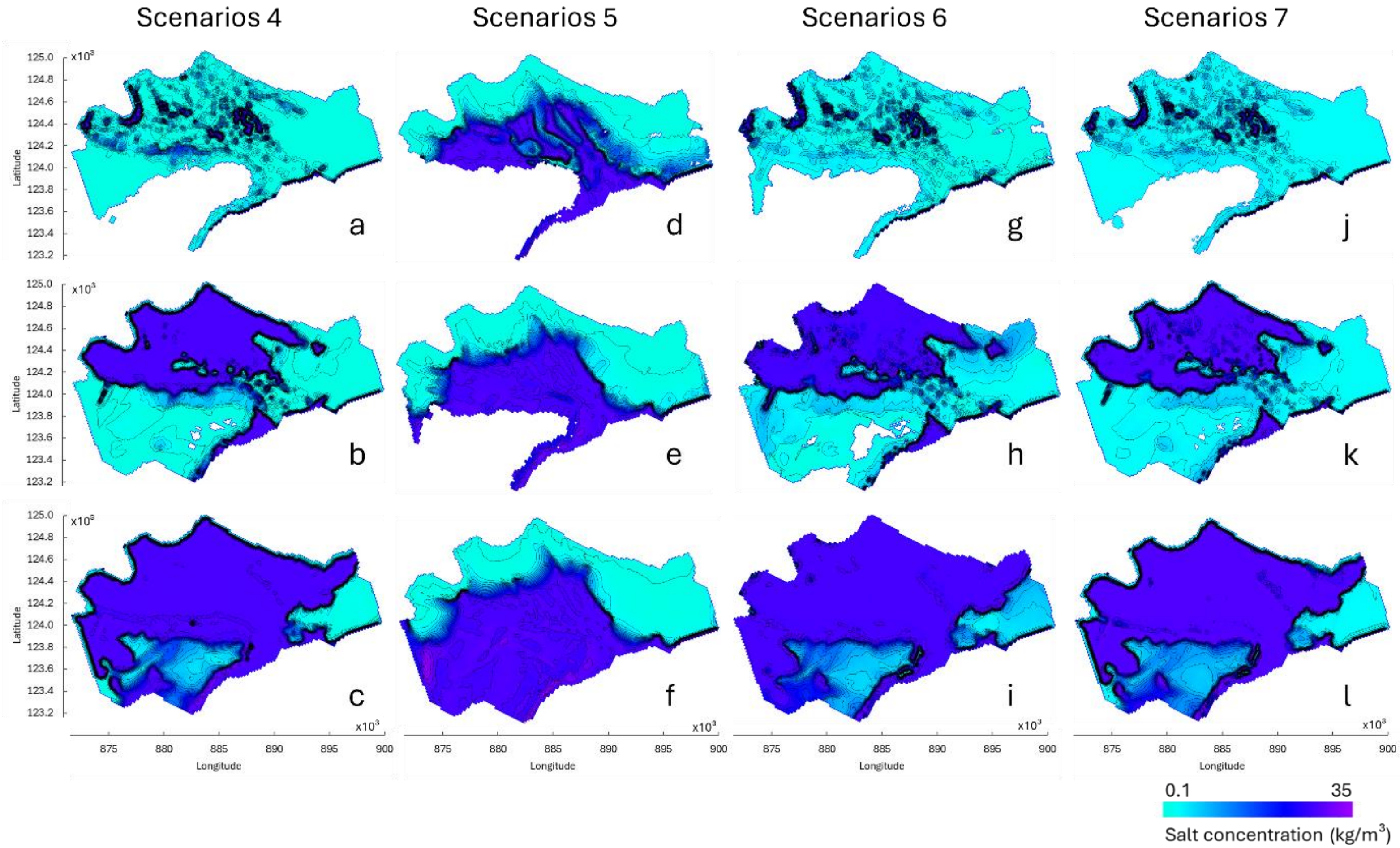

Figure 5.14 Saltwater distribution in the layers 3, 6, 9 from the top to bottom for scenarios 4, 5, 6, 7 simulated in 100 years. The last layer in all cases is still fully saline.

5.5 Discussion

The simulated scenarios with uniform hydraulic conductivity showed that the freshening process in the unconsolidated aquifer occurs slowly, taking roughly 1600 years for full freshening, for low-permeability sediments (HK = 0.8 m/d) characteristic of the Quaternary aquitard, and faster, about 1000 years, for the medium-permeability sediments (HK = 8 m/d) characteristics of the Holocene aquifer, and around 500 years for the high-permeability sediment (HK = 18 m/d) characteristics of the Pleistocene aquifer.

The freshening rate is not only dependent on the hydraulic conductivity of the sediment but also on the elevation of the top, bottom, and thickness of the aquifer. Since the elevation of the alluvial plain is close to sea level, while the hard rock is found below sea level, the higher density of saltwater contributes to maintaining salty conditions in the deeper layers. The recharge rate, interaction with rivers, and freshwater coming from upstream also contribute to the complex pattern of salinity, even in homogeneous conditions. The higher the freshwater incoming flux, either from surrounding or surface waters, the faster the freshening process occurs.

In the simulation of the realistic hydrostratigraphic structure, it was found that saltwater was trapped in the (discontinuous) clay layer distributed throughout the catchment area, delaying the freshening of the deeper layers compared to homogeneous conditions. Extrapolating the simulated freshening rate, it would take more than five thousand years to fully freshen the Luy river aquifer system, which is coherent with the proposed hydrogeological conceptual model from hydrochemistry. In particular, the groundwater model confirms that:

- higher salinity values are expected in the deepest part of the unconsolidated aquifer and the hard rock aquifer;
- the presence of aquitards delays the freshening process in semi-confined layers;
- saltwater can be trapped in low permeability sediments that can constitute secondary sources for salinization;

- the dune systems act as preferential recharge zone that freshen very fast and constitute freshwater reservoirs;
- the river and streams tend to drain the shallow aquifer and prevent freshwater to percolate deeper in the aquifer.

Considering the limitations of the simulation approach and all the simplifying assumptions, the model does not allow to predict accurate freshening rate nor to reproduce the current situation. However, it allows to estimate the order of magnitude for the freshening rate, which is a few hundred years in the shallow part of the aquifer and in the dune systems to several thousand of year below the confining clay layer. The main limitations of the model are:

- Hydrostratigraphic units are simulated as homogeneous, while field tests show there are extremely heterogeneous. The presence of clay lenses within the Holocene and Pleistocene aquifer could further exacerbate the presence of trapped saltwater as observed in wells and geophysical data (Pham et al., 2022, Cong-Thi et al., 2021, 2024a) and further delay locally the freshening process by influencing the flow paths.
- The river system, in particular the downstream part has been simulated with fixed head and freshwater conditions, while the estuary of the Luy river is influenced by the tides, and brackish water can be found upstream up to 5 km from the sea. Therefore, riverine saltwater intrusion is not taken into account.
- The geological model, boundary conditions and recharge rate have been taken as constant for the whole simulation period, ignoring variations in climatic conditions, deposition systems and land use. Especially the recharge rate was estimated to be about 400 mm/year in the current conditions, but this was likely different in the past.
- Anthropic activities have been ignored. Current irrigation practices in the study area have led to wells being contaminated by saltwater, likely through upconing of the saltwater trapped in low permeability layers. Irrigation of rice fields with surface

water from dams can locally speed up the freshening processes. However, these activities are supposed to be significant only for the last decades.

Saltwater patterns are matching quite well with the actual observation points described in Chapter 4. This suggests that the hydraulic conductivity values used in the realistic scenario, even if using a homogenous value per layer constitutes an acceptable simplification.

5.6 Conclusion

This study involved the construction of a 3D hydrogeological stratigraphical solid model using well logs and other existing data. In order to create a three-dimensional hydrogeological stratigraphic solid model, it is crucial to accurately determine the boundaries between different lithological units. These contacts serve as the basis for grouping lithological classes into hydrogeological units that have significant meaning. A hydrogeological model was created using a 3D stratigraphical solid model consisting of four layers: the Holocene aquifer, the Quaternary aquitard, the Pleistocene aquifer, and the hard-rock or secondary aquifer.

The coupled density-dependent groundwater flow and transport model SEAWAT was used to simulate freshening processes in the study zone. The recharge rate was computed from a soil moisture balance model accounting for current climatic conditions and land use (Chapter 3). Additionally, hydraulic conductivity values were obtained from previous field studies carried out in the study area. Several scenarios were simulated to estimate the impact of heterogeneity on the freshening processes.

The findings suggest that during long-term freshening, saltwater becomes trapped inside the clay aquitard and the lower aquifers. This trend is exacerbated by the difference in density between saltwater and freshwater. The top and bottom elevation of the aquifers is also affecting the saltwater distribution.

The saltwater distribution pattern identified in the most realistic scenario is in line with the findings of the geophysical investigation conducted by Cong-Thi et al. (2021) and the hydrochemical conceptual model proposed by Pham et al. (2022). The findings of this study can serve as a foundation for predicting the saltwater intrusion in the study area under different climate change scenarios. This information will aid government officials in evaluating the capacity of groundwater resources and implementing effective strategies for maintaining groundwater sustainability in the study area. This will be further investigated in Chapter 6.

Chapter 6. Simulating groundwater management scenarios in the salinized Luy River aquifer systems under climate change

6.1 Introduction

Ensuring the sustainable use of drinkable water resources is critical for the world's overall well-being (World Health Organization, 2004; United Nations, 2007). Nevertheless, despite many efforts, the utilization of several groundwater resources has become ineffective due to overexploitation and pollution caused by population growth, urban expansion, industrialization, agricultural development, and climate change. These factors lead to a decline in water quality and groundwater levels in many regions (Hughes et al., 2011; Taylor et al., 2013; Cosgrove and Rijsberman, 2014).

Various studies have been conducted for groundwater sustainable management, focusing not only on long-term aquifer health (Meinzer, 1923), but also on aquifer drawdown, dewatering, and saltwater intrusion, which are the most important issues in coastal areas (Conkling, 1946; Fetter, 1988; Schwartz and Zhang, 2003). Globally, groundwater management is based on the efficient and sustainable use of groundwater. Planning typically addresses three main management concerns: 1) Adjust groundwater abstractions to meet future sustainable supply and demand requirements, considering other groundwater functions such as maintaining baseflow in rivers and recharge. 2) When figuring out acceptable extraction rates, an integrated aquifer system management should consider in which aquifer units to extract and how to optimize well locations. 3) Additionally, one should take into account the economics, social impact, local regulations, and changes in water quality (Zekâi Ş. 2015; Wendy A. K. and Alex K. M., 2019).

People commonly use the term "climate change" to refer to global warming, which is defined as the continuous increase in average global temperatures. More generally, higher average temperatures are also causing more intense storms, droughts, and other weather extremes (Summerhayes, 2015; Foster et al., 2017; IPCC, 2021). There will be variations in the patterns and magnitude of changes in precipitation, evapotranspiration, and the timing of rainy and dry seasons. In aquifers, the main sources of groundwater recharge are precipitation and interaction with surface water bodies. As a result, any climate changes that directly impact precipitation and surface water will ultimately have an effect on groundwater systems. Similarly, Climate Change is expected to impact water demand, and therefore the need for groundwater extraction.

Seawater intrusion is particularly likely where groundwater extraction leads to water tables lying below sea level, including upconing, but fossil saltwater trapped in clay can also play a significant role in the distribution of seawater (Park et al., 2005; Bennetts et al., 2006; Werner et al., 2009). The perturbation of the water cycle through Climate Change inevitably impacts seawater intrusion processes. The impacts of saltwater intrusion, global climate change, and sea level rise have profound effects on the local communities living in coastal areas in terms of access to groundwater and water demand. The situation becomes even worse when the population grows over time.

The findings of previous chapters show that the Luy River aquifer system located in a semi-arid climate zone is salinized. The growing population, combined with industry and agriculture developments, requires a lot of freshwater. Furthermore, the overexploitation of private wells by farmers might cause the migration of saltwater from the depth towards the shallower layers. All of these issues, combined with global climate change and sea level rise, make groundwater management in the study area more challenging.

Because of their susceptibility, it is critical to prioritize sustainable management of coastal fresh groundwater sources. One requirement is a precise delineation of the current spatial distribution of freshwater reservoirs or saltwater distribution patterns. Obtaining an accurate description is challenging, whereas measurements are sparse, particularly at greater depths. Salinity fluctuates over short distances, influenced by relatively low hydraulic gradients that change over time and the heterogenous nature of sediments (Cong-Thi et al., 2021).

Modelling studies are valuable for determining the relative significance of various factors influencing SWI, as well as ensuring the model accurately incorporates all relevant processes (Werner A.D. and Simmons CT., 2009; Storlazzi, C.D et al., 2011; Tam, V.T., et al., 2016). In addition, models are helpful in predicting the future behaviour of groundwater systems in response to climate change, sea level rise, and human activities.

The objective of this chapter is to evaluate the influence of global climate change and sea level rise on the groundwater system of the coastal plain in the Luy River catchment (south-central Vietnam). The primary objective is to simulate groundwater management scenarios in the salinized Luy River aquifer systems. We suggest applying a combined method that utilizes the patterns of recharge and sea level rise based on the latest IPCC predictions (IPCC 2021), along with a density-dependent groundwater flow model developed for the study area using SEAWAT (Gue and Langevin, 2002).

We simulate the impacts of saltwater intrusion on the groundwater system, taking into account predicted sea level rise, the yearly variable groundwater recharge, groundwater abstraction, the initial salinity map, and the hydrogeological conditions of the study area. Finally, the analysis of the variations of the simulated groundwater head and salt-freshwater interface pattern enables us to assess the likely impacts of climate change on the groundwater resources of the study area. Following this, we will provide recommendations for the sustainable management of groundwater resources in the study area.

6.2 Study area and available data

The study area is characterized by short, steep rivers whose upstream tributaries originate in hills in the west, while their downstream courses run through narrow and shallow coastal plains toward the east. The semi-arid climate conditions have a typical temporal pattern of dryness from November to April and rain from May to August. Quaternary aquifers in the

Luy River Plain play an important role in water supply for the local community and their agricultural activities.

The model domain and structure of aquifers are similar to the one described in Chapter 5. It represents the Holocene aquifer, semi-continuous Quaternary aquitard, Pleistocene aquifer, and secondary hard-rock aquifer. The alluvial plain slopes from the west at the foot of the mountain at about 50 m (ASL) to the east at the coastline level, while sand dunes are present along the coastline both to the south and the north of the river, culminating at an elevation up to 160 m. During the dry season, irrigation water for rice fields was insufficient most of the time so that farmers recently changed the type of plant in parts of the study area from rice fields to dragon fruits and coconut plants, as they are more drought and salt tolerant, allowing the farmers to use groundwater as an irrigation source. However, experience shows that irrigation wells are often becoming too salty after a few irrigation seasons (Tran T.D., 2020).

Based on the pumping test results provided by Nawapi (2008, 2015) in the study area, the hydraulic conductivity of the Holocene aquifer ranges from 0.7 to 47 m/d and the Pleistocene's from 0.9 to 7.2 m/d. Figure 6.1 and Figure 6.2 illustrate the hydraulic conductivity distribution of the Holocene and Pleistocene aquifers obtained by inverse distance interpolation from 19 and 10 pumping test points in the two aquifers, respectively. Obviously, the majority of pumping test points are situated in the alluvial plain on the left bank of the Luy River, with no available data on the dunes. There are two tests in the Holocene aquifer showing a high value of hydraulic conductivity of 30.1 and 46.9 m/d, which were taken from the shallow wells (at 6.5 m and 3.5 m depth from ground surface, respectively) in the local sand parts. This may overestimate the hydraulic conductivity for the Holocene aquifer, which is globally less conductive that the Pleistocene aquifer, but it can serve as an indication for the distribution of hydraulic conductivity during calibration. Note that this data set is more restricted than the one used in Chapter 5 that considered more data located outside the study area and that it is only meant for illustration as the hydraulic conductivity estimation is part of the calibration process.

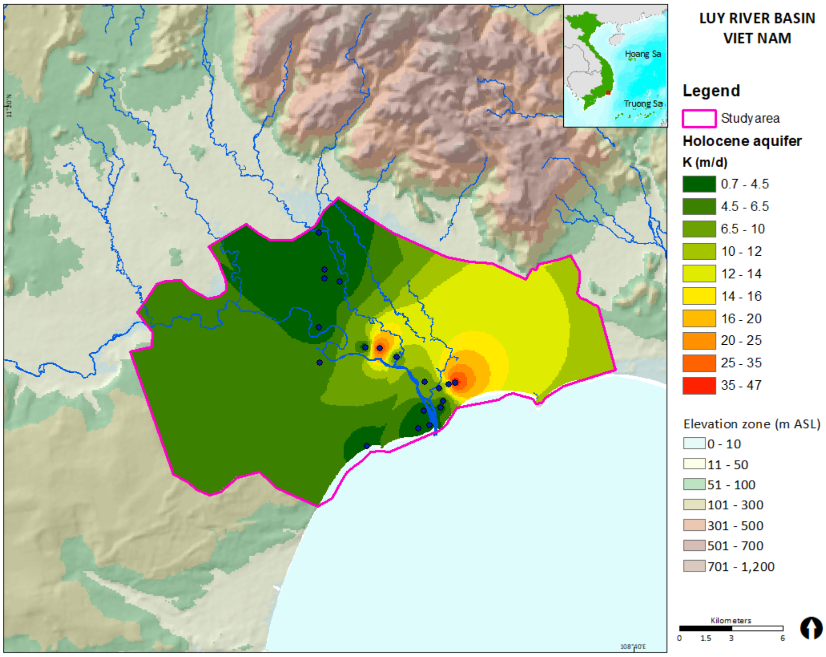

Figure 6.1 Hydraulic conductivity distribution in Holocene aquifer interpolated from the pumping test of Nawapi.

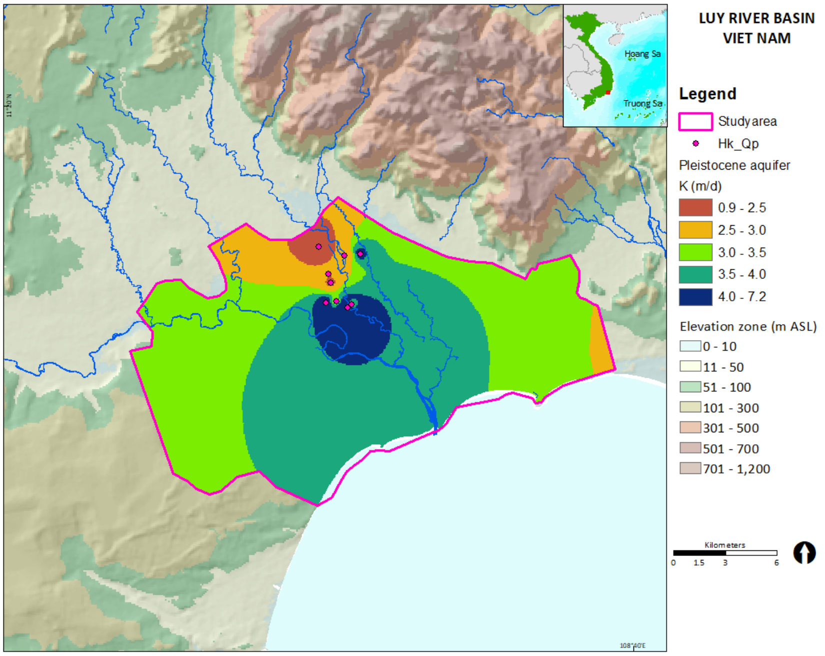

Figure 6.2 Hydraulic conductivity distribution in Pleistocene aquifer interpolated from the pumping test from Nawapi.

Nawapi (2008, 2015) reported that water levels observed in wells drilled in the dunes were sometimes deep, from 20 to 60–70 m from the ground surface, with some wells having even water levels deeper than 100 m under the surface. This suggests that important abstraction of groundwater might take place in the sand dunes.

The groundwater potential in the area is erratic, with varying hydraulic conductivities related to the presence of clayey sediments, and a distribution of fresh groundwater that does not follow any obvious trend; it primarily exists as a shallow freshwater lens lying over a more saline aquifer (Cong-Thi et al., 2021, 2024a: Pham et al., 2022). Furthermore, riverine saltwater intrusion exacerbates the situation. The potential for groundwater abstraction in the whole Bac Binh district was estimated at about 622587 m^3/day according to Nawapi (2008).

Field campaigns recorded groundwater levels during the rainy season of 2020 and the dry season of 2021. We selected 35 wells where freshwater level was determined and used the average value between the seasons for the steady-state model calibration. At some locations, the water level is below sea level, likely due to local groundwater extraction. Next to groundwater levels, the electrical conductivity of both Holocene and Pleistocene aquifers and the observed salinity are used to calibrate the groundwater model.

The Holocene and Pleistocene aquifers used to be the main source for drinking water and domestic water for residents. Recently, during the rural development program of the government, tank water was supplied for living. However, the householder still needs to abstract groundwater for agricultural activities.

According to BTPC (2018), the abstraction rate for each individual irrigation well in the study area ranges from 40 to 80 m^3/day and can reach up to 172m^3/day locally. In addition, MONREMEDIA (2022) reported that there are 7 groundwater abstraction wells distributed in the Bac Binh district (i.e. not necessarily within the model boundaries), which are operated by the government, with a total abstraction rate of about 3170 m^3/day.

In addition, we set up an interview campaign during the field campaign in 2020, where farmers having wells were asked about their water extraction. It appears that the abstraction volume ranges from 5 to 50 m^3/day, in hundreds of shallow production wells drilled in both the Holocene and Pleistocene aquifers, scattered over many villages of the study area. These estimated pumping rates will be used as the initial rate for current and future groundwater abstraction scenarios.

As described in Chapter 5, the salinity evolution in the coastal aquifer is highly dependent on the initial conditions and the heterogeneity of the aquifer which is largely unknown. An initial estimate of the salinity is therefore required to make any meaningful prediction of the future evolution of the salinity distribution. Cong-Thi (2024b) constructed an updated salinity map at three different levels corresponding to the depth ranges 0 to 5 m, 5 to 10 m, and 10 to 30 m combining electrical resistivity data and groundwater samples using Indicator Kriging. The salinity map is shown in Figure 6.3. This salinity map is used as the initial salt concentration for all simulations involving solute transport.

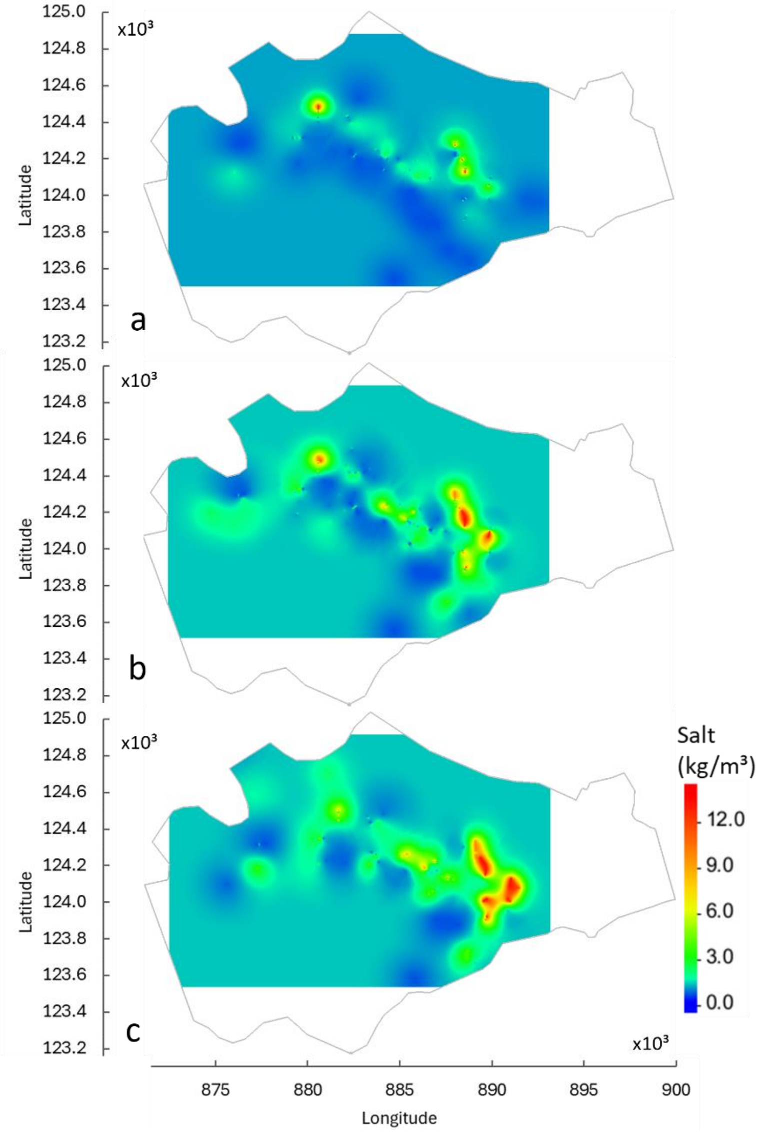

Figure 6.3 Salinity map at 0-5m depth (a), 5-10m depth (b), and 10-30m depth (c) (modified from Cong-Thi 2024a) which is added as initial salt concentration for SEAWAT simulation.

The average recharge estimation of Chapter 3 is used to simulate the current situation. Note that for transient simulations, the recharge is varying according to monthly average values.

6.3 Methodology

6.3.1 Climate change and sea level rise

Climate change presents many aspects and directly affects human life. This study considers two key factors: rainfall and sea level rise. According to the report of the Scenarios of Climate Change (MONRE, 2021) (RCP4.5), based on the latest IPCC predictions, the temperature recorded in the stations in Vietnam increased during the period 1958–2018 by about 0.15 °C per 10 years. The amount of rainfall tends to decrease in the north and increase in the south of the country.

The study area is located in a zone where the rain amount is expected to increase by about 10-15% by 2050 and by 10-20% at the end of this century. The SMB method, as presented in Chapter 3, provides the initial recharge input for the model. We consider the fluctuations expected at the mid-century and end-of-century to estimate the recharge for this century. Climate change naturally affects temperatures, humidity, radiation, and wind, leading to variations in evapotranspiration. However, due to the limited information available, we can only estimate the recharge variability based on the rate that corresponds to the monthly rain amount, using the initial estimates from the SMB method for the 1979–2021 period. Similarly, one can calculate the sea level starting from the initial level and continuing for the next 50 years. The satellite data (MONRE, 2021) showed that the sea level rose by about 3.6 mm per year along the Vietnamese coastal line in the period 1993–2018. The RCP4.5 scenario shows that sea level in Binh Thuan coastal area should increase by 12 cm, 17 cm, 23 cm, 29 cm, 35 cm, 41 cm, 47 cm, and 54 cm in the years 2030, 2040, 2050, 2060, 2070, 2080, 2090, and 2100, respectively.

The initial sea level imported to the model boundary at the coastal line is taken from the average value recorded at Phu Quy station during the period 1980–2018 (referenced to the Vietnamese national vertical datum). The above-mentioned increasing trend will be added to the simulations until the end of the simulation period. Following that, the recharge rate and sea level fluctuations are illustrated in Figure 6.4 and Figure 6.5.

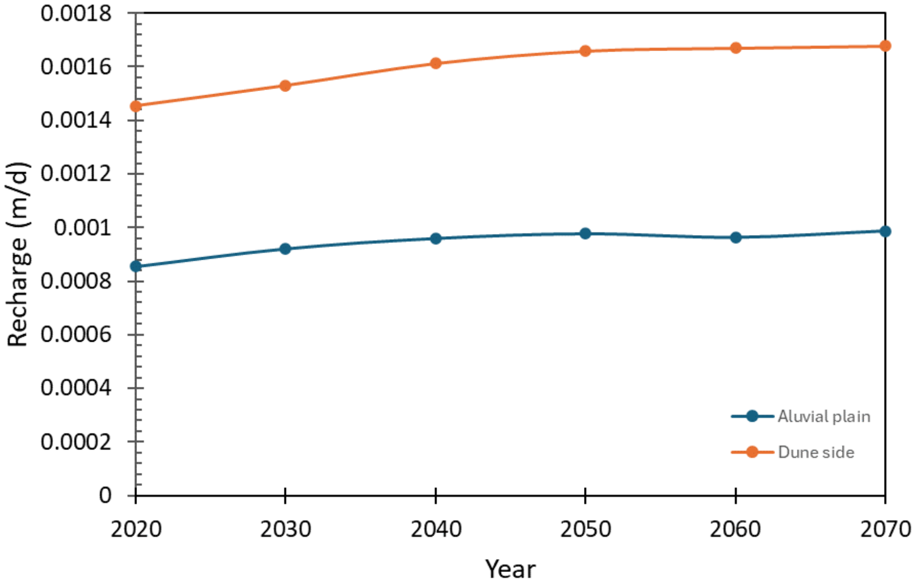

Figure 6.4 Estimated recharge under the climate change conditions during the simulation period.

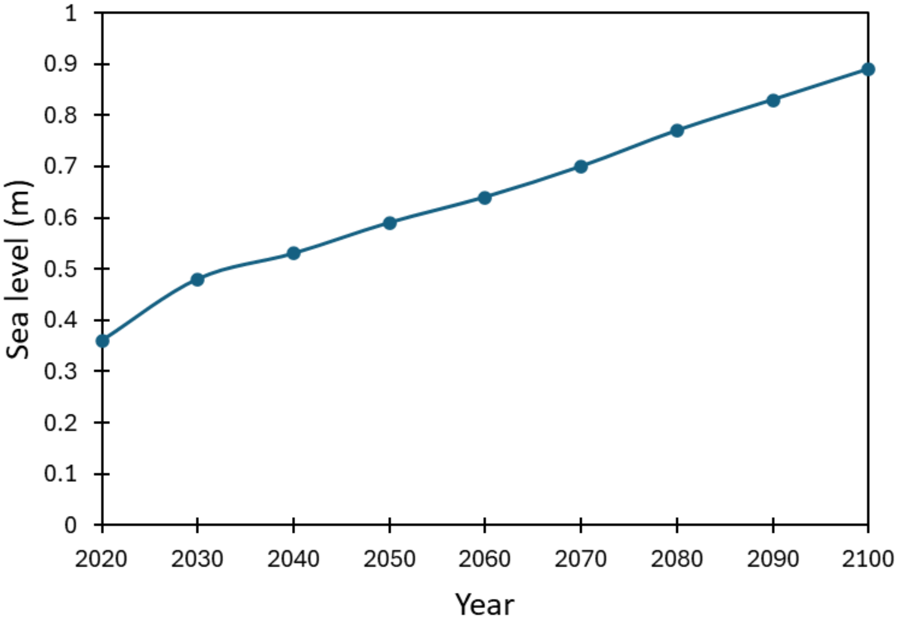

Figure 6.5 Sea level fluctuations under the climate change conditions during the simulation period.

6.3.2 Groundwater modelling

To assess the impact of global climate change and sea-level rise on groundwater resources, a variable-density groundwater flow model was built with MODFLOW coupled to MT3DMS through the SEAWAT code. The model is inherited from the model developed in Chapter 5. In particular, the structure of hydrogeological units, boundary conditions, drains, and rivers are the same. We are nevertheless considering the flux boundary, river and drainage conductance, and hydraulic conductivity values, which are sensitive components of the model during the calibration. We calibrate the model parameters using observation wells and water level measurements from two field campaigns during both the rainy and dry seasons.

We use the recent salinity map to set up the initial salt concentration for the model operating at different densities. For the lowest layers, the lack of data led to an overestimation of the salinity by indicator kriging at several locations. We then interpolated the initial salt concentration from water samples taken from deeper wells or from other sources, such as interviews during the field campaigns. We added the salt concentration from the 2019 field campaign in the Luy River estuary to the model as the imposed salinity along the river. The initial salt concentration setup for the model ranges from 0.45 to 35 kg/m^3 for fresh and salt water, respectively.

Groundwater extraction is also included in the groundwater model, with 40 production wells at a pumping rate of 30 m^3/day in both Holocene and Pleistocene aquifers, representing the numerous shallow wells in villages scattered in the coastal plain. We selected a smaller number of production wells than those in reality due to the large size of the model cell (200x200 m), the proximity of some wells, and the fact that their pumping rate is not always 30 m^3/day.

For all simulations in this study, we simulate a period of 50 years, with monthly stress periods. We first calibrated the model in steady state using groundwater levels collected from two field campaigns in 2020 and 2021. After that, we used the water level from three observation wells in the study area to evaluate the model in a transient state. The number of observation points is not sufficient for a real transient calibration. For each stress period, the areal recharge to the groundwater system was divided into 2 zones estimated by SMB model as described in Chapter 3. Each zone receives a uniform recharge equal to the monthly average of the distributed recharge in the respective area. The monthly average is obtained from the SBM model calculated with daily time steps on a 42-year period and adjusted in future scenarios based on the estimated rainfall. Another climate change variable input to the model is the sea level, which increased by 34 cm at the end of the century compared to the baseline period. We interpolated, when relevant, this rise in level linearly for each stress period throughout the simulation period.

Calibration pays attention to the root mean square error (RMSE) and the mean absolute error (MAE), keeping them as small as possible. However, the majority of the observation wells are also production wells, at least during the dry seasons, where the pumping rate and period of activity (pumping is not constant, but only active during irrigation) affects the water level. Some water level measured in wells are indeed below sea level indicating a groundwater extraction influence. Part of the calibration errors can be attributed to water levels collected mostly from the abstraction wells. In addition, the coarseness of the grid inevitably leads to approximated levels when compared to actual observation.

6.3.3 Formulation of scenarios

When forming the scenarios for the modeling, we consider the sea level rise, global climate change, the location, and the pumping rate of the production well. Eventually, we want to identify scenarios where groundwater extraction can sustain irrigation practices, under the effects of global climate change and sea level rise, while minimizing further salinization of the aquifer. Therefore, 3 scenarios are formulated:

1. Saltwater intrusion scenario in natural conditions (no extraction) under climate change and sea level rise. Here we will use the fluctuation of the recharge and sea level calculated based on the Scenarios of Climate Change (MONRE, 2021) (RCP4.5). We take the initial condition from current observations and see how the situations will evolve in the future if groundwater extraction would stop.
2. We integrate the impacts of climate change and sea level rise with the estimated pumping rates of production wells. This helps us see how the current situation will evolve in the future without any change in the pumping rate.
3. Finally, the model is tested where the totality of the extraction is transferred to the dune system to see if long-term groundwater extraction in the dunes can be a sustainable groundwater management option.

6.4 Results and discussion

6.4.1 Model calibration

We first calibrated the four-layer model in steady-state using trial-and-error, focusing on the hydraulic conductivity, the flux boundary, and river and drainage conductance. The whole recharge from rainfall in the highland region does not always enter the model as assumed in Chapter 5, as evidenced by first model runs that indicated water level too high. As a result, since this component of the model is highly uncertain, the incoming flow was lowered throughout the calibration process. The hydraulic conductivity was calibrated using the available data and considering sediment materials for each model layer. By examining the sediment material in the different branches of the river and drain locations, we were able to modify their conductance. The calibration was done when finding out the minimum residual values between the calculated and observed hydraulic heads.

The average groundwater levels observed in 2020–2021 (two field campaigns during the dry and wet seasons) were used for the calibration. Figure 6.6a show the hydraulic conductivity in the first model layer (Holocene aquifer), while Figure 6.6b shows the groundwater head for the Pleistocene aquifer and the head differences of simulated versus observed values for the 45 observed boreholes for the steady state calibrated model. The root mean square error (RMSE) is 2.15 m, while the mean absolute error (MAE) is 1.75 m. Given the grid cell size of 200x200 m, there are in practice significant variations of hydraulic head at this scale. Additionally, most of the observed wells are also production wells, so that discrepancies will happen related to the simulation of pumping wells at arbitrary location. We cannot really hope to get a better result. This is clearly illustrated by a series of wells having observed head below sea levels (Figure 6.7). In general, the total resulting error is acceptable and the water level follows the gradient trend in the study area.

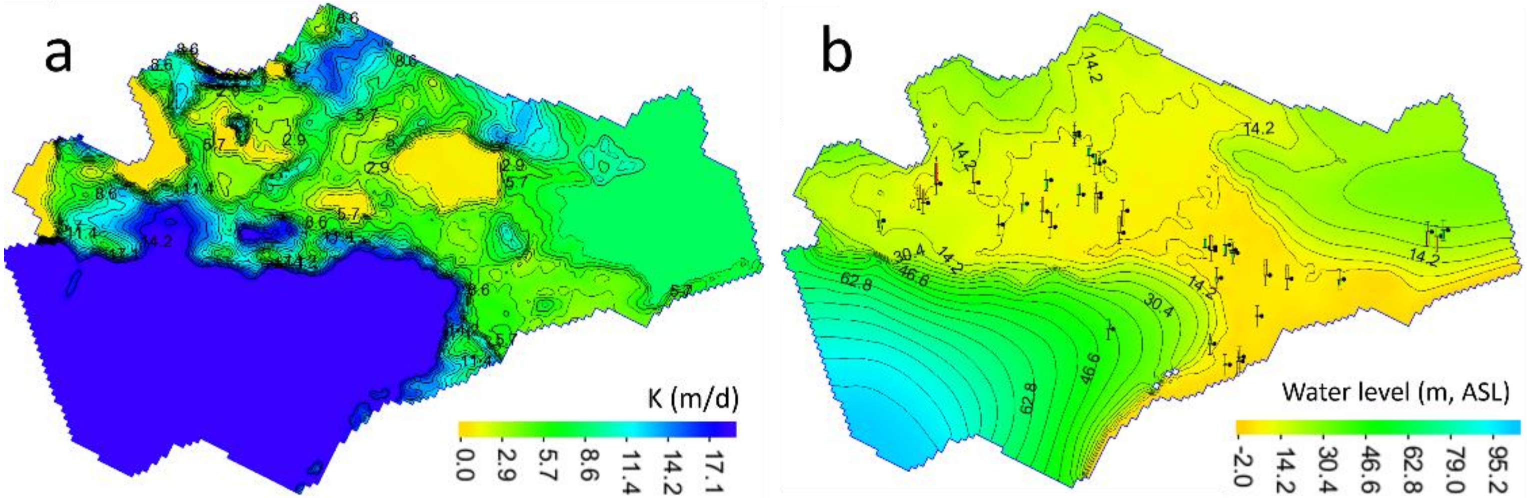

Figure 6.6 a – Hydraulic conductivity of the first model layer; b – Simulated hydraulic head after model calibration in steady state using static groundwater level observed in 45 boreholes.

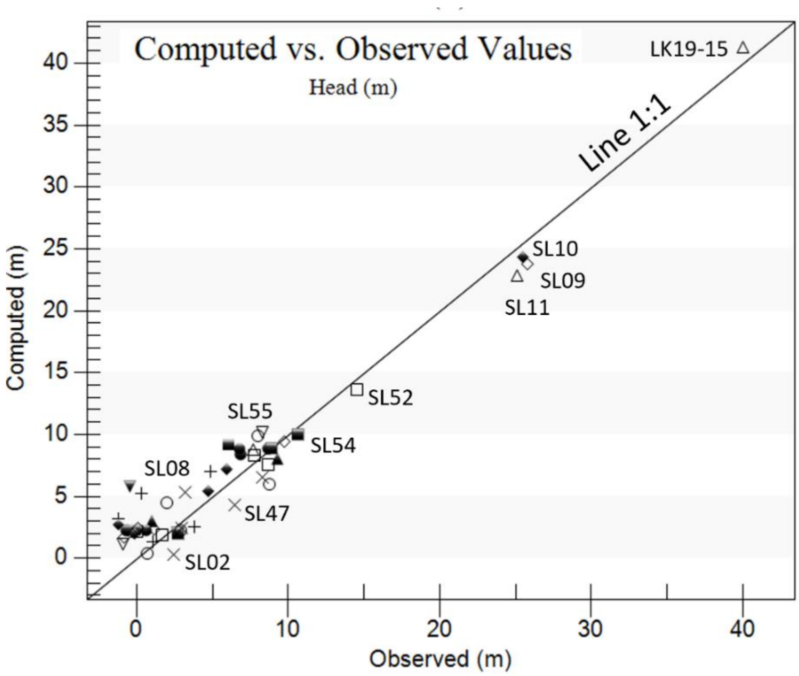

Figure 6.7. Scatter plot of calculated groundwater head versus observed groundwater head for the Holocene and Pleistocene aquifers in the model calibration.

The obtained calibrated parameters were then validated using transient flow simulations for 2020–2021 using the daily (converted from hourly) observed time series of groundwater levels in the boreholes LK02BT, LK12BT, and LK14BT (Figure 6.8). The recharge input for this validation was taken from the corresponding daily recharge calculated by the soil moisture balance method for the 2020–2021 period.

The difference between simulated and observed heads is globally acceptable. An example is shown for LK12BT. It can be seen that, as expected, water levels are increasing after rainy periods and then recessing during dryer periods. This particular well is particularly influenced by the proximity of a draining canal that prevents the actual head to rise above a preset level, a behavior difficult to reproduce with the model because the grid is too coarse.

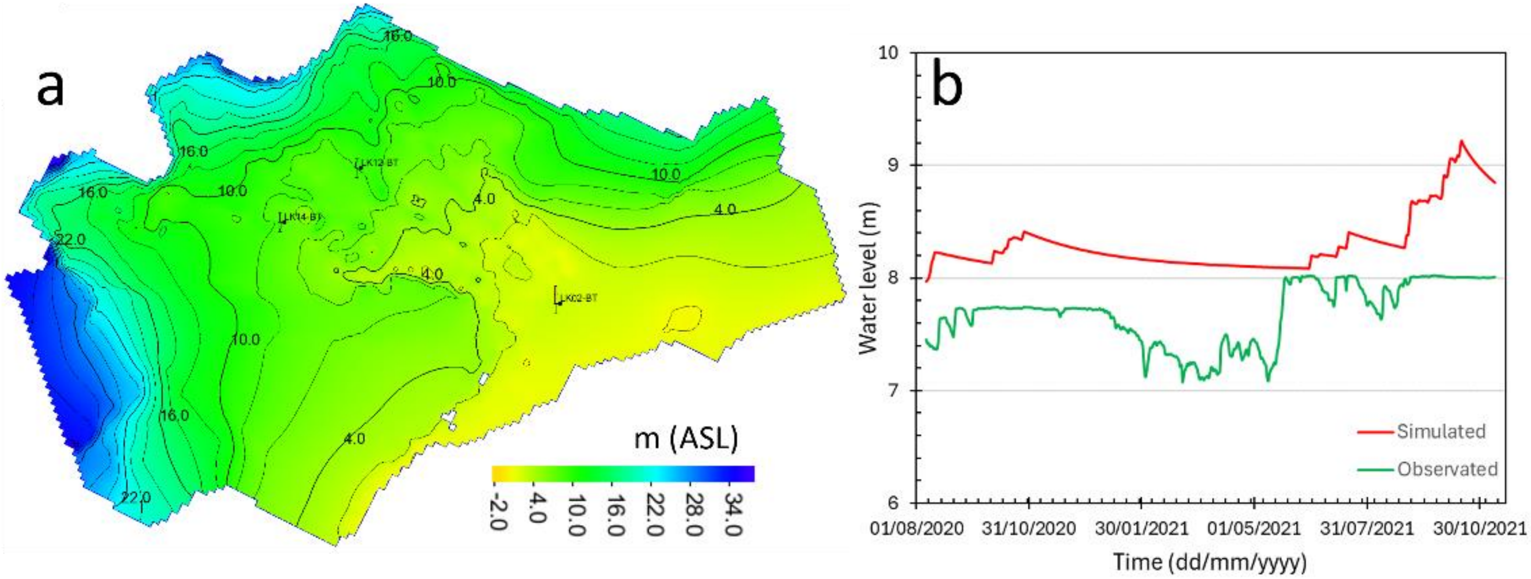

Figure 6.8 a - Valuate calibration in the transient state; b - Comparison of the simulated groundwater head with the observed in 2020‑2021 of the well LK12BT.

Table 6.1 The major input data and hydraulic parameters after calibration for the SEAWAT model.

Input data, hydraulic parameters	**Value range and data source**
Increasing recharge for both dune and alluvial plain	From 0.000854 m/d to 0.0009871 m/d for alluvial plain and from 0.001454 m/d to 0.0016771 m/d for dunes
Increasing Mean Sea level	From 0.36 m in 2020 to 0.7 m in 2070 (referenced to Vietnamese national vertical datum), as observed in Phu Quy meteorological Station
Salt concentration	35 kg/m^3 for the sea boundary, 22-25 kg/m^3 for river estuary, 0.45 kg/m^3 for fresh water
NW flux boundary	30417 m^3/day
Hydraulic conductivity	range from 0.7 - 9.5 m/d in Holocene aquifer and 0.9 - 17.5 m/d in Pleistocene aquifer, 0.57 for aquitard
River and drain conductance	River conductance 22.8 m/d, drain conductance 0.57 m/d - polygon in alluvial plain, 1 m below the surface

Table 6.1 presents the major input data and hydraulic parameters after calibration for the SEAWAT model.

During a short calibration period, the salinity distribution changes only slightly as already observed during the long-team simulations of Chapter 5. In addition, we used the realistic estimated values as the initial values for the salinity. Therefore, we did not calibrate the model for salinity transport.

6.4.2 Simulation of scenarios

The model was simulated under steady-state conditions for flow, incorporating stress periods with a rise in sea level and recharge across the time span from 2020 to 2070. For each scenario, our analysis is focused on three specific depth ranges: 0 - 5 m, 5 - 10 m, and 10 - 30 m. The initial objective of setting up the salinity map (Figure 6.9) was to examine if the salinity pattern undergoes significant changes in response to climate change. We also pay attention to the river estuary and the sea boundary to assess the presence of saltwater intrusion and its potential impacts.

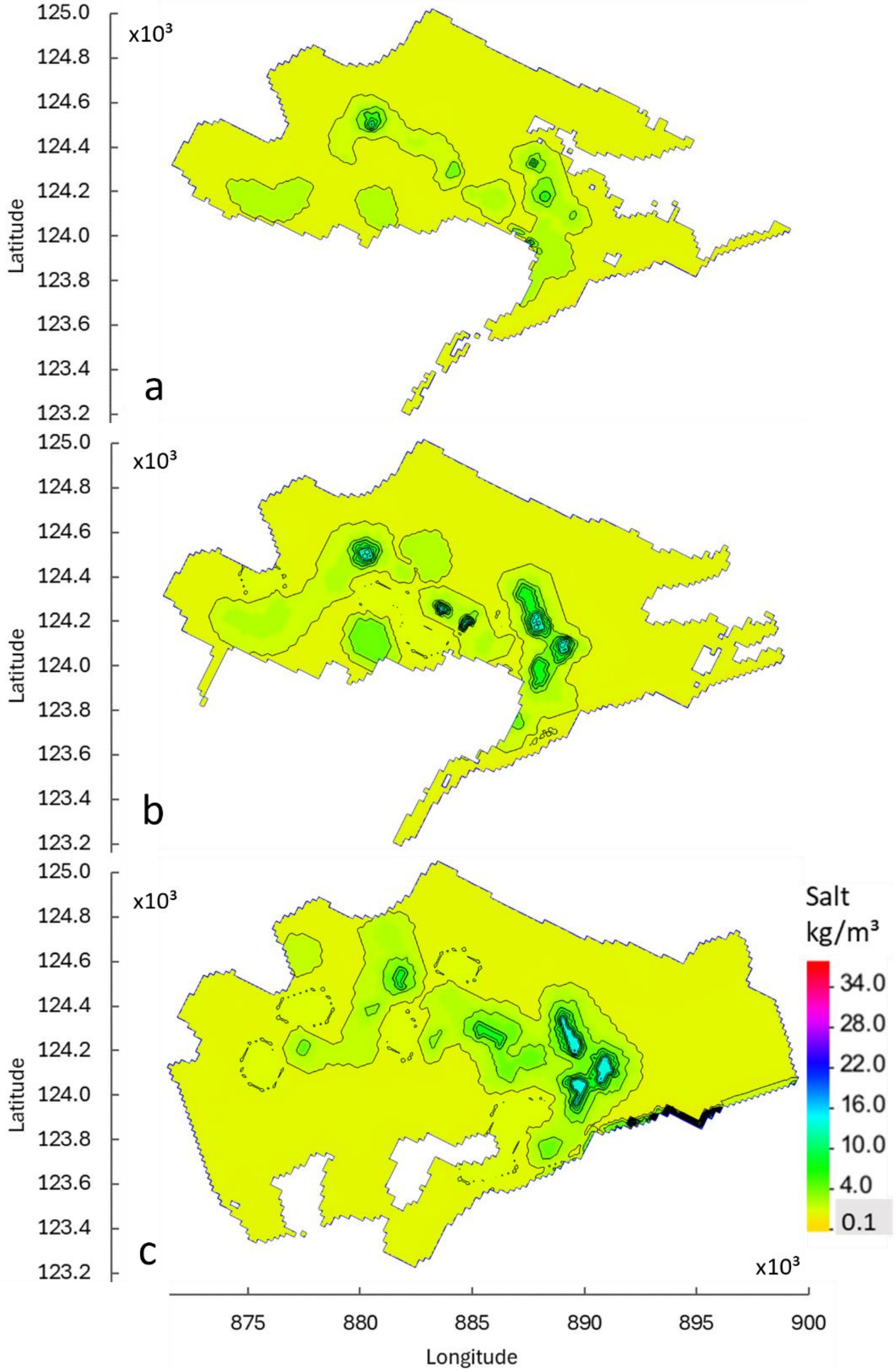

Figure 6.9 Salinity patterns at 0-5m depth (a), 5-10m depth (b), and 10-30m depth (c) imported from the salinity map (Cong-Thi 2024b) in the beginning of a 50-year simulation.

6.4.2.1 Scenario 1

Figure 6.10 shows the salinity patterns after a 50-year simulation in the case of no groundwater abstraction and increasing sea level and recharge. It seems freshening occurs faster at depths of 0 - 5 m (Figure 6.10a) compared to the depths of 5 - 10 m (Figure 6.10b) and 10 - 30 m (Figure 6.10c) in the alluvial plain. Nevertheless, the salinity intrusion occurring in the river estuary is more pronounced at a depth of 0 - 5 m (as it appears 3 - 4 km from the river mouth, Figure 6.10a), whilst it is less significant at depths of 5 - 10 m and 10 - 30 m. This could indicate that the river salt boundary conditions is not in equilibrium with the salinity map observations, because of a lack of observation points. Generally, salinity persists at depth even in the absence of pumping in the alluvial plain, which is coherent with the freshening time estimated in Chapter 5.

Sea level rise significantly affects salinity along the coastal zone, with salinity seen up to 600 meters inland from the coastline at depths ranging from 0 to 5 meters. The impact is even more pronounced at depths of 5 to 10 meters (up to 700 m) and 10 to 30 meters (up to 900 m) as expected from the density-difference. Nevertheless, the size of the grid is likely too coarse to accurately represent the salinity interface at the coast. Because of the high elevation, the top section of the dune (as shown in Fig. 6.10a and 6.10b) contain a greater number of dry cells (the white portion within the model domain) compared to the lower parts (as shown in Fig. 6.10c).

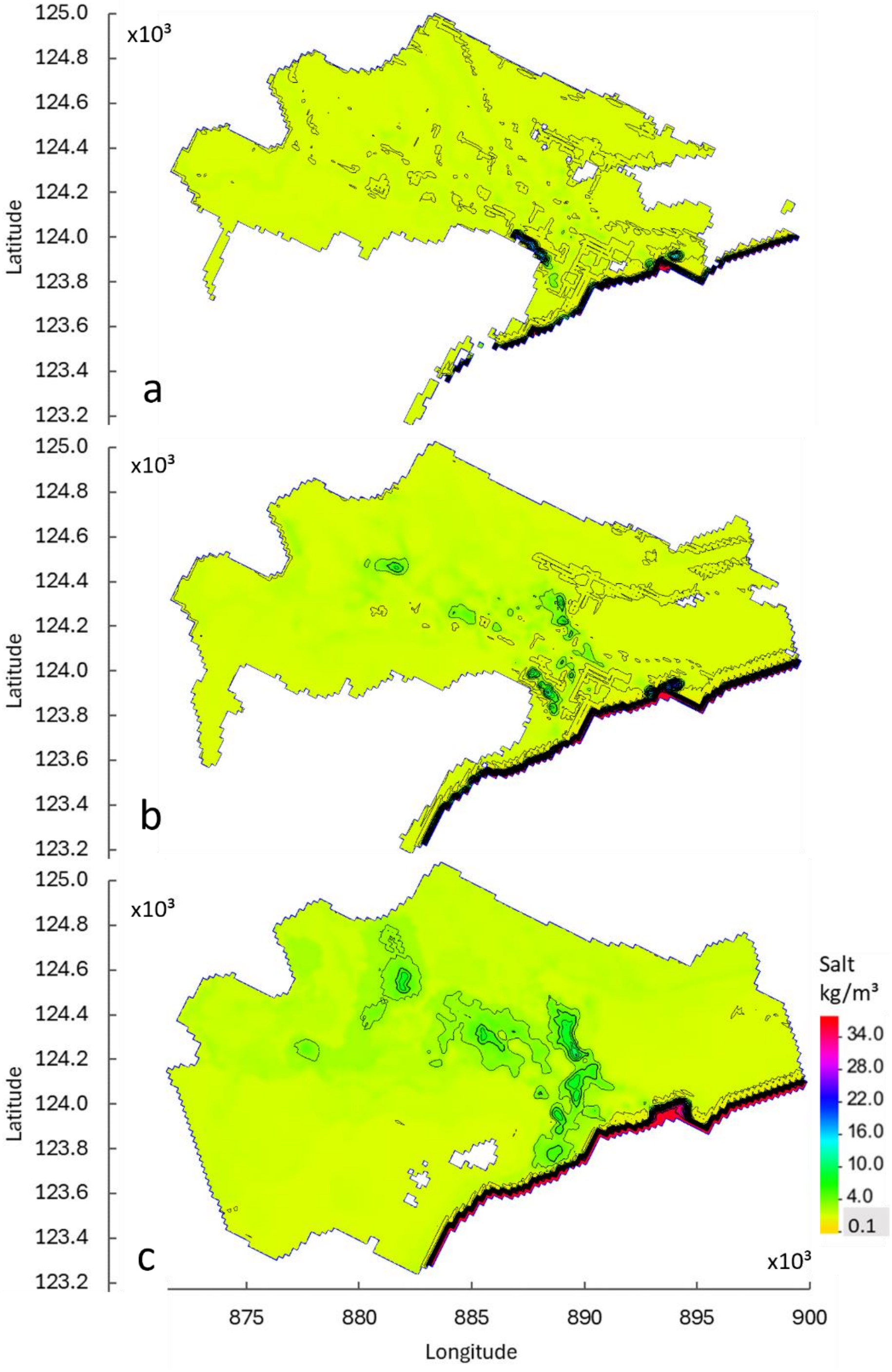

Figure 6.10 Salinity patterns at 0-5m depth (a), 5-10m depth (b), and 10-30m depth (c) after a 50-year simulation under sea level rise and climate change in the natural conditions (no abstraction)

6.4.2.2 Scenario 2

Figure 6.11 depicts the salinity patterns resulting from a 45-year simulation. This simulation involves the addition of 40 pumping wells, each with a rate of 30 m³/d, positioned in the alluvial plain. The simulation also takes into account the effects of climate change and sea level rise. The simulation did not converge for longer simulation periods. The continuous pumping is yielding to important changes in salinity locally, likely explaining the convergence problem, considering the relatively coarse grid used for simulations. Note also that a constant pumping throughout the whole year concentrated at a specific point is not representative of the actual extraction patters. Anyway, the 45-year period gives a realistic picture of how the salinity would evolve if current groundwater extraction were maintained. In this case, salinity increases at all depth levels (Figure 6.11) and the footprint is larger when compared to the original salinity map (Figure 6.3 or Figure 6.9).

The saltwater intrusion is especially pronounced in the river estuary, extending approximately 5.5 km at a depth ranging from 0 to 5 m. It slightly decreases at depths of 5 to 10 meters and 10 to 30 m. In this scenario, sea level rise has major impacts as saltwater penetrates nearly 1 kilometer inland at depths ranging from 10 to 30 m. Compared to scenario 1, this is the result of the lower hydraulic head inland related to pumping activities. The extent of saltwater intrusion marginally lowers at depths of 5 to 10 meters and 0 to 5 meters. Both the alluvial plain and dunes display a greater number of dry cells which is also explained by the pumping activities.

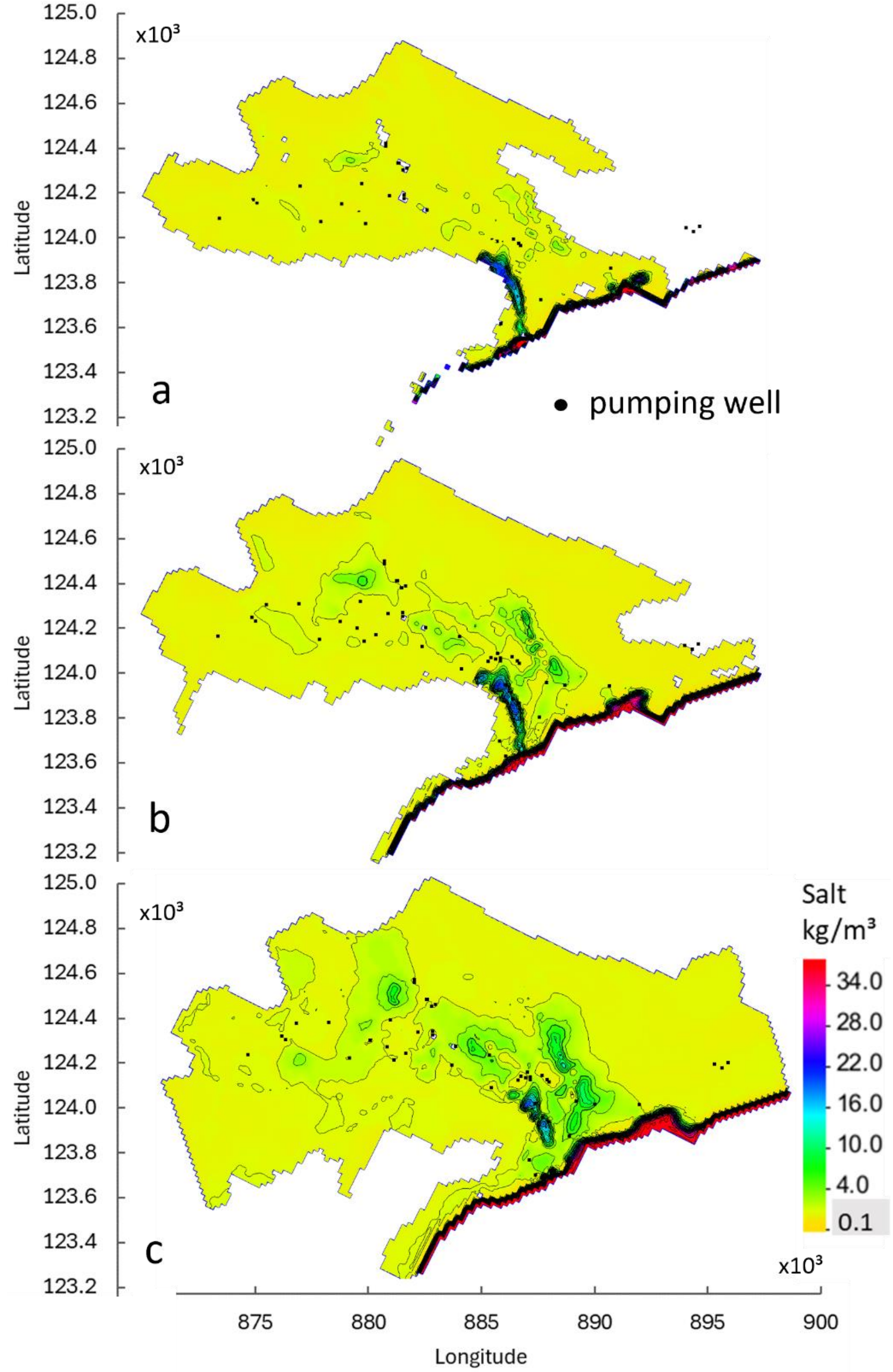

Figure 6.11 Salinity patterns at 0-5m depth (a), 5-10m depth (b), and 10-30m depth (c) after a 45-year simulation under sea level rise and climate change in the case of pumping in the alluvial plain

6.4.2.3 Scenario 3

In this scenario, we tested the model where the totality of 40 abstraction wells in the alluvial plain is transferred to 10 production wells (W_1-10) set up in the dune on the right bank of the Luy River (Figure 6.12). We chose the well location based on the stratigraphical model in Chapter 5 and the water level distribution in the calibration maps (Figure 6.6 and Figure 6.8). The production wells were consistently pumping at a rate of 135 m^3/d during the 50-year simulation, considering sea level rise and evolving recharge rate. The purpose of this setting is to assess the viability of extracting groundwater from the dunes as a long-term sustainable management strategy.

Figure 6.12 and Figure 6.13 depict the water level and salinity distribution, respectively, after a 50-year simulation. Our investigation revealed that the water level remains relatively constant in layer 7 of the model, without systematic lowering throughout the simulation period, which corresponds to the Pleistocene aquifer located in the dune on the right bank of the Luy River. This indicates that the proposed pumping rates can be sustained under the simulated recharge patterns. The optimal depth for the production wells is approximately 60-80 m for wells W_1-5 and 40-60 m for wells W_6-10. The salinity pattern in the alluvial plain on the left bank of the Luy River remains constant at depths of 5-10m and 10-30m, as shown in Figure 6.13b, c. Moreover, at depths of 0-5m, a fresher pattern is obvious, indicating that freshwater recharge is playing its role of further freshening the aquifer as expected from the long-term simulation (Chapter 5). The saltwater intrusion from the river estuary closely resembles scenario 1, which occurs when the model is operating under natural conditions without any pumping abstractions in the research region.

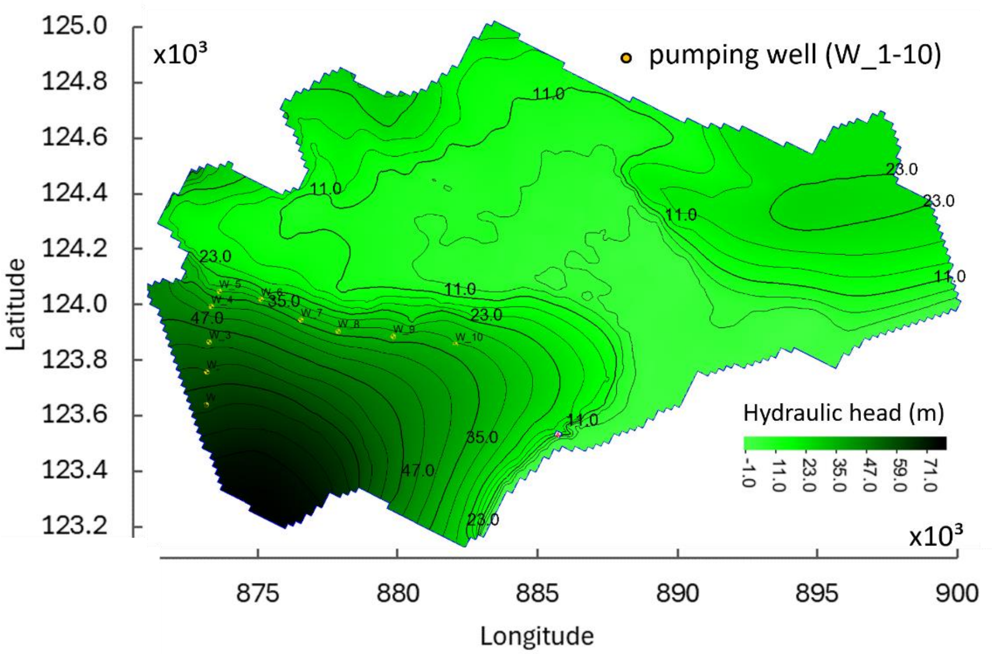

Figure 6.12 Figure 10. Location of the 10 potential production wells in the dune and the water level after a 50-year simulation associated with pumping

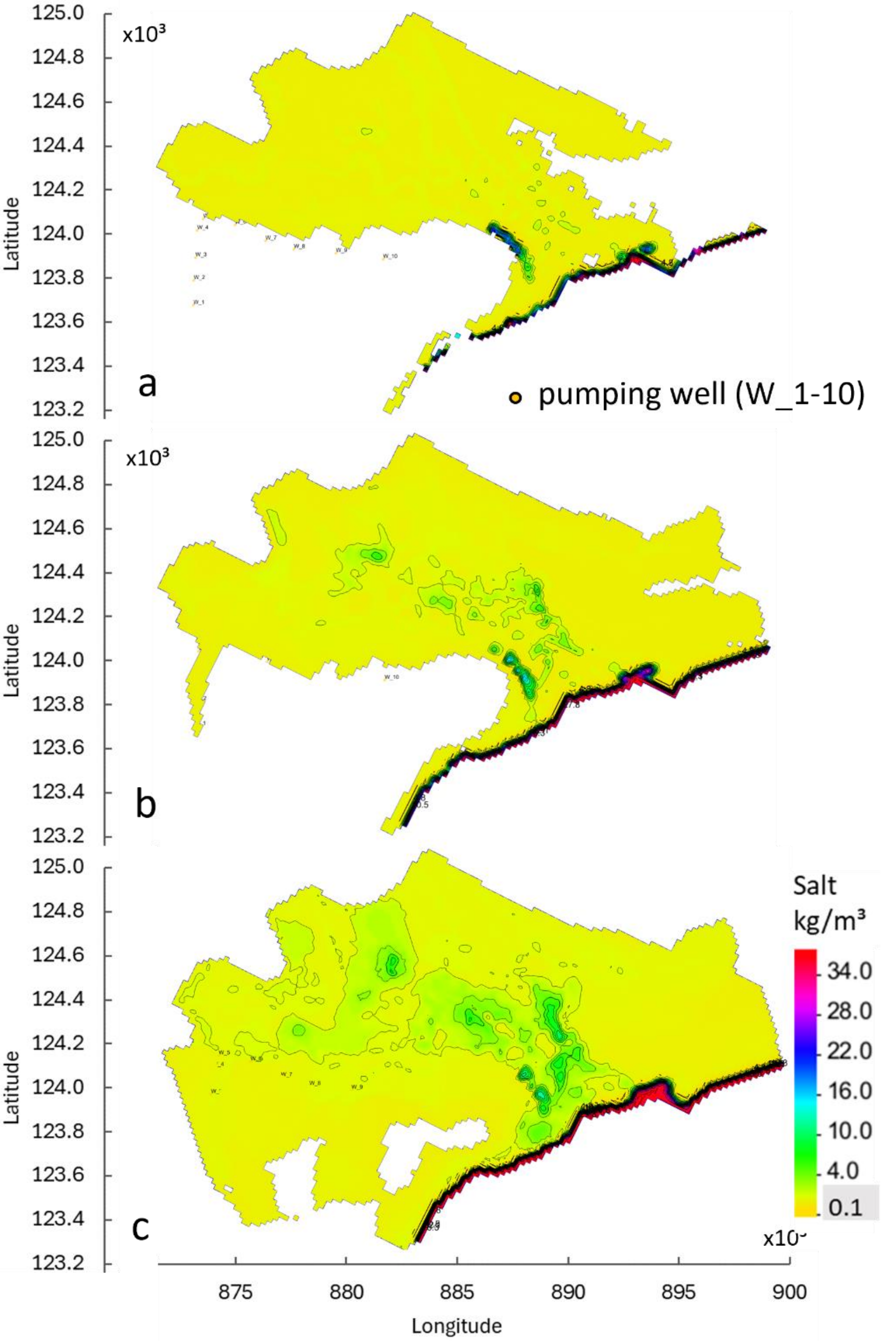

Figure 6.13 Figure 11b. Salinity patterns at 0-5m depth (a), 5-10m depth (b), and 10-30m depth (c) after a 50-year simulation under the same sea level and recharge rate as scenario 2. Groundwater pumping in the alluvial plain in scenario 2 has been switched to 10 wells on the dune in order to assess the potential of determining long-term production wells in the dune.

6.4.3 Discussion

Ideally, the model should be simulated with a fully transient approach with at least monthly time steps. Under those circumstances, we would be able to visually perceive the periodic variations in recharge and sea level, thereby enabling us to correctly monitor the distinct fluctuations in water levels within the aquifers and the specific consequences of saltwater intrusion. Due to the convergence problems encountered in SEAWAT in transient state, likely related to the combination of large initial heterogeneity in salinity, dynamics of the saltwater intrusion processes, and size of the model forcing us to work with a relatively coarse grid, we opted to simplify our simulation to a pseudo steady-state in which the stress factors do not very seasonally, and only the salt concentration is varying with time. We think this approach is reasonable to simulate long-term variations for which short-term dynamics (tides, seasonal variations) are less important. Nevertheless, this simplification prevents us to conclude on the viability of the proposed scenarios during the dry season.

Similarly, examining the impact of increasing pumping rates on the distribution of salinity would be interesting. Nevertheless, we observe during first tests convergence problem when increased rates were used. During scenario 2, when the model is run at a consistent pumping rate in the alluvial plain, a notable number of dry cells are observed, especially in the first layer. This concurs with the empirical evidence we gathered in the field, where a significant number of irrigation wells used by farmers were devoid of water after several seasons of production. This complicates the use of SEAWAT which relies on a MODFLOW-2000 in which less options are available to deal with dry cells. More care should therefore be given to the gridding and initial conditions to solve these kinds of issues.

When developing a groundwater model, it can be challenging to ensure that everything aligns precisely with reality, especially when working at the catchment scale. However, we tried our best to have the closest model to reality with simplifications always considering the final objectives of the model. Specifically, the groundwater model supports the following findings:

- Over the next 50 years, saltwater will continue to be present in the aquifers in its natural state, even without any pumping. However, if humans continue to extract groundwater at the current rate in the alluvial plain, the salinity will further increase.
- In the next 50 years, if groundwater remains abstracted as it currently is, saltwater may infiltrate inland, approximately 1 km from the coastline. In combination with the pumping in the alluvial and sea level rise, saltwater is forecast to intrude to the inland about 5 km from the river mouth. The salinity will increase in the shallow aquifer due to upconing and lateral migration.
- The dune system has a significant capacity for freshwater and could serve as freshwater reservoirs in the future. This is particularly valuable since it assists in reducing the problem of saltwater intrusion on the alluvial plain. However, more realistic pumping scenarios, including seasonally, should be performed to confirm this.

The Scenarios of Climate Change report (MONRE, 2021) (RCP4.5) indicates an increase in rainfall in the research region. However, the report also highlights the impact of extreme weather conditions, such as excessive rainfall during the rainy season, the dried months extending longer and prolonged droughts. During the rainy season, the study area may have enough freshwater for agriculture and living requirements. However, if the dried months extend longer than normal, pumping groundwater from the dunes with an amount of about 1350 m^3/d at depths of 40-80 m could help the community overcome the prolonged drought. This could be combined with managed aquifer recharge in which the excess of rainwater in the rainy period could be stored in the dune system to increase the amount of groundwater stored in the dune system. However, future water management plans should also consider changes in evapotranspiration to more accurately simulate the recharge.

6.5 Conclusion

In this study, we used the model that was developed in Chapter 5 to assess the impact of global climate change and sea-level rise on groundwater resources. In particular, the structure of hydrogeological units, boundary conditions, drains, and rivers were the same. In addition, we calibrated the model parameters the flux boundary, river and drainage conductance, and hydraulic conductivity values using observation wells and water level measurements from two field campaigns during both the rainy and dry seasons.

We use the recent salinity map from Cong-Thi (2024b) to set up the initial salt concentration for the model operating at different densities. For some parts with data missing, we interpolated the initial salt concentration from water samples taken from deeper wells or from other sources, such as interviews during the field campaigns. We used the salt concentration obtained from the 2019 field campaign in the Luy River estuary in the model as the initial salinity of the river. The initial salt concentration setup for the model varies from 0.45 to 35 kg/m^3 for fresh and salt water, respectively.

For the initial recharge, we used the values estimated from the SMB model in Chapter 3, while the initial sea level was taken from the average value recorded at Phu Quy station during the period 1980–2018. The recharge and sea level in the next 50 years were estimated from the climate change forecast reported in MONRE, 2021.

The coupled density-dependent groundwater flow and transport model SEAWAT was used for our simulation. Several scenarios were simulated to evaluate the impact of global climate change and sea-level rise on groundwater resources.

The findings suggest that in the next 50 years, salt water will still remain in the aquifers of the study area which is coherent with the findings of Chapter 5. Seawater might reach up to 1 km inland from the coastal line if groundwater is abstracted at the current rate and salinity will increase in the shallow aquifer.

The dune systems have a high potential for groundwater abstraction in the area and will be a valuable resource since they help reduce the problem of saltwater intrusion on the alluvial plain. Water should be preferentially extracted from these reservoirs as the risk of increasing the salinity of water is more limited. If saltwater is present in the bedrock, this should preferentially be combined with managed aquifer recharge to ensure that the resource is not over exploited. A dedicated study should be undertaken to assess the potential of the dune system to provide irrigation water to the community.

The results of this study will assist government officials in assessing the capabilities of groundwater resources and adopting effective strategies to ensure the long-term viability of groundwater in the research region.

Chapter 7. Conclusion and Recommendation

In this study, we used recharge estimates, hydrochemical analyses and numerical models as tools to examine the sources and evolution of saltwater, thus improving our comprehension of the forces and key elements that control the extent of saltwater intrusion in the Luy River catchment, Binh Thuan province, Vietnam. A hydrogeological system is defined by a complex and interrelated set of factors, including precipitation, evapotranspiration, land use, soil composition, sediment characteristics, groundwater extraction, sediment depth, among others. Hydrogeological models experience uncertainty when the presence, characteristics, and scope of these factors are not sufficiently specified, as is always the case in practice. Although groundwater model predictions are always uncertain, we can investigate and more efficiently manage areas that are vulnerable to climate change and sea level rise by applying integrated methodologies that include numerical model coupled with field observations. This allows us to predict future groundwater behavior, facilitates decision-making, and enables the examination of various management strategies for the study area.

Groundwater recharge is an essential component of the water balance and is a critical part in any sustainable groundwater management plan. Precisely evaluating this factor is difficult; however, it is crucial in the management of aquifers. To achieve this objective, we initially employed the SMB method to estimate daily groundwater recharge. This involved utilizing 42 years of recorded meteorological data, as well as describing the soil types, land use, and plant vegetation in the study area. The average recharge achieved using the SMB methodology is 312 mm/year in the alluvial plain and 531 mm/year in the dunes. Subsequently, we utilized the WTF approach to compute the recharge, which relies on the observable data obtained from the water table in the wells within the area. The objective of this procedure is to cross-validate the recharge value computed by SMB. The period of water level observations in the wells is rather brief, typically around one year. Consequently, the obtained results were indicative of short-term observations and not long-term average. In addition, fluctuations in water levels were influenced not only by the infiltration of rainwater for recharging, but also by factors such as ocean tides, earth tides, barometric pressure variations, pumping, drainage, lateral flow, irrigation practices and estimated specific yield that could only be partly taken into account. It is evident that more observations should be made in the future across the study area to better estimate recharge through the WTF method. Nevertheless, we still employ it as a means of validating recharge estimate from the SMB. Consequently, we have confidence in the estimation derived from the SMB approach, which was achieved over a longer duration, as a reliable approximation of the average recharge rate in the research region (Chapter 3). Our estimation constitutes the first attempt to quantify the recharge in the study area. In the future, we recommend to develop a more comprehensive water balance model for the whole catchment, including the upstream part in the mountain. We think that a model explicitly accounting for surface water processes such as run-off, should be investigated. Models such as SWAT (Neitsch et al 2009) or WetSpass (Batelaan and De Smedt, 2001, 2007) would help to better constrain the water balance in the study area, but they would require to systematically measure the river discharge at the outlet of the catchment.

In Chapter 4, we conducted a novel hydrogeochemical study in the Luy river watershed. This survey encompassed both shallow and deep wells, as well as samples obtained during both the dry and wet seasons. Our study represented the initial comprehensive examination of the hydrochemical analysis of seawater freshening/intrusion processes, focusing on water composition. Additionally, it was the first endeavor to discover the seasonal fluctuations associated with these processes. Furthermore, we suggested combining the new datasets with existing geophysical findings to differentiate the impact of recent saltwater intrusion from the prevailing freshening mechanisms that currently govern water quality within the catchment area.

Given that the Luy River and its tributaries drain the shallow aquifer, the bottom of the aquifer is up to several tens of meters below sea level, and the climate is semi-arid with limited recharge, particularly during the dry season. The analysis corroborates the ongoing slow process of freshening in the aquifer. The freshening characteristics are more pronounced in the rainy season than in the dry season. Salinization is more pronounced in the lower aquifer and during periods of low rainfall, which is caused by a lack of replenishment and excessive extraction of water from the aquifer. Additionally, the analysis validated the findings from geophysical data that indicated the presence of saline intrusion not just near the river but also further inland and at greater depths. Furthermore, the salt levels can change rapidly over short distances.

This led us to reject the initial hypothesis about the origin of saltwater, that was attributed to riverine intrusion in the estuary and develop a new conceptual model for understanding the progression of salinization in the Luy river catchment. This framework clarified the patterns of salinity distribution, the trend of freshening, and the occurrence of salinization during the dry season. We proposed that the saltwater that was initially present after the last high-water level has gradually become fresher due to the influx of precipitation and water from the hilly region. This is why samples taken from higher elevations exhibit characteristics of freshwater and are in a state of balance. The process of freshening is not fully finished in locations that are at a low elevation, at depth, and have a high clay content, where the ancient groundwater is still trapped. The seawater serves as a second source of salinization during the dry season when the farmers extract the limited shallow freshwater layer in the Holocene aquifer. Similar situations have been observed in Vietnam, such as in the River Delta (Tran D.D., et al. 2024; Bauer J., et al. 2022), and it is very likely that other coastal aquifer systems in the Binh Thuan province and adjacent provinces experienced a similar evolution. This conceptual model could be further validated by analyzing the age of groundwater through dedicated isotopic studies and integrating more comprehensively the hydrogeological processes with the stratigraphy of the study area.

This new conceptual model plays a crucial role in managing water resources in this semi-arid region of Vietnam, which is particularly susceptible to the impacts of climate change. By integrating an examination of the water balance including evaporation, precipitation, fluxes, river and canal recharges and discharge, and groundwater abstraction with an assessment of the hydraulic conductivity of the aquifer layers, a groundwater model of the study area was established.

Chapter 5 involves the first attempt for a three-dimensional (3D) stratigraphic model using the available well logs, geophysical, and geochemical data in the study area. The simulation includes looking at the effects of aquifer properties on the distribution of freshwater and saltwater over long periods of time. The goal is to verify the hydro-chemical conceptual model by examining if the time scale of the freshening process aligns with the hydraulic properties and water balance in the catchment area, assuming no groundwater exploitation. Additionally, the simulation aims to analyze the current distribution of saline groundwater from different hypotheses of saltwater sources. Lastly, it attempts to evaluate the potential for groundwater resource development in the face of freshening process and saltwater intrusion threats.

For these specific purposes, we developed a numerical groundwater flow and saltwater transport model using the SEAWAT package combining MODFLOW-2000 and MT3DMS. We used the necessary input data, including natural recharge, and river and drainage packages as stress factors and boundary conditions, with no attempt to calibrate it in this chapter given the absence of hydrogeological observation in natural conditions (no water extraction). The recharge rate was derived from the soil moisture balance model described in Chapter 4. In addition, hydraulic conductivity values were taken from prior field experiments conducted in the study region. Multiple scenarios were simulated to assess the influence of heterogeneity on the freshening processes.

The results indicated that during prolonged stages of freshening, seawater becomes trapped in the clay aquitard and the lower aquifers. The density difference between saltwater and freshwater exacerbates this phenomenon. The observed distribution pattern of saltwater in the most realistic scenario using the most advanced aquifer complexity, that includes the actual aquifer geometry, aligns with the results of the geophysical study conducted by Cong-Thi et al. (2021) and the hydrochemical conceptual of Chapter 4. It indicates that in the current condition, the full freshening of the aquifer would take several thousands of years, with saltwater being trapped in clay-rich zones, as well as at depth larger than the current sea level as well as in the basement aquifer. Of course, the limitations of the model related to the coarseness of the grid, the assumption of constant recharge through the millennia as well as the fixed distribution of layers do no allow to interpret quantitatively the outcomes. Nevertheless, this numerical study validates the conceptual model as a realistic hypothesis for the functioning of the aquifer system. As for Chapter 4, we can assume that a similar evolution has taken place in adjacent catchments. One of the challenges of these simulations is the computational cost: the 5000-year simulation took 17 days to complete. As a result, a supercomputer would be required for more advanced modeling works. In particular, it would be interesting to refine the model and to integrate the stratigraphy evolution in the model, as the catchment continued to evolve during the last 5000 years. It would also be interesting to integrate the results of calibration (Chapter 6), to further improve this simulation.

To determine to which extent groundwater will be affected by climate change and rising sea levels, we utilized the model created in Chapter 5 also in Chapter 6. Specifically, there was no difference in the layout of hydrogeological units, boundary conditions, drainage systems. However, to make the outcome of the model reliable, a realistic distribution of salinity was used along the river and a calibration was carried out. We used observation wells and water level data from two field campaigns in the rainy and dry seasons to calibrate the model parameters, including the hydraulic conductivity values, the incoming flux at the Northwest boundary, and the conductance of rivers and drains.

To avoid long simulations and produce realistic salinity estimations, the initial salt concentration for the model operating at varying densities was obtained from the newest salinity map from Cong-Thi (2024). We used the salt content measured during the 2019 field campaign in the estuary of the Luy River. The starting concentration of the model ranges from 0.45 to 35 kg/m^3.

A variety of scenarios were simulated to assess the effects of global climate change and rising sea levels on groundwater resources. Based on the results, it is projected that saltwater will continue to be present in the aquifers of the research area for the next 50 years, particularly in the alluvial plain, which is line with the order of magnitude of freshening times obtained in Chapter 5. If groundwater continues to be extracted at the current rate, seawater might potentially penetrate up to 1 kilometer inland from the coastline, while the occurrence of saline water in shallow waters would become exacerbated. In contrast, the dunes in the area have a significant recharge capacity and significant freshwater reserves and should serve as a valuable resource for groundwater production in a sustainable water management plan. They would play a crucial role in mitigating the issue of saltwater intrusion on the alluvial plain. This information will aid government officials in evaluating the capacity of groundwater resources and implementing efficient policies to ensure the sustainable viability of groundwater in the research region. However, this model is still in its infancy. Its main limitations are its steady-state nature in terms of stress factors (recharge and extraction) and its limited resolution. This prevents to currently draw any conclusion about the seasonality of groundwater extraction nor the local evolution of salinity for different scenarios. The input of the model should also be adapted to account for other impacts of climate change on the water cycle, such as change in the evapotranspiration due to change in temperature.

These simplifications were necessary during the modeling process because of convergence problems while executing SEAWAT. Typically, SEAWAT would terminate the execution of the simulation before the end because of a lack of convergence. We discovered that the coarse model grid within our relatively large study area could be contributing to the convergence problem. The significant elevation difference between the dunes (160 m ASL) and the alluvial plain (around 10 m ASL) may also contribute to the convergence issue. In this case, the higher elevation leads to a high quantity of dried cells in the upper layers. The coarse grid was necessary and sufficient for the long-term simulations of Chapter 5, characterizing slow natural freshening processes, but not anymore for the faster evolution resulting from anthropic activities. Future endeavors should therefore focus on refining the grid to allow more accurate simulations of the temporal evolution of salinity in the study area.

The chapters' findings suggest the following strategies for sustainable groundwater use in the study area:

1) Groundwater abstraction in the alluvial plain should be banned or at least strictly managed by the government officer, especially in the vicinity of zones where higher salinity have been mapped. Indeed, upconing and lateral migration of saltwater still trapped in the aquifer, in particular in low hydraulic conductivity zones, is explaining why farmers are observing salinity increases in their wells when exploiting the thin freshwater lens present at shallow depth. Since this situation is inherent to the evolution of the catchment, avoiding extraction of groundwater is the only viable option to limit salinization.

2) Instead, pumping should be limited to freshwater zones. Considering that the current salinity map is still facing a lack of data in many areas of the alluvial plain, only the dune system where freshwater is present everywhere should be used. The pumping rate should be controlled according to the estimated seasonal recharge and the actual capacity of the dune to ensure sustainability. Since the presence of saltwater in the bedrock under the dune is not excluded, such management strategy should be accompanied by further investigations (wells drilled in the bedrock, dedicated numerical model, monitoring network).

3) To assess the potential for sustainable extraction, the dunes should therefore be investigated in more detail, such as by doing long-term pumping tests, increasing the number of piezometers to access the actual groundwater levels and their seasonal variation. The estimation of the recharge should be improved and accounts for local agricultural practice. Current extraction rates should also be estimated. Deep wells should be drilled to verify the presence of saltwater in the basement aquifer.

4) Based on the above-mentioned investigations, the numerical model should be refined to assess various management scenarios. If necessary, managed aquifer recharge could be

implemented in order to increase sustainable groundwater extraction rate. For example, when dams have excess water, it could be infiltrated in the dunes instead of being released in the Luy River. Similarly, water drained through canals could be reinjected in the dunes at the condition that its quality is sufficient.

References

1. Alcalá, F.J., Custodio, E., 2008. Using the Cl/Br ratio as a tracer to identify the origin of salinity in aquifers in Spain and Portugal. J. Hydrol. 359, 189–207.
2. Alfarrah, N., Walraevens, K., 2018. Groundwater Overexploitation and Seawater Intrusion in Coastal Areas of Arid and Semi-Arid Regions. Water 2018, 10, 143. https://doi.org/10.3390/w10020143
3. Alvin Lal, Bithin Datta (2019). Multi-objective groundwater management strategy under uncertainties for sustainable control of saltwater intrusion: Solution for an island country in the South Pacific, Journal of Environmental Management, Volume 234, Pages 115-130, ISSN 0301-4797, https://doi.org/10.1016/j.jenvman.2018.12.054.
4. Arlen W. Harbaugh, Edward R. Banta, Mary C. Hill, and Michael G. McDonald, 2000. MODFLOW-2000, The U.S. Geological Survey modular ground-water model: User guide to modularization concepts and the ground-water flow process. U.S. Geological Survey https://doi.org/10.3133/ofr200092.
5. Antonellini, M., Allen, D.M., Mollema, P.N. et al. Groundwater freshening following coastal progradation and land reclamation of the Po Plain, Italy. Hydrogeol J 23, 1009–1026 (2015). https://doi.org/10.1007/s10040-015-1263-0.
6. Andreasen, D.C., Fleck, W.B., 1997. Use of Bromide: chloride ratios to differentiate potential sources of chloride in a shallow, unconfined aquifer affected by brackish-water intrusion. Hydrogeol. J. 5, 17–26.
7. Andersen, M.S., Nyvang, V., Jakobsen, R., Postma, D., 2005. Geochemical processes and solute transport at the seawater/freshwater interface of a sandy aquifer. Geochim. Cosmochim. Acta 69, 3979–3994.
8. Anne Gobin, Le Trinh Hai, Pham Ha Linh, Luc Hens, Pierre Ozer, Le Thi Thu Hien, Nguyen Thanh Binh, Pham Quang Vinh, 2012. Impact of global climate change and desertification on the environment and society in the southern centre of Vietnam

(case study in the Binh Thuan province). Final Report, of the bilateral Belgian - Vietnamese project, 2012.

9. Appelo, C.A.J., 1994. Cation and proton exchange, pH variations, and carbonate reactions in a freshening aquifer. Water Resour. Res. 20, 2793–2805

10. Appelo, C., Postma, D., 2005. Geochemistry, Groundwater and Pollution. 2nd ed. Balkema, Rotterdam, pp. 119–174.

11. Ayers, R.S. and Westcot, D.W., 1989. Water quality for agriculture. FAO Irrigation and Drainage Paper. Food and Agriculture Organization of the United Nations Rome, M-56 ISBN 92-5-102263-1.

12. Batelaan, O., De Smedt, F., 2001. Wetspass: a flexible, GIS based, distributed recharge methodology for regional groundwater modelling. In: Gehrels, H., Peters, J., Hoehn, E., Jensen, K., Leibundgut, C., Griffioen, J., Webb, B., Zaadnoordijk, W.-J. (Eds.), Impact of Human Activity on Groundwater Dynamics, vol. Publ. No. 269. IAHS, Wallingford, pp. 11–17.

13. Batelaan, O. and De Smedt, F., 2007, GIS-based recharge estimation by coupling surface-subsurface water balances. Journal of Hydrology, 337(3-4), 337-355, doi: 10.1016/j.jhydrol.2007.02.001.

14. Bauer, J., Borsig, N., Pham, V.C., Tran, V.H., Nguyen, T.H., Norra, S., 2022. Geochemistry and evolution of groundwater resources in the context of salinization and freshening in the southernmost Mekong Delta, Vietnam. Journal of Hydrology: Regional Studies 40, 101010.

15. Barnett et al, 2012, Australian groundwater modelling guidelines, Waterlines report, National Water Commission, Canberra.

16. Barlow, P.M. & Reichard, E.G., (2010). Saltwater intrusion in coastal regions of North America. Hydrogeology Journal, 18: 247–260.

17. Barlow, P.M., 2013. Saltwater intrusion. Retrieved from: http://water.usgs.gov/ogw/gwrp/saltwater/salt.html Accessed: February 4, 2014.

18. Bakundukize, C., Marc, V.C., Kristine, W., 2011. Estimation of groundwater recharge in Bugesera region (Burundi) using soil moisture budget approach. Geol. BELGICA 14, 86–102.

19. Bear, J. (1999). Seawater intrusion in coastal aquifers: concepts, methods and practices. Boston. Mass: Kluwer Academic.

20. Bennetts, D.A. Webb, J.A., Stone, D.J.M. and Hill, D.M. (2006). Understanding the salinization process for groundwater in an area of south-eastern Australia, using hydrochemical and isotopic evidence. Journal of Hydrology, 323, 178-192.

21. Binh Thuan Department of Natural Resources and Environment (BTDNRE). Inventory the current state of water resource exploitation and wastewater discharge in Binh Thuan province, 2007.

22. Binh Thuan Province Committee (BTPC). Distribution and protection planning for groundwater resources in coastal areas of Binh Thuan province, 2018.

23. Binh Thuan Department of Natural Resources and Environment, 2020. Report on the 5-year environmental status (2016–2020) of Binh Thuan province (in Vietnamese).

24. Bosserelle, A. L., Morgan, L. K., &Hughes, M. W. (2022). Groundwater rise and associated flooding in coastal settlements due to sea-level rise: A review of processes and methods. Earth's Future, 10, e2021EF002580. https://doi.org/10.1029/2021EF002580

25. British Business Group Vietnam, 2017. Vietnam Water Sector Briefing (PDF).. Archived from the original (PDF) on 11 January 2019.

26. Casillas-Trasvina, A., Zhou, Y., Stigter, T.Y. *et al.* Application of numerical models to assess multi-source saltwater intrusion under natural and pumping conditions in the Great Maputo aquifer, Mozambique. *Hydrogeol J* **27**, 2973–2992 (2019). https://doi.org/10.1007/s10040-019-02053-5

27. Cherubini, C. and Pastore, N.: Critical stress scenarios for a coastal aquifer in southeastern Italy, Nat. Hazards Earth Syst. Sci., 11, 1381–1393, https://doi.org/10.5194/nhess-11-1381-2011, 2011.

28. Cong-Thi, D., Pham, D.L., Thibaut, R., Paepen, M., Ho, H.H., Nguyen, F., Hermans, T., (2021). Imaging the structure and the saltwater intrusion extent of the Luy River coastal aquifer (Binh Thuan, Vietnam) using electrical resistivity tomography. Water 13, 1743. https://doi.org/10.3390/w13131743.
29. Cong-Thi, D. 2024b. Hydrogeophysical Characterization of Saltwater Intrusions in the Southern Central Region, Vietnam. Ph.D. thesis, Ghent University, Ghent, Belgium.
30. Cong-Thi D., Pham, D.L., Caterina, D., Pauw, X. D., Dang, T.H., Ho, H.H., Nguyen, F., Hermans, T., (2024a) Quantifying salinity in heterogeneous coastal aquifers through ERT and IP: Insights from laboratory and field investigations. Journal of Contaminant Hydrology, 262 (2024) 104322. https://doi.org/10.1016/j.jconhyd.2024.104322
31. Claassen, H.C., 1982. Guidelines and Techniques for Obtaining Water Samples that Accurately Represent the Water Chemistry of an Aquifer. US Geological Survey.
32. Craig, H., 1961. Isotopic variations in meteoric waters. Science 133, 1702–1703.
33. Custodio, E., 1997. Studying, monitoring and controlling seawater intrusion in coastal aquifer. In: Guideline for Study, Monitoring and Control, FAO Water Reports No. 11, 7-13.
34. Custodio, E (2010) Coastal aquifers of Europe: an overview. Hydrogeol J 18:269–280
35. Department of Natural Resources and Environment of Binh Thuan province (DONREBT), 2020. Report on environmental status for 5 years (2016 - 2020) of Binh Thuan province.
36. De Louw, P. G. B., Eeman, S., Siemon, B., Voortman, B. R., Gunnink, J., van Baaren, E. S., and Oude Essink, G. H. P.: Shallow rainwater lenses in deltaic areas with saline seepage, Hydrol. Earth Syst. Sci., 15, 3659–3678, doi:10.5194/hess-15-3659- 2011, 2011.

37. Dodd C, Rishworth GM. Coastal urban reliance on groundwater during drought cycles: Opportunities, threats and state of knowledge. Cambridge Prisms: Coastal Futures. 2023; 1: e11. doi:10.1017/cft.2022.
38. Domenico, P.A. and F.W. Schwartz, 1990. Physical and Chemical Hydrogeology, John Wiley & Sons, New York, 824 p.
39. Eriksson E, Khunakasem V (1969) Chloride concentrations in groundwater, recharge rate and rate of deposition of chloride in the Israel coastal plain. J Hydrol 7:178–179.
40. FAO (2012) AquaCrop—reference Manual. Land and Water Division, Rome.
41. Fetter C.W. 2001. Applied Hydrogeology (4th edition), Prentice Hall
42. Fisher, R.S., Mullican III, W.F., 1997. Hydrochemical evolution of sodium-sulfate and sodium-chloride groundwater beneath the northern Chihuahuan Desert, TransPecos, Texas, USA. Hydrogeol. J. 5, 4–16
43. Fox weather, 2024. World's population forecast to peak in 2080 before declining, new projections show. https://www.foxweather.com/earth-space/world-population-peak-2080-before-decline.
44. Fritz, P., Fontes, J.C., 1989. Handbook of Environmental Isotope Geochemistry. Elsevier Scientific Pub. Co., New York.
45. Gee, G.W., Zhang, Z.F., Tyler, S.W., 2004. Chloride-mass-balance for Predicting Increased Recharge after Land-Use Change. University of California, California, pp. 1–26. Available from: http://repositories.cdlib.org/lbnl/LBNL-55584.
46. Giambastiani BMS, Antonellini M, Oude Essink GHP, Stuurman RJ (2007) Saltwater intrusion in the unconfined coastal aquifer of Ravenna (Italy): a numerical model. J Hydrol 340:91–104.
47. Giménez, F.E., (2014). Space/time development of seawater intrusion: a study case in Vinaroz coastal plain (Eastern Spain) using HFE-Diagram, and spatial distribution of hydrochemical facies. Journal of Hydrology 517, 617–627.
48. Giménez, F. E., Sánchez San Román, F.J., 2015. An excel macro to plot the HFE-diagram to identify sea water intrusion phases. Groundwater 53, 819–824.

49. Giménez, F. E., 2019. Use of the Hydrochemical Facies Diagram (HFE-D) for the evaluation of salinization by seawater intrusion in the coastal Oropesa Plain: Comparative analysis with the coastal Vinaroz Plain, Spain, HydroResearch, 2, 76-84.

50. Gomis, Y.V., Boluda, B.N., and Ruiz, B.F.. 2000. Gypsum precipitation/dissolution as an explanation of the decrease of sulphate concentration during seawater intrusion. J. Hydrol. 228, 48–55.

51. Gobin, A., Le, T.H., Pham, H.L., Luc, H., Pierre, O., Le, T.T.H., Nguyen, T.B., Pham, Q.V., 2012. Impact of global climate change and desertification on the environment and society in the southern centre of Vietnam (case study in the Binh Thuan province). Final Report, of the bilateral Belgian - Vietnamese project, 2012.

52. Gobin, A., Nguyen, H. T., Pham, V.Q., Pham, H.T.T., 2016. Heavy rainfall patterns in Vietnam and their relation with ENSO cycles. International Journal of Climatology, Int. J. Climatol. 36: 1686–1699, 2016.

53. Ha, Q.H., Tran, N.T.D., Vo, P.L., Nguyen, H.Q., Dang, D.H., 2022. Groundwater in Southern Vietnam: Understanding geochemical processes to better preserve the critical water resource. Science of the Total Environment 807, 151345.

54. Healy, R.W., 2010. Estimating Groundwater Recharge. Cambridge University Press, Cambridge, p. 245.

55. Hem, J.D., 1985. Study and Interpretation of the Chemical Characteristics of Natural Water. Department of the Interior, US Geological Survey.

56. Hermans, T., Goderniaux, P., Jougnot, D., Fleckenstein, J.H., Brunner, P., Nguyen, F., Linde, N., Huisman, J.A., Bour, O., Lopez Alvis, J., Hoffmann, R., Palacios, A., Cooke, A.-K., Pardo-Álvarez, Á., Blazevic, L., Pouladi, B., Haruzi, P., Fernandez Visentini, A., Nogueira, G.E.H., Tirado-Conde, J., Looms, M.C., Kenshilikova, M., Davy, P., Le Borgne, T., 2023. Advancing measurements and representations of subsurface heterogeneity and dynamic processes: towards 4D hydrogeology. Hydrol. Earth Syst. Sci. 27, 255–287. https://doi.org/10.5194/hess-27-255-2023

57. Hill M.C. & Tiedeman C.R., 2007, Effective Groundwater Model Calibration: With Analysis of Data, Sensitivities, Predictions, and Uncertainty, Wiley, 480p.

58. Hoang, P. (ed), 1997. Geological and Mineral Resources map of Phan Thiet - Vietnam on 1:50.000 scale. Department of Geology and Minerals of Vietnam, Ha Noi (in Vietnamese).

59. Hoang, V.H., Larsen, F., Nguyen, V.L., Dang, D.N., Tran, T.T., Pham Q.N., 2018. Salt Groundwater Intrusion in the Pleistocene Aquifer in the Southern Part of the Red River Delta, Vietnam. VNU Journal of Science: Earth and Environmental Sciences, Vol. 34, No.1, 11-22.

60. Idowu, T.E. and Lasisi, K.H., (2020). Seawater intrusion in the coastal aquifers of East and Horn of Africa: A review from a regional perspective, Scientific African 8.

61. Johnson AI (1967) Specific yield – compilation of specific yields for various materials. US Geol Surv Water-Supply Paper 1662-D, 74 pp.

62. IPCC 2006: 2006 IPCC Guidelines for National Greenhouse Gas Inventories. In Prepared by the National Greenhouse Gas Inventories Programe, Eds. Eggleston HS, Miwa K, Ngara T, Tanabe K, Published: IGES, Japan.

63. IPCC AR6 WG1 (2021). Chapter 11: Weather and climate extreme events in a changing climate. Eds. Seneviratne S. I., Zhang X,. Adnan M., Badi, W.

64. Kim, J.H., Kim, K.H., Nguyen, T.T., Batsaikhan, B., Yun, S.T., 2017. Hydrochemical assessment of freshening saline groundwater using multiple end-members mixing modelling: A study of Red River delta aquifer, Vietnam. Journal of Hydrology 549, 703–714.

65. Kinzelbach W. et al. "A Survey of Methods for Groundwater Recharge in Arid and Semi-arid regions." Early Warning and Assessment Report Series, UNEP/DEWA/RS.02-2. United Nations Environment Programme, Nairobi, Kenya. 2002.

66. Kotchoni, D.O.V., Vouillamoz, JM., Lawson, F.M.A. *et al.* Relationships between rainfall and groundwater recharge in seasonally humid Benin: a comparative analysis of long-term hydrographs in sedimentary and crystalline

aquifers. *Hydrogeol J* **27**, 447–457 (2019). https://doi.org/10.1007/s10040-018-1806-2.

67. Lambrakis, N., 2006. Multicomponent heterovalent chromatography in aquifers. Modelling salinization and freshening phenomena in field conditions. J. Hydrol. 323, 230–243.

68. Langevin 2005. Simulation of Submarine Ground Water Discharge to a Marine Estuary: Biscayne Bay, Florida Volume 41, Issue 6, Pages 758-771. https://doi.org/10.1111/j.1745-6584.2003.tb02417.x

69. Larsen, F., Tran, L.V., Hoang, V.H., Tran, T.L., Christiansen, A.V., and Pham, Q.N., 2017. Groundwater salinity influenced by Holocene seawater trapped in incised valleys in the Red River delta plain. Nature Geoscience, Advance Online Publication.

70. Le, T.T.H., Gobin, A., Pham, T.T.H., 2019. Spatial indicators for desertification in southeast Vietnam. Nat. Hazards Earth Syst. Sci., 19, 2325–2337, 2019.

71. Lebbe, L., Adams, R., and De Deckere, E.: Modeling of historical evolution of saltwater distribution on the right bank of the Scheldt in the Antwerp harbor, in: Proc. 22nd Salt Water Intrusion Meeting., 2012.

72. Lebbe, L., Depret, D., Claus J., and Devriese, G.J., 2018. Saltwater intrusion in the breakthrough valley of the river Aa between the Flemish coastal plain and the Saint Omer basin (France) E3S Web of Conferences 54, 00017. https://doi.org/10.1051/e3sconf/20185400017.

73. Lerner DN, Issar AS, Simmers I (1990) Groundwater recharge. A guide to understanding and estimating natural recharge. Int Contrib Hydrogeol Verlang Heinz Heise 8, 345 p.

74. Lyles, J.R., (2000). Is seawater intrusion affecting ground water on Lopez Island, Washington? USGS Numbered Series, U.S. Geological Survey. Fact Sheet FS-057-00.

75. Meyer, R., Engesgaard, P., & Sonnenborg, T. O. (2019). Origin and dynamics of saltwater intrusion in a regional aquifer: Combining 3-D saltwater modeling with

geophysical and geochemical data. *Water Resources Research*, 55, 1792– 1813. https://doi.org/10.1029/2018WR023624

76. Michelli, M., 2008. Sea-level changes, coastal evolution and paleoceanography of coastal waters in SE-Vietnam since the mid-Holocene. (Ph.D. Thesis) Christian Albrechts Universität Kiel, Germany (159 pp.)

77. Montcoudiol, N., Molson, J., Lemieux, J. M., (2017): Numerical modelling in support of a conceptual model for groundwater flow and geochemical evolution in the southern Outaouais Region, Quebec, Canada, Canadian Water Resources Journal / Revue canadienne des ressources hydriques, DOI: 10.1080/07011784.2017.1323560.

78. MONRE, Ministry of Natural Resources and Environment, 2021. Scenarios of climate change for Vietnam from 2020.

79. MONREMEDIA. The management of water resources in Binh Thuan province, 2022. Online in the link: Công tác quản lý về tài nguyên nước trên địa bản tỉnh Bình Thuận (tainguyenmoitruong.gov.vn)

80. Morgan, L.K., Werner, A.D., (2015). A national inventory of seawater intrusion vulnerability for Australia. Journal of Hydrology: Regional Studies 4, 686–698.

81. Mu. Ramkumar, David Menier, K. Kumaraswamy, Chapter 1 - Coastal Zone Management During Changing Climate and Rising Sea Level: Transcendence of Institutional, Geographic, and Subject Field Barriers Is the Key, Editor(s): Mu. Ramkumar, R. Arthur James, David Menier, K. Kumaraswamy, Coastal Zone Management, Elsevier, 2019, Pages 1-12, ISBN 9780128143506, https://doi.org/10.1016/B978-0-12-814350-6.00001-X.

82. Nawapi, (2015) Groundwater resource in Binh Thuan – Groundwater mapping at 1:50000 scale

83. Nawapi, (2018) Groundwater resource in Binh Thuan – Groundwater mapping at 1:200000 scale.

84. Neitsch S.L., Arnold J.G., Kiniry J.R., Williams J.R., 2009. Soil and Water assessment tool theoretical documentation Version 2009. Texas Water Resources Institute

Technical Report No.406. Texas A&M University System College Station, Texas 77843-2118.

85. Neumann, B., Vafeidis, A.T., Zimmermann, J., Nicholls, R.J., 2015. Future Coastal Population Growth and Exposure to Sea-Level Rise and Coastal Flooding - A Global Assessment. PLOS ONE 10, e0118571. https://doi.org/10.1371/journal.pone.0118571

86. Nguyen DT (ed) (1999) Geological Maps and Explanatory notes of B'Lao, Da Lat - Cam Ranh, Gia Ray - Ba Ria and Phan Thiet, 1:200,000 Scale. Department of Geology and Minerals of Vietnam, Ha Noi (in Vietnamese).

87. Nguyen M.K. Characterization of groundwater reservoirs forming in coastal river basins in Ninh Thuan and Binh Thuan provinces. PhD. Thesis, Hanoi University of Mining and Geology, 2015.

88. Nguyen, T.T., Kawamura, A., Tong, T.N., Nakagawa, N., Amaguchi, H., Gilbuena, J.R., 2014. Hydrogeochemical characteristics of groundwater from the two main aquifers in the Red River Delta, Vietnam. Journal of Asian Earth Sciences 93, 180–192.

89. Nguyen, V.T. Doctoral thesis: Characteristics of sedimentary facies and sequence stratigraphy of the Quaternary sand formations in the coastal areas of Ninh Thuan - Binh Thuan provinces. VNU University of Sciences, Vietnam National University, Hanoi 2019.

90. Park, S.C., Yun, S.T., Chae, G.T., Yoo, I.S., Shin, K.S., Heo, C.H. and Lee, S.K., (2005). Regional hydrochemical study on salinization of coastal aquifers, western coastal area of South Korea. Journal of Hydrology, 313, 182-194.

91. Parck, Y., Lee J.Y., Kim, J.H., Song S.H., (2012) National scale evaluation of groundwater chemistry in Korea coastal aquifers: evidence of seawater intrusion. Environ Earth Sci 66:707–718

92. Parkhurst, D.L., Appelo, C., 2013. Description of Input and Examples for PHREEQC Version 3: A Computer Program for Speciation, Batch-reaction, One-dimensional Transport, and Inverse Geochemical Calculations. US Geological Survey.

93. Paepen, M., Deleersnyder, W., De Latte, S., Walraevens, K., Hermans, T. Effect of Groundwater Extraction and Artificial Recharge on the Geophysical Footprints of Fresh Submarine Groundwater Discharge in the Western Belgian Coastal Area. Water 2022, 14, 1040. https:// doi.org/10.3390/w14071040

94. Petalas, C. and Lambrakis, N., (2006). Simulation of intense salinization phenomena in coastal aquifers—the case of the coastal aquifers of Thrace. Journal of Hydrology, 324, 51-64.

95. Prusty, P., Farooq, S.H., 2020. Seawater intrusion in the coastal aquifers of India - A review. Hydro Research 3, 61–74.

96. Piper, A.M., 1944. A graphic procedure in the geochemical interpretation of water-analyses. Eos Trans Am Geophys Union 25(6):914–928.

97. Ritter, M.E. 2006. The physical environment: An introduction to Physical Geography. Available online at http://www.uwsp.edu/geo/faculty/ritter/geog101/textbook/title_page.html.

98. Russak, A., Sivan, O., 2010. Hydrogeochemical tool to identify salinization or freshening of coastal aquifers determined from combine field work, experiments, and modelling. Environ. Sci. Technol, 44, 4096-4102.

99. Sarker, MM.R., Van Camp, M., Hossain, H., Islam, M., Ahmed, N., Karim, M., Bhuiyan, A.Q., Walraevens, K., 2021. Groundwater salinization and freshening processes in coastal aquifers from southwest Bangladesh. Science of The Total Environment, ISSN 0048-9697, https://doi.org/10.1016/j.scitotenv.2021.146339.

100. Scanlon BR, Healy RW, Cook PG (2002) Choosing appropriate techniques for quantifying groundwater recharge. Hydrogeol J (in press). DOI 10.1007/s10040-001-0176-2

101. Scanlon. B.R. et al. Global synthesis of groundwater recharge in semiarid and arid regions. Hydrol. Process. 20, 3335–3370 (2006). doi: 10.1002/hyp.6335

102. Scanlon, B. R. Evaluation of methods of estimating recharge in semiarid and arid regions in the southwestern U.S., in Hogan, J. F., Phillips, F. M., & Scanlon, B. R., eds., Groundwater recharge in a desert environment: the southwestern United

States: Washington, D.C., American Geophysical Union, Water Science and Applications Series, 9, 235–254 (2004).

103. SCS (1985) National engineering handbook (Sect. 4). US Dept. of Agriculture, Soil Conservation Service, Washington, DC.

104. Simmers I (ed) (1997) Recharge of phreatic aquifers in (semi-) arid areas. Balkema, Rotterdam, 277 pp.

105. Stattegger, K., Tjallingii, R., Saito, Y., Michelli, M., Nguyen, T.T., Wetzel, A., 2013. Mid to late Holocene sea-level reconstruction of Southeast Vietnam using beachrock and beach-ridge deposits. Global and Planetary Change 110 (2013) 214–222.

106. Stuyfzand, P., 1986. A New Hydrochemical Classification of Water Types with Examples of Application to The Netherlands. H20 19. pp. 562–568.

107. Storlazzi, C.D., E. Elias, M.E. Field, and M.K. Presto, 2011: Numerical modeling of the impact of sea-level rise on fringing coral reef hydrodynamics and sediment transport. Coral Reefs, 30, 83-96.

108. Ta T.T., Tran T.L., Pham Q.N., Le V.H. The scientific and technological solutions to limit saltwater intrusion in the coastal aquifers in the Southern Central region of Vietnam under climate change—a study case in Ninh Thuan province. Project Report, Hanoi University of Natural Resources and Environment, 2019.

109. Thornthwaite, C.W., Mather, J.R., 1957. Instructions and Tables for Computing Potential Evapotranspiration and Water Balance. Publ.Climatol, Centerton, NJ (EUA).

110. Tirado, M.C., R. Clarke, L.A. Jaykus, A. McQuatters-Gollop, and J.M. Frank, 2010: Climate change and food safety: A review. Climate Change and Food Science, 43(7), 1745-1765.

111. Tokarevich, N.K.,A.A.Tronin, O.V. Blinova, R.V. Buzinov,V.P. Boltenkov, E.D.Yurasova, and J. Nurse, 2011: The impact of climate change on the expansion of Ixodes persulcatus habitat and the incidence of tick-borne encephalitis in the

north of European Russia. Global Health Action, 4, 8448, doi:10.3402/gha.v4i0. 8448.

112. Tran, D. H., Hoang, T. N., Tokida, T., Tirol-Padre, A., & Minamikawa, K. (2017). Impacts of alternate wetting and drying on greenhouse gas emission from paddy field in Central Vietnam. Soil Science and Plant Nutrition, 64(1), 14–22. https://doi.org/10.1080/00380768.2017.1409601.

113. Tran T.D., 2020. Survey on the effect of drought and saltwater intrusion on agricultural production and irrigation in Binh Thuan. Report, of the bilateral Belgian - Vietnamese project by the VLIR-UOS, 2020.

114. Tran D.D., Pham T.B.T., Park E., Phan T.T.H., Duong B.M., Wang J., 2024. Extent of saltwater intrusion and freshwater exploitability in the coastal Vietnamese Mekong Delta assessed by gauging records and numerical simulations, Journal of Hydrology, Volume 630, 130655, ISSN 0022-1694, https://doi.org/10.1016/j.jhydrol.2024.130655.

115. Turekian, K.K. ,1968.- Oceans, Prentice Hall

116. UNESCO, 1987. Groundwater problems in coastal areas. International Hydrological Programme.

117. USDA-SCS (1986) Urban hydrology for small watersheds, Technical Release 55 (TR-55). Soil Conservation Service.

118. United States Department of Agriculture (USDA). Urban Hydrology for Small Watersheds; Technical Release 55 (TR-55); Soil Conservation Service (SCS): Washington, DC, USA, 1986.

119. USGS, 2021. "The Fundamentals of the Water Cycle". www.usgs.gov. Archived from the original on 27 November 2019. Retrieved 17 September 2021.

120. United Nations, 2020. Percentage of total population living in coastal areas. https://www.un.org/esa/sustdev/natlinfo/indicators/methodology_sheets/oceans_seas_coasts/pop_coastal_areas.pdf.

121. University of Technology Sydney (2018). "Hundreds of Vietnamese children access safe water". University of Technology Sydney. Archived from the original on 11 January 2019.

122. UNICEF (2015). "Viet Nam [Sanitation]". UNICEF. Archived from the original on 11 January 2019. Retrieved 11 January 2019.

123. Van Camp, M., Mtoni, Y., Mjemah, I.C., Bakundukize, C., Walraevens, K., 2014. Investigating seawater intrusion due to groundwater pumping with schematic model simulations: the example of the Dar es Salaam coastal aquifer in Tanzania. J. Afr. Earth Sci. 96, 71–78.

124. Vandenbohede, A. (2003). Solute transport in heterogeneous aquifers parameter identification and its use in groundwater pollution and saltwater intrusion problems [PhD thesis, Universiteit Gent]. Gent.

125. Vietnam-Netherlands Center for Water and Environment (VINWATER) and the Sub-institute of Hydrometeorology and Climate Change (SIHYMECC), 2017. Project: Integrated water resources management and urban development related to climate change in Binh Thuan Province.

126. Vietnam News, 2019a. Water industry needs smart tech. Archived from the original on 16 January 2019. Retrieved 16 January 2019.

127. Vietnam News, 2019b. Water quality inspections to be held nationwide. Archived from the original on 16 January 2019. Retrieved 16 January 2019.

128. Walraevens, K., Lebbe L., Van Camp, M., Angius, G., Serra, M., Vacca, A., Massidda, R., Debreuck, W., 1993. Salt Fresh-water Flow and Distribution in a Cross-section at Oostduinkerke (Western Coastal-plain of Belgium). Study and Modelling of Saltwater Intrusion into Aquifers. pp. 407–420.

129. Walraevens, K., Van Camp, M., 2004. Advances in understanding natural groundwater quality controls in coastal aquifers. Proceedings of the 18th Salt Water Intrusion Meeting, pp. 449–463.

130. Walraevens K, Cardenal J, Van Camp M (2007) Reaction transport modelling of a freshening aquifer (Tertiary Ledo-Paniselian Aquifer, Flanders-Belgium). Appl Geochem 22:289–305.

131. Weixing Guo and Christian D. Langevin 2002. User's Guide to SEAWAT: A Computer Program for Simulation of Three-Dimensional Variable-Density Ground-Water Flow. U.S. Geological Survey Techniques of Water-Resources Investigations 6-A7.

132. Werner, A.D., Gallagher, M.R., (2006) Characterisation of sea-water intrusion in the Pioneer Valley, Australia using hydrochemistry and three-dimensional numerical modelling. Hydrogeology Journal 14:1452–1469.

133. Werner AD, Jakovovic D, Simmons CT. Experimental observations of saltwater up-coning. J Hydrol 2009; 373:230–41.

134. Werner, A. D., Bakker, M., Post, V. E. A., Vandenbohede, A., Lu, C., Ataie-Ashtiani, B., 2013. Seawater intrusion processes, investigation and management: Recent advances and future challenges. Advances in Water Resources, 51, 3–26. https://doi.org/10.1016/j.advwatres.2012.03.004

135. Werner, A.D.; Jakovovic, D.; Simmons, C.T. Experimental observations of saltwater up-coning. J. Hydrol. 2009, 373, 230–241.

136. WHO Library Cataloguing-in-Publication Data, 2017. Guidelines for drinking-water quality: fourth edition incorporating the first addendum ISBN 978-92-4-154995-0.

137. Wong, P.P., I.J. Losada, J.-P. Gattuso, J. Hinkel, A. Khattabi, K.L. McInnes, Y. Saito, and A. Sallenger, 2014: Coastal systems and low-lying areas. In: Climate Change 2014: Impacts, Adaptation, and Vulnerability. Part A: Global and Sectoral Aspects. Contribution of Working Group II to the Fifth Assessment Report of the Intergovernmental Panel on Climate Change, [Field, C.B., V.R. Barros, D.J. Dokken, K.J. Mach, M.D. Mastrandrea, T.E. Bilir, M. Chatterjee, K.L. Ebi, Y.O. Estrada, R.C. Genova, B. Girma, E.S. Kissel, A.N. Levy, S. MacCracken, P.R. Mastrandrea, and L.L. White (eds.)]. Cambridge University Press, Cambridge, United Kingdom and New York, NY, USA, pp. 361-409.

138. Woessner, W. W., & Poeter, E. P. (2020). Hydrogeologic Properties of Earth Materials and Principles of Groundwater Flow. The Groundwater Project, 2020, ISBN: 978-1-7770541-2-0.

139. Worthington, S. R., Foley, A. E., & Soley, R. W. (2019). Transient characteristics of effective porosity and specific yield in bedrock aquifers. Journal of Hydrology, 578, 124129.

140. Worthington, S. R. (2022). Estimating effective porosity in bedrock aquifers. Groundwater, 60(2), 169-179. https://doi.org/10.1111/gwat.13171.

141. Zwertvaegher, A., Finke, P., De Reu, J., Vandenbohede, A., Lebbe, L., Bats, M., et al. (2013). Reconstructing Phreatic Palaeogroundwater Levels in a Geoarchaeological Context: A Case Study in Flanders, Belgium: RECONSTRUCTING PHREATIC PALAEOGROUNDWATER LEVELS. Geoarchaeology, 28(2), 170–189. https://doi.org/10.1002/gea.21435.

142. Zamrsky, D., Oude Essink, G. H. P.,& Bierkens, M. F. P. (2024). Global impact of sea level rise on coastal fresh groundwater resources. Earth's Future, 12, e2023EF003581. https://doi.org/10.1029/2023EF003581

143. Zekâi Şen, Chapter 1 - Water Science Basic Information, Editor(s): Zekâi Şen, Practical and Applied Hydrogeology, Elsevier, 2015, Pages 1-41, ISBN 9780128000755, https://doi.org/10.1016/B978-0-12-800075-5.00001-7.

144. Zghibi, A., Zouhri, L. and Tarhouni, J. (2011), Groundwater modelling and marine intrusion in the semi-arid systems (Cap-Bon, Tunisia). Hydrol. Process., 25: 1822-1836. https://doi.org/10.1002/hyp.7948. Zheng. C. and Wang. P. P. (1999): MT3DMS. A modular three-dimensional multispecies transport model for simulation of advection. dispersion. and chemical reactions of contaminants in groundwater systems; documentation and user's guide. Contract Report SERDP-99-1. U.S. Army Engineer Research and Development Center. Vicksburg. MS https://doi.org/10.13031/2013.42263

145. Zwertvaegher, A., Finke, P., De Reu, J., Vandenbohede, A., Lebbe, L., Bats, M., De Clercq, W., De Smedt, P., Gelorini, V., Sergant, J., Antrop, M., Bourgeois, J., De

Maeyer, P., Van Meirvenne, M., Verniers, J., Crombé, P., 2013. Reconstructing Phreatic Palaeogroundwater Levels in a Geoarchaeological Context: A Case Study in Flanders, Belgium: RECONSTRUCTING PHREATIC PALAEOGROUNDWATER LEVELS. Geoarchaeology 28, 170–189. https://doi.org/10.1002/gea.21435

Appendix

Appendix 1 Geological map of Bac Binh and Tuy Phong districts (Segers, 2024)

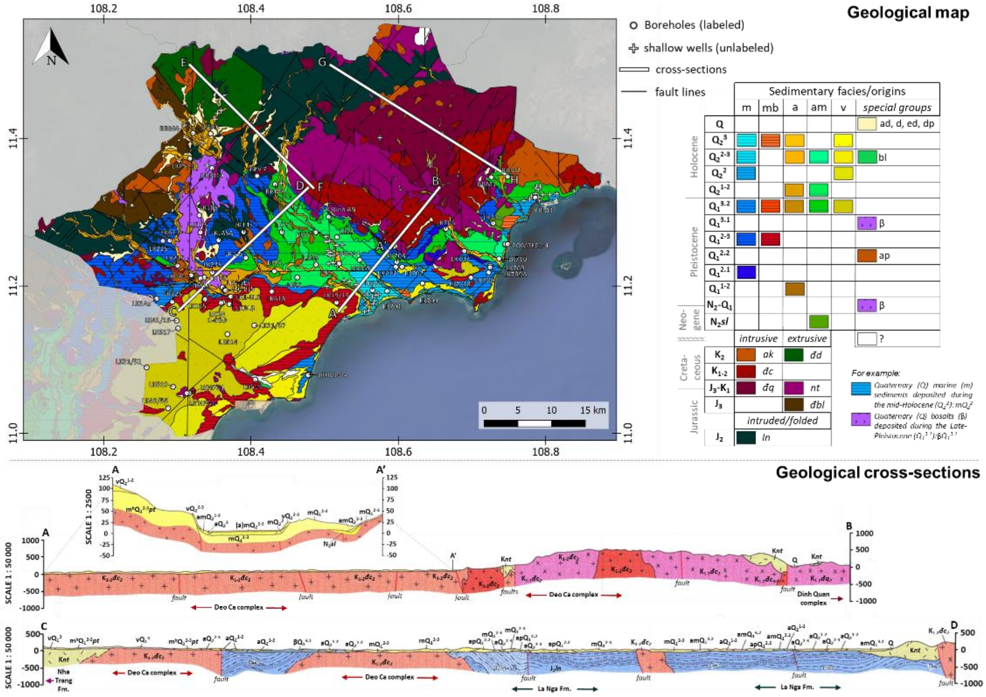

Appendix 2 Compilation of relevant geological formations and deposits (sedimentary facies), derived from multiple sources (Segers, 2024)

Age		Formation (*sed. facies*)		Lithological description	Thickness
		Name	Symbol		
Holocene	L	*Undivided*	ad,ed,d,dpQ	Sand, clayey-silty sand, pebbles, gravels, breccia, etc.[6,12,13]	0,5-28 m[6,14]
	M-L	*Aeolian*	vQ_2^3, vQ_2^{2-3}	Small-grained quartz sand[13]	1-40 m[6,14], ~10 m Average[6]
		Alluvial	aQ_2^3, aQ_2^{2-3}	Sand, clayey-silty sand, gravel and pebbles[12,13]	
		Alluvial-marine	amQ_2^{2-3}	Silty and sandy clay[13]	
		Marine	mQ_2^3, mQ_2^{2-3}	Medium-grained quartz sand, containing mollusc fragments and ilmenite in Late and Mid-Late deposits respectively[13]	
		Marine-bog	mbQ_2^3	Black sandy silt-clay, containing molluscs[13]	
	E-M	*Aeolian*	vQ_2^{1-2}, vQ_2^2	Small-grained, yellowish-brown quartz sand near the coast[13], with white glass sand further inland[12]	
		Alluvial	aQ_2^{1-2}	Gravel sand, sand and sand mixed with silty clay[12]	
		Alluvial-marine	amQ_2^{1-2}	Silty and sandy clay near coast[13], with silty sand further inland[12]	
		Marine	mQ_2^{1-2}, mQ_2^2	Quartz sand, silty-clayey sand and gravel[13]	
Pleistocene	L	*Aeolian*	vQ_1^3	Small-grained quartz sand mixed with pink-brownish silt[12,13]	N/P
		Alluvial	$aQ_1^{3.2}$	Sand, gravel, silty-clayey sand[12]	N/P
		Alluvial-marine	$amQ_1^{3.2}$	Sandy silt, silty-clayey sand and clayey silt with sand[12,13]	N/P
		Marine	$mQ_1^{3.2}$	White, small-grained quartz sand near the coast[13] and gray quartz sands mixed with silt further inland[12]	N/P
		Marine-barrier	$m^bQ_1^{3.2}$	Gravel sand, sandstone containing mollusc fragments and coral[13]	N/P
		Phuoc Tan Fm.	βQ_1^3*pht* or $BQ_1^{3.1}$	Blackish-grey, vesicular, porous olivine (andesito)basalt with upper layer weathered to clay[6,10,14]	3-40 m[6,10]
	M-L	*Marine*	mQ_1^{2-3}	Yellow-grey sand and silty clay mixed with gravel[12,13]	N/P
		Phan Thiet Fm.	m,mv,m^b Q_1^{2-3}*pt*	(a) a lowermost greyish marine (m) sand unit strongly indurated by carbonates; (b) a thin and discontinuous white sand layer (c) a thick yellow-reddish quartz marine sand bar sequence	50 m to > 100 m[9,10]

				(m^b) with partial aeolian reworking (mv). Clay% increases with depth[1,9]	
		Alluvial-proluvial	ap$Q_1^{2.2}$	Gravel, quartz pebbles and sand[12,13]	N/P
		Mui Ne Fm.	m$Q_1^{2.1}$*mn*	Grey, silty to silty-clayey sand mixed with gravel[9,12,13]	N/P
	E-M	Tuy Phong Fm.	aQ_1^{1-2}*tp*	Gravel sand, gravel and lateritized mineral stone[9]	2-30 m[9]
		Tuc Trung Fm.	βN_2-Q_1*tt* or BN_2-Q_1	Blackish-grey, vesicular, porous olivine-doleritic basalt with upper layer weathered to clay[6,10,14]	3-15 m[6,10]
Pliocene	L	Song Luy or Lien Huong Fm.	N_2sl or N_2lh	(a) a lower white-grey, well-cemented silty sandstone; (b) white grey, well-cemented pebbly sandstone and conglomerate; and (c) upper white-to-dark medium-bedded grey claystones (argillite) and sandstones that contain plant remains.[2,5,6,10] Locally, rocks are cut by thin quartz veins.[5]	3,6-20 m[6,14] 10-20 m in Luy valley[2,5,6]
Cretaceous	L	Ankroet (or Cana)	ɤK_2*ak*	Primarily leucocratic, sub-alkaline granites[5] with subordinate gabbro and granodiorite[5,15]: biotite-bearing[2,5]	N/P
		Don Duong	K_2*đd*	Series of felsic and calc-alkaline volcano-sedimentary beds, composed of: (porphyry) rhyolite, rhyodacite, (porphyry) dacite, felsite and their tuffs + beds of tuffaceous sandstone[2,6,11] + weathering crust of clays mixed with sand[6]	~750 m[6,14] + 5-6 m[6] crust
	M	Deo Ca	ɤξK*đc* or GSyK*dc*	Biotite granosyenite, biotite granite, porphyry granite[10,14] and granodiorites.[2,3] Calc-alkaline series, similar to Dinh Quan suite.[4]	N/P
L-Jurassic to E-Cretaceous		Nha Trang	K*nt*	Series of felsic and sub-alkaline volcano-sedimentary beds, composed of: dacite, rhyodacite, felsite, trachyrhyolite, rhyolite and their tuffs.[2,6,10,14] Same magmatic origin as Deo Ca complex.[2]	500-600m[2], max. 750[14]
		Dinh Quan	ɤδJ_3*đq* or ɤδJ_3-K_1*đq*	Hornblende-biotite diorites, granodiorites[1,10] and biotite granites[1,14]	N/P
Jurassic	L	Deo Bao Loc	J_3*đbl*	Series of volcano-sedimentary beds, composed of: andesito-basalt, andesite, andesito-dacite, dacite-rhyodacite, (porphyry) rhyolite and their tuffs[2,6,7,14]	Max. 650-800 m[9,10]
	M	La Nga Fm. (or Ma Da & Song Phan Fm.)[2,11]	J_2*ln*	Lower part (gulf-lagoonal facies): clayey schist interbedded with siltstone, sandstone and silty-clayey sandstone + argillaceous shale, plant remains and pyrite crystals[2,6,14] Upper part (shallow marine facies): sandstone and siltstone + fewer beds of argillaceous shale and less pyrite[2,6,14] Local metamorphism: hornfels and sericite schist[2]	300-1500 m[14] 500-850 m[2,10]

Appendix 3 Chemical component of groundwater samples in the Luy River catchment collected in the rainy season 2020

Name	PH	TDS	Na+	K+	Ca^2+	Mg^2+	Fe^2+/Fe^3+	Mn^2+	NH_4+	Cl-	SO_4^{2-}	NO_3^-	NO_2^-	HCO_3^-	PO_4^{2-}
		mg/l	mg/l	mg/l	mg/l	mg/l	mg/l	mg/l	mg/l	mg/l	mg/l	mg/l	mg/l	mg/l	mg/l
SL001	7.7	1054	124.3	29.5	94.6	37.6	0.0	0.0	1.6	106.1	93.4	93.7	0.4	472.8	0.1
SL002	8.7	470	45.5	1.4	59.4	9.1	0.0	0.0	0.1	44.4	37.4	55.7	0.1	215.9	0.9
SL003	7.8	914	78.3	24.1	112.1	10.3	0.0	0.1	3.7	76.1	66.3	125.1	8.9	396.5	12.6
SL004	8.1	1068	219.6	21.8	53.2	28.3	0.0	0.1	0.0	256.1	76.8	0.2	0.0	411.8	0.3
SL005	5.7	5040	1186.9	120.1	252.6	278.8	0.0	0.7	0.0	2691.6	403.8	14.0	0.0	91.5	0.0
SL006	7.3	3410	417.4	40.3	269.2	225.4	25.1	4.2	4.0	465.0	1562.3	0.7	0.1	396.5	0.0
SL007	8.1	711	87.1	14.0	99.2	28.4	0.0	0.0	0.0	188.0	55.9	68.1	2.0	167.8	0.2
SL008	7.8	684	75.8	59.8	47.0	12.9	0.0	0.0	0.0	62.3	68.8	89.4	1.0	247.7	19.5
SL009	4.2	286	11.5	23.8	33.1	11.2	0.1	0.9	0.0	40.5	29.6	132.6	0.1	0.0	0.0
SL010	4.5	360	41.1	8.5	29.6	12.6	0.0	4.3	0.0	70.0	62.3	69.3	0.1	61.0	0.1
SL011	4.5	493	39.8	29.8	47.7	17.4	0.0	1.0	0.0	86.9	62.0	131.0	0.1	76.3	0.0
SL012	6.3	85	8.9	4.5	6.0	2.8	0.0	0.5	0.0	16.2	1.5	20.8	0.7	23.2	0.2
SL013	6.3	449	69.5	23.1	34.6	23.7	4.5	1.1	0.2	138.7	50.5	24.8	0.2	76.3	2.3
SL014	7.1	885	195.3	15.6	32.1	42.9	12.8	4.9	3.4	328.1	3.5	2.0	0.0	244.0	0.0
SL015	6.8	5269	1543.2	64.7	366.8	321.4	3.4	7.4	3.2	2738.0	19.5	2.5	0.6	198.3	0.0
SL016	7.4	847	150.7	20.9	44.1	29.6	2.9	0.2	1.5	163.7	112.1	1.0	0.0	320.3	0.0
SL017	7.4	1078	213.9	16.1	47.7	30.7	0.0	0.0	0.0	147.6	293.5	66.9	1.6	259.3	0.6
SL018	6.7	5607	1614.8	32.4	313.9	239.9	0.1	0.4	0.0	2597.6	545.3	3.0	0.1	259.3	0.5
SL019		1032	138.8	74.1	47.6	18.6	0.0	0.0	0.4	68.8	110.3	67.3	0.1	503.3	2.5

SL020	7.4	335	63.8	3.7	17.7	11.0	4.3	0.3	0.4	57.3	31.5	7.2	0.3	137.3	0.0
SL021	7.4	1781	285.5	150.3	40.1	27.9	0.0	0.0	2.0	177.6	168.2	29.2	0.3	899.8	0.4
SL022	7.1	1437	198.4	76.0	118.6	40.9	0.8	0.5	0.0	142.5	178.8	99.1	1.4	579.5	0.1
SL023	7.5	2087	389.1	59.3	96.6	84.6	0.0	0.2	0.1	396.8	250.5	59.4	0.8	747.3	2.6
SL024	8.4	1528	217.4	107.2	115.9	25.6	0.0	0.2	0.0	207.8	145.7	19.8	0.4	686.3	2.3
SL025	7.7	1627	228.1	103.3	72.5	42.7	0.1	0.0	13.2	171.6	104.9	51.2	0.1	838.8	0.5
SL026	7.9	1546	233.6	120.7	56.6	33.6	0.0	0.0	8.0	175.8	107.7	44.7	1.9	762.5	0.6
SL027	7.7	1274	191.8	5.3	107.3	33.9	0.0	0.1	0.1	175.4	104.9	212.3	0.7	442.3	0.1
SL028	7.6	880	147.2	2.8	54.8	26.8	0.0	0.1	0.0	119.2	80.8	66.7	0.8	381.3	0.1
SL029	7.4	1390	348.8	4.0	47.2	26.1	0.5	0.3	0.7	332.9	39.9	24.9	0.2	564.3	0.1
SL030	7.5	624	97.7	1.6	36.5	11.5	0.1	1.4	0.0	50.6	64.4	8.6	0.7	350.8	0.0
SL031	7.6	2696	514.6	80.2	149.2	77.1	0.0	0.0	0.8	563.4	250.8	51.7	0.3	1006.5	1.4
SL032	7.4	662	97.2	18.7	27.9	18.9	3.6	0.8	0.5	77.7	79.1	2.0	0.0	335.5	0.0
SL033	6.9	1196	291.3	0.9	35.0	33.6	0.0	0.0	0.0	280.0	316.1	40.6	0.0	198.3	0.0
SL034		1735	272.5	50.9	107.6	66.6	0.0	0.0	0.0	268.6	215.3	172.0	0.5	579.5	1.0
SL035	7.3	2303	509.6	58.4	36.2	39.4	0.3	0.1	0.0	317.1	409.5	1.2	0.1	930.3	0.8
SL036	7.1	2825	734.1	17.0	48.1	62.1	0.4	0.8	2.0	823.6	525.5	0.9	0.3	610.0	0.1
SL037	6.9	880	187.3	2.1	21.0	27.2	1.4	0.3	0.5	142.0	177.7	0.3	0.1	320.3	0.0
SL038	7.2	1392	335.5	5.9	26.6	26.0	1.2	0.4	0.6	262.3	304.7	0.2	0.1	427.0	1.3
SL039	6.2	754	108.0	2.5	69.3	31.4	0.3	4.1	0.0	91.5	192.6	51.3	4.8	198.3	0.0
SL040	6.3	729	123.5	3.5	31.6	24.2	30.5	0.7	0.0	66.7	322.6	3.8	0.0	122.0	0.0
SL041	7.1	975	185.0	4.9	33.7	28.3	6.4	0.7	0.1	112.2	267.3	1.1	0.0	335.5	0.0
SL042	7.0	990	174.2	10.8	43.5	27.5	4.7	0.5	0.4	114.0	226.3	7.1	0.0	381.3	0.0
SL043	6.7	1729	334.9	2.2	69.5	58.4	0.0	0.9	0.2	161.3	716.4	96.4	0.9	287.9	0.1
SL044	6.4	1156	215.8	1.5	72.6	39.1	0.0	0.0	0.1	168.7	372.6	85.6	1.2	198.3	0.1
SL045	6.8	567	94.5	1.6	31.6	20.0	0.0	0.0	0.5	64.9	115.5	9.2	0.0	228.8	0.3
SL046	6.9	497	91.7	0.5	23.0	12.6	0.0	0.1	0.0	41.5	78.3	16.0	0.3	231.8	0.5

SL047	7.1	1412	168.2	16.8	160.8	31.7	0.0	0.0	0.0	158.8	132.8	340.7	0.6	396.5	5.3
SL048	7.1	1430	296.7	14.2	66.7	22.3	0.0	0.0	0.0	176.9	128.1	112.9	1.3	610.0	0.8
SL049	7.6	572	70.7	1.1	45.2	16.7	0.0	0.6	0.0	27.5	26.2	2.7	0.0	381.3	0.5
SL050	7.5	853	134.3	1.4	56.5	20.4	0.0	0.1	0.0	80.4	116.6	61.8	0.2	381.3	0.4
SL051	7.2	595	55.9	4.2	72.1	17.2	0.0	0.0	0.0	55.3	73.5	25.1	0.1	289.8	1.8
SL052	7.7	1028	92.2	72.6	73.4	21.3	0.0	0.6	15.1	78.8	21.9	23.7	0.3	625.3	2.5
SL053	6.8	674	95.4	2.3	50.3	21.4	0.0	0.2	0.2	67.3	69.7	46.2	0.1	320.3	0.2
SL054	7.3	748	118.8	29.2	64.6	15.5	0.0	0.0	0.0	147.4	50.2	28.7	0.2	289.8	3.8
SL055	6.8	688	64.5	24.2	89.1	19.6	0.0	0.0	0.0	99.9	90.2	132.3	0.0	167.8	0.9
SL056	6.8	517	93.8	1.9	29.6	7.3	0.2	0.4	0.0	35.8	22.6	1.7	0.0	323.3	0.0
SL057	7.8	579	70.8	15.1	48.7	8.6	0.0	0.0	0.0	27.7	58.1	27.6	0.1	320.3	1.7
SL058	7.0	840	104.2	1.8	86.0	32.3	0.0	0.0	0.0	90.6	135.3	47.6	0.1	341.6	0.1
SL059	7.9	2296	639.1	14.6	50.3	8.5	2.1	0.1	0.0	558.7	0.0	0.5	0.0	1021.8	0.0
SL060	7.5	1412	284.9	2.7	54.3	26.3	0.0	0.1	0.4	138.2	130.0	72.7	0.1	701.7	0.6
SL061	7.5	337	32.6	7.5	34.8	8.0	0.1	0.3	1.6	35.5	18.1	16.2	0.5	179.3	2.9
SL062	6.7	145	10.9	2.1	15.1	5.5	0.5	0.2	0.1	16.4	10.2	16.6	0.7	67.1	0.0
SL063	7.1	8924	2288.2	4.0	979.3	530.2	0.2	1.4	0.2	4837.4	35.8	2.6	0.1	245.2	0.0
SL064	7.7	1182	140.6	0.6	14.1	7.4	0.0	0.0	0.1	67.6	110.0	132.0	0.4	706.4	2.4
SL065	7.4	1095	108.5	0.4	113.2	44.8	0.0	0.0	0.0	86.9	83.1	168.9	0.0	488.0	0.9
SL066	7.5	1525	237.9	0.5	90.6	41.8	0.0	0.3	0.0	117.1	97.9	137.7	1.0	800.2	0.4
SL067	7.0	881	177.7	2.7	33.8	22.9	0.0	0.0	0.0	153.7	76.3	27.0	0.1	386.6	0.4
SL068	7.3	1115	214.7	4.3	70.5	27.7	0.0	0.0	0.0	242.9	232.1	63.4	0.3	259.3	0.1
SL069	7.6	1209	209.5	3.6	54.4	35.9	0.0	0.3	0.0	116.8	125.5	141.5	3.2	518.5	0.0
SL070	8.5	819	160.8	1.0	22.3	7.7	0.0	0.0	0.0	61.7	29.2	9.1	0.0	525.8	1.1
SL071	7.6	652	121.3	0.4	18.6	7.7	0.9	0.1	0.1	40.3	25.4	16.1	0.2	419.7	0.8
SL072	7.8	1400	289.4	0.3	41.2	11.9	0.0	0.1	0.0	367.4	106.7	3.1	0.3	578.3	1.1
SL073	8.1	1749	406.1	1.3	16.9	6.1	0.0	0.0	0.3	148.2	125.2	124.9	0.9	915.0	4.4

SL074	7.2	828	166.4	0.9	34.2	14.7	0.0	0.1	0.0	118.8	89.7	111.0	0.7	290.4	0.8
SL075	7.0	692	117.9	1.2	28.8	26.1	0.0	0.0	0.0	121.0	102.8	50.3	0.1	244.0	0.1
SL076	7.1	928	95.3	16.0	89.5	31.1	0.0	0.5	0.0	116.6	140.5	100.8	2.1	335.5	0.0
SL077	7.4	5288	1628.8	3.1	189.3	85.7	0.0	2.0	0.0	2019.8	536.0	71.9	4.0	747.3	0.1
SL078	7.5	2081	528.0	4.8	93.6	25.8	0.0	0.2	0.0	582.7	165.2	8.4	0.5	671.0	1.0
SL079	7.3	1772	383.4	4.9	104.8	37.0	0.0	0.0	0.0	423.5	153.4	99.7	0.4	564.3	0.7
SL080	7.2	324	22.7	11.3	40.0	8.6	0.0	0.0	0.0	30.2	40.5	20.2	0.4	150.1	0.3
SL081	7.1	3242	832.3	23.0	165.5	20.2	0.2	0.0	0.1	1454.4	211.7	45.1	0.6	488.0	0.5
SL082	7.2	1702	423.1	32.5	85.3	3.6	0.0	0.4	0.0	488.6	147.0	168.9	1.6	350.8	0.0
SL083	7.2	1658	420.7	57.6	193.9	3.8	0.0	0.8	0.0	169.1	397.1	71.5	1.7	341.6	0.1
SL084	6.9	418	79.0	18.8	28.6	4.1	0.0	0.1	0.2	136.9	17.8	8.1	1.0	122.0	1.1
SL085	7.8	2068	509.0	28.0	46.6	3.8	0.0	0.4	0.8	406.4	181.9	141.8	0.6	747.3	1.8
SL086	7.3	614	54.7	1.0	57.6	17.9	0.3	0.6	0.2	29.3	7.2	1.8	0.0	442.3	0.7
SL087	7.7	704	160.4	0.6	18.9	3.2	0.1	0.0	0.2	94.9	23.9	18.0	0.1	383.1	0.6
SL088	7.6	926	91.1	1.6	118.9	37.2	0.0	0.1	0.0	161.5	84.5	293.5	0.4	137.3	0.1
SL089	7.6	1645	278.6	2.4	110.5	82.5	0.0	0.0	0.0	419.5	67.6	104.3	0.1	579.5	0.0
SL090	7.7	851	127.0	0.6	40.4	16.9	0.0	0.0	0.1	16.6	5.8	11.4	0.4	632.0	0.0
LK01BT	7.5	7457	2284.0	106.0	102.8	264.1	0.1	3.4	3.5	3380.2	896.2	0.4	0.1	416.0	0.0
LK02BT	7.7	1979	446.4	29.0	16.0	28.7	0.1	0.2	2.9	291.7	456.2	7.2	0.3	697.8	2.8
LK03BT	7.5	6692	2135.4	11.2	139.2	164.5	2.5	2.0	1.7	2992.0	397.4	1.1	0.1	844.2	0.4
LK04BT	7.1	1748	359.1	6.7	69.0	69.4	0.1	1.8	1.1	374.1	553.9	1.6	0.1	311.7	0.0
LK05BT	7.2	1483	321.8	6.9	40.5	42.0	3.9	0.5	0.4	307.2	323.3	1.7	0.0	434.3	0.4
LK06BT	7.0	3387	806.8	14.8	154.1	115.1	9.3	1.1	0.6	1095.2	713.9	1.3	0.0	475.2	0.0
LK07BT	7.1	16047	4902.7	15.7	872.2	912.1	0.0	22.9	1.7	4935.2	4219.4	3.5	0.0	161.0	0.2
LK08BT	7.3	605	137.5	0.6	17.0	13.6	1.5	2.8	0.7	131.0	101.7	1.5	0.0	197.0	0.0
LK09BT	7.3	965	173.2	1.6	52.8	30.0	2.2	1.5	0.0	154.3	154.2	3.2	0.0	392.2	0.0
LK10BT	7.5	525	72.0	0.9	38.4	17.3	0.1	0.0	0.8	54.0	52.9	8.2	0.0	280.0	0.5

LK11BT	6.9	540	58.7	0.5	59.0	18.5	0.0	0.7	0.2	59.3	72.1	7.3	0.3	262.9	0.4
LK12BT	6.8	595	65.6	0.7	81.1	26.6	0.2	0.2	0.2	104.9	105.6	3.3	0.0	206.2	0.3
LK13BT	7.7	963	210.7	0.3	3.3	2.0	0.1	0.0	0.0	54.9	49.9	17.9	2.0	619.8	1.8
LK14BT	7.5	1533	340.3	1.3	5.4	4.9	13.5	0.3	0.2	78.4	73.1	24.4	0.7	976.0	0.8
LK15BT	7.3	693	98.5	0.7	63.6	12.2	0.9	0.3	0.6	45.5	20.0	1.1	0.1	449.0	0.3
LK16BT	6.9	455	48.2	0.5	60.2	9.6	0.1	0.2	0.4	36.6	11.9	1.7	0.1	284.9	0.2
LK17BT	7.0	3967	1091.5	56.6	56.2	106.4	1.0	0.3	0.0	1352.7	772.4	1.4	0.1	527.7	1.2
LK18BT	6.5	526	91.7	5.1	34.9	30.9	15.4	0.3	0.5	119.7	104.4	3.3	0.0	120.2	0.0
LK19BT	6.2	827	248.7	42.0	14.8	16.1	1.2	0.2	0.0	435.7	33.3	15.5	0.1	18.3	0.0
LK20BT	7.1	284	49.2	8.9	26.3	5.6	0.7	0.3	0.8	80.7	21.0	14.0	1.5	73.8	0.2

Appendix 4 Chemical component of groundwater samples in the Luy River catchment collected in the dry season 2021

Name	PH	TDS	Na+	K+	Ca^2+	Mg^2+	Fe^2+/Fe^3+	Mn^2+	NH_4+	Cl-	SO_4^{2-}	NO_3^-	NO_2^-	HCO_3^-	PO_4^{2-}
		mg/l	mg/l	mg/l	mg/l	mg/l	mg/l	mg/l	mg/l	mg/l	mg/l	mg/l	mg/l	mg/l	mg/l
SL005	5.8	5931	1317	137.5	311.5	347.4	0.0	0.7	0.2	3479	323.8	13.1	0.1	0.0	0.0
SL015	6.2	12437	2901	104.0	625.9	664.8	39.0	12.1	4.9	6970	1037	0.3	0.6	77.5	0.2
SL017	6.6	1555	279.4	24.8	135.9	85.3	0.0	2.3	0.6	381.5	514.7	30.8	0.6	99.4	0.0
SL021	7.1	3630	763.0	244.8	114.4	84.1	0.0	0.1	2.6	854.6	527.2	201.6	112.7	724.7	0.2
SL024	7.7	2768	627.9	174.2	89.2	45.9	0.0	0.0	0.1	583.2	329.5	53.2	0.2	861.9	2.3
SL033	6.8	1742	485.1	1.4	54.8	54.6	0.0	0.0	0.1	478.6	342.1	18.3	0.2	306.8	0.0
SL036	7.2	3099	918.5	22.6	51.7	66.7	0.5	0.8	3.2	1066	433.3	0.0	0.2	534.4	0.3
SL054	7.4	2772	649.3	6.2	282.5	54.0	0.0	0.0	0.1	1289	12.4	112.2	0.6	364.8	0.1
SL063	7.1	13313	2997	4.3	849.9	564.7	0.0	0.4	0.4	8437	43.1	0.6	0.1	415.4	0.0
SL064	7.5	1789	444.1	2.1	43.7	23.7	0.0	0.0	0.1	154.5	142.7	200.0	0.5	775.3	2.4
SL068	7.1	1693	398.8	7.5	118.1	45.1	0.0	0.0	0.1	540.6	272.0	27.3	0.2	283.0	0.0
SL075	7.1	1647	423.2	3.0	47.4	39.2	0.0	0.0	0.1	305.0	175.7	165.4	0.3	487.4	0.2
SL077	7.1	7271	1817.2	4.6	346.9	177.2	0.0	5.8	0.4	3406	595.1	119.1	0.2	797.9	0.0
SL079	7.3	2608	741.1	7.5	106.9	36.7	0.0	0.0	0.1	923.8	126.3	96.6	0.2	567.9	0.8
SL081	7.2	1202	320.8	11.4	72.3	11.2	0.0	0.0	0.1	464.0	70.5	30.4	0.2	220.8	0.5
LK01BT	7.1	31239	8205	409.6	409.1	1421.8	0.0	8.4	15.1	19752	274.6	9.0	76.3	657.6	0.2
LK02BT	7.5	1927	515.1	30.0	12.0	22.2	1.1	0.1	0.1	352.6	387.2	4.6	45.1	552.7	3.3
LK03BT	7.5	8572	2484	13.4	174.3	195.9	0.7	2.4	0.3	4606	323.2	4.6	1.2	764.3	1.2
LK05BT	7.4	1563	406.5	8.0	41.9	46.2	2.2	0.5	1.1	355.9	279.4	0.0	0.0	420.9	0.7
LK06BT	7.4	4453	1091	19.3	220.8	159.2	1.8	1.2	0.1	1555	918.1	0.2	0.2	485.6	0.0
LK07BT	7.0	24805	5478	21.5	1120	1248	0.0	33.5	0.7	10994	5865	3.8	0.2	39.7	0.2

LK08BT	7.1	967	243.6	0.8	28.0	24.7	11.2	5.0	1.1	296.6	115.3	0.0	0.9	239.7	0.1
LK09BT	7.2	1239	281.1	2.0	65.9	38.3	7.8	0.9	0.1	270.5	166.8	0.6	0.3	405.0	0.0
LK11BT	7.4	585	67.1	1.2	81.4	24.6	0.0	0.4	0.1	105.5	49.2	0.3	0.2	254.4	0.3
LK12BT	7.4	601	66.0	1.5	79.1	25.1	2.3	0.3	0.1	104.5	47.1	0.0	0.4	272.1	0.5
LK13BT	7.9	1415	408.3	0.5	4.5	2.8	1.4	0.0	0.1	96.7	99.7	22.3	0.2	775.3	1.5
LK14BT	8.0	2325	674.6	0.4	7.8	4.9	0.2	0.0	0.1	198.1	164.0	50.5	0.2	1222.4	1.8
LK15BT	7.3	444	65.9	0.4	41.8	8.4	0.1	0.2	0.1	39.4	22.2	1.8	0.2	262.9	0.3
LK16BT	7.1	333	52.4	0.6	36.4	6.8	0.1	0.0	0.1	43.9	18.3	1.0	0.2	173.2	0.2
LK17BT	7.5	4558	1278.0	56.4	62.8	93.9	0.3	0.3	2.1	1906.3	602.1	0.0	0.2	553.9	1.3
LK18BT	7.2	1294	297.4	11.9	56.1	54.5	1.4	0.3	0.1	532.8	138.6	0.4	0.6	199.5	0.1
LK19BT	6.5	1049	337.1	40.6	14.2	17.2	1.3	0.2	0.1	591.7	31.0	9.1	0.5	5.5	0.1
LK20BT	7.4	659	178.8	26.7	27.7	12.4	0.0	0.3	0.1	279.3	26.9	11.6	0.3	95.2	0.3

Appendix 5 Fresh-Salt waters in the mixing line

Saltwater is taken from Turekian, K.K. ,1968.- Oceans, Prentice Hall and Freshwater is taken from freshwater sample in the study area.

Mixing line mg/l	TDS	Na+	K	Ca2+	Mg2+	Cl-	SO42-	NO3-	HCO3-	Br
Sea water	35000	10500	380	410	1290	19000	2750	0.22	140	65
Fresh water	325.1	22.7	11.3	40.0	8.6	30.2	40.5	20.2	150.1	0.9

Appendix 6. Lithological well logs

VIETNAM INSTITUTE OF GEOSCIENCES AND MINERAL RESOURCES

LITHOLOGICAL WELL LOG

Well LK01-BT

Location: Lâm Lộc village, Hòa Minh ward, Tuy Phong district, Bình Thuận province
Coordinate: X: 889826.813; Y: 1239041.552; Z: 5m UTM zone 48
Lat: 11.18622; Long: 108.5703
Project: Impact of saltwater intrusion on water resources and irrigation in the Southern Central region of Vietnam under climate change
Date: 20/7/2020 ; Ending depth: 31.5m

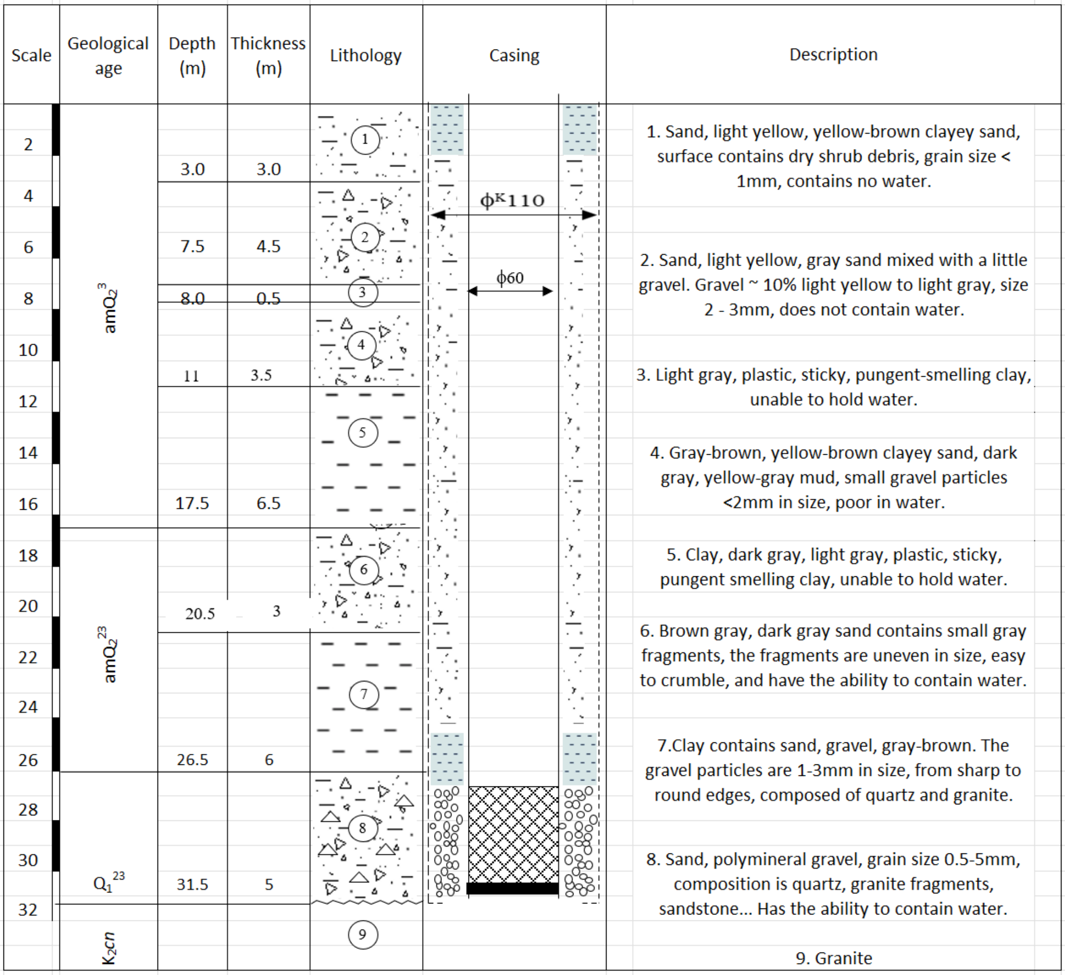

Scale	Geological age	Depth (m)	Thickness (m)	Lithology	Casing	Description
	amQ_2^3	3.0	3.0	①		1. Sand, light yellow, yellow-brown clayey sand, surface contains dry shrub debris, grain size < 1mm, contains no water.
		7.5	4.5	②		2. Sand, light yellow, gray sand mixed with a little gravel. Gravel ~ 10% light yellow to light gray, size 2 - 3mm, does not contain water.
		8.0	0.5	③		3. Light gray, plastic, sticky, pungent-smelling clay, unable to hold water.
		11	3.5	④		4. Gray-brown, yellow-brown clayey sand, dark gray, yellow-gray mud, small gravel particles <2mm in size, poor in water.
		17.5	6.5	⑤		5. Clay, dark gray, light gray, plastic, sticky, pungent smelling clay, unable to hold water.
	amQ_2^{23}	20.5	3	⑥		6. Brown gray, dark gray sand contains small gray fragments, the fragments are uneven in size, easy to crumble, and have the ability to contain water.
		26.5	6	⑦		7.Clay contains sand, gravel, gray-brown. The gravel particles are 1-3mm in size, from sharp to round edges, composed of quartz and granite.
	Q_1^{23}	31.5	5	⑧		8. Sand, polymineral gravel, grain size 0.5-5mm, composition is quartz, granite fragments, sandstone... Has the ability to contain water.
	K_2cn			⑨		9. Granite

VIETNAM INSTITUTE OF GEOSCIENCES AND MINERAL RESOURCES

LITHOLOGICAL WELL LOG

Well LK03-BT

Location: Bình Liêm village, Phan Rí Thành ward, Bắc Bình district, Bình Thuận province

Coordinate: X: 886164.266; Y: 1241949.916; Z: 4 m UTM zone 48

Lat: 11.21392; Long: 108.53533

Project: Impact of saltwater intrusion on water resources and irrigation in the Southern Central region of Vietnam under climate change

Date: 22/7/2020 ; Ending depth: 17m

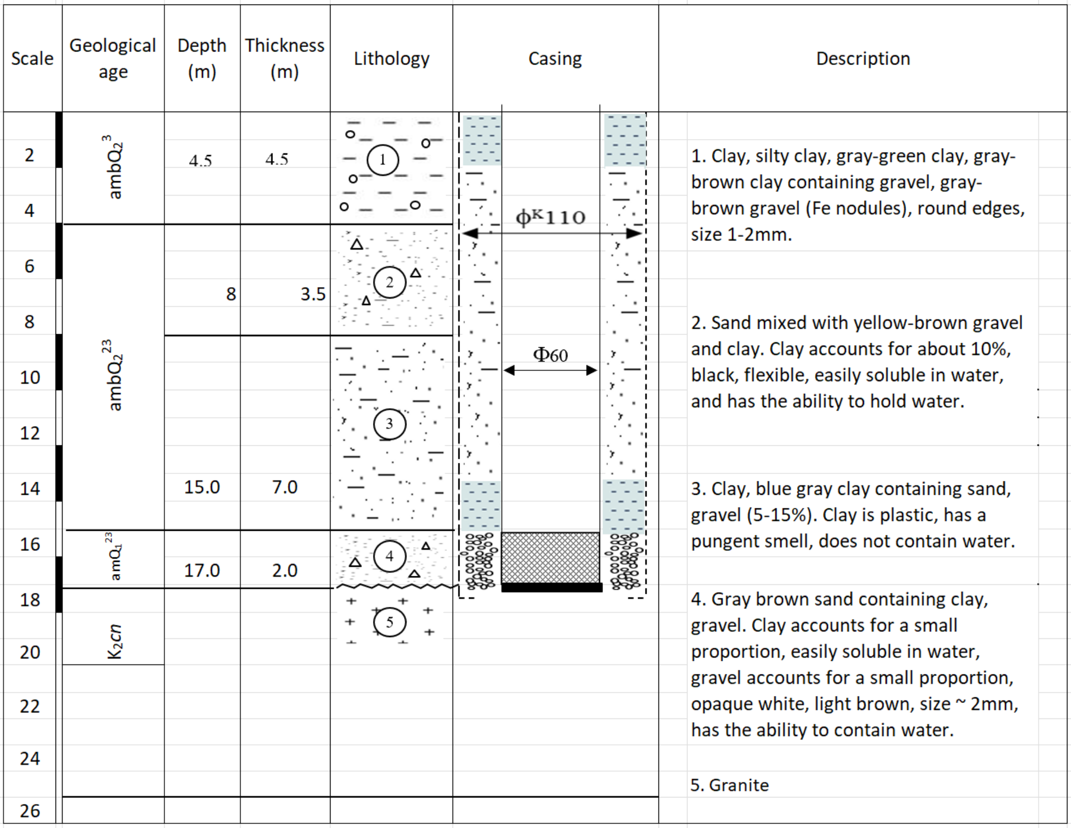

1. Clay, silty clay, gray-green clay, gray-brown clay containing gravel, gray-brown gravel (Fe nodules), round edges, size 1-2mm.

2. Sand mixed with yellow-brown gravel and clay. Clay accounts for about 10%, black, flexible, easily soluble in water, and has the ability to hold water.

3. Clay, blue gray clay containing sand, gravel (5-15%). Clay is plastic, has a pungent smell, does not contain water.

4. Gray brown sand containing clay, gravel. Clay accounts for a small proportion, easily soluble in water, gravel accounts for a small proportion, opaque white, light brown, size ~ 2mm, has the ability to contain water.

5. Granite

LITHOLOGICAL WELL LOG

Well LK05-BT

Location: Bình Liêm village, Phan Rí Thành ward, Bắc Bình district, Bình Thuận province
Tọa độ: X: 886252.857; Y: 1240501.045; Z: 5 m UTM Zone 48
Lat: 11.20082; Long: 108.53610
Project: Impact of saltwater intrusion on water resources and irrigation in the Southern Central region of Vietnam under climate change
Date: 23/7/2020 ; Ending depth: 19 m

Scale	Geological age	Depth (m)	Thickness (m)	Lithology
		1.0	1.0	①
2	$ambQ_2^3$	3.0	2.0	②
4 6 8		8.5	5.5	③
10 12	$ambQ_2^{23}$	11.5	3.0	④
14		15.0	3.5	⑤
16	$amvQ_1^{23}$	17.0	2.0	⑥
18		19.0	2.0	⑦
20				⑧

Casing

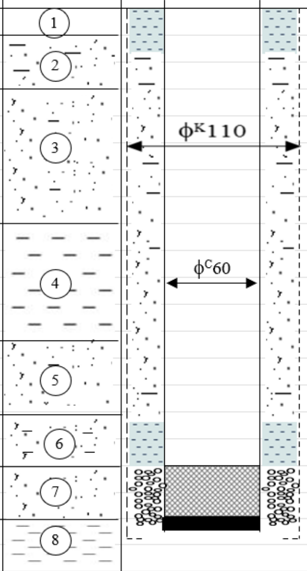

Description

1. Soil about 1 m thickness.composed of sand, sand mixed with gravel and fragments of construction materials.

2. Clay mixed with sand, gravel, yellow brown, sand and gravel ratio 20-25%.

3. Sand, light yellow clayey sand containing gravel, low clay ratio. Next is a layer of black sand with size from fine grained sand to coarse grained sand, capable of holding water.

4. Clay contains mud and organic matter, black, plastic, thick, pungent smell

5. Dark gray sand containing clay and gravel, clay is about 15%. Gravel accounts for about 3-5%, opaque white, light gray, and has the ability to contain water.

6. Yellow mixed sand containing clay and gravel. Clay accounts for about 25%, gravel accounts for a small percentage. Sand has fairly uniform size from fine to medium grain, poor in water.

7.Dark gray sand, dark gray containing clay and gravel. Small clay ratio of about 15%. Gravel accounts for about 3-5%, opaque white, light gray, and has the ability to contain water.

8. Clay contains mud and organic matter, black, plastic, thick, pungent

VIETNAM INSTITUTE OF GEOSCIENCES AND MINERAL RESOURCES

LITHOLOGICAL WELL LOG

Well LK07-BT

Location: E Chim rice field, Phan Hiệp ward, Bắc Bình district, Bình Thuận province
Coordinate: X: 884644.636; Y: 1242337.408; Z: 5 m UTM Zone 48
Lat: 11.21757; Long: 108.52152
Project: Impact of saltwater intrusion on water resources and irrigation in the Southern Central region of Vietnam under climate change
Date: 30/7/2020 ; Depth: 14.5 m

Scale	Geological age	Depth (m)	Thickness (m)	Lithology	Casing	Desciption
2 4 6 8 10 12	amQ_2^{23}	13	13.0	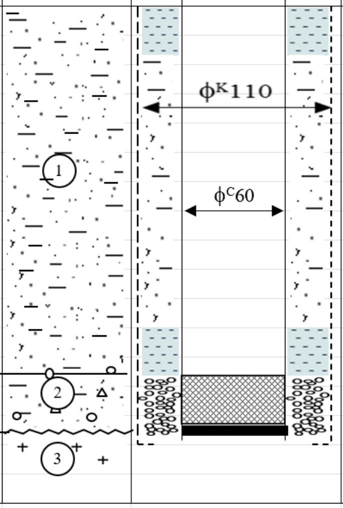		1.Clay, clay loam mixed with plant humus in the top layer, this layer is about 0.3m thick. Next is the clay layer, clay loam containing powder, sand, the ratio of powder, sand is about 10-15%. Plastic, viscous clay.
14	mQ_1^3	14.5	1.5			2. Yellow-gray clay mixed with gravel, grit, and sand. The ratio of gravel, grit, and sand is 30-35%, about 0.3 m thick. The ratio between clay and debris changes. The sand mixed with gravel, brown, gray, and has the ability to contain water.
16	K_2cn					3. Granite

LITHOLOGICAL WELL LOG

Well LK09-BT

Location: Bình Hiếu village, Phan Hiệp ward, Bắc Bình district, Bình Thuận province
Tọa độ: X: 884496.085; Y: 1241521.461; Z: 6 m UTM Zone 48
Lat: 11.20122; Long: 108.52013
Project: Impact of saltwater intrusion on water resources and irrigation in the Southern Central region of Vietnam under climate change
Date: 24/7/2020; Ending depth: 20.5 m

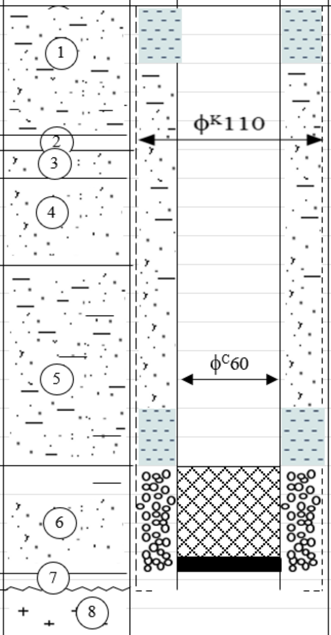

Scale	Geological age	Depth (m)	Thichkness (m)	Description
2 4	amQ_2^{23}	4.5	4.5	1. The upper part is a layer of yellow-brown soil, composed of clay and clay loam that becomes mushy when exposed to water. It changes in grain size at deeper, the bottom is sandy clay with an equivalent clay-sand ratio.
		5.0	0.5	2. The clay layer is gray-blue, thin, flexible, and has a pungent odor.
6		6	1	3. Medium - coarse sand, yellow brown clayey sand containing gravel, clay ratio ~ 10%, gravel 5-7%.
8		9.0	3.0	4. Sand, small grained polymineral sand containing clay, gravel. The proportion of fine clay is about 10%. The gravel is about 3-5% in white, light gray, and has the ability to contain water.
10 12 14 16	amQ_1^3	16.0	7.0	5. Gray clay containing large grains of sand and gravel. The clay-sand ratio varies unevenly, clay accounts for the largest proportion in the middle of the layer, the bottom and top of the layer the sand ratio fluctuates around 20-40%
18 20	Q_1^{23}	19.5	3.5	6. Dark gray sand, small-grained polymineral sand containing clay and grit. Blue-gray clay is about 10-15%. Grits is about 3-5% in opaque white, light gray. Sand varies in size with depth from fine to coarse, and has the ability to hold water.
				7. Mixed thin clay lens
	K_2cn			8. Granite

VIETNAM INSTITUTE OF GEOSCIENCES AND MINERAL RESOURCES

LITHOLOGICAL WELL LOG

Well LK11-BT

Location: Tailor house, Chợ Lầu ward, Bắc Bình district, Bình Thuận province
Coordinate: X: 883214.549; Y: 1244541.115; Z: 10 m UTM Zone 48
Lat: 11.23658; Long: 108.51045
Project: Impact of saltwater intrusion on water resources and irrigation in the Southern Central region of Vietnam under climate change
Date: 24/7/2020, Ending depth: 13.5m

Scale	Geological age	Depth (m)	Thickness (m)	Lithology	Casing	Description
2 4	amQ_2^{23}	5.0	5.0	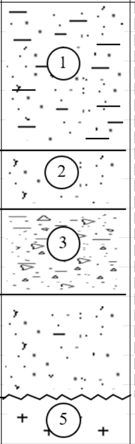	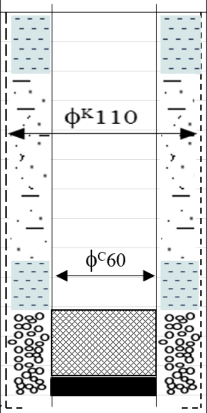	1. The upper part is a soil layer composed of clay and clay loam that becomes mushy when exposed to water. This layer has uneven grain size variation, the main components are clay; sand and powder is about 25-30% depending on the location.
6		7.0	2.0			2. Gray-brown sand, mixed clay with a ratio about 10-15%, soft, has water-holding capacity.
8 10	amQ_1^{3}	10	3.0			3. Sand containing light gray gravel and black, light gray fragments.
12	Q_1^{23}	13.5	3.5			4. Sand, silt, clay containing mica flakes, in situ weathering products of granite.
14 16 18	K_2*cn*					5. Granite

VIETNAM INSTITUTE OF GEOSCIENCES AND MINERAL RESOURCES

LITHOLOGICAL WELL LOG

Well LK13

Location: Primary school of Phan Thanh 1 , Phan Thanh ward, Bắc Bình district, Bình Thuận province

Coordinate: X: 880860.599; Y: 1242625.627; Z: 8 m UTM Zone 48

Lat: 11.22058; Long: 108.548695

Project: Impact of saltwater intrusion on water resources and irrigation in the Southern Central region of Vietnam under climate change

Date: 27/7/2020 ; Ending depth: 23 m

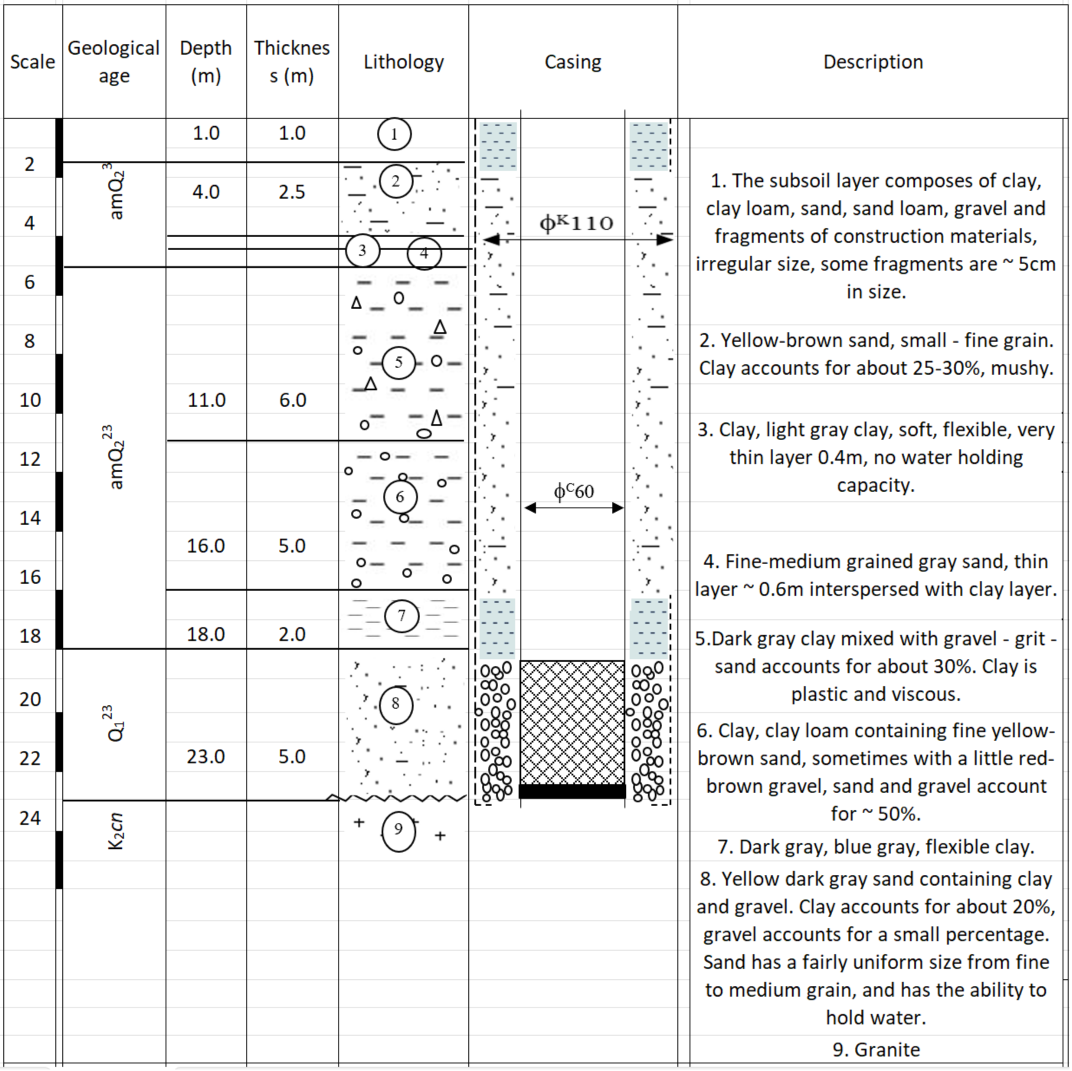

1. The subsoil layer composes of clay, clay loam, sand, sand loam, gravel and fragments of construction materials, irregular size, some fragments are ~ 5cm in size.

2. Yellow-brown sand, small - fine grain. Clay accounts for about 25-30%, mushy.

3. Clay, light gray clay, soft, flexible, very thin layer 0.4m, no water holding capacity.

4. Fine-medium grained gray sand, thin layer ~ 0.6m interspersed with clay layer.

5.Dark gray clay mixed with gravel - grit - sand accounts for about 30%. Clay is plastic and viscous.

6. Clay, clay loam containing fine yellow-brown sand, sometimes with a little red-brown gravel, sand and gravel account for ~ 50%.

7. Dark gray, blue gray, flexible clay.

8. Yellow dark gray sand containing clay and gravel. Clay accounts for about 20%, gravel accounts for a small percentage. Sand has a fairly uniform size from fine to medium grain, and has the ability to hold water.

9. Granite

VIETNAM INSTITUTE OF GEOSCIENCES AND MINERAL RESOURCES

LITHOLOGICAL WELL LOG

Well LK15-BT

Location: At the rice field, Phan Thanh ward, Bắc Bình district, Bình Thuận province
Tọa độ: X: 879957.698; Y: 1241837.396; Z: 9 m UTM Zone 48
Lat: 11.21363; Long: 108.47022
Project: Impact of saltwater intrusion on water resources and irrigation in the Southern Central region of Vietnam under climate change
Date: 26/7/2020 ; Ending depth: 13 m

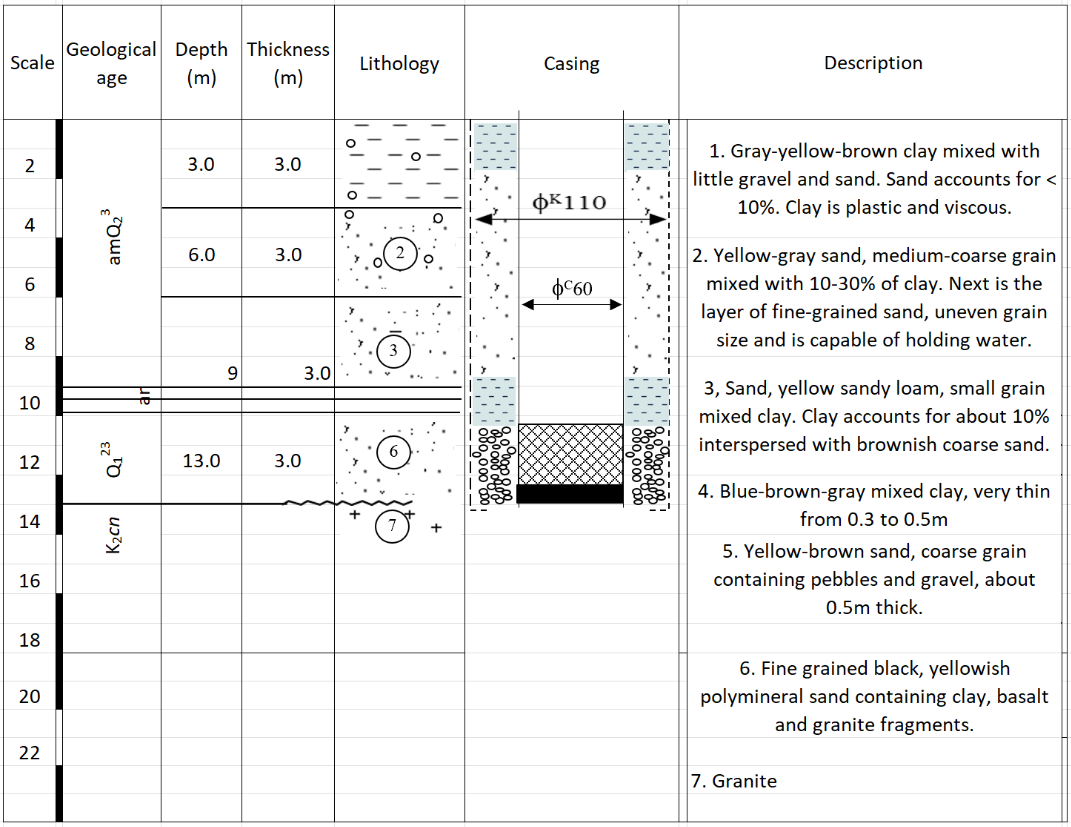

Scale	Geological age	Depth (m)	Thickness (m)	Lithology	Casing	Description
2	amQ_2^3	3.0	3.0		ϕK110	1. Gray-yellow-brown clay mixed with little gravel and sand. Sand accounts for < 10%. Clay is plastic and viscous.
4						
6		6.0	3.0	②	ϕC60	2. Yellow-gray sand, medium-coarse grain mixed with 10-30% of clay. Next is the layer of fine-grained sand, uneven grain size and is capable of holding water.
8		9	3.0	③		
10	ar					3, Sand, yellow sandy loam, small grain mixed clay. Clay accounts for about 10% interspersed with brownish coarse sand.
12	Q_1^{23}	13.0	3.0	⑥		4. Blue-brown-gray mixed clay, very thin from 0.3 to 0.5m
14	K_2cn			⑦		5. Yellow-brown sand, coarse grain containing pebbles and gravel, about 0.5m thick.
16						
18						
20						6. Fine grained black, yellowish polymineral sand containing clay, basalt and granite fragments.
22						7. Granite

VIETNAM INSTITUTE OF GEOSCIENCES AND MINERAL RESOURCES

LITHOLOGICAL WELL LOG

Well LK17-BT

Location: At the kailyard of Mr Thiên house, Phan Rí Thành ward, Bac Binh district, Bình Thuận

Coordinate: X: 888787.438; Y: 1238995.797; Z: 5 m UTM Zone 48

Lat: 11.18692; Long: 108.55903

Project: Impact of saltwater intrusion on water resources and irrigation in the Southern Central region of Vietnam under climate change

Date: 28/7/2020 ; Ending depth: 21.5m

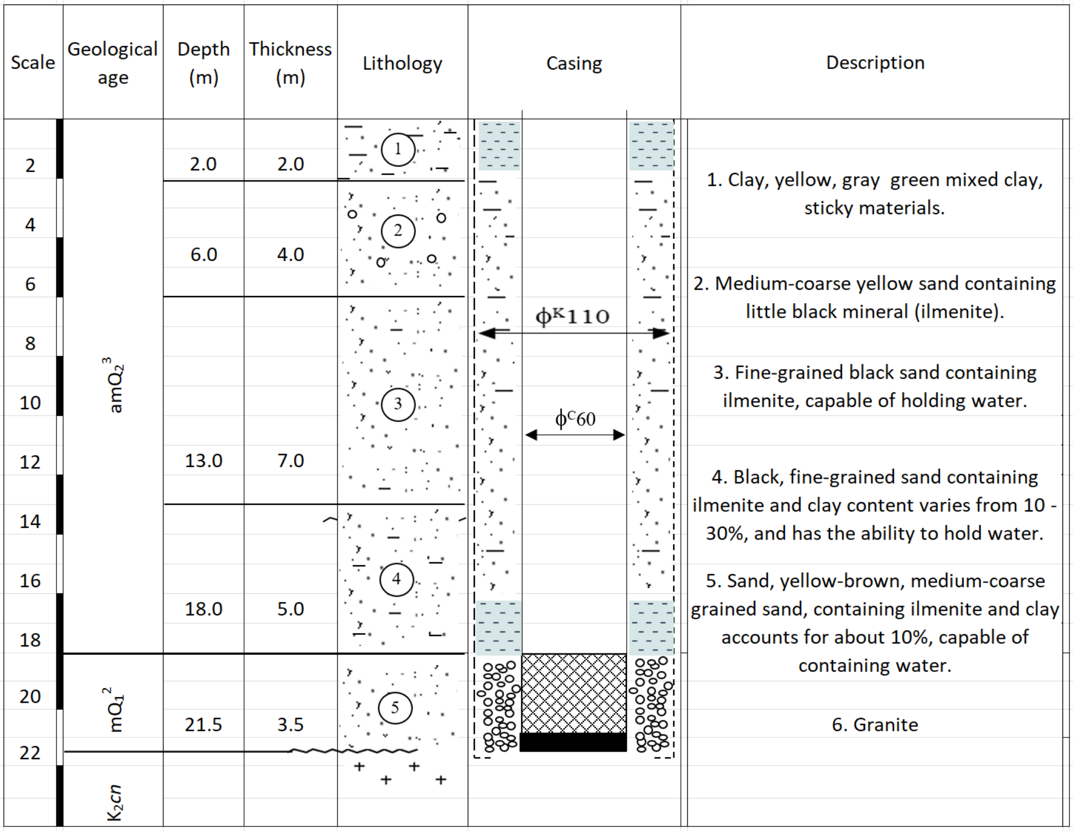

Geological age	Depth (m)	Thickness (m)	Lithology	Description
amQ_2^3	2.0	2.0	①	1. Clay, yellow, gray green mixed clay, sticky materials.
	6.0	4.0	②	2. Medium-coarse yellow sand containing little black mineral (ilmenite).
	13.0	7.0	③	3. Fine-grained black sand containing ilmenite, capable of holding water.
	18.0	5.0	④	4. Black, fine-grained sand containing ilmenite and clay content varies from 10 - 30%, and has the ability to hold water.
mQ_1^2	21.5	3.5	⑤	5. Sand, yellow-brown, medium-coarse grained sand, containing ilmenite and clay accounts for about 10%, capable of containing water.
K_2cn				6. Granite

VIETNAM INSTITUTE OF GEOSCIENCES AND MINERAL RESOURCES

LITHOLOGICAL WELL LOG

Well LK19-BT

Location: Hòa Phú village, Phan Rí Cửa ward, Tuy Phong district, Bình Thuận province
Coordinate: X: 887729.409; Y: 1237443.074; Z: 4 m UTM Zone 48
Lat: 11.17202; Long: 108.55095
Project: Impact of saltwater intrusion on water resources and irrigation in the Southern Central region of Vietnam under climate change
Date: 29/7/2020 ; Ending depth: 13.5 m

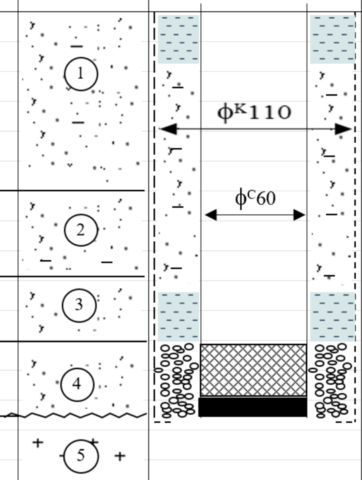

Scale	Geological age	Depth (m)	Thickness (m)	Lithology	Casing	Description
2 4 6	amQ_2^{2-3}	6.0	6.0	①		1. The upper part is a layer of white sand mixed with yellow-brown, small grain, containing many black minerals (ilmenite).
8		9.0	3.0	②		2. Yellow-brown medium-coarse sand containing white biological remains. This layer is ~30cm thick. Next is a layer of fine-medium white sand containing white biological remains similar to the yellow sand layer, interspersed with a few thin layers of ilmenite. The bottom of the layer is sandy loam, clay accounts for about 25-30%.
10		11.0	2.0	③		3. Medium-grained gray sand containing biological remains.
12	mQ_1^2	13.5	2.5	④		4. Fine to medium grained red sand,
14 16 18	K_2cn			⑤		5. Granite